UNIVERSITY OF NOTTINGHAM

EngD Centre in Efficient Fossil Energy Technologies

AVOIDING THE SINTERING OF COAL FIRED SHALLOW FLUIDISED BEDS

Daniel Tolulope Afilaka

MEng (Hons), AMIChemE, GradEI

Thesis submitted to the University of Nottingham for the degree of

Doctor of Engineering

September 2015

Abstract

Fluidised bed combustion (FBC) has been identified as one of the best technologies available for lump coal combustion. A major drawback during prolonged operation of FBC systems particularly bubbling fluidised bed (BFB) systems is sintering and agglomerate formation of bed material that affects performance efficiency and reliability in industrial applications as exemplified at Associated British Sugar (AB Sugar). The mechanisms responsible for sintering and agglomerate formation in this type of system need to be understood, to promote continual use of this technology for efficient coal utilisation.

The first set of investigations focused on agglomeration properties of bed material (Garside 14/25 sand) used in Industrial FBC at AB Sugar. Bed material was calcinated between 800 and 1200°C in a high temperature furnace in the absence and presence of coal (three types of bituminous coals) or coal ash. Results showed sintering and agglomerate formation of bed material can occur in the absence of coal or coal ash at a calcination temperature near 1200°C. Addition of coal or coal ash further promotes sintering and agglomerate formation at 1000°C. Combustion stages appears to influence surface morphology, chemistry and mechanisms of agglomerated bed material based on similarities observed in the agglomerated bed material formed from calcination of Garside 14/25 sand bed material mixed with coal, and those formed in industrial scale FBC during combustion of lump coal.

The second set of investigations used two different lump bituminous coals classified as washed (undergone washing process to remove mud/shale stone) or unwashed (still containing the mud/shale) from the same mine (Blyth, typically referred to as Blyth coals) as those used in the AB Sugar industrial FBC. Combustion of washed and unwashed Blyth lump coals (9 to 19 mm particle

size) was investigated in a 30 kW pilot scale bubbling fluidised bed combustor (PSBFBC) during normal combustion and crash stop combustion runs. This simulated conditions in the AB Sugar Industrial FBC system with a thermal rating of approximately 30 MW, which uses larger coal particle size of 12 to 25 mm.

Results reveal unwashed Blyth lump coal in the PSBFBC and industrial FBC causes some sintering and agglomerate formation of the bed material over short operation periods of 52 and 240 hours respectively, which was not observed in the washed Blyth coal system over a similar operating period. Observed sintering and agglomeration formation in unwashed Blyth coal is mainly attributed to accumulation of mud/shale stones in the bed, which would have been mostly removed by the washing process. The crash stop combustion run, done to simulate the fan trip scenario in the industrial FBC system, promoted sintering and agglomerate formation in the PSBFBC, possibly due to the 30 to 50°C temperature rise in the bed when fluidised air was stopped.

Continuous deposition and increasing concentration of mud/shale stones in the bed affects the localised temperature as well as the fluidising properties and quality, eventually promoting sintering and agglomerate formation. PSBFBC bed height, bed material particle size and measured pressure drop also increase with increasing operating time and mud/shale stones deposition in the bed.

Deposition of coal ash to the surface of the bed material (sand) in the PSBFBC was analysed by the use of SEM-EDX and XRF. The deposition of ash to the surface of PSBFBC bed material sand increases as the operation times increases, as identified by increasing concentration of Al, K and Ca on fluidised bed sand particle surfaces in their stable oxide forms of Al_2O_3, K_2O and CaO respectively.

Acknowledgement

I would like to express my sincere gratitude to God almighty for the wisdom, knowledge and kindness He has bestowed upon me during the course of completing this work and throughout my life up to this stage.

A special thanks goes to my supervisors Prof. Hao Liu and Dr. Carol Eastwick for their support and guidance. I would also like to acknowledge the support of staff and students at Nottingham University, particularly, Prof. Colin Snape, Dr. Anup Patel and Dianne Vincent who have all provided me with their time, support, and advice towards the successful completion of this work.

This research work would not have been possible without the financial support of EPSRC, BF2RA and Associated British Sugar. I would also like to give special thanks to the staffs and associates of Associated British Sugar for their support over the past four years, particularly, Nick Smalley, James Edwards, Maurice Fisher and David Gent.

Finally, a word of appreciation to my family for their constant care, support and understanding which has been incredible and to my wife Bukola Afilaka and my daughters Oluwadarasimi and Oluwadamilola Afilaka for their love, infinite patience and words of encouragement during the busy and tight schedule of completing this piece of work.

Dedication

I dedicate this thesis to my daughter Oluwadarasimi Elizabeth Afilaka whose entire childhood I have missed while carrying out this study. I love you more than words can express.

Table of Contents

List of Figures

List of Tables

Contributions to Knowledge

List of Publications

- Agglomeration Behaviour of Fluidised Bed Sand during Calcination in the Presence and Absence of Bituminous Coal (Currently Being Prepared)
- Mechanism of Sintering and Agglomerate Formation during the Combustion of Washed and Unwashed Bituminous Coal in a Pilot Scale Bubbling Fluidised Bed Combustor (Currently Being Prepared)

Conference Presentation

- An Investigation of Defluidisation within Bubbling Fluidised Bed Combustors Burning Washed and Unwashed Lump Coal. IEA Clean Coal Technology Conference (CCT 2015), Krakow, Poland. 17 – 25 May, 2015

Poster Presentations

- Characteristic Behaviour of Fluidised Bed Sand during Calcination. IEAGHG Carbon Capture and Storage Summer School 2013, Nottingham, United Kingdom. 21 – 26 July, 2013
- Avoiding the Sintering of Coal Fired Shallow Fluidised Beds. Biomass and Fossil Fuel Research Alliance Coal Science Lecture 2015, London, United Kingdom. 6 October, 2015

Nomenclatures

		Units
A	Cross sectional surface area	m^2
C_D	Discharge coefficient	-
$C_{D, h}$	Orifice discharge coefficient	-
$C_{D, plate}$	Plate discharge coefficient	-
d_{noz}	Nozzle diameter	m
d_s	Mean particle diameter	mm
ε	Voidage at combustion conditions	%
$ε_o$	Voidage at static conditions	%
F	Fuel feed-rate	kg/s
g	Acceleration due to gravity	m/s^2
Ga	Galileo's number	-
H	Expanded bed height at combustion conditions	m
H_o	Static bed height	m
$L_{B(av)}$	Average measured height of free space above the bed	mm
$\dot{m}$	Mass flow-rate of air	kg/s
n	Power factor	-
N_h	Number of orifice per unit area of distributor	-

		Units
ΔP	Pressure drop	mbar
ρ_b	Bulk density of bed	kg/m^3
ρ_g	Air density at elevated temperature	kg/m^3
$\rho_{g.amb}$	Air density at ambient temperature	kg/m^3
ρ_s	Particle density	kg/m^3
Q	Volumetric flow-rate at elevated temperature	m^3/s
Q_{amb}	Volumetric flow-rate at ambient temperature	m^3/s
Re_{mf}	Reynolds number at minimum fluidisation	-
T	Elevated temperature	°C
T_{amb}	Ambient temperature	°C
t_d	Distribution plate thickness	m
U	Superficial velocity	m/s
U_h	Superficial velocity in the orifice	m/s
u_{mf}	Minimum fluidisation velocity	m/s
μ	Dynamic air viscosity at elevated temperature	kg/m.s
μ_{amb}	Dynamic air viscosity at ambient temperature	kg/m.s
w_i	Initial weight	g
w_o	Final weight	g

Abbreviations

AB Sugar	Associated British Sugar
AFI	Ash Fusibility Index
AFT	Ash Fusion Temperature
ASTM	American Standard Test Method
BFB	Bubbling Fluidised Bed
BFBR	Bubbling Fluidised Bed Reactor
BSE	Back Scattered Electron
BS ISO	International Organisation for Standardisation
CFB	Circulating Fluidised Bed
DT	Differential Thermocouple
DTA	Differential Thermal Analysis
EDX	Energy Dispersed X-ray
ELIF	Excimer Laser Induced Fragmentation Florescence
FB	Fluidised Bed
FBC	Fluidised Bed Combustor
FSS	Full Scale Span
FT	Flow Temperature
HT	Hemispherical Temperature
ID	Internal Diameter

IDT	Initial Deformation Temperature
LFO	Light Fuel Oil
LPM	Litres Per Minute
OD	Outside Diameter
PEARLS	Plasma Exited Atomic Resonance Line Spectroscopy
PF	Pulverised Fuel
PI	Pressure Indicator
PID	Proportional Integral Derivative
PSBFBC	Pilot Scale Bubbling Fluidised Bed Combustor
PT	Pressure Transmitter
SEM	Scanning Electron Microscope
TC	Thermocouple
TGA	Thermo Gravimetric Analysis
TI	Temperature Indicator
tpd	Tonnes Per Day
tph	Tonnes Per Hour
wt	Weight
w/w	Weight to Weight
XRD	X-ray Diffraction
XRF	X-ray Fluorescence

CHAPTER ONE

INTRODUCTION AND OBJECTIVES

1.1. Introduction

This chapter provides an introduction and background to the project on “Avoiding the Sintering of Coal Fired Shallow Fluidised Beds” conducted in fulfilment of the award of Doctor of Engineering (EngD) Degree at the University of Nottingham, United Kingdom (UK)

The context of this research is covered in this chapter with a project brief, which is based on sintering and agglomeration problems currently facing an industrial operating lump coal fluidised bed combustor (FBC) located at Associated British Sugar (AB Sugar) Newark Factory, UK. This is followed by a brief overview on sintering and agglomerate formation in fluidised bed systems. Other details given in this chapter include scope and justification of this project, objectives of this project, and structure of this thesis.

1.2. Project Brief

AB Sugar operates a number of coal-fired FBC for producing animal feed by drying sugar beet pulp subsequent to the sugar extraction process. The schematic diagram of one of the FBC systems operated by AB Sugar based at Newark Factory is shown in Figure 1-1. As shown in the diagram, air is fed into a bed of quartz sand (Garside 14/25) made up of >96wt% SiO_2, particle size 0.5 – 1.0 mm, and typical static bed height of 150 – 200 mm through plenum chamber

(wind box) with the use of 2,100 standpipe air distribution (air nozzles) of 1 inch internal diameter.

Bituminous coal with a particle size of 12.5 – 28 mm (>90wt%), initial ash deformation temperature (IDT) no lower than 1150°C (at ash fusion conditions) and coal ash content not higher than 6wt% is used for the FBC operation. During normal operations, typical bed temperature is 900°C but the gas temperature can be as high as 1100°C, depending on whether flue gas recirculation is used or not.

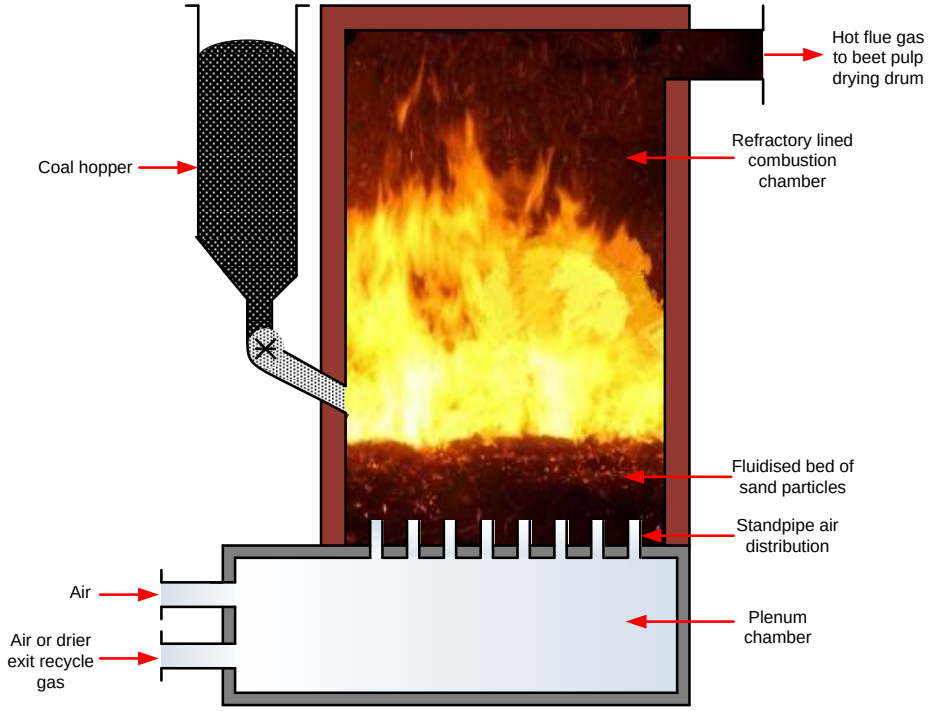

Figure 1-1: Schematic diagram of the industrial operated lump coal shallow FBC at AB Sugar Newark factory

During continual operation of the FBC system over a typical sugar production campaign period of 24 – 26 weeks, sintering and agglomeration of the bed material usually occurs over 6 – 8 weeks of continuous operation. The occurrence of unexpected fan failure after about 5 weeks of operation also increases the likelihood of sintering and agglomeration occurring earlier than the expected stipulated time. The occurrence of sintering and agglomerate formation

as a result of any of the identified reasons requires shutdown of the FBC to change the whole bed materials. This typically takes about 5 days from start to finish which causes suspension of the animal feed production process or switching to the use of a natural gas fired drier which is more expensive to operate causing serious financial losses to the company. The need to understand the mechanism/s responsible for the occurrence of sintering and agglomerate formation within the FBC system, including suitable detection techniques is therefore seen as very important in order to increase FBC operating time and reduce financial losses.

1.3. Overview of Sintering and Agglomerate Formation in Fluidised Bed Systems

Literature revealed that the use of fluidised beds (FB) for solid fuel (biomass, coal, petroleum coke, etc.) combustion or gasification processes has been of major interest in the past few decades due to high heat transfer efficiency, vast contact surface area, isothermal operating conditions, fuel flexibility, low NOx emissions and low maintenance cost associated with this technology (Basu 2006; Bartels et al. 2010b; Zhong et al. 2013). However, the sintering and agglomerate formation issue has been a major problem facing the usability of FB technology for this application (Skrifvars et al. 1992; Ohman et al. 2000).

Sintering can be described as a phenomenon whereby loosely attached bed material particles become denser through the adhesion of the bed material particles (Teixeira et al. 2012). Continuous adhesion of the bed material particles in the FB system can lead to agglomerate formation which inevitably causes a decrease in heat transfer and fluidisation quality resulting in the defluidisation of the FB bed (Skrifvars et al. 1998; Ohman et al. 2000). The occurrence of FB bed

defluidisation requires an unscheduled plant shut down to change the bed material (Llorente & Garcia 2005; Zhong et al. 2013).

Over many years of active research into understanding the causes of sintering and agglomerate formation, many researchers have studied sintering and agglomerate formation in FB system using various fuel types such as coal (Huffman et al. 1981; Manzoori & Agarwal 1992), petroleum coke (Anthony et al. 1997) and biomass (Brus et al. 2005; Chirone et al. 2006). From all the various research conducted in this subject area, scholars have been able to identify and propose sintering and agglomerate formation mechanisms, suitable detection techniques and mitigation approaches. The mechanisms that have been proposed to be responsible for sintering and agglomerate formation can be divided into three different types - namely hydrodynamics (Visser 1989; Seville et al. 2000), chemical reaction (Manzoori & Agarwal 1992; Olanders & Steenari 1995), and ash and bed interaction (Ohman et al. 2000; Lin et al. 2003) all explained in chapter 2.

Sintering and agglomerate formation detection approaches can be broadly classified into two types; ex-situ detection (Huffman et al. 1981; van der Drift & Olsen 1999; Llorente & Garcia 2005) and online agglomeration detection techniques (McDougall et al. 2005; Scala & Chirone 2006; Chirone et al. 2006; Mac an Bhaird et al. 2014). The ex-situ fly ash detection technique uses the properties of the fuel and ash to predict sintering and agglomerate formation while the latter technique focus on using real life data collected from the FB operating process.

However, it remains questionable if the identified and proposed sintering and agglomerate formation mechanisms and detection techniques from earlier scholars will be relevant to this situation. Thus the purpose of this study.

1.4. Scope and Justification

From the project brief and overview of sintering and agglomerate formation in FB system detailed in section 1.2 and 1.3 respectively, it can be seen that much work has been done to understand sintering and agglomerate formation. The focus of published research into this topic has mainly been on biomass fuel with a small number of reported investigations on low volatile bituminous coal. Hence, this study focused on understanding and developing a comprehensive sintering and agglomerate formation mechanism for highly volatile bituminous coal.

According to literature, various coal types react differently during sintering and agglomerate formation due to variation in their fuel properties and characteristics (composition, volatility and size) and combustion conditions (McCullough et al. 2011). It is therefore necessary to investigate the cause of sintering and agglomerate formation under these conditions, especially when using lump sized coal (9 to 19 mm particle size), which is a unique technology with no reported research outcome from previous scholars.

A comparison between sintering and agglomerate formation tendencies of washed coal over unwashed coal was not investigated or reported by previous scholars. Hence, another investigation performed and reported in this study.

In these studies, a 30 kW lump coal fired pilot scale bubbling fluidised bed combustor (PSBFBC) was designed, manufactured, installed and commissioned using the same minimum fluidising velocity and nozzle type (size, design and material) as the industrial operated FBC at AB Sugar. The PSBFBC was operated at similar operating temperature, using the same coal and bed material type as the industrial operating FBC at AB Sugar.

1.5. Research Objectives

To identify the cause of sintering and agglomerate formation and suitable detection techniques in a typical shallow FBC (usually BFB), the following objectives have been identified.

1. Investigate mechanisms of bed sintering and agglomerate formation during combustion of washed and unwashed lump coal in BFB, and establish the effect of coal quality on sintering and agglomerate formation during normal combustion operation.

2. Investigate the effect of fluidisation fan failure on bed sintering and agglomerate formation, and make recommendations for operational procedures to minimise or mitigate sintering and agglomerate formation in the BFB system.

1.6. Thesis Structure

This thesis is divided into seven chapters. Chapter one introduces the project including project brief, overview of sintering and agglomerate formation in FBC system, and justification, scope and objectives of the project.

Chapter two covers literature review of sintering and agglomerate formation during fluidised bed combustion of coal. A brief introduction to coal, its chemistry and general principles of coal combustion, and fluidised bed combustion of coal are explored. Discussion includes sintering and agglomerate formation in a bubbling fluidised bed (BFB), and detection techniques of sintering and agglomerate formation. The mechanism responsible for sintering and agglomerate formation during lump coal combustion is also proposed by the author of this work.

Chapter three covers design of the PSBFBC used for this investigation. Discussion includes pre-design decisions, hydrodynamic design parameters, fluidising air flowrate, coal feedrate, component design, and piping and instrumentation details.

Chapter four details the materials and experimental methodology implemented during this investigation. Topics covered include material specifications and methodologies of bed material calcination, PSBFBC coal combustion, and bed material characterisation techniques.

Chapter five covers results and discussion on agglomeration behaviour of fluidised bed sand during calcination. The discussion section in this chapter is divided into two different but linked investigative works carried out as part of this study. The first section detailed the calcination study of bed material at high temperature between 800 and 1200°C in a fuel and ash free environment. Colour change, weight loss, particle surface characteristics, and sintering and agglomerate formation types / mechanism are examined. The second section details the calcination study of bed material in the presence of coal / ash. Related are visual inspection of agglomerates, comparison of surface morphology of different agglomerated bed material samples, and sintering and agglomerate formation types and mechanism.

Chapter six investigates the effect of washed and unwashed coal on fluidised bed operation with respect to sintering and agglomerate formation using the PSBFBC system. This chapter covers a comparison between two bituminous coal types with discussion section divided into two investigations. The first section covers the normal operation of PSBFBC using the two coal types while the second focused on the crash stop effect on sintering and agglomerate formation with the same two coal types as before.

Chapter seven provides conclusions, recommendations for industrial applications, and proposed future investigations.

1.7. Summary

Sintering and agglomerate formation is a major problem facing the use of FBC technology. With the ever-increasing trend in sintering and agglomerate formation research in biomass combustion, additional research investigating this phenomenon in a coal environment is likewise imperative.

To achieve a comprehensive, conclusive and economically meaningful result from this investigation, a PSBFBC using similar design and operating parameters as the industrial operated FBC based at AB Sugar factory is necessary.

Various mechanisms of sintering and agglomerate formation have been identified from literature. These need to be investigated to determine the mechanisms responsible for sintering and agglomerate formation in the lump coal combustion FBC system. Suitable measures to detect sintering and agglomerate formation in a FBC also need to be identified using the PSBFBC.

CHAPTER TWO

REVIEW OF SINTERING AND AGGLOMERATE FORMATION DURING FLUIDISED BED COMBUSTION OF COAL

2.1. Introduction

The use of fluidised bed (FB) system as a coal conversion technology for both combustion and gasification processes have been widely studied over years of active research and development in both the academic and industrial world (Basu 2006). FB systems can be divided into two types namely circulating fluidised bed (CFB) and bubbling fluidised bed (BFB) systems. CFB systems are fast operating FB, where the fuel is burnt in a fast fluidisation regime of about 10 m/s while BFB are stationary or slow FB where coal is burnt in a slow fluidisation regime of between 1 and 2.5 m/s. However, a major drawback seen during prolonged operation of FB systems particularly BFB system which is the focus of this study, is the sintering and agglomeration of the bed material.

During coal combustion in the BFB system, a wide choice of coal particle size ranging from crushed to lump coal with, typical size of between 3 to 32 mm, are used depending on the type of system (National Coal Board 1980; Basu 2006). The typical operating bed temperature is usually between 750 and 950°C, under which soft, fine ash is produced. With continuous fluidisation occurring in the high temperature BFB environment, constant interaction and collision continually occurs between the fine ash produced from the combustion process, bed material and coal particles present in the system. Over time, sintering of the bed

occurs which is followed by agglomerate formation and in most cases leading to defluidisation of the bed in the BFB system. Different mechanisms have been identified to be responsible for this phenomenon by various scholars namely hydrodynamics (Visser 1989; Seville et al. 2000), ash and bed interaction (Ohman et al. 2000; Lin et al. 2003), and chemical reaction (Manzoori & Agarwal 1992; Olanders & Steenari 1995; Tardos & Pfeffer 1995) mechanisms which are all discussed in this chapter.

Discussions in this chapter also cover brief description of coal chemistry and properties, FB combustion of coal, and detection techniques of sintering and agglomerate formation in BFB system. Details of the discussions in this chapter are based on findings identified from literature survey with more focus on coal combustion applications.

2.2. Coal

Coal, a highly complex heterogeneous substance, is a fossil fuel formed from the decomposition of plant remains over millions of years in peat swamps under extreme heat and pressure in the absence of oxygen (Meyers 1981). Coal contains a mixture of organic and inorganic components, liquid and gaseous phases and varies widely in their physical and chemical properties depending on the region where they are found, time of deposition and degree of coalification (Liu et al. 2005). The organic portion of coal composes of carbon, oxygen, hydrogen, nitrogen and sulphur while the inorganic portion consists of sodium, magnesium, aluminium, silicon, potassium, calcium and iron (Benson et al. 1993). Example of the typical organic structure of coal is presented in Figure 2-1 which shows a network of macromolecular aromatic clusters linked to naphthenic rings by bridges of aliphatic and heterocyclic groups chains (Levine et al. 1982)

Coal types differ in their appearance, fixed carbon content, volatile matter, heating value and elemental composition. Generally, coals are characterised into different ranks using their fixed carbon content, heat content and or percentage of volatile matter (Jinsheng 2009). High rank coals are identified with high fixed carbon content, heating value and low hydrogen and oxygen contents, for example bituminous and anthracite coal. Low rank coals (lignite and sub-bituminous coal) on the other hand exhibit low fixed carbon content, heating values and high hydrogen, oxygen and sulphur content. A comparison between different coal types is presented in Table 2-1.

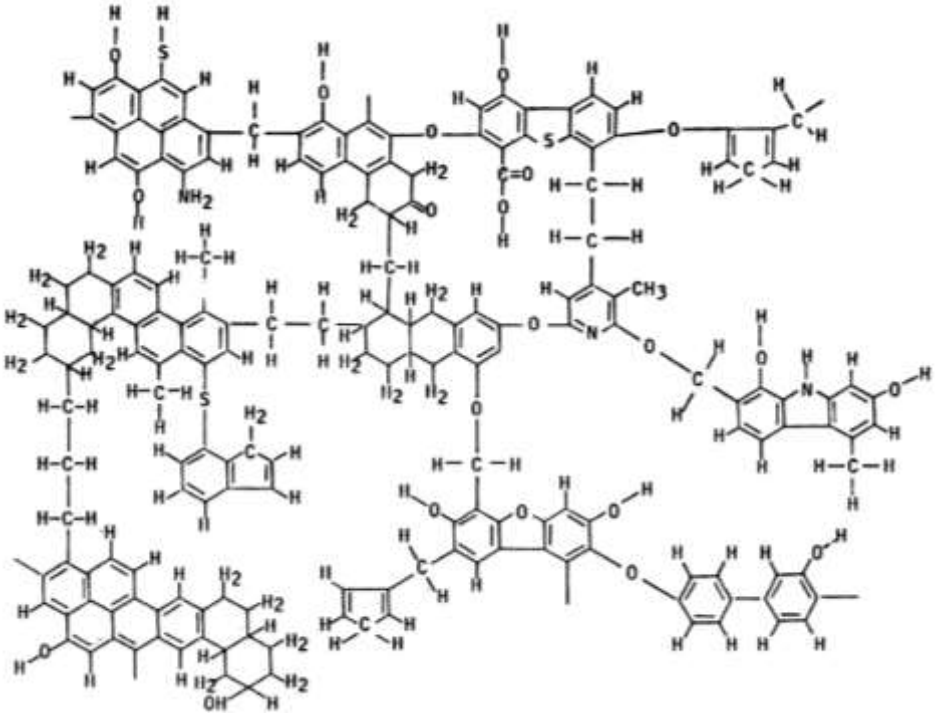

Figure 2-1: Typical structure of chemical groups in coal (Levine et al. 1982)

For the purpose of this work, the coal type of interest is high volatile bituminous (high rank) coal, which is currently used by AB Sugar in their FBC operation. Bituminous coal supplies the highest amount of energy that comes from coal based on global utilisation. It is generally used to produce heat, electricity and in steel making. Bituminous coal are also black in colour like every other coal type but frequently appear shiny due to alternating band layers of dull and glossy

black colouration (Matthews 2005). Large deposits of bituminous coal are found in Great Britain, Germany, Russia, India, China and Australia in terms of global resources (Schobert 1987). Analyses of the bituminous coals used in this investigation are presented in section 4.2.2.

Table 2-1: Different coal types ranked based on their fixed carbon content, heat content and elemental composition (Meyers 1981)

Coal Type	Limits of fixed carbon (% w/w)	Limits of heat content (MJ/kg)	Elemental Composition (% w/w)		
			Carbon	Hydrogen	Oxygen
Anthracite	86 - 98	≥ 32.48	90 - 97	3 - 5	1 - 3
Bituminous	69 - 86	26.68 - 32.48	85 - 90	4 - 5	5 - 10
Subbituminous	30 - 69	19.26 - 26.68	75 - 85	5	10 - 20
Lignite	25 - 30	14.62 - 19.26	70 - 75	4 - 5	20 - 25

2.2.1. Chemical Properties Characterisation of Coal

Chemical composition of coal can be determined using proximate and ultimate analyses. Proximate analysis is used to determine the moisture, fixed carbon, ash and volatile matter contents of the coal (Unsworth et al. 1991). The data generated and collected from this analytical technique has been interpreted by some researchers and used to predict coal behaviour during combustion (Bartels et al. 2008; Teixeira et al. 2012). Ultimate analysis on the other hand is used to determine the quantity of carbon, hydrogen, nitrogen, oxygen and sulphur present in coal (Schobert 1987). A major advantage of the ultimate analysis is that it can be used to estimate the maximum amount sulphur oxides emission expected to be released during combustion of the coal. It can however not be accurately used to estimate the amount of nitrogen oxide emission due to the fact that not all of the nitrogen in the fuel are converted to the oxide state (Khan et al. 2009). Various institutional standardised methods used to carry out proximate

and ultimate analysis are referenced in Table 2-2. Application of these institutional standards to determine the chemical properties of the bituminous coals used in this study is detailed in section 4.2.2.

Table 2-2: Standard methods for the chemical properties characterisation of coal

Properties	Standard Methods	
	ASTM	BS ISO
Proximate Analysis		
Moisture Content	D3172-13	17246:2010
Ash Content		
Volatile Matter Content		
Fixed Carbon		
Ultimate Analysis		
Total Sulphur Content	D3176 – 09	17247:2013
Carbon Content		
Hydrogen Content		
Nitrogen Content		
Oxygen Content		

2.2.2. Thermal Properties Characterisation of Coal

Ash fusion temperature and specific energy tests are two analytical techniques implemented to characterise the thermal properties of coal. The ash fusion temperature test, which is a function of ash fusibility index (AFI), is used to determine the softening and melting temperature of coal under reducing or oxidising condition. Various scholars have identified ash fusion temperature test as a suitable technique for predicting the sintering and agglomeration, slagging and fouling tendencies of a fuel with varying degree of accuracy (Bartels et al. 2008). The specific energy test is done to determine the total amount of energy present per unit mass of coal. This helps in estimating the quantity of heat

required or amount of coal required to achieve the required operating temperature during the combustion process. Institutional standardised methods used to determine ash fusion temperature and gross specific energy of coal are referenced in Table 2-3. Application of these institutional standards to determine the thermal properties (gross specific energy) of the bituminous coals used in this study are detailed in section 4.2.2

Table 2-3: Standard methods for the thermal properties characterisation of coal

Properties	Standard Methods	
	ASTM	BS ISO
Ash Fusion Temperature		
Initial Deformation Temperature (IDT)	D1857/ D1857M-04 (2010)	540:2008
Hemispherical Temperature (HT)		
Flow Temperature (FT)		
Gross Specific Energy	D5865-13	1928:2009

2.3. General Principles of Coal Combustion

Combustion can be described as an exothermic process where carbon and hydrocarbon are oxidised to produce carbon dioxide, water and heat. The heat generated from this process can be used for various purposes such as drying and steam production for power generation. During coal combustion, the coal particle undergoes three stages namely: heating and drying of the coal particle, devolatilisation and volatile combustion, and char combustion (Basu 2006; Liu 2011b). Char combustion is usually the most time consuming stage of the entire combustion process accounting for about 90% of the total combustion time (Basu 2006). The largest share of the total combustion energy is released during this stage depending on the volatile content of the coal (Liu 2011b). In cases where the coal has high moisture content, the heating and drying stage becomes the most time consuming process.

Combustion behaviour of coal is also influenced by their elemental constituents, which are classified into organic and inorganic matters. Over many years of active research the effect that each of these constituent has on combustion behaviour have been studied and broadly divided into three groups as shown in Figure 2-2 (Unsworth et al. 1991). The first group are those affected only by the organic constituent of coal, the second group are those affected by both the organic and inorganic constituent of the coal while the third group are those affected only by the inorganic constituent of the coal. For the purpose of this work, the group affected only by the inorganic constituent of the fuel (Group III) is of major interest.

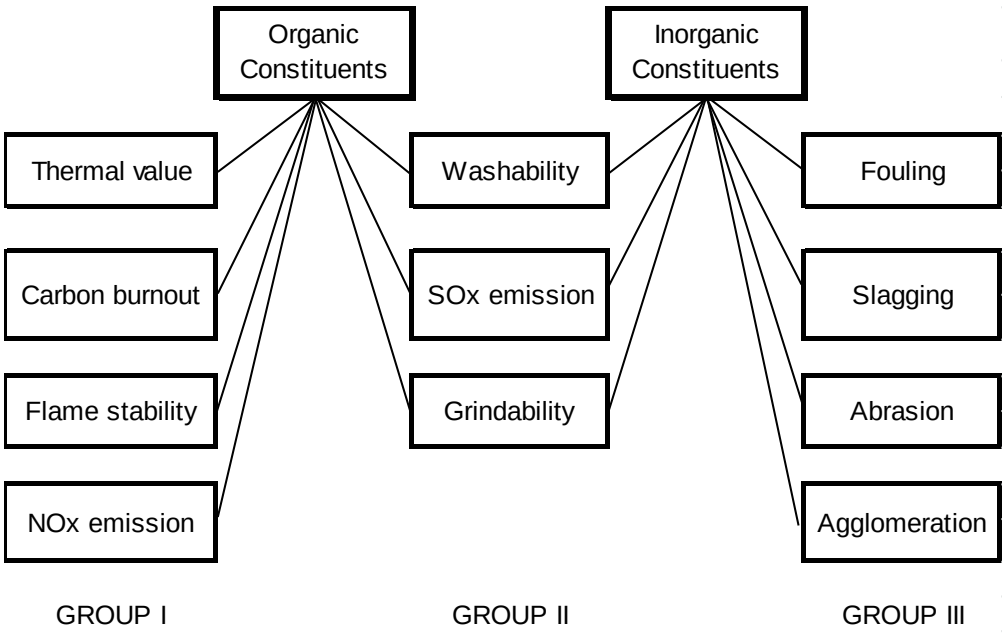

Figure 2-2: Relationship between technological areas and coal constituents
(Unsworth et al. 1991)

Fouling, slagging, abrasion and agglomeration formation have all been identified to influence the inorganic constituent of coal (Anthony et al. 1997; Anthony et al. 1998; Teixeira et al. 2012). During coal combustion, the inorganics (mineral matters) present in coal are transformed into ash (Benson et al. 1995). The chemistry and quantity of ash produced from the coal combustion process depends on the inorganic composition of the coal. The higher the inorganic

content in the coal, the greater the amount of ash produced from the fuel and the more problematic the fuel will be in causing ash deposition and ash related problems during combustion or gasification (Unsworth et al. 1991). Fusion and melting behaviour of produced from the combustion process is also influenced by the elemental ratio of the inorganics present in the fuel (Vassilev et al. 2015).

2.4. Fluidised Bed Combustion of Coal

Fluidised bed combustion (FBC) system has been identified as one of the best technologies available for lump coal combustion. In FBC, air is blown slowly upward through a set of nozzles into a bed of sand of particle size 0.03mm to 3mm depending on the application. A continuous increase of the air velocity causes individual sand particles present in the bed to move upward and become supported by the air stream in order to form a fairly defined surface (National Coal Board 1980). Further increase in the air velocity causes a turbulent briskly boiling effect of the bed material to occur which makes it behave like a fluid demonstrating the properties of a boiling liquid at which point it is described as a fluidised bed (FB). If the sand in the bed is heated up and coal is injected onto the bed surface continuously, the coal will burn and combust causing the whole bed of sand to assume a uniform temperature at which point we have a FBC (Dainton 1979).

The rapid mixing of the bed materials and the efficient combustion of coal in the FBC makes it possible to sustain combustion with reduced amount of unburnt coal left in the bed typically 0.5 to 5% (National Coal Board 1980). Most FBC are operated within temperature range of 750 to 950°C depending on the fuel used, at which a soft fine ash is produced. The use of FBC is of interest because it offers many advantages including lower operating temperature; reduced NO_x and SO_x formation; uniform operating temperature; low capital and operating cost and

high fuel flexibility when compared with other coal conversion technologies (Basu 2006). There are two main types of FBC system namely circulating fluidised bed (CFB) and bubbling fluidised bed (BFB).

2.4.1. Circulating Fluidised Bed

CFB can be described as a fast operating FB where the fuel is burnt in a fast fluidisation regime. The fluidising air velocity in this system is always around 10m/s which causes the bed material particles of particle size 0.05 to 0.5mm to become fully (or near fully) entrained (Koppejan & Van Loo 2003). The hot gases and entrained solids passes upwards into a gas-solid separator where the solid materials are captured and returned back into the CFB and the hot gases are made available downstream for drying purposes or steam generation depending on the application. A typical setup of a CFB system is presented in Figure 2-3. CFB systems are generally larger size system with higher operating cost when compared to BFB systems (Basu 2006).

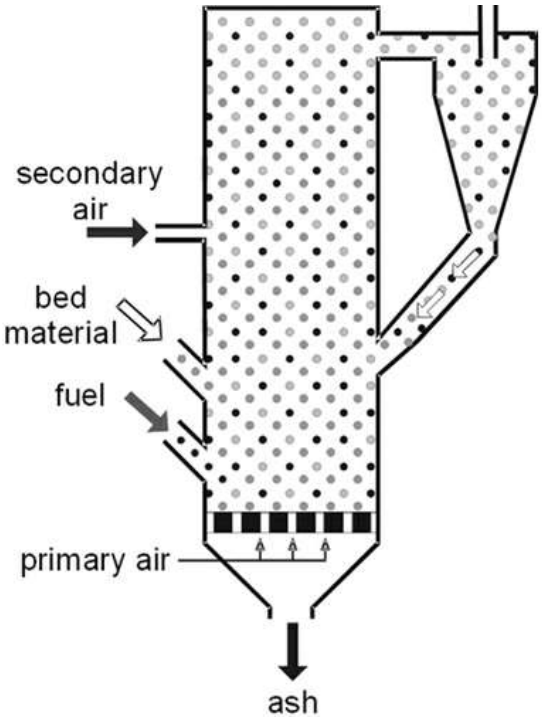

Figure 2-3: Typical setup of a CFB reactor section for a coal combustion system (Koppejan & Van Loo 2003)

2.4.2. Bubbling Fluidised Bed

BFB combustion systems can be described as a stationary or slow FB with air velocity between 1 and 2.5m/s. Schematic diagram for a typical BFB system is shown in Figure 2-4. A typical BFB combustion system comprises of three sections namely: plenum chamber, fluidising zone and free board zone. The primary combustion air is supplied into the plenum chamber above which a fluidising grate or a distributor nozzle plate sits and allows the primary combustion air to pass through into the bed zone. The fluidising zone where the primary combustion takes places typically contains bed material usually sand with a particle size of 0.03 to 3mm depending on the application (Basu 2006). Above the fluidising zone is the freeboard zone where unburnt fuel from the fluidising zone is burnt before being lost by entrainment. Depending on the application, the walls of the BFB can be lined with or without tubes to produce steam for power generation and / or hot gas for drying purpose respectively.

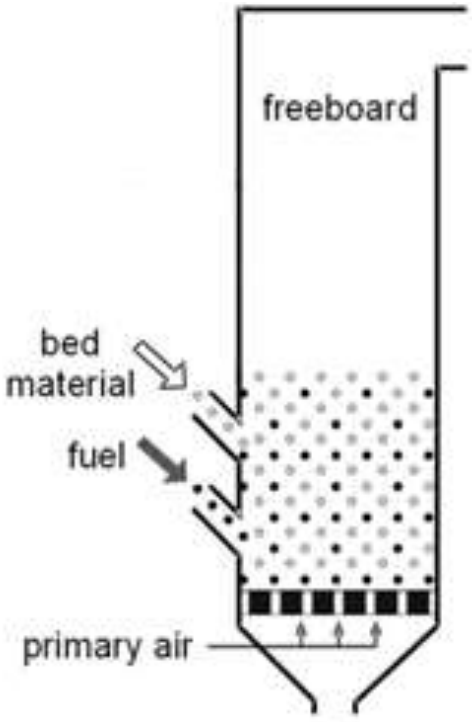

Figure 2-4: Typical setup of a BFB reactor section for a coal combustion system (Koppejan & Van Loo 2003)

2.4.2.1. Effect of Coal Particle Size on BFB

The particle size of coal burnt in a BFB ranges widely from crushed to lump coal with a typical size of between 6 to 32mm (National Coal Board 1980). During coal combustion in the BFB, the temperature of the char burning particle is always higher than that of the surroundings (sand bed) and this difference can be as high as 200°C (Park 1989). According to Park, the temperature difference between the burning char particles and the bulk of the sand bed is dependent on the particle size of char, oxygen concentration available in the bed and the reactivity of char. The temperature difference between the char particle and the bulk sand bed increases with a decrease in char particle size and falls rapidly with further decrease in char particle size (Park 1989). This high temperature effect exhibited by the char particles compared with their fluidised surrounding during combustion is supported by the findings of Lin and colleagues (Lin et al. 2003) who observed similar effect while studying char particle combustion in a lab-scale FB.

2.4.2.2. Effect of Coal Ash on BFB

As the temperature rises during the combustion of coal, a complex sequence of phase changes and reactions occur leading to ash formation as a by-product of the combustion process. Some of the ash produced from the combustion process forms a coating layer on the surface of the bed material particles and is also deposited in the bed (Ohman et al. 2000). If the temperature within the bed becomes high enough, the inorganic components present in the ash will melt to form a liquid phase ash. This liquid phase ash formed can act as glue which causes a glassy sintering of the remaining un-melted ash particles present within the bed and those deposited on the surface of the bed particles (Schobert 1990). The sintered ash in combination with the sand bed can form aggregate which are

too large to be fluidised by the air stream passing through the bed. This description follows bed material and ash particle sintering and agglomerate formation mechanism discussed in details in section 2.5.2. It is important to point out that for this ash sintering to occur two conditions needs to be met which are: the presence of ash in the bed and a high enough temperature above the ash fusion temperature to cause the deposited ash to melt. This shows that using coal with high ash content might increase the possibility of ash sintering occurring hence causing the formation of sintered aggregates (agglomerate).

2.5. Sintering and Agglomerate Formation in BFB

Sintering (agglomeration) can simply be described as a high temperature process for fusing solid powdered particles together (Simpson 2009). It is a widely used processing technique in the ceramic and metal industry to produce bulk ceramic components and powder metallurgical parts which is achieved by applying thermal energy on ceramic and/or metal powders (Kang 2005). Sintering processes can be divided into two types namely: solid state and liquid phase sintering (German 1996; Kang 2005). Solid state sintering occurs when the powder particles are wholly densified in a solid state at the sintering temperature (Tanaka et al. 2012) while liquid phase sintering occurs when a liquid phase is present in the compact during sintering to act as a binder (German et al. 2009). Comparison between these two types of sintering processes is shown in Figure 2-5.

Liquid phase sintering is of two types: viscous flow sintering and transient liquid phase sintering. Viscous flow sintering occurs when the volume fraction of liquid present in the system is significantly high that a full densification can be achieved by a viscous flow of grain – liquid mixture without causing a change to the structure of the grain during densification (Kang 2005). Transient liquid phase

occurs when a liquid phase is formed in the compact at the early stages of sintering but disappears as sintering progresses causing densification to be completed in the solid state(Kang 2005). The ceramic and metal industries have identified various variables, which influence sintering formation and have divided these variables into two categories: material variables and process variables. Material variables include chemical composition of powder material, size, shape, particle size distribution and degree of powder agglomeration. The process variables category are mostly thermodynamic variables such as temperature, pressure, heating and cooling rate, time and atmosphere (Kang 2005).

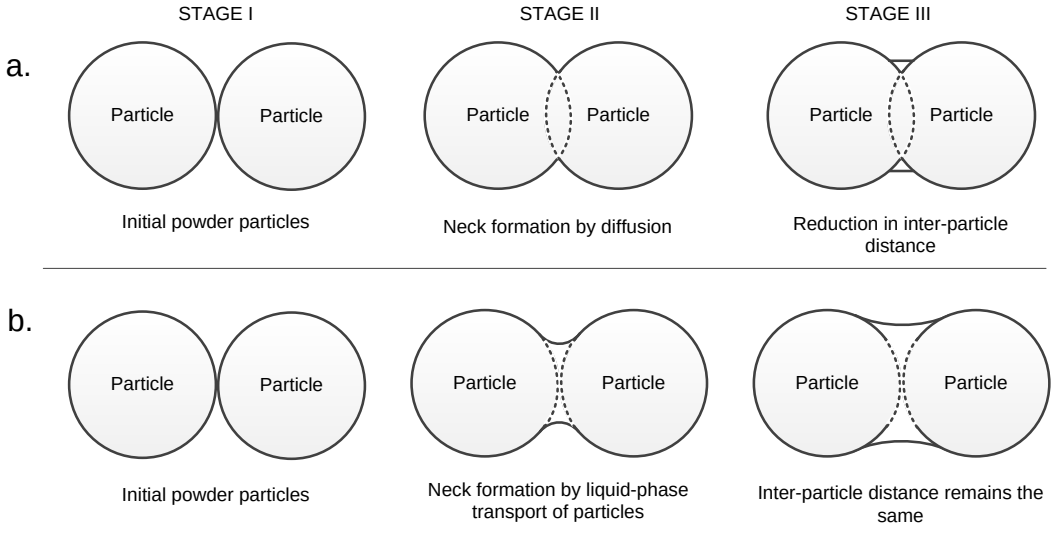

Figure 2-5: Schematic illustration of the types of sintering process of compact between two particles. (a) Solid state diffusion. (b) Liquid phase. (Rajput 2007)

In BFB operation, sintering of the bed material is a major problem facing the use of BFB for combustion processes (Bartels et al. 2010b). Bed sintering in BFB operation causes agglomerate formation and in most cases results in defluidisation of the bed requiring a lengthy and expensive unscheduled shutdown of the FBC system (Ohman et al. 2000; Zhong et al. 2013). It is very difficult to separate sintering from agglomerate formation as agglomerate formation can be expressed as product of sintering prior to defluidisation (Teixeira et al. 2012).

Agglomerate can be described as the sintering of bed particles or partial melting of a binder within the system causing the bed particles to form an aggregate in a high temperature process (Teixeira et al. 2012). The gas-solid fluidisation phenomenon that occurs in BFB at high temperature is a complex process and becomes even more complex for agglomeration at high temperatures where chemical reaction, transport phenomena and particle interactions are involved (Bartels et al. 2008).

In order to have a better understanding of sintering and agglomerate formation under these conditions, a comprehensive study needs to be undertaken on the inter-particle interaction that occurs between the bed material particles, the ash produced from the combustion processes and the chemical reaction effects of the combustion process in the BFB system. Discussion in this section covers agglomeration formation mechanisms from the perspective of hydrodynamics, bed and ash particle interaction and chemical reaction mechanisms, which have been identified by various scholars in literature. The question being answered from this discussion is to determine if any of these mechanisms are solely responsible for sintering and agglomerate formation or if a combination of them is required during lump coal combustion in a BFB system?

2.5.1. Hydrodynamic Mechanism

As explained earlier in section 2.4.2, a BFB consist of a bed of sand made up of identical sized sand particles blown upward by a stream of fluidising air to attain fluidisation. The sand particles used in BFB are classified as B types based on Geldart particle classification which categorises powder into four types: A, B, C and D according to their fluidisation behaviour as a function of their particle size and density as presented in Figure 2-6 (Geldart 1973; Basu 2006). At fluidised conditions, inter-particle interaction occurs in the form of gas-particle and

particle-particle interactions within the BFB system. The gas-particle interaction describes the boundary characteristics that occur between fixed and fluidised bed conditions in a BFB system, which can be influenced by the particle-particle interaction within the same system. Particle-particle interaction are associated with the presence of inter-particle forces which can exist as van der Waals and electrostatic forces of attraction in a homogenous powder particle environment when the particle collision is inelastic (Visser 1989; Chaivatamaset et al. 2013) or due to the occurrence of a strong liquid bridge in a heterogeneous environment when a liquid binder is present (Seville et al. 2000).

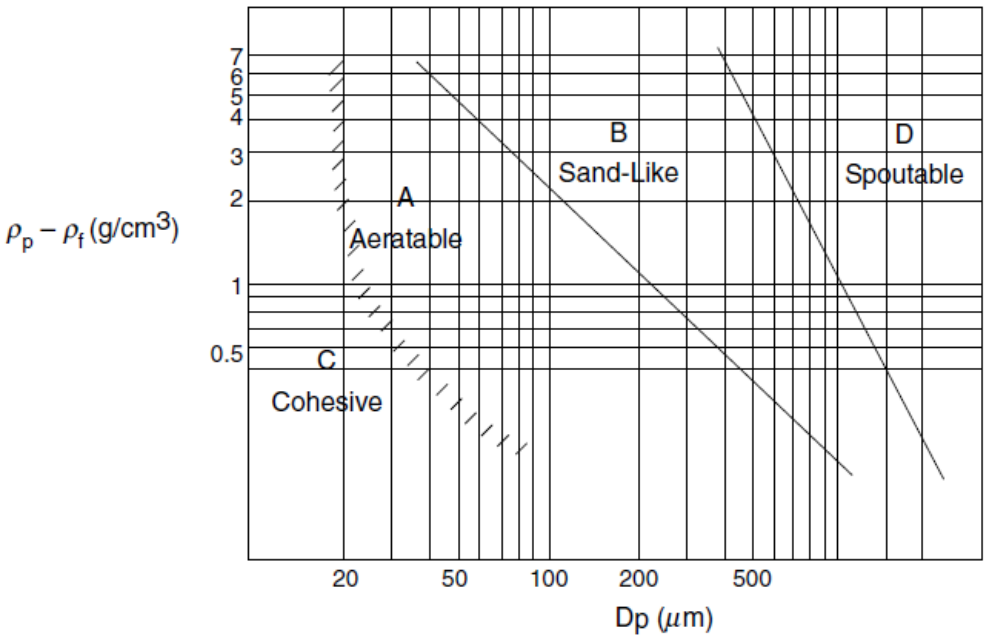

Figure 2-6: Powder classification developed by Geldart

The liquid binder in a heterogeneous environment can be formed from the melting of deposited ash in the BFB system, which can be achieved if the bed temperature is operated above the AFT of the deposited ash. One possible cause of this temperature rise can be attributed to the coal particle size burnt in the BFB during the combustion process. The introduction of lump sized coal into the bed causes an increase in the mean particle size of the bed. This increase in mean particle size will reduce the fluidisation quality of the bed and change the

fluidisation regime of the system from a B type to D type according to Geldart classification making it difficult to fluidise the bed (Basu 2006). The degree of particle size variation increase within the system will depend on the amount and particle size of the coal introduced into the BFB. As a result of the change in the fluidisation quality and regime of the bed due to increase in average particle size of the bed, the mixing and vigorousity of the bed fluidisation becomes poor. This in turn will lead to poor heat transfer and uneven temperature distribution across the bed, causing the creation of hot spots which will result in the melting of deposited ash and production of liquid binder needed for the formation of the strong inter-particle liquid bridge (Atakul & Ekinci 1990).

Molerus explains that when one of the inter-particle forces present in the system is of the same order of magnitude as the gravitational force, the particles present within the bed becomes sticky and this stickiness can alter the fluidisation quality and characteristics of the bed (Molerus 1982). This implies that the bed particles can adhere together when they collide if the inter-particle forces present in the system are strong enough. According to Seville and Clift, bed particles become sticky and exhibit a higher form of inter-particle force of attraction in the form of liquid bridge and sintering when a liquid binder is present (Seville & Clift 1984). Increase in the amount of liquid present in the system increases the stickiness of the bed particles to each other causing a change in the fluidisation quality and regime of the bed hence, making the bed more difficult to fluidise (Molerus 1982).

In summary, the hydrodynamics mechanism depends on the presence of a strong inter-particle force of attraction between the particles present in the bed to cause the alteration of the bed fluidisation regime due to an increase in the mean particle size profile of the bed. This effect causes the creation of a hot spot and temperature rise in the bed followed by melting of deposited ash to produce liquid binder for the formation of strong inter-particle liquid bridges and sintering

between the bed particles. It can be concluded that the hydrodynamic mechanism can easily occur in a BFB during lump coal combustion. However, this mechanism cannot be solely responsible for sintering and agglomerate formation in the system as it depends on other factors such as the presence of a liquid binder in the form of molten ash which is influenced by the chemical composition of the ash and temperature profile in the bed.

2.5.2. Bed Material and Ash Particle Interaction Mechanism

This mechanism attributes sintering and agglomerate formation to the interaction that occurs between the ashes produced during the combustion of coal described in section 2.4.2.2., and the bed material. It has been suggested that the ash produced during combustion acts like a glue and adhere with the bed material particles present in the bed on collision (Schobert 1990). Over the years, many researchers have studied this interaction and have proposed various formation routes for this mechanism. These various routes have been classified by Mac an Bhaird and colleagues into two pathways which are melt induced and coating induced (Mac an Bhaird et al. 2014).

The melting induced pathway can be attributed to the formation of liquid molten ash particles which adheres up on to the surface of the bed material particles on collision (Mac an Bhaird et al. 2014). This pathway can be likened to the transient liquid phase sintering earlier described in section 2.5. The fusing together of the sand bed particles is induced by the presence of the liquid molten ash but as the sintering and agglomerate formation process progresses, the molten liquid ash becomes absent causing the process to be completed in the solid state. Melting induced pathway can be characterised by its low viscosity and the absence of silica in the neck region of the linked bridge formed between the bed material particles (Teixeira et al. 2012).

Coating induced pathway has been identified as the most common type observed in industrial-scale FB systems (Bartels et al. 2008). This agglomeration pathway has been associated with the interaction that occurs between the gas phase inorganic compounds present in the deposited ash and the surface of bed material particles in the BFB bed (Visser 1989). Continuous deposition of ash onto the surface of the bed material particles has been identified to promote the formation of a neck link between ash coated bed material particles upon collision with each other, which initiates sintering and agglomeration formation. Coating induced pathway can be characterised by its high viscosity and the presence of silica in the neck region of the linked bridge formed between the bed material particles (Teixeira et al. 2012).

Ohman and colleagues proposed a three-step mechanism route for the coating induced pathway which is shown in Figure 2-7 (Ohman et al. 2000) and are described as follows: Step 1: Deposition of ash on the bed material particles via a combination of attachment of small particles to the surface of the bed material particles, condensation of gaseous alkali species on the bed material particles and chemical reaction of the gaseous alkali on the surface of the bed material particles. Step 2: Continuous deposition of ash on the surface of the bed material particles to create a homogenised layer strengthened by sintering. Step 3: Melting behaviour of the homogeneous ash layer formed on the surface of bed material particles, which is responsible for the strong inter-particle adhesive forces causing sintering and agglomerate formation. The presence of this strong inter-particle adhesive force identified to be present in the coating induced pathway, which was also described earlier as part of the hydrodynamic mechanism in section 2.5.1, shows the relationship between these two mechanisms and their dependency on each other for sintering and agglomerate formation.

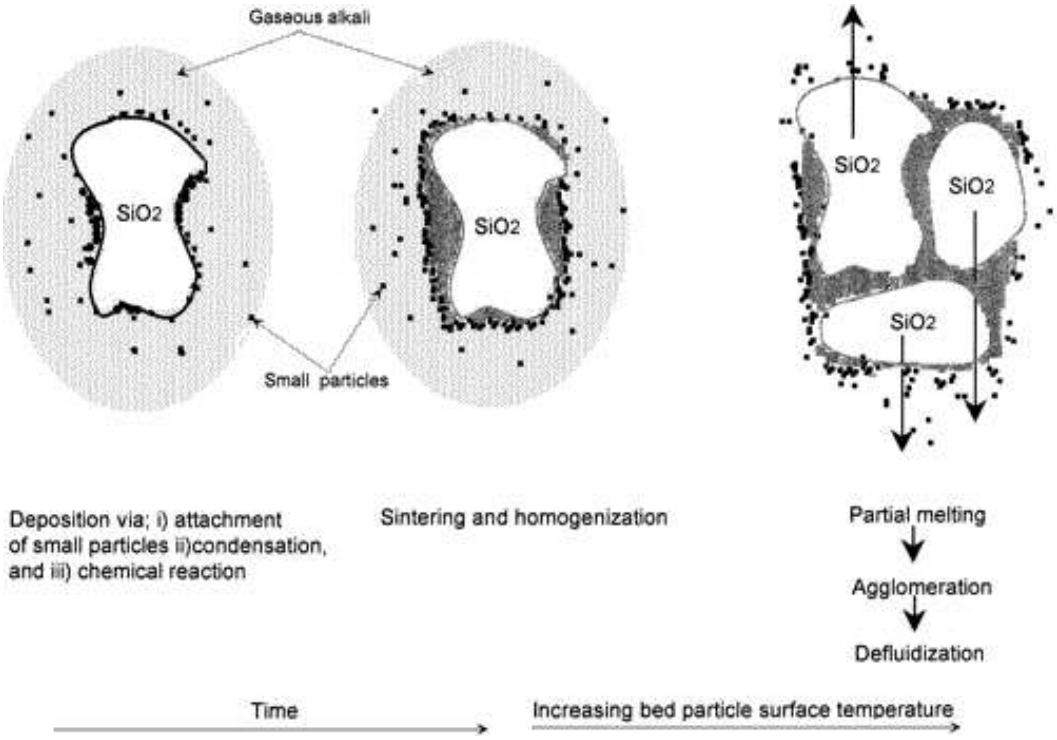

Figure 2-7: Schematic illustration of the coating induced sintering and agglomeration formation pathway for bed material and particle interaction mechanism (Ohman et al. 2000)

Both the melting induced and coating induced pathways are temperature dependent for sintering process, which precedes agglomerate formation. As discussed earlier in section 2.4.2.1, a temperature difference of up to 200°C can be measured between the combusting char particles and the bed temperature in the BFB (Park 1989). It is therefore possible to observe hot spots in the regions where the char particles are burning across the bed and have localised elevated temperature high enough to initiate ash melting or softening. This view can be supported by the findings of Lin and colleagues (Lin et al. 2003) who associated the high combustion temperature of char particles as the source of elevated temperature which initiates ash sintering.

Their views are further supported by the findings of Chirone and colleagues while studying the mechanism and prevention of agglomeration in a BFB (Chirone et al. 2006). It is also important to mention that ash with a high IDT sometimes sinter and form agglomerate at lower temperature because ash soften and

agglomeration have been reported to occur at temperature below the IDT (Llorente & Garcia 2005). The other possible source of temperature build up in the BFB system to initiate the ash melting process is described in section 2.5.1 caused by the change in the fluidisation regime due to the lump coal size introduced into the BFB system and deposition of mud/shale stones into the bed later discussed in section 2.5.4.

In summary, both melting and coating induced forms of bed material and ash particles interaction mechanisms can occur in a BFB during lump coal combustion. The occurrence of this mechanism however depends on the presence and deposition of ash in the bed and on the surface of the bed material particles, chemical reaction of the gaseous alkali on the surface of the bed material particles, high elevated temperature above the AFT of the ash produced from the combustion process to initiate ash melting, a form of collision between the ash and the bed material particles and the presence of strong inter-particle adhesive forces existing as liquid bridge which is a hydrodynamic mechanism parameter.

2.5.3. Chemical Reaction Mechanism

It is a generally accepted opinion that sintering and agglomerate formation in a BFB is mainly caused by the melting of ash produced from the combustion process (Ohman et al. 2000). Ash melting can be attributed to the high temperature build-up in the BFB above the AFT of the ash produced during the combustion process as described in section 2.5.1 and 2.5.2 or due to the formation of low melting temperature ash eutectics (alkali-silicate salts) which melts under standard combustion temperature of between 750 – 950°C. The formation of these low temperature melting ash eutectics, which interacts and adheres to the surface of the bed material particle initiating sintering and

agglomerate formation has been identified to be influenced by the chemical composition of the fuel. These chemical constituent reacts together and undergoes a series of chemical reactions in gaseous and solid states during the combustion and gasification process (Bartels et al. 2008).

From various studies on the chemical reaction mechanism for sintering and agglomerate formation during the combustion and gasification of coal in a FB system, the presence of different alkali and alkali earth elements in the ash has been associated with the making of low temperature melting ash eutectics (Olanders & Steenari 1995). Some of the alkali and alkali earth elements that have been identified to be responsible for the formation of this low temperature melting ash eutectics includes sodium, calcium, magnesium and sulphur discovered during the combustion and gasification of lignite coal with high sodium content (Kyi & Chadwick 1999; Vuthaluru et al. 2000; Vassileva & Vassilev 2005; Dahlin et al. 2009; McCullough et al. 2011); iron, calcium and magnesium identified during the combustion of lignite and sub-bituminous coals in a fixed bed furnace (Namkung et al. 2015); and iron and aluminium recognised during the gasification of high ash Chinese (Wu et al. 2009) and Indian (Datta et al. 2015) coals respectively.

High amount of each identified alkali and alkali earth elements were found to be present in their oxides states in the inter-particle liquid bridge formed between the bed material particles and in the coating layer deposited on the bed material particle surface. The liquid bridges were found to be formed from molten alkali–silicate salts of sodium, calcium, magnesium, iron and /or aluminium oxides depending on the chemical composition of the fuel. Different alkali–silicate salt have different melting temperature and the type of alkali–silicate formed is dependent on the percentage composition of the alkali elements present in the system (Schairer & Yagi 1952). The coating layer on the surface of the bed

material particle has been attributed to the chemical reaction that occurs between the silica present in the bed material particles and the alkali and alkaline elements present in the fuel. The use of silica sand or bed material containing high composition of silica has been identified in some literatures as a bad choice of bed material during the combustion or gasification of high alkali fuel in a FBC (Ergudenler & Ghaly 1993; Grubor et al. 1995). This is because silica has a high alkali absorbing tendencies to create a low-melting surface due to the fluxing action of alkalis which promotes ash deposition and condensation of gaseous alkali species to form a coating layer (van der Drift & Olsen 1999).

In summary, chemical reaction mechanism has been identified to be responsible for both the chemical reaction that occurs between the chemical constituent of the fuel to form a low melting temperature ash eutectic and also the reaction between the silica content of the bed material and the gaseous alkali species of the fuel released during the combustion or gasification process. This mechanism can easily occur during the combustion of lump coal in a BFB provided that alkali and alkaline elements are present in the fuel and/or silica is present in the bed material particles.

2.5.4. Summary and Commentary on Sintering and Agglomerate Formation Mechanisms

From all the from literature findings on sintering and agglomerate formation mechanism detailed in section 2.5.1 to 2.5.3, it is proposed by the author of this work that the combination of hydrodynamic, chemical reaction, and bed material and ash interaction mechanisms is responsible for sintering and agglomerate formation during lump coal combustion in a BFB system. The literature survey shows the inter-relationship, inter-dependency and reliance of the discussed mechanisms on each other during sintering and agglomeration formation in a

BFB system. Hence, a proposed pathway for sintering and agglomerate formation in a BFB system during lump coal combustion based on all the mechanisms integrated together is presented in Figure 2-8.

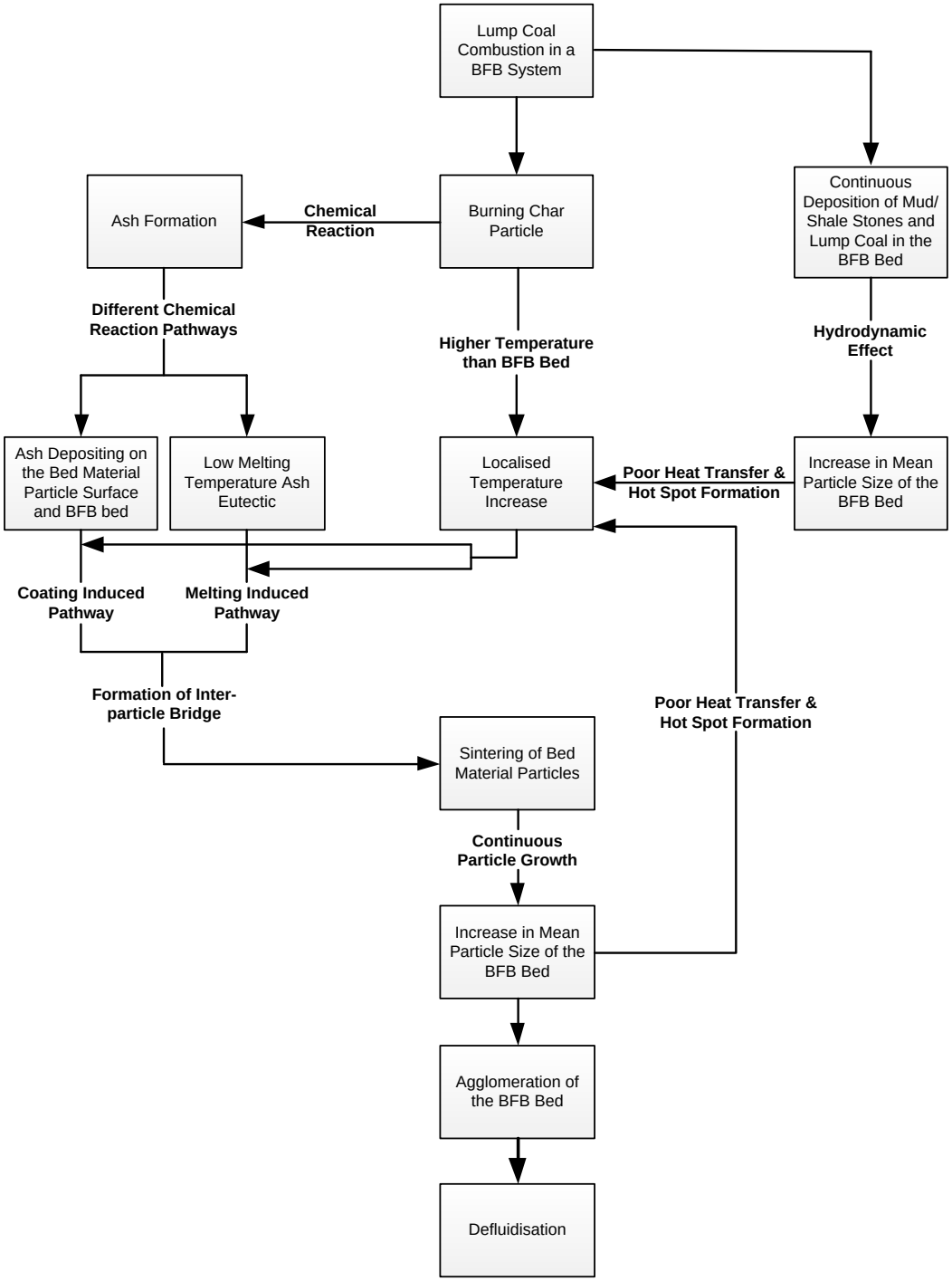

Figure 2-8: Proposed reaction pathway for sintering and agglomeration formation in a BFB system without ash removal during combustion of lump coal (proposed by author of this work)

From the proposed sintering and agglomerate formation pathway presented in Figure 2-8, the formation of ash and production of low melting temperature ash eutectic from the combustion process have been identified as a chemical reaction mechanism step. The deposition of ash on the surface of the bed material particles is described by both the bed material and ash interaction, and the chemical reaction mechanisms. The bed material and ash particle interaction mechanism is suggested to be responsible for the initial deposition of ash on the surface of the bed while the adhesion (binding) of the ash onto the surface of the bed material is influenced by the chemical reaction that occurs between the silica sand in the bed material and the gaseous phase alkali and alkaline elements present in the fuel ash. The interaction that occurs between the bed material particles and molten low temperature ash eutectic has been identified as a bed material and ash particle interaction mechanism. It is a proven fact from the literature that the formation of a liquid binder from the ash present in the BFB system for both the coating induced and melting induced pathway, which is responsible for the liquid bridge formation, is a temperature influenced condition (Ohman et al. 2000).

The temperature needed to induce this full or partial melt has been attributed to be caused by the high temperature of the burning char particles in the bed as discussed in section 2.4.2.1 and/or the continuous deposition of lump coal and mud/shale stone in the bed which changes the hydrodynamics of the bed as earlier discussed in section 2.5.1. However, it was observed from the literature survey that scholars who have earlier studied sintering and agglomerate formation mechanisms have not reported the effect of continuous deposition of mud/shale stone in the bed of a BFB system. During combustion of lump coal, deposition of mud/shale stones occurs in the bed especially when using unwashed coal, which contains high amount of mud/shale stone. Typically in a

pulverised fuel (PF) fired system, the mud/shale stones would be pulverised alongside with the coal during the milling process and be released as ash from the combustion process. In this situation, higher amount of ash and more ash related problem are reported in the PF system.

In BFB systems where the coal has not been pulverised, the mud/shale are fed into to the BFB system with coal as they have the same physical appearance as coal. On combusting the fuel, the coal present in the feed will burn while the mud/shale stone are deposited and remain in the bed in the absence of an ash removal device in the BFB system. The continuous deposition of the stones in the bed causes an increase in the mean bed material particle size and over time a change in the fluidisation regime occurs. This then leads to poor heat transfer across the bed, generation of hot spots and finally high temperature build-up in the bed which can initiate ash melting promoting sintering and agglomerate formation. The mud/shale stones deposited in the bed are usually the same size as the lump coal introduced into the bed. Mud/shale stone can also be deposited from the use of washed coal as the washing process does not remove all the mud/shale stone present in the fuel but only removes 75 - 80% (Fonseca 1995).

The presence of this high temperature promotes the formation of the liquid binder, which causes the formation of strong inter-particle liquid bridge or sintering. Continuous deposition of the ash and formation of more liquid bridge causes further particle growth resulting in poorer heat transfer across the bed and generation of more hot spots and high localised temperature. Continuous operation of the BFB system will cause the sintered bed material to form agglomerate, which will later lead to defluidisation of the BFB system. In conclusion, the applicability of this proposed sintering and agglomerate formation pathway will be studied during the course of this investigation in order to determine its relevance to lump coal combustion in a BFB system.

2.6. Detection of Sintering and Agglomeration

In order to be able to control sintering and agglomerate formation in a FB system, a suitable and effective tool is needed to detect its formation in the early stages. To achieve this, a number of methods have been identified and proposed by scholars. These methods have been broadly categorised into two groups' namely ex-situ fly ash characterisation and process measurement detection approach. Discussion in this section covers detailed description of the methods identified under each group, which is applicable to FB systems.

2.6.1. Ex-situ Fuel Ash Characterisation

As earlier identified in section 2.5, sintering and agglomerate formation in a FB system is an ash related problem formed from the interaction and chemical reaction that occurs between the inorganic components of the ash and that of the bed material present in the FB system. It is assumed that understanding the characteristic behaviour of the fuel ash can help to determine the sintering and agglomeration tendency of the fuel. Hence, the rationale behind the ex-situ fly ash measurement approach. The ex-situ fly ash measurements approach is associated with the use of different analytical techniques to study the sintering and agglomerate formation tendencies of the fuel ash outside the actual FB combustion or gasification environment.

One of the ex-situ fly ash measurement approaches is the standard ash fusion temperature (AFT) test as determined according to ASTM-D1857 or BS-ISO 540:2008 earlier described in section 2.2.2. This AFT technique, which was designed to determine the slagging tendencies of coal based on the visual observation of the deformation of the ash cone during heat treatment, has been proposed to predict sintering and agglomerate formation (Skrifvars et al. 1999; Llorente & Garcia 2005). However, the accuracy of this test to correctly

determine the ash deformation temperature and relating it to sintering and agglomerate prediction has been widely argued. According to Huffman and colleagues during their investigation on high temperature behaviour of coal ash in reducing and oxidising environment, it was reported that the initial deformation of coal ash occurred at temperatures between 200 and 400°C lower than the one visually observed during AFT test (Huffman et al. 1981). This argument has been supported by other researchers who reported that the measured temperature from the AFT test is higher than those measured from other techniques (van der Drift & Olsen 1999; Skrifvars et al. 1999). Hence it was concluded by Llorente and Garcia during their investigation that the AFT is not completely suitable to predict sintering and agglomerate formation due to this inconsistencies (Llorente & Garcia 2005).

Another method proposed for predicting sintering and agglomerate formation is the empirical correlation between standard fusion temperature and inorganic composition of the fuel ash. This is done by representing the inorganic composition of the fuel ash in a phase diagram based on their mass composition to determine their fusion temperature. This method has been identified to be very reliable in predicting the melting behaviour of coal ash melting temperatures (Wall et al. 1996). However, the suitability of this method to correctly predict sintering and agglomerate formation still remains questionable due to the ambiguous assumption of predicting the eutectic point of ash based on only two or three inorganic component of the ash which is represented on the phase diagram and ignoring other inorganic components present. Also the application of this method is limited to the available resource in literature on the phase equilibria between the element/elemental oxides of interest.

Scanning electron microscopy (SEM) is another common technique which has been used to study sintering and agglomerate formation in various high

temperature processes such as combustion and gasification processes (Öhman & Nordin 2000; Teixeira et al. 2012; Mac an Bhaird et al. 2014). Some of these researcher have focussed the use of SEM study sintering and agglomerate formation in low rank coal (Vassilev et al. 2005; Vassileva & Vassilev 2005; Vassileva & Vassilev 2006) and biomass (Bartels et al. 2008; Chirone et al. 2006; Brus et al. 2005). The results which was obtained from their investigations shows that SEM imaging technique helps in creating a visual representation of the interaction between the bed particles and the binders present in an agglomerated particle. However, this technique has only being used to study agglomerate formed from sintering and agglomerate formation mechanism.

Energy dispersed x-ray (EDX) which is an elemental or chemical characterisation technique has also being used in combination with SEM to study sintering and agglomerate formation by various researchers (Wu et al. 2009; Coda Zabetta et al. 2013; Zhong et al. 2013; Luan et al. 2014). This technique was used to identify and semi quantify the elements present in the particles and binder of an agglomerated bed sample. The ability to identify the elemental composition of an agglomerated bed sample helps in understanding its formation mechanism. The major drawback for applying this technique is that the quantitative data obtained from this analysis are semi quantitative and does not account for the bulk sample composition of the agglomerated sample. Also this analytical technique can only be applied to study the chemistry of the aggregate formed and not to detect sintering and agglomerate formation.

X-ray fluorescence (XRF) is one of the best quantitative and qualitative analytical techniques available to determine the elemental and elemental oxide constituent of a inorganic sample ranging from oxygen through to uranium at major, minor and trace (ppm) levels (Shackley 2011). XRF has been used for sintering and agglomeration investigation during the gasification of lignite coal (McCullough et

al. 2011) and works by bombarding the prepared sample being analysed with high energy x-ray causing the ejection of electrons from the inner shells (typically K and L) surrounding the nucleus of the atoms present in the sample. Even though XRF analysis is one of the best analytical techniques available, it has not been universally utilised for sintering agglomerate formation by researchers into this topic area when compared to SEM and EDX

Other ex-situ methods which have been investigated and proposed for sintering and agglomeration detecting in biomass applications but have not be studied for coal applications includes: the combination of differential thermal analysis (DTA) with thermo gravimetric analysis (TGA) to characterise the melting and volatilisation behaviour of the ash (van der Drift & Olsen 1999), and the correlation of the mass ratio of the alkaline earth oxides to alkaline oxides present in the ash which is expressed by equation 2.1 (Llorente & Garcia 2005).

$$I = \frac{CaO + MgO}{K_2O + Na_2O} \tag{2.1}$$

The suitability of many of the techniques under this approach for accurately predicting or detecting sintering and agglomerate formation is uncertain. This is because the ex-situ approach is tested outside the FB system, which ignores the reactions and interactions that occurs between the fuel ash and the bed material as well as the effect of the operating conditions on the system during the combustion or gasification process. However, based on the success report of SEM, EDX and XRF analytical techniques by previous researchers for sintering and agglomerate formation studies, these techniques will be implemented to study sintering and agglomerate formation during this investigation the lack of suitability of this approach for sintering and agglomeration detection, it was not further investigated during the course of this study.

2.6.2. Process Measurements Approach

The process measurement approach can be described as an on-line or continuous detection system, which is setup to measure one or more process variable during the operation of the FB system for combustion or gasification purposes. The most commonly measured process variables in a FB system are pressure, temperature, acoustic (sound) emission and gas-phase alkali component, which are used as the basis for this type of detection system. The process measurement approach is highly suitable for industrial applications as opposed to the ex-situ fly ash measurement characterisation because it takes into consideration the whole bed interaction and hydrodynamic effects that occurs in a fluidisation environment in the FB system during combustion or gasification condition.

2.6.2.1. Pressure Measurement

Differential and absolute pressures are the most frequently measured and analysed process variable in industrial FB systems, which are used to monitor the fluidisation quality and hydrodynamics of the bed. With the relationship between the pressure measurements and the fluidisation quality of the bed, the use of this measured process variable has been proposed for detecting sintering and agglomerate formation. In order to do this various scholars have identified different techniques of analysing the pressure parameter measurement for accurate sintering and agglomerate formation detection. This technique can be broadly classified into two methods namely linear, and nonlinear measurements.

Linear measurement method is setup to measures the average pressure drop across the vertical section of the FB system, which provides detailed information on the fluidisation properties of the FB system such as bed height and density. The linear vertical pressure measurement method has been investigated by a

number of scholars (Kai & Furusaki 1987; Fuller et al. 1993; Daw et al. 1998). Kai and Furusaki proposed the application of average deviation of differential pressure fluctuation technique which was determined by applying standard deviation and variance to the vertical pressure measurements taken during their studies on methanation of CO_2 and fluidisation quality in a FB system (Kai & Furusaki 1987). The differential pressure during their investigation was measured between the top of the column and 5cm above the nozzle plate at a sampling frequency of 100Hz. The bubble size of the airflow was also measured using an optical probe. It was reported from their investigation that a correlation was observed between standard deviations of the different pressure fluctuations and fluidisation quality. However, it was also observed that this correlation was strongly influenced by fluidisation velocity.

Other proposed techniques under the linear measurement method includes variance of high frequency (100Hz) pressure fluctuations proposed during FB combustion of pine seed shell (Chirone et al. 2006); fluidisation quality analyser technology measuring high frequency pressure (>30Hz) across the FB system connected to a buffer amplifier, low pass filter, differentiator, rectifier and a PID controller (Daw & Hawk 1995); and principal component analysis of three or more pressure differential measurement across the FB system (Fuller et al. 1993).

Non-linear pressure measurement method on the other hand has been developed based on state-space projection of the dynamics in a FB system. This in essence means that the dynamic state of a FB system at a particular time can be determined by projecting all state variables of the system into a multi-dimensional space model to generate a collection of successive dynamic state during its evolution in time. This collection of successive dynamic state can be described as an attractor, which is a characteristic measure of the dynamic state

of the FB system. With just one variable such as local pressure of the FB system, the dynamic state of the FB system can be reconstructed using time delay coordinates (Takens 1981). Some of the techniques which have been proposed under the state-space projection theory for sintering and agglomeration detection are bin method (Fuller et al. 1993), symbol statistics (Daw et al. 1998) and attractor comparison method (van Ommen et al. 2000).

Another proposed theory under the non-linear pressure measurement method is the statistical distance theory. This approach depends on using statistical models to determine the distance between the probability distribution of a reference pressure signal and the real time pressure measurement in the FB system. Some of the techniques proposed under the statistical theory includes Kullback-Leibler distribution distance (Gheorghiu et al. 2004) and the Kolmogorov–Smirnov statistic (Bartels et al. 2010a). Both techniques have been claimed to be suitable for early sintering and agglomerate formation detection. It has also been reported that, the Kolmogorov-Smirnov distribution distance technique is not sensitive to fluctuating fluidisation velocities while the effect of fluctuating fluidisation velocities on Kullback-Leibler distribution is unknown.

In summary, the proposed linear analysis method based on standard deviation and variance of pressure differential fluctuations can be used to detect sintering and agglomeration formation. However a major drawback, which might affect their applicability in industrial scale FB system is that they are very sensitive to fluidisation velocities, which fluctuate frequently in industrial system. Non-linear analysis methods have received great attentions in reviewed publication as a suitable sintering and agglomerate formation detection approach but the implementation of this method for industrial application remains questionable due to the difficulty of obtaining accurate and reproducible pressure data from the industrial FB system in order to generate the state space projection correlation or

probability distribution reference pressure signal points. The linear analysis method will be further investigated as part of this study as given in section 4.5 and 6.3.1.

2.6.2.2. Temperature Measurement

It is a well know phenomena that one of the products released from the combustion or gasification of solid fuel irrespective of the conversion technology is heat (Lowry 1945; Schobert 1987). This released heat is usually measured as temperature which starts off as a localised property but with continuous mixing in a well fluidised FB system especially BFB, the localised temperature develops into a homogenous property by becoming evenly spread across the bed (Basu 2006). From earlier discussion on sintering and agglomerate formation mechanism given in section 2.5, temperature was identified as an important parameter required to initiate sintering and agglomerate formation in an ash environment especially when localised (absence of well mixing or fluidisation). This dependency of sintering and agglomerate formation on temperature in an ash environment supports the rationale of using temperature measurement as a sintering detection tool. However, the positioning of temperature measurement in the FB system might be critical to the suitability of this approach for sintering and agglomerate formation detection especially in industrial applications.

From various research into the use of temperature measurement as a sintering and agglomerate formation detection tool, two methods for measuring temperature across the FB system has been proposed. The first proposed method is a radial bed temperature difference measurement technique identified during the investigation of anticipated defluidisation of caking coal in a laboratory scale electrically wall heated FB system (Lau & Whalley 1981). From this study the proposed detection setup is based on measuring the temperature difference

between two radially separated points (centre of the bed and wall of the FB vessel) in the FB system using a differential thermocouple (DT). It was reported that the initial differential temperature measured between the two radial points was relatively low in the order of 2 – 4°C until a point of defluidisation when this rapidly increased. The reason for this increase was attributed to the slow down effect of the bed circulation caused by sticky bed material adhering together which causes the thermal boundary surface to shift away from the wall of the FB system towards the centre of the bed (Lau & Whalley 1981).

However, the suitability of this method as an effective tool in an industrially operated FB system remains questionable due some limitations. Firstly, during solid fuel combustion or gasification, the heat generated is not directly localised at the vessel walls but internally at the fuel particle combustion or gasification zone. Hence, the mechanism for radial heat transfer is not applicable in this situation. Secondly, industrially operated FB systems used for combustion or gasification purposes always have a huge diameter and the suggestion of using the temperature measured between two radial points as an indicator of sintering and agglomerate formation does not properly represent the temperature profile of the FB system. Thirdly, coal injection into an industrially operated FB system is done using screw feeder or coal flicker system to ensure proper coal distribution across the large bed surface; hence radial heat transfer mechanism again becomes not applicable. For these reasons, the radial method theory has been identified not to be valid and might not work in practice in an industrially operated FB system therefore this method will not be further investigated in this study.

The second proposed method is the absolute temperature variance and vertical temperature measurement across the FB system. This method was proposed by Scala and Chirone during their investigation on characterisation and early detection of bed agglomeration during fluidised bed combustion of olive husk in

an electrically wall heat laboratory scale BFB system (Scala & Chirone 2006). During their investigation, operating conditions in the laboratory scale BFB system were held constant until defluidisation occurred. It was observed from their investigation that the variance of the temperature measured by the upper thermocouple probe decreased as it approaches the initial defluidisation point as well as an increase in the normalised relative temperature difference.

The temperature variance measured between two vertical temperature points is expected to decrease as the defluidisation point is reached and the relative temperature difference is also expected to increase due to sintering and agglomerate formation as they are both influenced by the quality of fluidisation or mixing occurring in the FB system (Hamidi et al. 2015) . The findings from this investigation looks promising but the practicability of this method in an industrial scale FBC system remains questionable as the authors did not report the effect flue gas recycle stream, bed mass and fluidisation velocity have on the applicability of this method. This method will however be further investigated during the course of this investigation.

In summary, the temperature uniformity in the FB system is closely related to the fluidization quality. A decrease in the bed fluidity causes the temperature difference between different locations of the bed to increases while the variance in local temperatures decreases at the same time making it an important tool for detecting sintering and agglomerate formation. The absolute temperature variance and vertical temperature difference method seems more practically applicable as a sintering and agglomerate formation detecting tool than the radial temperature difference method in industrial scale FBC system. The absolute temperature variance and vertical temperature difference method will be further investigated as part of this study as given in section 4.4 and 6.3.1.

2.6.2.3. Acoustics Emission

This method involves measuring broad ranges of frequencies emitted from the FB system at various operating conditions during combustion or gasification which are not necessarily confined to human audible range. During solid fuel combustion or gasification, various beat patterns and harmonics are generated when particles present in the FB system collides with each other. It has been identified that various particle size and shapes emits various harmonics and beat patterns on collision (Hamidi et al. 2015). From research into the use of acoustics emission for the detection of sintering and agglomerate formation by many scholars, various characteristics of acoustics have been identified to be useful and proposed as methods.

The first proposed method is the correlation between beat patterns and particle size, reciprocal to frequency. This method was proposed by Leach and colleagues while investigating the effect of particle size and shape on acoustics emission (Leach et al. 1977; Leach et al. 1978). From their investigations, a characteristic frequency correlation was drawn between particle size and beat pattern using Gaussian size distribution to categorise the distribution of sound frequencies emitted from various particle size upon collision (Leach et al. 1978).

The authors reported that a linear correlation exist between the beat pattern and particle size and claimed that shape and width of a narrow Gaussian size distribution can be characterised from the sound signal emitted upon collision. The suitability of this method for sintering and agglomerate formation detection in a FB system still remains uncertain as various sounds of similar frequencies within the characterised limit might be generated from other machineries within the facility which might affect the reliability of this method.

The second proposed method is based on measuring the amplitude signal of the acoustic emission. This was proposed by Zukowski during the combustion of gaseous fuel in a laboratory scale bubbling fluidised bed (Zukowski 1999). The proposed method required the use of microphones, which were placed outside the FB system to measure sound waves within the audible range. It was observed from this investigation that different operating temperature regime could be identified by the mean intensity of the acoustic signal measured. It was also reported that the amplitude of the signals generated at low temperature up to 850°C were higher due to gas explosion taking place, but at higher temperatures above 950°C, the amplitude of the signal measured became relatively low and smooth. Although this study was not done to investigate sintering and agglomerate formation detection during solid fuel combustion or gasification, it however demonstrates that clear acoustic signals contain valuable information about the bubbling behaviour in a FB system.

The third proposed method is based on using what is described as chaos and energy fraction analyses to characterise acoustic emission signals sampled by an accelerometer. This method was proposed by Wang and colleagues who identified this approach while studying agglomeration detection by acoustics emission sensors in FB system during the production of polyolefin (Wang et al. 2009). The setup for this method requires division of the acquired acoustic emission signals into micro-, meso- and macroscales by wavelet transform and on the basis of the energy of mesoscale fraction. It was reported that from this analysis a coefficient of malfunction could be defined based on Kolmogorov entropy and correlation to obtain and measure the unpredictability of the signals, which is sensitive to adhering particles on collision. The authors claimed that agglomerated particle movement in the FB system and their particle size can be predicted from the empirical model and also reported that successful tests have

been conducted both in the laboratory and industrial scale FB system. However, the suitability of this method for sintering and agglomerate formation detection during solid fuel combustion or gasification is unknown.

In summary, the use of acoustic emission approach has been employed under various conditions to characterise the fluidisation regime and agglomeration detection in FBC systems except during solid fuel combustion or gasification. Findings reported by various researchers into this approach shows a clear relationship between particle size and acoustic patterns emitted when they collide with each other but care needs to be taken when selecting measuring equipment and location for this purpose due to the fact that other acoustic source can affect the signal recorded. The prospect of implementing acoustic emission detection approach during solid fuel combustion in a FB system sounds like a viable option. However, more studies need to be done to support this view.

2.6.2.4. Gas Phase Alkali Measurement

Measuring the gas-phase alkali component present in the gas stream from the FB system is another proposed approach, which can be used for sintering and agglomerate formation detection. Under this approach, two methods have been suggested which are plasma exited atomic resonance line spectroscopy (PEARLS) and excimer laser induced fragmentation fluorescence (ELIF). PEARLS method requires the measurement of specific gas phase alkali components present in the flue gas stream of the FB system using atomic absorption spectroscopy (Hayrinen et al. 2004). The setup for this method as described by Hayrinen and colleagues requires a continuous sampling of gas phase components in the flue gas stream via a horizontal sampling line. The sample gas is then mixed with a nitrogen plasma jet to separate the alkali compounds present in the stream before being analysed by atomic absorption

spectroscopy. The PEARLS method was found to be very effective in measuring gaseous alkali present in the flue gas stream however, the focus of their work was not based on using this method for sintering and agglomerate formation detection and therefore the suitability of this method for this purpose remains uncertain.

ELIF method has been used to determine the presence of sodium and potassium in the gas stream of a CFB system during an investigation on the combustion of biomass with coal (Glazer et al. 2005). During this investigation, it was reported that alkali species measured from the co-firing of biomass with coal was lower than expected when compared with values obtained from their mass balance calculation. The authors associated this observation with the formation of alkali-alumina-silicate in the bed which is thermodynamically favoured by the introduction of coal into the biomass combustion system (Glazer et al. 2005). This observation supports the findings of Kyi and colleagues (Kyi & Chadwick 1999), Vuthaluru and colleagues (Vuthaluru et al. 2000), Dahlin and colleagues (Dahlin et al. 2009) and many other researchers who have also identified the deposition of alkali metal on the surface of the bed material during the combustion or gasification of high sodium coal in a FB system. These findings support the argument that the alkali content present in the flue gas stream does not represent the quantity of alkali metals present in the system as some are deposited in the solid state on the bed material and on the walls of the FB system.

In summary, the use of these two methods for measuring the amount of gas phase alkali component present in the gas stream in the FB system has been successfully demonstrated in the laboratory scale setup. However, the suitability of this approach for sintering and agglomerate formation detection in an industrial scale FB system still remains uncertain because the presence of gas alkali

species is not sufficient for indicating sintering and agglomerate formation. Also, this approach only measures the alkali present in the gas phase which does not represent the alkali components present in the FB system as some are deposited on the bed material surface as reported in sintering and agglomerate formation mechanism studies.

2.7. Conclusion and Summary of Findings

The literature survey has helped in identifying the major mechanisms responsible for sintering and agglomerate formation in a FB system during combustion and gasification processes. It was however discovered that the focus of research into this topic area has mainly been on biomass fuel and a small number of reported investigation on low rank coal under combustion and gasification processes. With the increasing interest and heavy reliance on coal as a major source of energy for the foreseeable future and the growing interest of using FB system as a coal conversion technology of choice, more work needs to be done to understand this formation mechanism in other coal types especially bituminous coal which currently supplies the highest amount of energy from coal based on utilisation.

All the sintering mechanisms identified by previous scholars have been associated with liquid phase sintering due to the presence of molten phase ash. However, previous scholars have not reported the existence of solid state sintering which might occur between the bed material particles at high temperatures. It will be beneficial to investigate if the solid state sintering effect occurs in sintering and agglomerate formation during lump coal combustion in a FB system

Many sintering and agglomerate formation detection approaches were also identified to have been proposed in literature but their practical implementation remains uncertain. This is because sintering and agglomeration studies have

been described as a very complex phenomenon, which are different for every system due to the wide variation in fuel chemistry, equipment design and operating conditions. Hence more work is needed to provide more robust understanding on the effect each of these conditions has, not just on detection approach, but also on the formation mechanism.

CHAPTER THREE

PILOT SCALE BUBBLING FLUIDISED BED COMBUSTOR DESIGN

3.1. Introduction

This chapter provides detailed information on the design parameters, principles and considerations implemented in the design of the 30kW lump coal fired PSBFBC for investigating sintering and agglomerate formation. Discussion in this chapter includes predesign decisions; hydrodynamic design parameters and design validation, component and equipment design, control and instrumentation of the PSBFBC.

The process flow diagram of the 154mm I.D., 30kW lump coal fired PSBFBC system designed and built for the investigation of sintering and agglomerate formation is shown in Figure 3-1. The PSBFBC system consists of a bubbling fluidised bed reactor (BFBR), gas-solid cyclone, lump coal screw feeder, fluidising fan, flue gas sampling, flue gas analyser and data logging system. The BFBR is made from stainless steel pipe 312 (ASTM A-312) with a total height of 2000mm divided into three sections namely: plenum chamber, fluidising zone and freeboard zone with a height of 200mm, 750mm and 1050mm respectively. A lump coal feed inlet port is located in the freeboard section at a height of 1200mm from the base of the BFBR. Flue gas and fine solids exit the BFBR via an exit port located on the centreline of the freeboard section at a height of 1880mm from the base of the BFBR into a gas-solid cyclone to separate the

entrained fine particles collected in the cyclone reject container from the flue gas effluent which is continuously sampled and analysed via a sampling port located at the top of the cyclone before it is released into the atmosphere through the exhaust stack.

At the bottom of the BFBR, a 50mm O.D. flexible stainless steel pipe is connected to the plenum chamber to supply the fluidising air into the BFBR in-line with ball valves and a variable area volumetric air flowmeter (range 120 to 1100LPM at 15°C) with a repeatability of ±0.5% of flow on a full scale span (FSS). The fluidising air is supplied by a Fans and Blowers Ltd 2900rpm centrifugal fan (model BM 841) which is powered by an 11kW Brook Crompton IP55 motor and controlled by a Weg technology variable speed drive (model CFM-11). The fan and variable frequency drive operations are controlled remotely using the Super Drive G2 software supplied by Weg.

At start-up, two semi cylindrical Watlow ceramic fibre heaters (VS108A18T-0001R), 203mm ID by 457mm long with electrical rating of 240V - 3900W (total power rating of 7800W) and a maximum operating temperature of 982°C are used to provide the bed temperature required prior to coal injection. The ceramic fibre heaters are wrapped with 50mm thick layer of calcium magnesium silicate thermal insulating sheet with a maximum operating temperature of 1150°C and enclosed in a 3mm thick aluminium sheet casing. In order to minimise heat loss during operation, the outer walls of the BFBR and the gas-solid cyclone are wrapped with 38mm of the same insulating sheet (calcium magnesium silicate) used for the fibre heater and held together by aluminium tape.

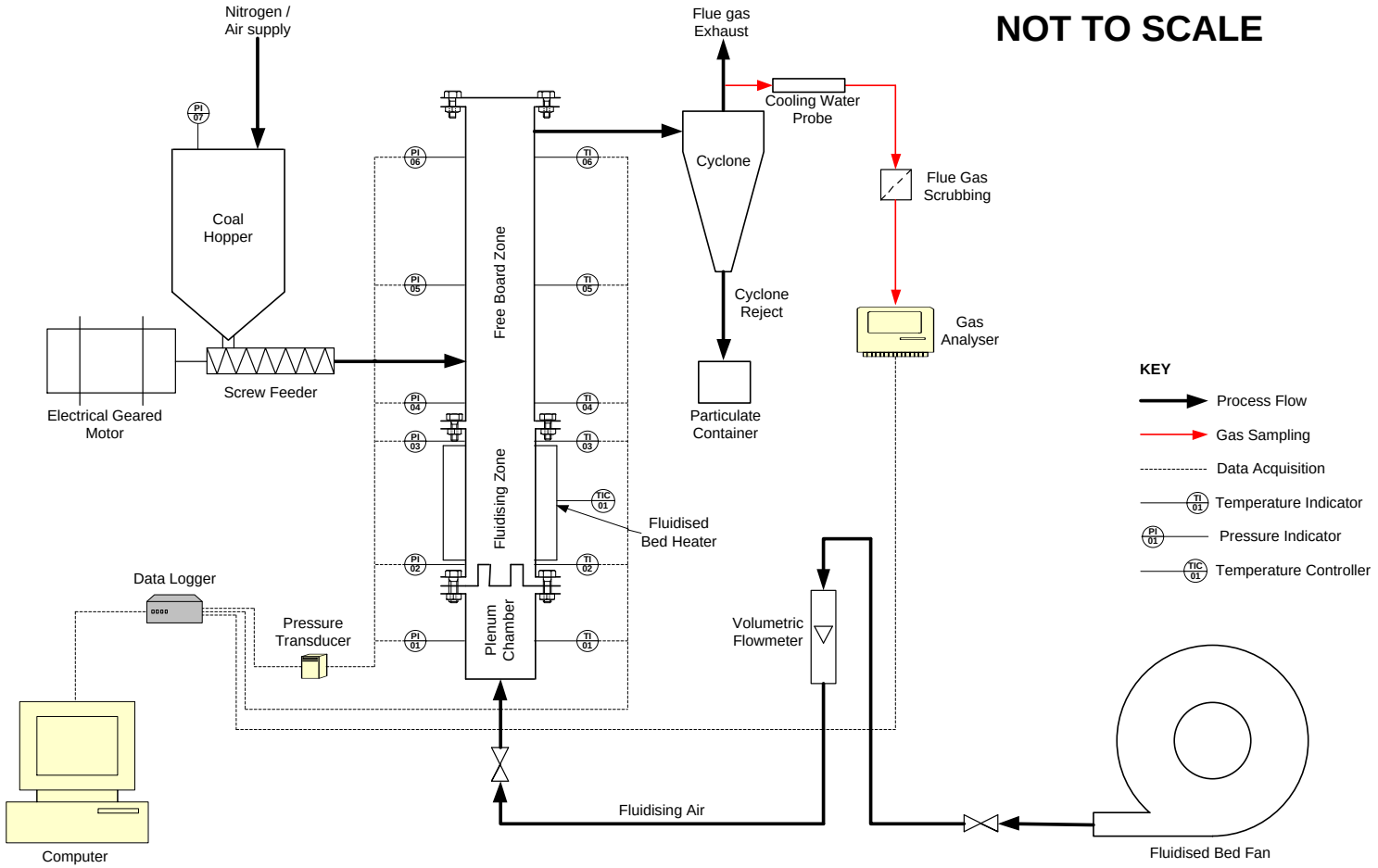

Figure 3-1: Process Flow Diagram of the PSBFBC system

The lump coal feeder system consist of a cylindrical coal hopper (ID: 254mm, height: 500mm) with a holding capacity of up to 17kg of coal, a spiral screw auger (spiral diameter: 44mm, spiral pitch: 40mm, flight height: 17mm) powered by a SEW-EURODRIVE helical geared motor (model R67 DRE80M4/TF) which is controlled by an Allen – Bradley IP20 variable speed drive (model PowerFlex 4 AC Drive) to regulate the coal feeding rate. The hopper has a separate air and nitrogen supply line to create an inert environment and provide backpressure to prevent hot gas flow into the coal feed line of the BFBR coal hopper.

3.2. Pre-Design Decisions

Due to space restriction, design constraints and health and safety issues, the following design decisions were made and agreed with industrial partner (AB Sugar) from the start of the project to serve as a guide for the PSBFBC design:

I. The casing of the BFBR of the PSBFBC shall be made with high-grade 154 mm (nominal I.D size) austenitic stainless steel 312 pipe (ASTM A-312) 40S (wall thickness of 7.11mm). This material has a service temperature of up to 1200°C and the wall thickness of 7.11mm will provide strong resistance against erosion / abrasion of the reactor section caused by fluidising sand, coal particles and shale/mud stones during combustion runs.

II. The length of the BFBR of the PSBFBC shall not exceed 2 metres (2000mm). This shall be divided into three sections namely plenum chamber, fluidising zone and freeboard zone with a height of 200mm, 750mm and 1050mm respectively.

III. The same nozzle type and size (diameter, hole dimension and placement) as those used in the industrial scale FBC shall be used in the

BFBR. To accommodate for the absence of refractory layer at the base of the distribution plate in the BFBR which is typically present in the industrial scale FBC, the length of the nozzle in the BFBR shall be shorten to the height of the nozzle above the refractory in the industrial scale FBC which is 50mm.

IV. Due to health and safety reasons, electrical heaters shall be used for start-up in the BFBR section of the PSBFBC as opposed to light fuel oil (LFO) used in the industrial scale FBC based at AB Sugar. The decision was made to use two Watlow semi cylindrical ceramic fibre heaters (VS108A18T-0001R), 203mm I.D. by 457mm long with electrical rating of 240V - 3900W (total power rating of 7800W).

V. The coal particle size to be used in the PSBFBC shall be 10 - 19mm as opposed to 12 - 25mm used in the industrial scale FBC based at AB Sugar due to lump coal feeder design constraints for a pilot-scale system.

VI. The same Garside 14/25 sand bed material used in the industrial scale FBC shall be used in the BFBR.

VII. The PSBFBC shall be operated at similar conditions (temperature, fluidising velocity and oxygen concentration in the flue gas stream) as the industrial scale FBC. However, the operating time scale shall be a maximum of 10 hours per day as opposed to 24/7 operating setup in the industrial FBC.

3.3. Hydrodynamic Design Parameters

During fluidisation, a hydrodynamic gas-solid interaction occurs in the system causing a transformation in the behaviour of the fine solid to act in a fluid like state. This gas-solid interaction affects the environmental and operating

characteristics of the FBC and also serves as a differentiating factor between various types of FBC. To ensure that the BFBR gas-solid behaviour corresponds with the expectation of a bubbling fluidised system, basic hydrodynamic parameters which affects this interaction needs to be determined and used as design specification for the BFBR design. The hydrodynamic design parameter route used for the PSBFBC design is detailed in Figure 3-2.

3.3.1. Fluidisation Velocity

3.3.1.1. Minimum Fluidisation Velocity

The minimum fluidisation velocity (u_{mf}) used as the basis for the BFBR design was determined using equation 3.1 (Richardson et al. 2002):

$$u_{mf} = \left(\frac{\mu}{d_s \rho_g}\right) Re_{mf} \tag{3.1}$$

where μ is the fluidising air viscosity, ρ_g is the fluidising air density, d_s is the mean particle diameter of the fluidised bed sand and Re_{mf} is the particle Reynolds number at minimum fluidisation velocity defined by equation 3.4. The fluidising air viscosity (μ) and density (ρ_g) are temperature dependent and are expected to change at elevated temperatures between the start-up (ambient) condition and combustion (elevated) condition (900°C). Hence this change needs to be accounted for.

Fluidising air viscosity

The fluidising air viscosity at elevated temperature was determined using a power-law viscosity relationship (ANSYS. 2006) given in equation 3.2.

$$\mu = \mu_{amb}\left[\frac{(T + 273)}{(T_{amb} + 273)}\right]^n \tag{3.2}$$

where μ is the fluidising air viscosity at temperature T, μ_{amb} is the fluidising air viscosity at ambient temperature T_{amb} and n is the power factor.

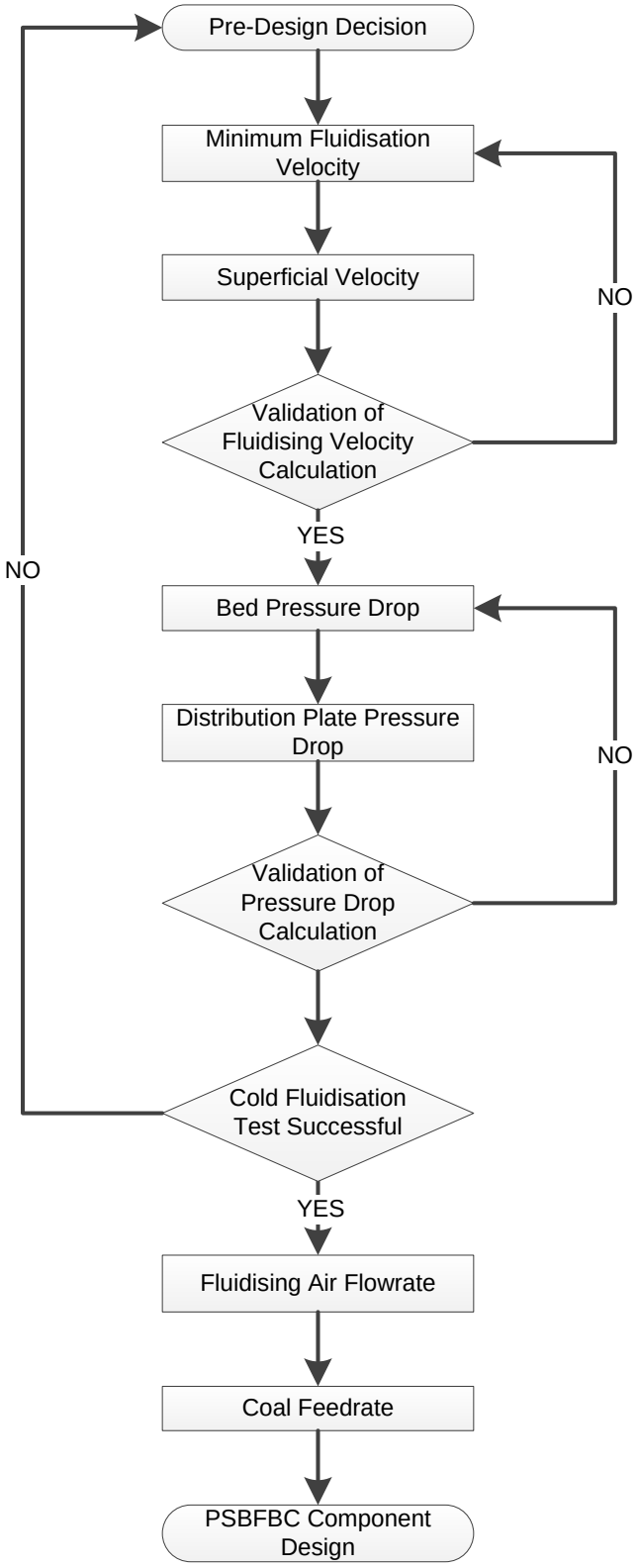

Figure 3-2: PSBFBC hydrodynamic design parameter process

Fluidising air density

The fluidising air density at elevated temperature was calculated using an ideal gas relationship (Sánchez-Prieto et al. 2014) given in equation 3.3.

$$\rho_g = \rho_{g,amb}\left[\frac{(T_{amb}+273)}{(T+273)}\right] \quad (3.3)$$

where ρ_g is the fluidising air density at temperature T, $\rho_{g,amb}$ is the fluidising air density at ambient temperature T_{amb}.

Reynolds number

Reynolds number at minimum fluidisation velocity (Re_{mf}) given as part of equation 3.1 was determined using Wen and Yu equation (Wen & Yu 1966) given in equation 3.4. Galileo's number (Ga) which is a function of Reynolds number was determined using equation 3.5 (Richardson et al. 2002) where ρ_s is particle density of the bed material and g is acceleration due to gravity

$$Re_{mf} = \left[(33.7)^2 + 0.0408Ga\right] - 33.7 \quad (3.4)$$

$$Ga = \frac{d_s^3 \rho_g(\rho_s - \rho_g)g}{\mu^2} \quad (3.5)$$

For the purpose of this work, the design parameters for the fluidising velocity calculation are as follows: T_{amb} = 20ºC; μ_{amb} = 1.8 x 10^5 kg/m.s, $\rho_{g,amb}$ = 1.2 kg/m^3, ρ_s = 2650 kg/m^3 , d_s = 0.8 mm, n = 2/3, and g = 9.81 m/s^2

3.3.1.2. Superficial Velocity

Superficial velocity is a function of the minimum fluidisation velocity which has been quantified by various scholars as 5 to 20 times (Holdich 2002), and 5 to 30 times (Levenspiel 1999; Liu 2011a) the minimum fluidisation velocity. For the purpose of the BFBR design in this work, the air superficial velocity has been

specified as 8 times the minimum fluidisation velocity, the same as the specification for the industrial scale FBC based at AB Sugar. This is given in equation 3.6

$$U = 8u_{mf} \quad (3.6)$$

3.3.1.3. Validation of Fluidising Velocity

The calculated minimum fluidisation velocity using equation 3.1 to 3.5 is 0.40m/s at ambient conditions (20°C) and 0.21 m/s at combustion conditions (900°C). On using equation 3.6 the superficial velocity was calculated as 1.68m/s at 900°C. According to Basu, the superficial velocity for a BFB combustion system should be between 1.5 to 2.5m/s (Basu 2006), while Van Loo suggested that this value should be between 1 to 2m/s (Van Loo & Koppejan 2008). It can be seen that the calculated superficial velocity for this case is within the range of the values suggested by both Basu and Van Loo. Hence, the calculated values of 0.21 and 1.68m/s for the minimum and superficial velocities are valid for the BFBR application in the PSBFBC system. The calculated superficial velocity for BFBR was also confirmed to be the same as that for the industrial scale FBC based at AB Sugar.

3.3.2. Pressure Drop

As part of the BFBR design, the theoretical pressure drop (ΔP), which affects the uniformity and stability of fluidisation in the BFBR, needs to be determined. In BFB, the cause of ΔP which influences the uniformity of airflow distribution through all the section of the bed has been attributed to two factors which are bed pressure drop (ΔP_{bed}) and distributor pressure drop (ΔP_{dist}) given by equation 3.7 (Basu 2006).

$$\Delta P_{total} = \Delta P_{bed} + \Delta P_{dist} \quad (3.7)$$

According to Basu, the expected ratio of ΔP_{dist} to ΔP_{bed} should be between 0.15 and 0.3 for a BFBR in order to ensure that a uniform and stable fluidisation is achieved (Basu 2006). The pressure drop across the BFBR is also an important parameter required for fluidised bed fan sizing as the fan, needs to be able to supply a higher pressure than the ΔP across the bed and distribution plate for fluidisation to occur.

3.3.2.1. Bed Pressure Drop

The pressure drop through the BFBR bubbling bed was determined using equation 3.8 (Oka 2010).

$$\Delta P_{bed} = (1-\varepsilon)\rho_s H g \tag{3.8}$$

where H is the expanded bed height at combustion conditions and ε is the bed voidage at combustion conditions. The expanded bed height H was determined using equation 3.9 (Oka 2010)

$$\frac{H_o}{H} = \frac{1-\varepsilon}{1-\varepsilon_o} \tag{3.9}$$

where H_o is the static bed height and ε_o is the bed voidage at static conditions both at ambient conditions. Bed voidage ε at combustion condition was determined using equation 3.10 (Basu 2006) and bed voidage at static condition ε_o was determined using equation 3.11 (Fueyo & Dopazo 1995) where ρ_b is the bulk density of the bed.

$$\varepsilon = \frac{U+1}{U+2} \tag{3.10}$$

$$\varepsilon_o = 1-\frac{\rho_b}{\rho_s} \tag{3.11}$$

3.3.2.2. Distributor Pressure Drop

The distributor pressure drop was determined using the orifice theory given in equation 3.12 (Saberi et al. 1995)

$$\Delta P_{dist} = \frac{\rho_g}{C_D^2}\frac{U_h^2}{2} \quad (3.12)$$

where C_D is the orifice discharge coefficient described and determined using equation 3.13 to 3.15 and U_h is the air superficial velocity in the orifices.

Orifice discharge coefficient

The orifice discharge coefficient, C_D was determined using a correlation given in equation 3.13 which comprises of the sum of discharge coefficient through the perforated plate ($C_{D,plate}$) and discharge coefficient through the orifices ($C_{D,h}$) (Sánchez-Prieto et al. 2014).

$$C_D = \frac{1}{\sqrt{\frac{1}{C_{D,plate}^2} + \frac{1}{C_{D,h}^2}}} \quad (3.13)$$

$C_{D,plate}$ was determined using discharge coefficient equation deduced by Quereshi and Creasy given in equation 3.14 (Qureshi & Creasy 1979) where d_{noz} is the nozzle diameter which accounts for the perforated plate contribution and t_d is the distributor plate thickness.

$$C_{D,plate} = 0.82\left(\frac{t_d}{d_{noz}}\right)^{0.13} \quad (3.14)$$

To determine $C_{D,h}$, a slightly corrected version of equation 3.14 was used given in equation 3.15 as described by Quereshi and Creasy where d_h is the orifice diameter which accounts for the orifice contribution to the distributor pressure drop.

$$C_{D,h} = 0.82\left(\frac{t_d}{d_h}\right)^{0.13} \quad (3.15)$$

Air superficial velocity in the orifice

The air superficial velocity in the orifices U_h was determined using equation 3.16 where N_h is the number of orifice per unit area of the distributor (Saberi et al. 1995; Basu 2006).

$$U_h = \left(\frac{4}{\pi}\right)\left(\frac{1}{N_h\, d_h^2}\right)U \quad (3.16)$$

For the purpose of this work, the design parameters for the pressure drop calculation were measured and are as follow: ρ_b = 1560 kg/m^3 d_{noz} = 0.0275 m, d_h = 0.003 m, t_d = 0.02 m, N_h = 6875 orifice/m^2, and H_o = 0.2m

3.3.2.3. Validation of Pressure Drop

A summary of the calculated pressure drop hydrodynamic parameters using equation 3.7 to 3.16 is shown in Table 3-1. From the calculation summary, it can be seen that the calculated values for the bed voidage "ε", orifice discharge coefficient "C_D", air superficial velocity in the orifice "U_h" and ratio of distributor pressure drop ΔP_{dist} to bed pressure drop ΔP_{bed} are all within the limit specified in various literatures for a BFB system. Hence this validates that the design approach implemented for the BFBR design so far is applicable.

3.3.3. BFBR Prototype Cold Rig Testing

After all hydrodynamic design parameter calculations were completed; a decision was made to build a prototype of the BFBR section of the PSBFBC system using clear polycarbonate material. This enabled the validation of the hydrodynamic design parameters calculated in section 3.3.1 and 3.3.2, and also provided a

visual representation which enhanced the understanding of the fluidisation quality expected in the BFBR at cold conditions. The process flow diagram of the cold visualisation rig setup is shown in Figure 3-3.

Table 3-1: Calculated pressure drop hydrodynamic parameters

Parameters	Calculated Value	Expected	Reference
ε	0.73	0.5 – 0.85	(Basu 2006)
H (m)	0.433	-	-
C_D	0.62	0.60 – 0.80	(Zenz 1981; Sánchez-Prieto et al. 2014)
U_h (m/s)	34.6	$30 > U_h < 90$	(Basu 2006)
ΔP_{dist} (mbar)	5.22	-	-
ΔP_{bed} (mbar)	30.21	-	-
$\frac{\Delta P_{dist}}{\Delta P_{bed}}$	0.17	0.15 – 0.3	(Basu 2006)
		0.15 – 0.4	(Sánchez-Prieto et al. 2014)

The set up matched the design and comprises of a BFBR with an I.D. of 154mm and a total height of 2000mm, which was divided into plenum chamber, fluidising zone and freeboard zone using dimensions specified in the pre-design decisions (see section 3.2). The flanges were cut out of 20mm thick polycarbonate sheet into standard flange size for 154 mm pipes. These were glued to the ends of the cut polycarbonate tube section using high adhesive polycarbonate glue.

A nozzle distribution plate was made using 20mm thick polycarbonate sheet, which was drilled to accommodate four nozzles following the dimensions specified in the nozzle arrangement design for the PSBFBC distribution plate discussed later in section 3.6.2. The nozzles were screwed into the distribution plate and placed in between the air chamber and the fluidising zone of the BFBR. One pressure tapping port was created in the air inlet pipe into the air chamber, which was connected to an Omega Engineering electronic differential pressure

transmitter (model PX 2300 – 2DI) with an accuracy of ±0.25% on a FSS and repeatability of 0.05% on a FSS. The pressure transmitter constantly provides a 4 – 20 mA signal calibrated range for pressure measurement of 0 to 137.90mbar. This is connected to a dataTaker Technology five-channel logger (model DT80 series 2) with an accuracy of ±0.01% on a FSS for data logging purposes.

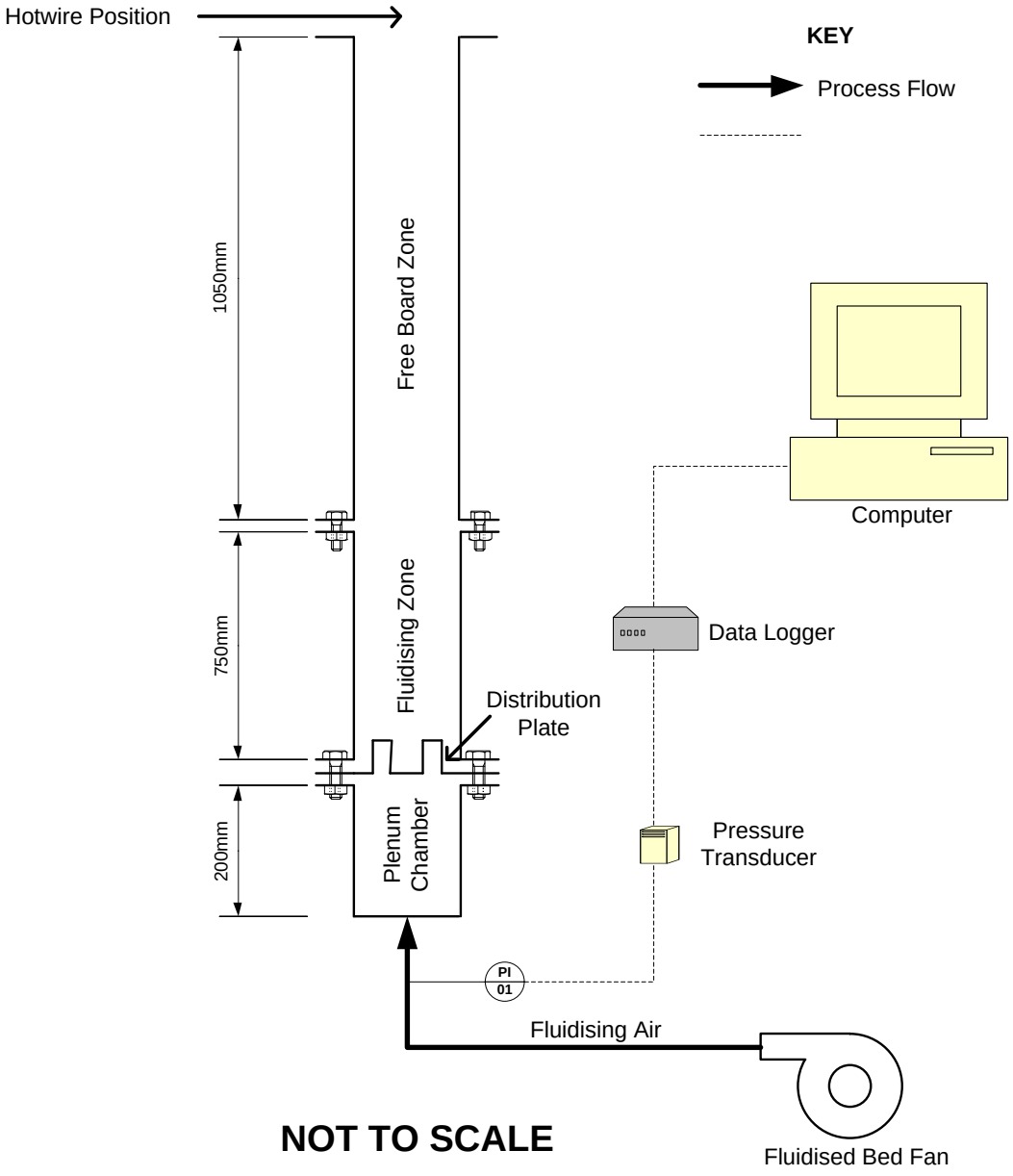

Figure 3-3: Process flow diagram of the cold fluidised bed rig made from Perspex tube

The fluidising air was supplied by a B.O.B Stevenson Ltd 2600 rpm centrifugal fan which is powered by a 5.5kW Brook Crompton IP55 motor controlled by an

in-house built variable speed drive inverter. The top section of the freeboard zone was left open in order to measure the velocity of the air supplied into the cold rig using a TES-1340 Hotwire digital Thermo Anemometer. The velocities were measured at distances of 80mm, 120mm and 150mm from the edge of the cold BFBR wall across the top opened surface represented by point A, B and C respectively in Figure 3-4.

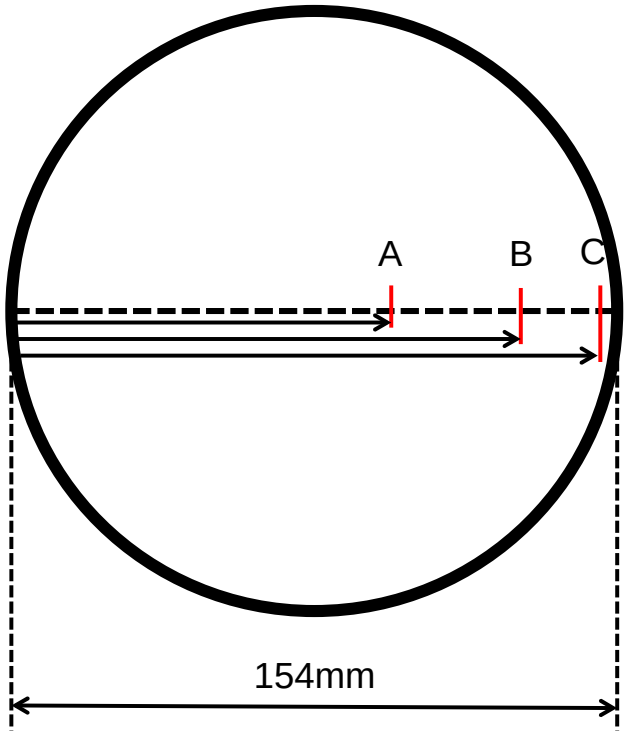

Figure 3-4: Schematic diagram to show hot wire measuring positions (A, B and C) across the top section of the freeboard zone during the cold fluidisation test

The two variables that were measured during the cold fluidisation test are fluidising air velocity and pressure drop. Due to the absence of a volumetric flow meter in the setup, it was impossible to be able to measure the volumetric flowrate of the air supplied into the air chamber. Fluidisation quality was judged by visual observation of the bed.

From visual observation of the bed during this investigation, it was seen that a slight movement occurred in the bed at a fan speed of 6 and the bed mixing became more vigorous as the fan speed was ramped up from 6 to the maximum

setting of 10 on the fan inverter regulator. On comparing this observation with the air velocity measurements taken during the investigation plotted against fan speed shown in Figure 3-5, it was noticed that the air velocity measured at fan speed 6 across the top opening of the BFBR were 0.41m/s, 0.48m/s and 0.52m/s at the three measurement point 150mm, 80mm and 120mm, respectively with an average of 0.47m/s. This measured velocity equates to the theoretically calculated minimum fluidisation of 0.41 m/s at ambient conditions in section 3.3.1.3. It can therefore be said that this point is the minimum fluidisation point.

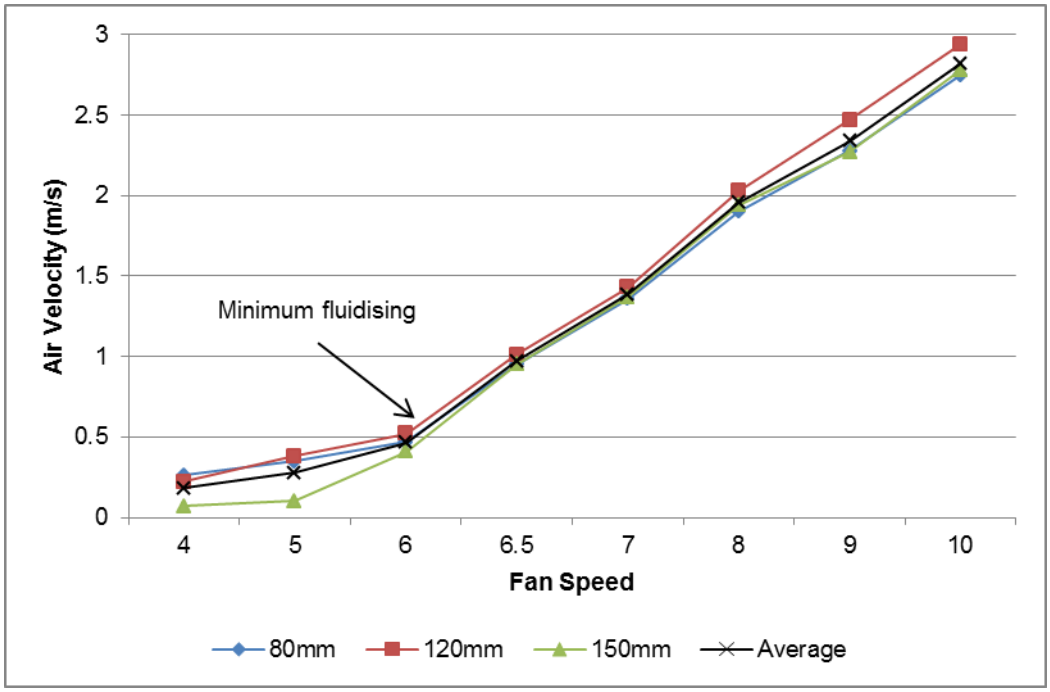

Figure 3-5: Plot of air velocity against fan speed during cold fluidisation test at room temperatures

The slight variation between the theoretically calculated and measured minimum fluidisation velocity can be attributed to the pressure drop across the distribution plate and the lower fluidising air temperature than the assumed ambient conditions used in the theoretical calculation. The measured velocity across the BFBR was also observed to increase, as the fan speed was increased from 6 to 10. This finding correlates with that reported from the visual observation that the

vigour and quality of fluidisation observed increases as the fan speed was increased.

The plot presented in Figure 3-6 shows the average air velocities measured across the top open section of the BFBR (which equates to fan speed) plotted against the pressure drop measured at each velocity every 10 seconds over a 5 minutes time period (30 data points per measured air velocity or fan speed). The average pressure drop data shown in Figure 3-6 was determined by finding the average of all the pressure drop data collected at each air velocity or fan speed.

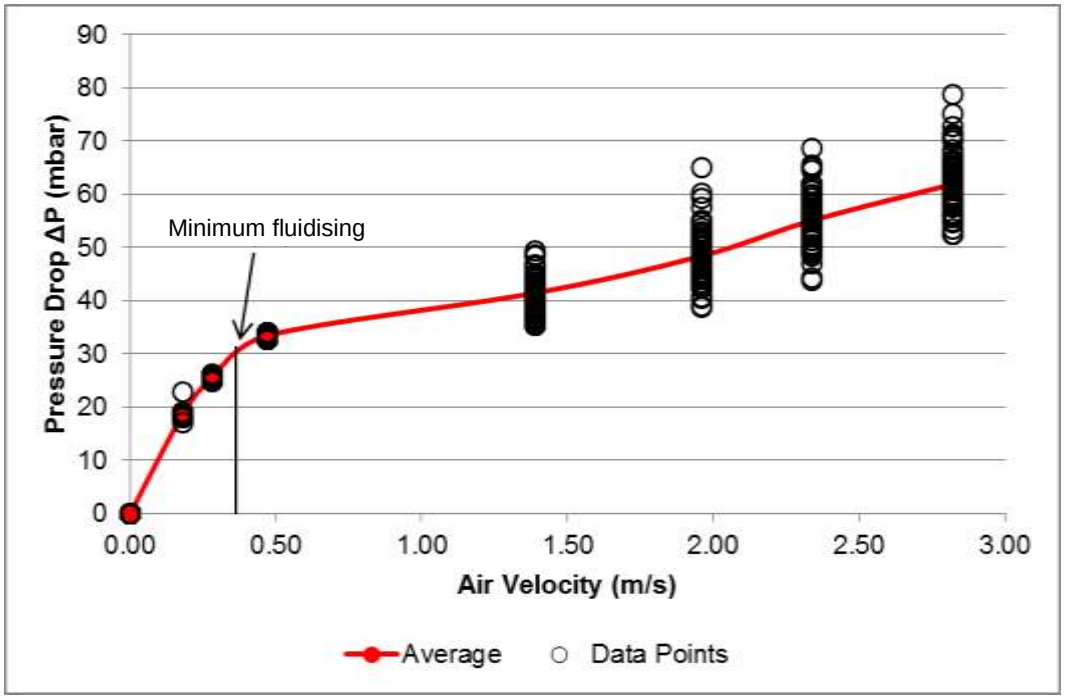

Figure 3-6: Plot of pressure drop against air velocity during cold fluidisation test at room temperatures

On analysing the measured pressure drop and air velocity relationship, it was observed that both the measured pressure drop across the distributor plus bed and pressure drop variation increased as the fluidising air velocity increases. This increasing trend in the pressure drop variation can be associated with the increase in quality of fluidisation achieved across the bed as the fluidising velocity increases (Basu 2006; Zhang et al. 2014). The minimum fluidisation

point was also identified to be about 0.40 m/s as pointed out in Figure 3-6 which is close to the theoretically calculated minimum fluidisation velocity of 0.41m/s.

3.3.4. Conclusion

The calculated design parameter values correlate very well with the literature data for a BFB system as identified in the validation sections for the fluidising velocities and pressure drop comparison (see section 3.3.1.3. and 3.3.2.3. respectively). The cold visualisation test rig provided a visual confirmation that quality fluidisation can be achieved in the proposed BFBR for sintering and agglomerate formation investigation. Hence, the calculated design parameter values, specified reactor diameter and length, bed height and proposed nozzle arrangement can all be carried forward and established as the basis for the BFBR design for the PSBFBC system.

However, the cold visualisation test pointed out that the following needs to be included in the final PSBFBC system setup

1. The need of a volumetric flowmeter in order to be able to measure the fluidising air flowrate supplied by the fluidised bed fan going into the BFBR.

2. Installation of manual ball valves in the fluidising air supply line in-between the fluidised bed fan and inlet into the air chamber in-order to be able to control the air supply flowrate as required during combustion runs.

3. More pressure tappings are required across the length of the reactor (one in the plenum chamber, two in the fluidising zone and three in the free board zone) in order to have a clearer source of information on the pressure profile across the system especially when trying to measure the differential pressure across two points.

3.4. Fluidising Air Flow rate

3.4.1. Volumetric air flowrate

The volumetric air flow rate (m^3/s) required for the combustion process in the PSBFBC was determined using equation 3.17 where U is the fluidising air superficial velocity (m/s) assumed to be eight times the u_{mf} calculated earlier in section 3.3.1.2 and A is the cross sectional area (m^2) of the BFBR.

$$Q = U A \tag{3.17}$$

The volumetric airflow rate calculated using the above equation is that required at combustion conditions in the BFBR. Hence, the volumetric airflow rate was corrected “normalised”, to ambient conditions using equation 3.18 to determine the amount of air needed to be supplied at ambient conditions to meet the combustion conditions requirement.

$$Q = Q_{amb}\left[\frac{(T_{amb} + 273)}{(T + 273)}\right] \tag{3.18}$$

where Q is the volumetric flowrate at temperature T (°C) and Q_{amb} is the volumetric flow rate at ambient temperature T_{amb} (°C)

3.4.2. Mass air flowrate

The mass airflow rate required for combustion in the BFBR was determined using equation 3.19 where $\dot{m}$ is the mass flowrate of air (kg/s)

$$\dot{m} = \rho_{g,amb}\, Q_{amb} \tag{3.19}$$

3.5. Coal Feed rate

By using the stoichiometric combustion of solid fuel in air equation given in equation 3.20, where F is the fuel (coal) feed rate (kg/s), the amount of coal required for the combustion process at stoichiometric conditions was determined (Liu 2011a). The C, H, N, S and O values were given as weight percentage of each element identified to be present in the coal by ultimate analysis discussed in section 2.2.1 and 4.2.2.

$$\left(\frac{\dot{m}}{F}\right)_{stoic,mass} = 0.1144C + 0.3433H + 0.098N + 0.0429(S - O) \quad (3.20)$$

Since all fluidised bed combustion processes operate in excess air conditions and not stoichiometric, the coal feed rate had to be adjusted for this condition. This was done by using equation 3.21.

$$F_{\%ExcessAir} = \frac{F_{stoic}}{\left(1 + \frac{\%ExcessAir}{100}\right)} \quad (3.21)$$

3.6. Components Design

3.6.1. BFBR Sizing

Based on the pre-design decision that the length of the BFBR shall not exceed 2 metres (see section 3.2) and the confirmation of the suitability of the specified length for this application from the BFBR cold rig testing (see section 3.3.3.), it was decided that the 2 metres length will be used as the basis of the BFBR design in the PSBFBC. This specified length was divided into the three standard zones typically present in a BFB combustion reactor following the same ratio as for the BFBR cold rig test (see section 3.3.3). The schematic diagram of the BFBR section of the PSBFBC is shown in Figure 3-7.

The cut end of each section was welded to a 6 inches pipe standard austenitic stainless steel 310 flange using 3.2mm stainless steel 312 welding rods, which is the same for every other welding carried during the construction of PSBFBC. Pressure tapping were made using ¼ inches austenitic stainless steel 304 pipe arranged across the centreline of the BFBR wall at a height of 100mm, 300mm, 900mm, 1130mm, 1450mm and 1770mm respectively measured from the base of the BFBR and marked PI-01 to PI-06.

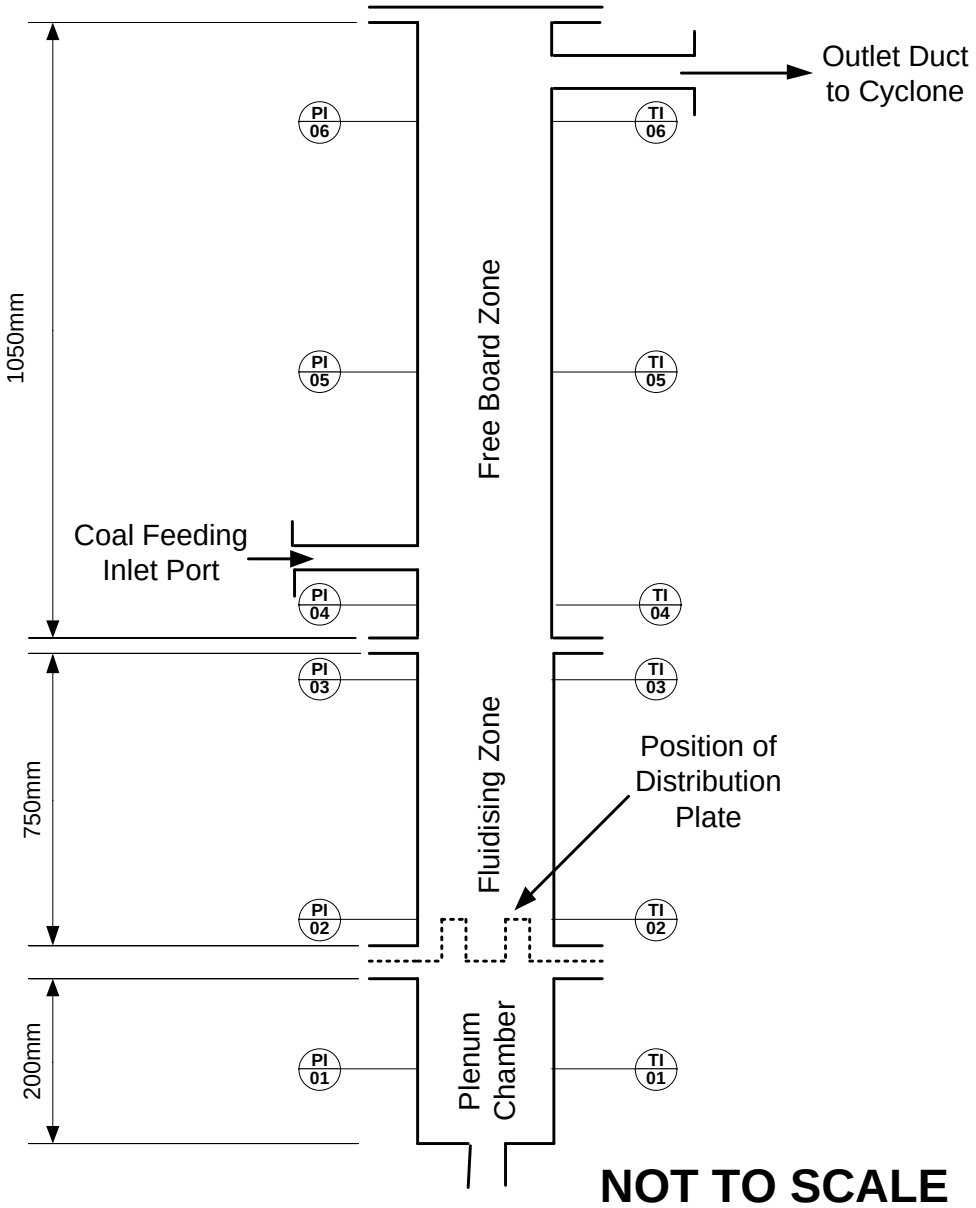

Figure 3-7: Schematic diagram and dimensions of the BFBR section of the PSBFBC

The thermocouple ports were arranged at the same height on the opposite side of the pressure tapping across the centreline of the BFBR wall and using stainless steel 316 bored-through male connector ⅛ inches (O.D) by ⅜ inches male pipe weld for the thermocouple port fittings. The wall of the BFBR case was drilled for the appropriate fitting size and welded. The pressure tappings and thermocouple port were arranged in the ratio of 1:2:3 across the zones of the BFBR from the plenum chamber to the freeboard zone to effectively optimise pressure and temperature measurement across various zones of the BFBR.

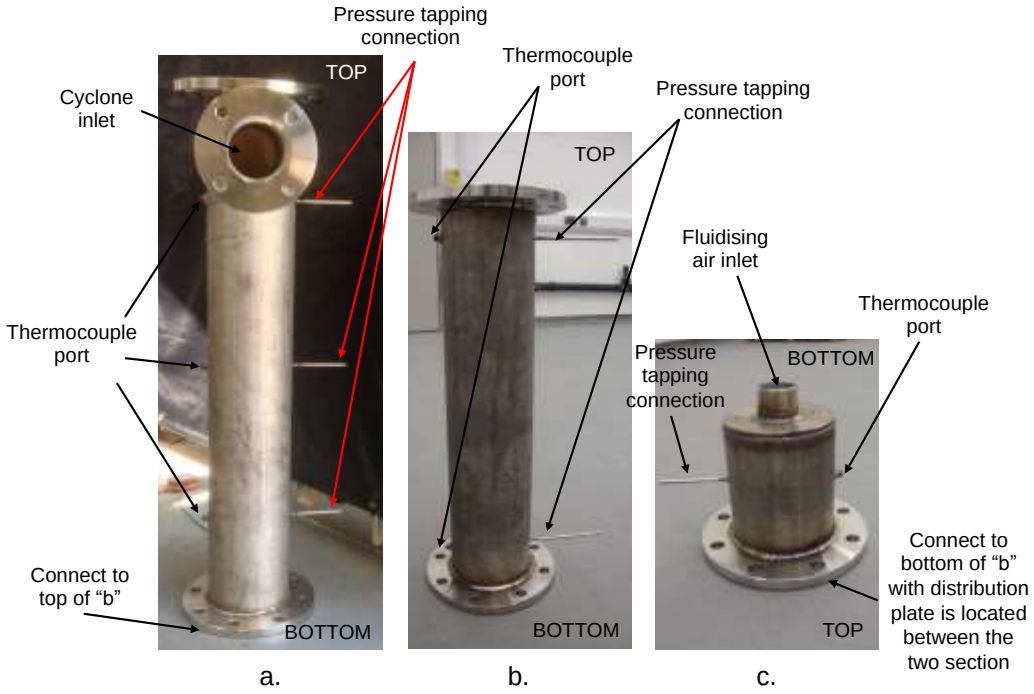

Figure 3-8: Pictures showing fabricated sections of the BFBR for the PSBFBC system. (a) Freeboard zone. (b) Fluidising zone. (c) Plenum chamber

The gap between the pressure tapping and temperature ports in the fluidising zone was set at 600mm to allow proper positioning of the electrical heaters around the BFBR walls. A 3 inches (76mm O.D) austenitic stainless steel 304 pipe was welded to a drilled hole at the top side of the freeboard zone measured at a height of 1880mm from the base of the BFBR to serve as a cyclone inlet flue gas stream. On the opposite side of the flue gas inlet pipe to the cyclone at a height of 1200mm from the base of the BFBR located in the lower section of the

freeboard zone, a hole was drilled for the welding of a 2 inches (50mm O.D) austenitic stainless steel 304 pipe to serve as the lump coal feeding inlet port. Picture of the finished fabricated sections of the BFBR for the PSBFBC system are shown in Figure 3-8

3.6.2. Nozzle Design and Arrangement

As mentioned earlier in section 3.2, the choice of nozzles to be used in the BFBR shall be the same as the ones currently used in the industrial operated FBC system. After deliberating on the number of nozzles and their arrangements in the BFBR distribution plate, a four nozzle arrangement was chosen based on the suitability of the pattern to the specified diameter of the BFBR. The suitability of this nozzle arrangement for this application was further reinforced by meeting pressure drop criteria expected for a BFB system as discussed in section nozzle 3.3.2.3, and the ability to attain quality fluidisation as discussed in section 3.3.3 and 3.3.4. A schematic diagram and picture of the distribution plate is shown in Figure 3-9.

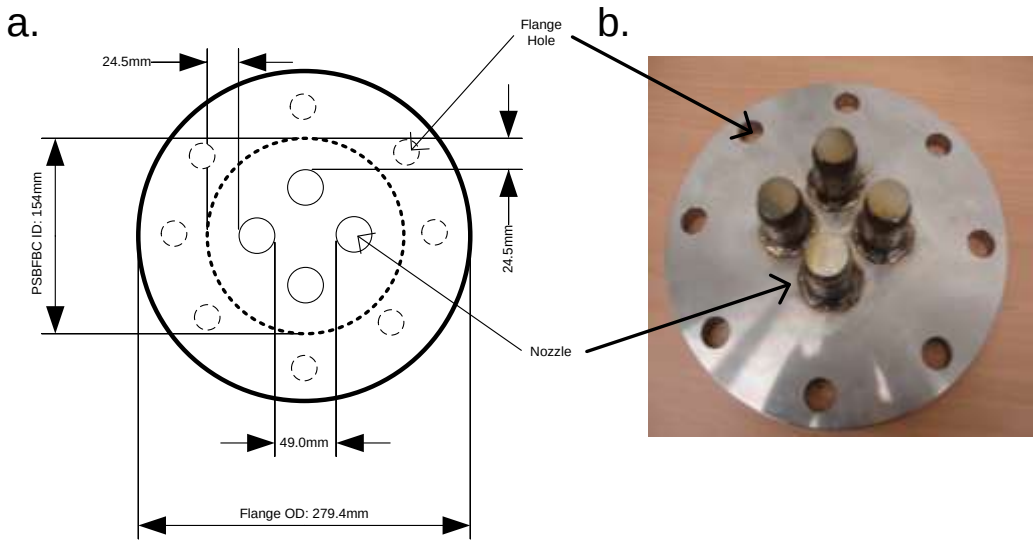

Figure 3-9: Nozzle design and arrangement for the PSBFBC distribution plate. (a) Schematic diagram and dimensions. (b) Image after fabrication

The positioning and dimensions of a single nozzle on the distribution plate of the BFBR in the PSBFBC system is shown in Figure 3-10. The nozzle plate was made using a 6 inches pipe standard austenitic stainless steel 310 blank flange with a thickness of 20mm. This flange was drilled following the nozzle arrangement dimensions given in Figure 3-9 with hole sizes of 34mm (O.D) onto which the nozzles were then welded.

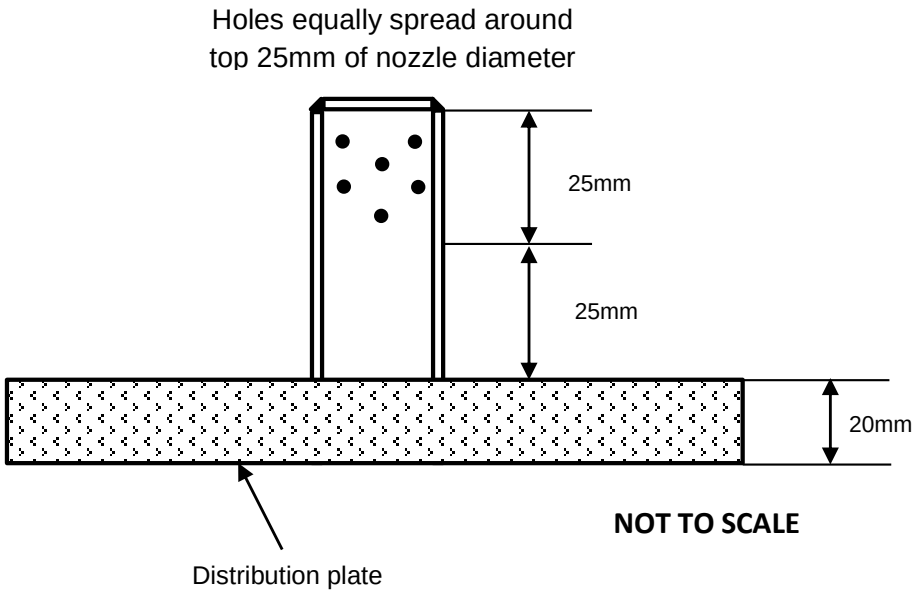

Figure 3-10: Single nozzle positioning on the distribution plate of the BFBR in PSBFBC system with dimensions

3.6.3. Coal Feeder

Having specified the particle size of the coal to be fed into the PSBFBC as 10 to 19mm as part of the pre-design decisions (see section 3.2), further decisions had to be made on the type of coal supply system to be employed for this purpose. After detailed consideration on safety, suitability and feasibility of various coal supply systems ranging from a coal flicker system similar to the mechanism used in industrial scale FBC to a screw feeder system, the decision was made to use an enclosed screw feeder system in the PSBFBC. A schematic diagram of the screw auger designed and used as the coal conveyor in the screw feeder system for the PSBFBC is shown in Figure 3-11.

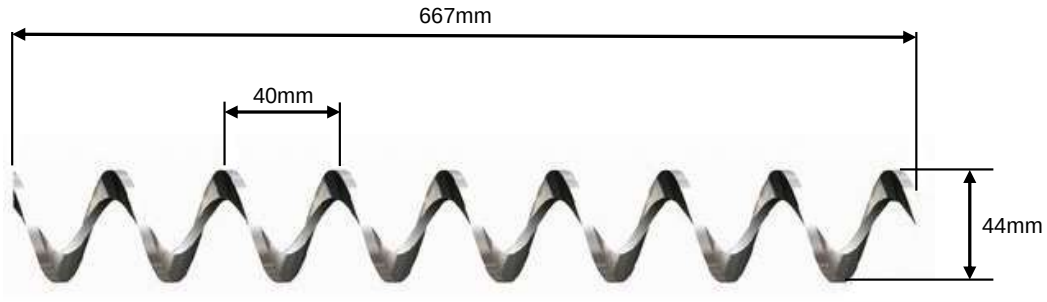

NOT TO SCALE

Figure 3-11: Schematic diagram and dimension of the PSBFBC coal feeder shaft-less screw auger

The screw auger is made from high grade austenitic stainless steel 316 of 3mm thickness with service temperature up to 1400°C. To increase the strength and rigidity of the screw auger for this application, a 16mm austenitic stainless steel 316 rod was inserted into the ring hole in the screw auger and then welded on to serve as a centre shaft. As part of the conveyor section of the screw feeder design, a shaft containing ball bearing shown in Figure 3-12 was made from austenitic stainless steel 304 for the ease of rotation of the screw auger.

Figure 3-12: Ball bearing shaft for PSBFBC screw auger

Complete assembling of the conveyor section of the screw feeder system for the PSBFBC is shown in Figure 3-13. The conveyor section comprises of the screw auger, hollow shaft housing bearing and a motor driving shaft.

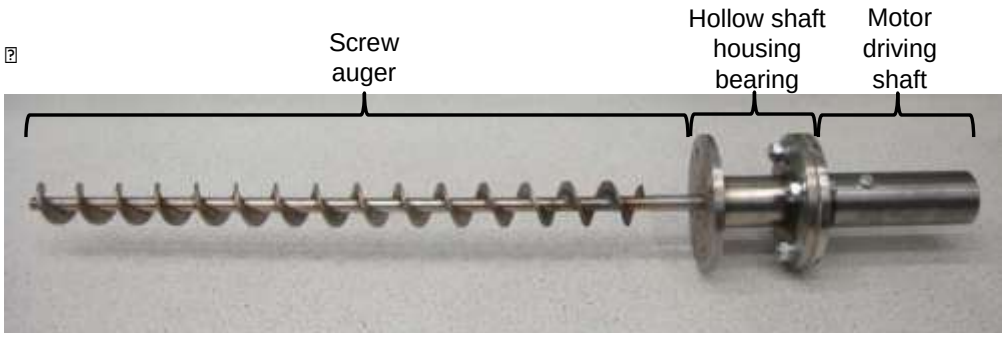

Figure 3-13: Coal conveyor section of the PSBFBC screw feeder system

The remaining sections of the screw feeder system for the PSBFBC are shown in Figure 3-14 which includes a coal hopper with a holding capacity of up to 17kg of lump coal and a SEW-EURODRIVE helical geared motor (mode R67 DRE80M4/TF) which powers the coal conveyor. The speed of the geared motor, which dictates the coal feeding rate supplied into the BFBR, is controlled by an Allen – Bradley IP20 variable speed drive (model PowerFlex 4 AC Drive). As part of the screw feeder system design with strong emphasis on system safety, the system is designed with two main safety features located on the top of the coal hopper as shown in Figure 3-15.

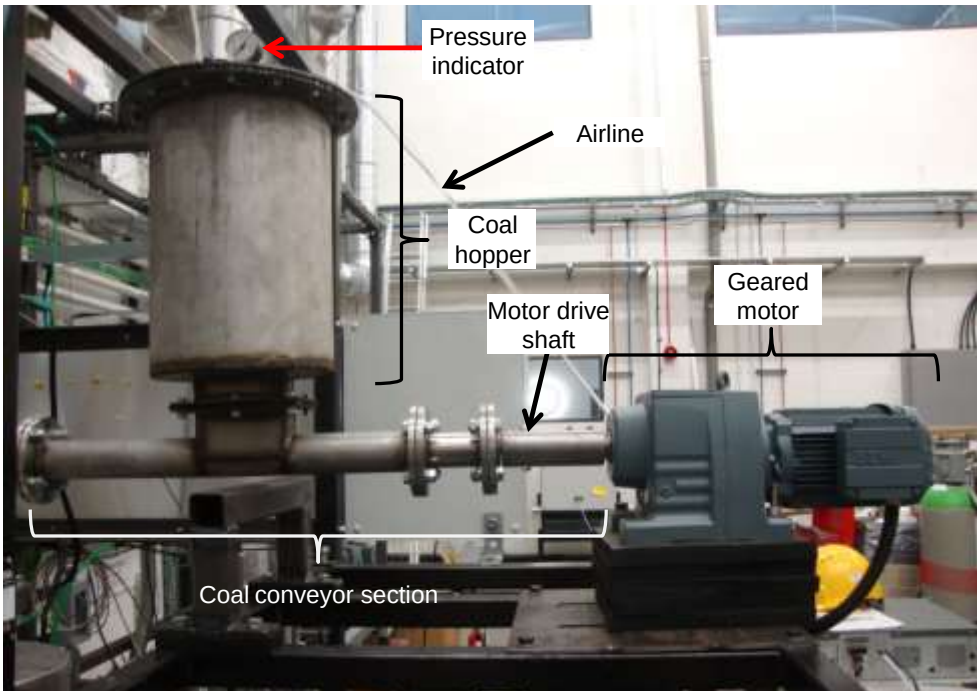

Figure 3-14: Complete coal screw feeder system for the PSBFBC

The first safety feature is an air / nitrogen inlet line, which constantly supplies air or nitrogen into the coal conveyor system to create a positive pressure flow, which will prevent hot-gas flash back that might occur during the PSBFBC operation. The second feature is a pressure indicator, which measures pressure in the coal hopper. This helps the PSBFBC operator to monitor the pressure and / or identify pressure build-up which might arise from a blockage in the conveyor section of the screw feeder system. The coal feeder calibration chart is shown in Appendix A.

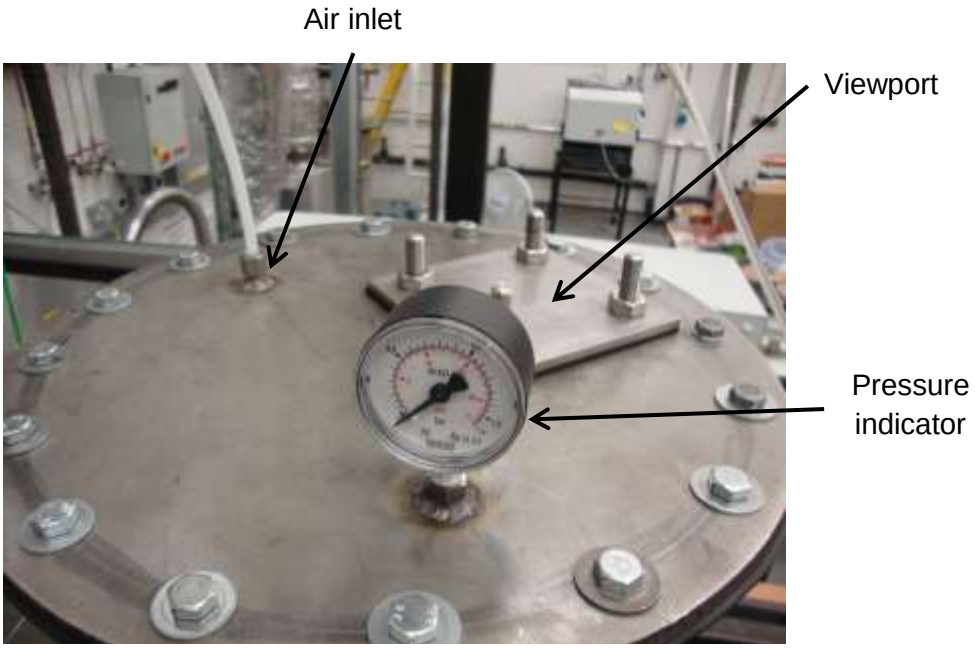

Figure 3-15: Top section of the coal hopper in the screw feeder system for the PSCFBC showing safety features of the system

3.6.4. BFBR Fan Sizing

The BFBR fan sizing was outsourced to Fan and Blowers Ltd, UK, which is a centrifugal fan designer and manufacturer. The BFBR fan was sized based on the fluidising volumetric air flowrate requirement of the PSBFBC and the estimated pressure drop across the BFBR section of the PSBFBC calculated from expressions in section 3.4 and 3.3.2 respectively. The specified design volumetric flowrate for the BFBR fan was given as fifteen times the calculated

requirement at ambient conditions and the supply pressure requirement was given as three times the calculated pressure drop across the BFBR.

A schematic diagram of the BFBR fan size as specified by the manufacturer based on the design specification given is shown in Appendix B. The resulting BFBR fan specified for this application is a 2900rpm centrifugal fan (model BM 841) which is powered by an 11kW Brook Crompton IP55 motor controlled by a Weg technology variable speed drive (model CFM-11) and has a total weight of 210kg. The BFBR fan and variable speed drive operations are controlled remotely using Super Drive G2 software supplied by Weg. For the operation of the fan, air is drawn from laboratory room and the size of the room is sufficient that it does not impact the fan or vice versa.

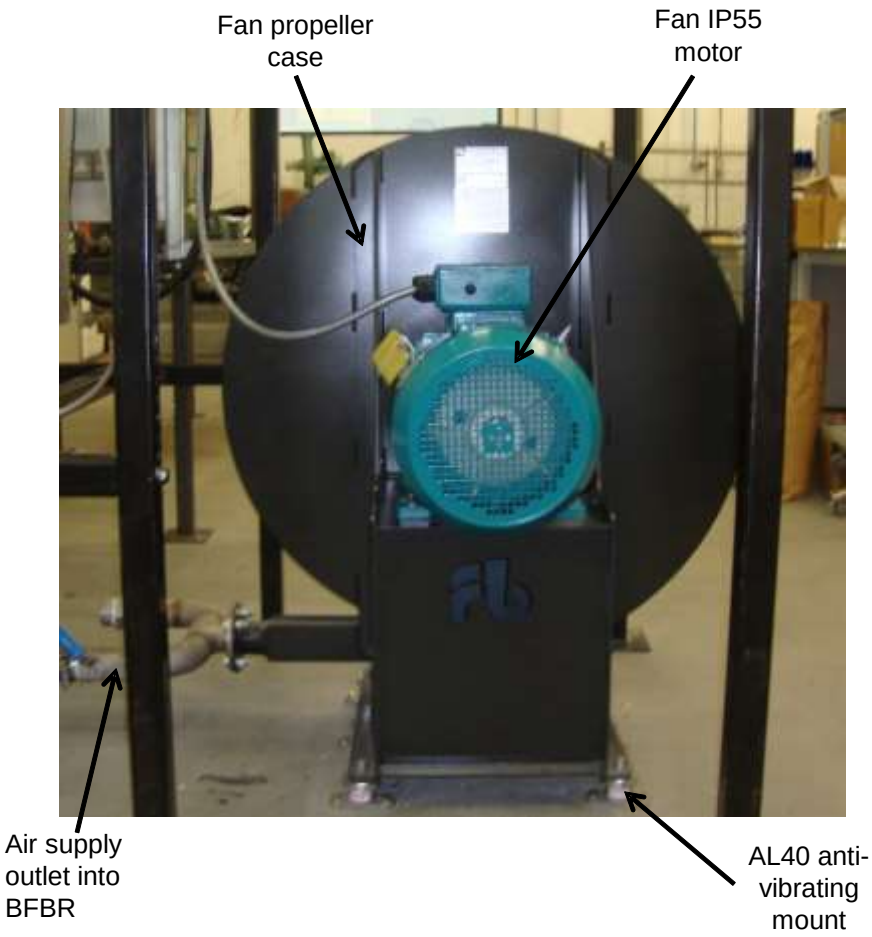

Figure 3-16: Picture showing the back view of the installed BFBR fan sitting on the AL40 anti vibrating mounts

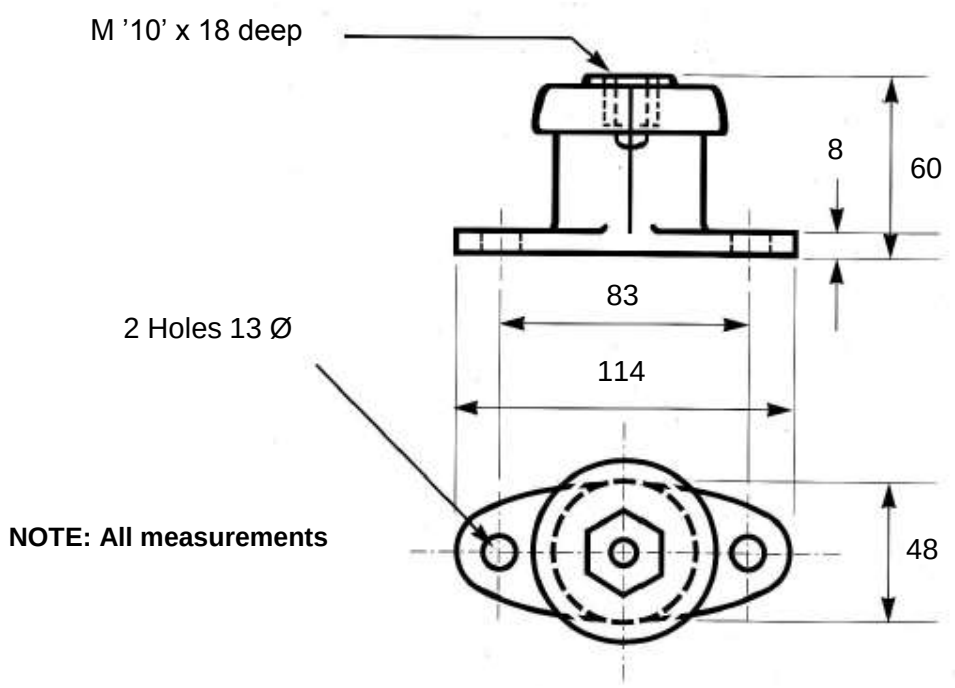

Figure 3-17: Schematic diagram and dimensions of a single AL40 BFBR fan anti-vibrating mount

From the operational safety assessment done on the BFBR fan prior to installation, it was concluded that the use of anti-vibrating mounts were required for the safe operation of the fluidised bed fan especially at high speed operation. Six pieces of AL40 anti-vibrating mount with a total weight rating equal to the weight of the BFBR fan was purchased from the fan manufacturer and installed as shown in Figure 3-16. The anti-vibrating mount casing is made from aluminium with a compressible rubber packing which absorb vibration during operation. The schematic diagram and dimensions of a single anti-vibrating mount is shown in Figure 3-17

3.6.5. Cyclone Design

The gas-solid cyclone for the PSBFBC was designed to achieve a high efficiency standard by using the high-efficiency cyclone engineering design principle shown in Figure 3-18a (Sinnott 2005). However, from cyclone design and operation experience, certain parameters within this standard design principle can be slightly adjusted without having a major effect on the efficiency of the cyclone.

These adjustments were done for the ease of fabrication (material sourcing), space restriction within the laboratory and cost reduction. The altered high-efficiency cyclone design used in the PSBFBC system is shown in Figure 3-18b where D_c is given as the diameter of the cylindrical section of the cyclone in this case which is 10.5 inches (266mm ID). The schematic diagram of the PSBFBC cyclone design specification given to the manufacturer is shown in Figure 3-19. The cyclone was fabricated using high grade austenitic stainless steel 304

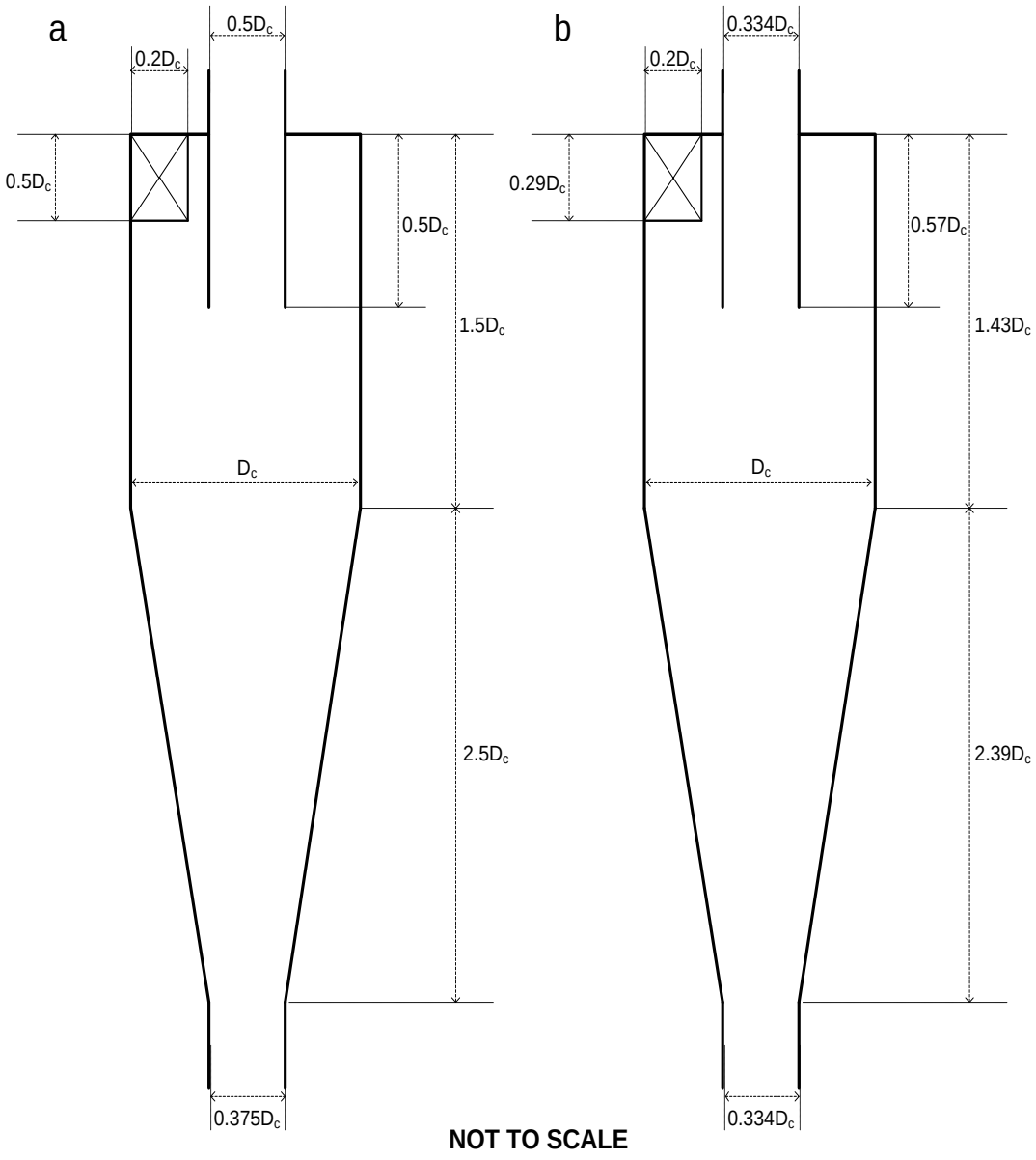

Figure 3-18: Cyclone design dimensions. (a) Standard high-efficiency cyclone. (b) Altered high-efficiency cyclone

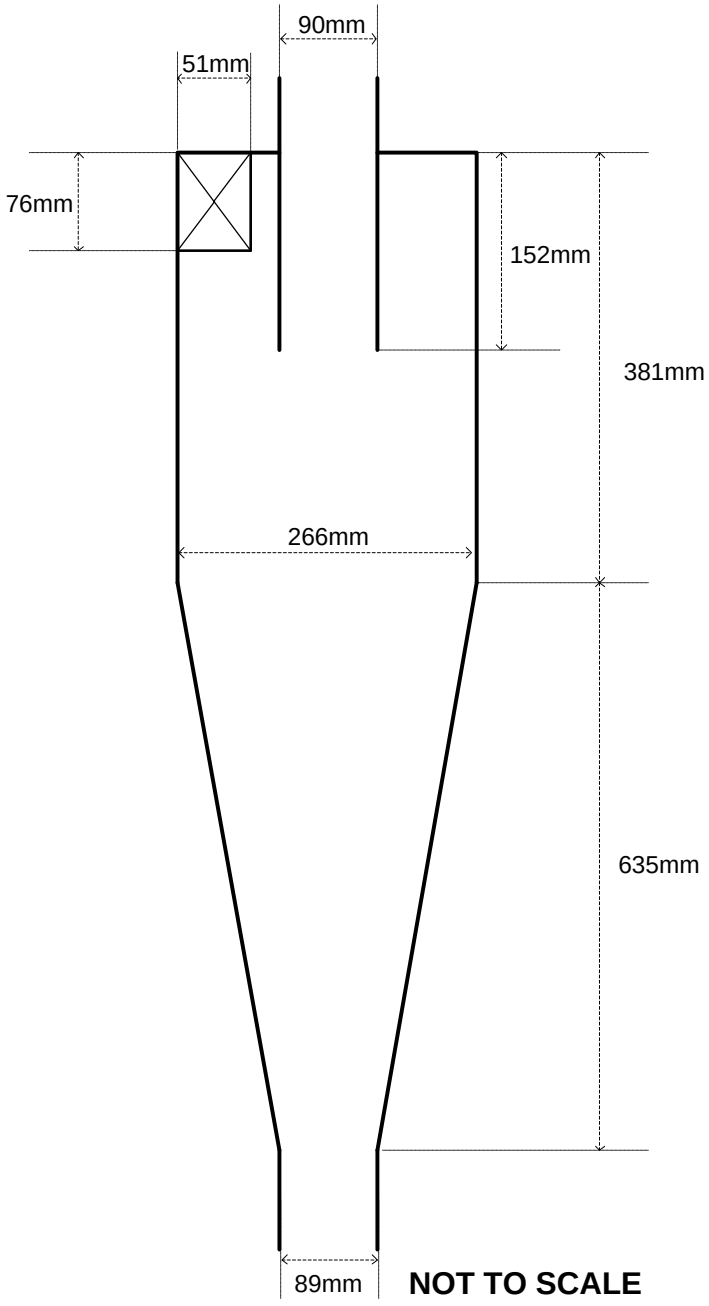

Figure 3-19: Schematic diagram of the PSBFBC cyclone design showing all dimensions

3.6.6. Flue Gas Sampling Probe

The flue gas cooling water sampling probe size specification was based on practical engineering experience. The justification for this is that the flowrate of the flue gas to be sampled is very low (0.5 l/min) and operational modifications can easily be made to improve the cooling effect across the probe for flow rate of this size by increasing the cooling water flowrate. The specific exit temperature of

the flue gas from the probe is not critical as allowance is made for secondary cooling to occur around the gas conditioning unit prior to the gas analyser.

The schematic diagram and dimensions of the flue gas cooling water probe design is shown in Figure 3-20. The probe consists of three concentric tube layers namely inner, middle and outer tube with varied I.D of 6mm, 12mm, and 18mm respectively. The material used for the fabrication of the flue gas cooling water probe is stainless steel 316 seamless pipes with a wall thickness of 1.25mm.

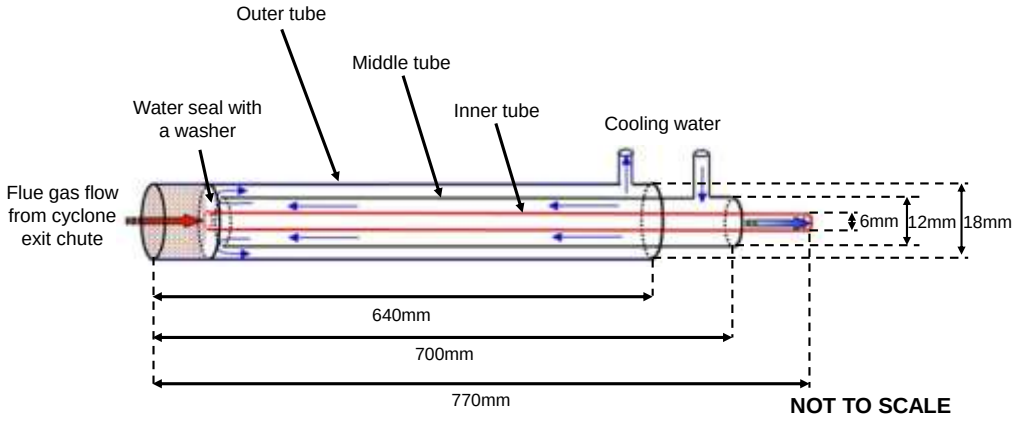

Figure 3-20: Schematic diagram and dimensions of the cooling water flue gas sampling probe for the PSBFBC

3.6.7. Volumetric Flowmeter

The volumetric flowrate of the fluidising air supply from the BFBR fan into the plenum chamber of the BFBR was monitored using a low pressure drop variable area volumetric flowmeter shown in Figure 3-21. The flowmeter was designed by Cache Instrumentation Ltd with a measuring range of between 120 - 1100 l/min (air equivalent) at 1.013bar and 20°C. It has a high repeatability of ±0.5% of flow and a maximum operation temperature of 120°C. The flowmeter was only used as an operational indicator device to provide an estimate measurement of fluidising air flowrate supplied into the BFBR during combustion runs.

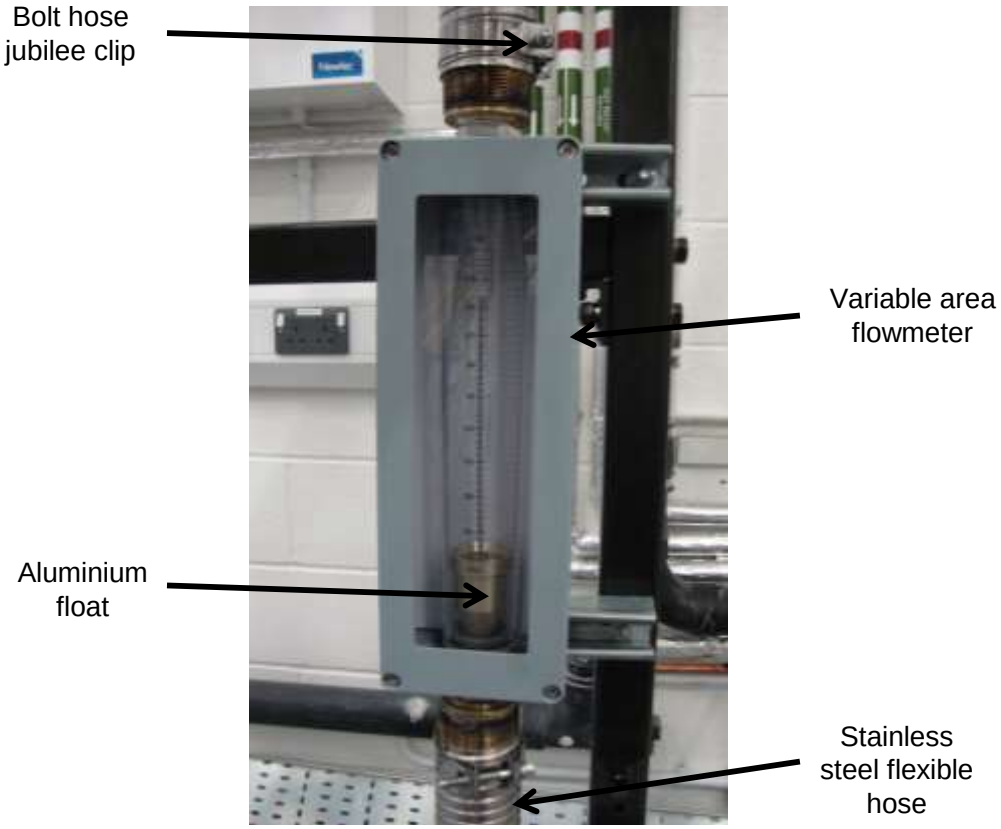

Figure 3-21: PSBFBC variable area volumetric flowmeter with air supply hose connections

3.6.8. Bed Material Sampling Probe

In order to be able to carry out bed material sampling from the BFBR, a bed material sampling probe shown in Figure 3-22 was designed and assembled for this purpose. The bed material sampling probe consists of a 6mm stainless steel rod with a length of 2500mm and a sample collector made of plastic with a diameter of 50mm and depth of 10mm.

The length of the bed material sampling probe was designed to be 700mm longer than the total height of the fluidising and freeboard zone of the BFBR to provide enough space for holding and manoeuvring the probe during sampling. The diameter of the sample collector was restricted to 50mm for easy passage into the BFBR without being blocked by the thermocouple probes.

a.

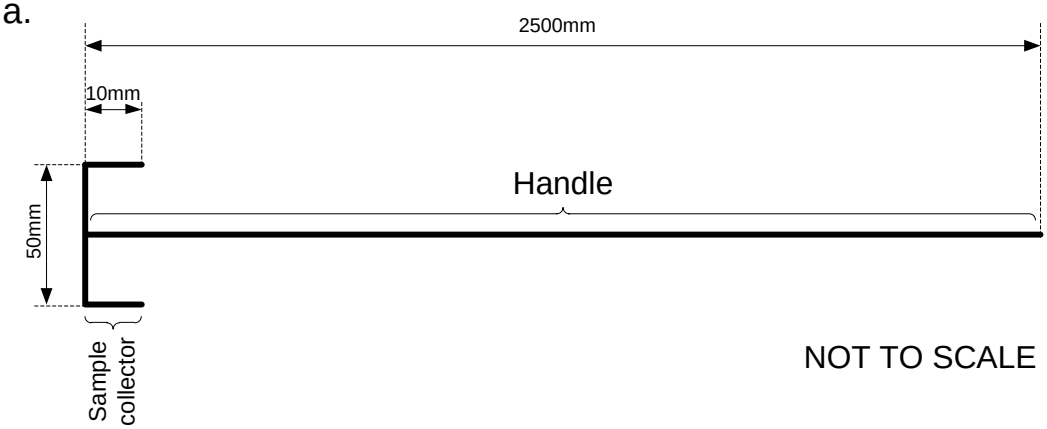

b.

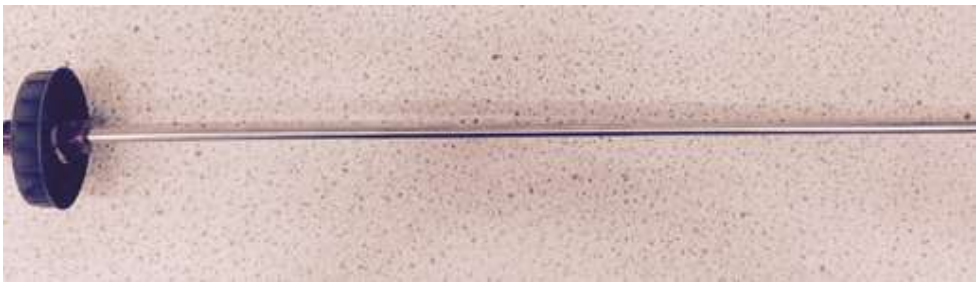

Figure 3-22: PSBFBC bed material sampling probe. (a) Schematic diagram and dimensions. (b) Picture after been assembled.

3.6.9. PSBFBC Frame

The PSBFBC support frame was produced using 50mm by 50mm mild steel square box section pipes with a wall thickness of 3mm. A detailed schematic diagram of the design specification for the PSBFBC support frame is shown in Figure 3-23. The support frame is divided into three sections namely coal feeder, fluidised bed and cyclone sections. The support frame has a total footprint of 2200mm (length) by 1200mm (width) and a height of 2650mm.

The frame metal bars were made and produced as single / individual pieces for the ease of transportation and were assembled together on site using stainless steel M19 bolt. The use of bolts also makes it easy to take apart when trying to open up the BFBR section of the PSBFBC to check the condition of the bed and / or change the bed material. Each of the joints are supported and reinforced by cut pieces of 50mm by 50mm mild steel angle bar to carry the force and stresses

of the PSBFBC system during operation. The entire structure is bolted to the floor using 12 pieces of M12 brass raw bolts (2 on each leg plate). The base support of the PSBFBC frame is specified to be located at 1850mm in order to accommodate the BFBR expansion height downwards due to thermal growth which is expected to be about 25mm for a 900°C operating temperature.

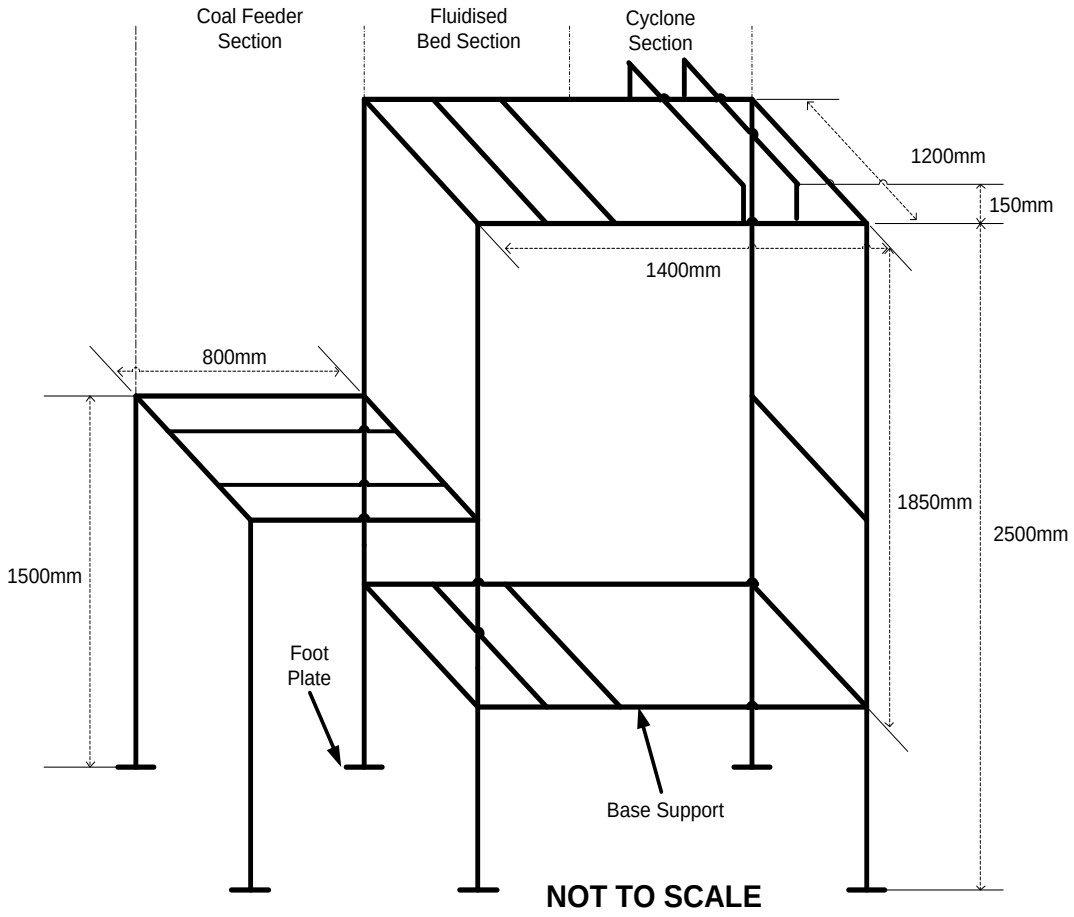

Figure 3-23: Schematic diagram and dimensions of the PSBFBC support frame

3.7. Piping

3.7.1. Fluidising Air Supply

For the supply of air into the plenum chamber of the BFBR from the BFBR fan via the variable area flowmeter, a high temperature flexible interlock stainless metallic tubing made from austenitic stainless steel 304 S16 shown in Figure

3-21 was used. The metallic tubing used has a bore size of 2⅜ inches (I.D. 60mm, thickness 3mm) and with a maximum working temperature of 650°C. It was connected using a stainless steel bolt hose jubilee clip (size 63 – 68mm).

3.7.2. Cooling Water and Flue Gas Supply

The cooling water supply in and out of the flue gas sampling probe, flue gas supply from the sampling probe into the gas analyser via the gas cooling and scrubbing system and the exhaust gas supply from the gas analyser into the atmosphere were all done using natural nylon flexible hose (O.D. 6mm). The nylon hose can withstand an operating temperature range of – 40°C to + 80°C and was connected using ¼ inch straight coupler brass compression fitting.

3.8. Instrumentation

3.8.1. Temperature Measurement

K-type thermocouples (250mm length; 3mm O.D.) with temperature measuring range of 0°C to 1100°C were used for temperature measurement in the BFBR. The thermocouples are arranged and labelled sequentially from TI-1 to TI-6 along the centreline of the BFBR using the welded stainless steel 316 bored-through male connector ⅛ inches (O.D) by ⅜ inches male pipe port fitted to the walls of the BFBR as discussed in section 3.6.1. The thermocouple signal monitoring and data logging connections are discussed in section 3.8.4.

3.8.2. Pressure Measurement

Austenitic stainless steel 304 (¼ inches pipe size) arranged on the opposite side of the thermocouples as discussed in section 3.6.1., are used as pressure measuring ports. The six pressure tappings labelled sequentially from PI-1 to PI-6 along the centreline of the BFBR are each connected to a ¼ inches manual ball

valve, which is used for selecting the pressure tapping point of choice. The pressure measuring port is connected to an Omega Engineering electronic differential pressure transmitter (model PX2300 – 2DI) with an accuracy of ±0.25% on a FSS and repeatability of 0.05% on a FSS to measure the pressure by providing a 4 – 20 mA signal calibrated range for pressure measure 0 to 137.90mbar connected to dataTaker process monitor. The pressure signal monitoring and data logging connections are discussed in section 3.8.4.

3.8.3. Flue Gas Measurement

The flue gas sampling was done using the flue gas-sampling probe (see section 3.3.6.), which was connected to a Horiba technology gas sampler (model VS-3000) via an in-house designed gas cooling and conditioning unit. The Horiba gas sampler is connected to a regularly calibrated Horiba technology gas analyser (model VA-3000) with a repeatability of ±0.5% on a full scale range (FSR), which was used to analyse the composition of NO_x in the flue gas. The composition of O_2, CO_2 and CO in the flue gas stream were measured using a regularly calibrated ABB technology gas analyser (model EL 3020) with a repeatability of ≤0.5% on a FSR. The flue gas monitoring and data logging connections are discussed in section 3.8.4.

3.8.4. Data Monitoring and Logging

Temperature, pressure drop and flue gas composition signals across the PSBFBC are continuously monitored using dataTaker Technology five-channel logger (model DT80 series 2). This is connected to dataTaker Technology twenty-channel expansion module (CEM20) each with an accuracy of ±0.01% on a FSS and logged at a pre-selected time intervals of (10 seconds) for the entire duration of the experiment using dEX data logger software supplied by dataTaker installed on the PSBFBC computer.

CHAPTER FOUR

MATERIALS AND EXPERIMENTATION METHODS

4.1. Introduction

This chapter provides a detailed description of the materials and experimental methods employed during the course of this research. The choice and specifications of materials used for the purpose of this research were specified to meet criteria V - VI of the pre-design decision specification given in section 3.2. Discussion in the material specification section covers details of the physical, chemical and thermal properties of the materials used during the course of this study.

The experimentation methods employed for this research have been divided into three phases as presented in the overall experimental flow sheet shown in Figure 4-1. Phase 1 covers the industrial case study investigation carried out to understand the mechanism/s responsible for sintering and agglomeration formation in the industrial scale FBC system during lump coal combustion. The setup for this investigation focussed on the use of SEM-EDX and XRF characterisation techniques to study the surface morphology and chemical composition of the loose and agglomerated bed material particles collected from the industrial scale operated FBC. This preliminary study serves as a basis or standard for comparison in deducing the sintering and agglomeration formation mechanism in this system. Details of the experimental methods employed for this phase of investigation will be discussed in the bed material characterisation

techniques section (see section 4.6). Results for this phase of investigation are discussed in chapter 5 and 6.

Phase 2 is based on bed material calcination investigation which was done in order to study the characteristics behaviour of Garside 14/25 sand in the absence and presence of fuel (coal) and fuel ash at high temperature fixed bed conditions using an electrically heated high temperature furnace (Vecstar VF1). Detailed descriptions of the sample preparation and calcination procedure used for this phase of investigation are outlined under this section. Details of the characterisation techniques used to study the surface morphology and the chemical composition of the Garside 14/25 sand bed material or mix before and after the calcination process are given in the bed material characterisation techniques section (see section 4.6). Results for this phase of investigation are discussed in chapter 5.

The operation of the PSBFBC system designed and described in chapter 3 for lump coal combustion to investigate sintering and agglomerate formation was the focus of experimental methods in Phase 3. This investigation was carried out using washed and unwashed bituminous coal in-order to understand the effect they have on sintering and agglomerate formation. Description of the combustion procedures implemented for the PSBFBC lump coal combustion starting from pre- start up checks to shut down during normal operation, emergency shutdown procedures, measurements, samples and data collection are fully outlined in this section. Details of the characterisation techniques used to study the surface morphology and the chemical composition of the loose and agglomerated bed material produced during lump coal combustion in the PSBFBC are given in the bed material characterisation techniques section (see section 4.6). Results for this phase of investigation are discussed in chapter 6.

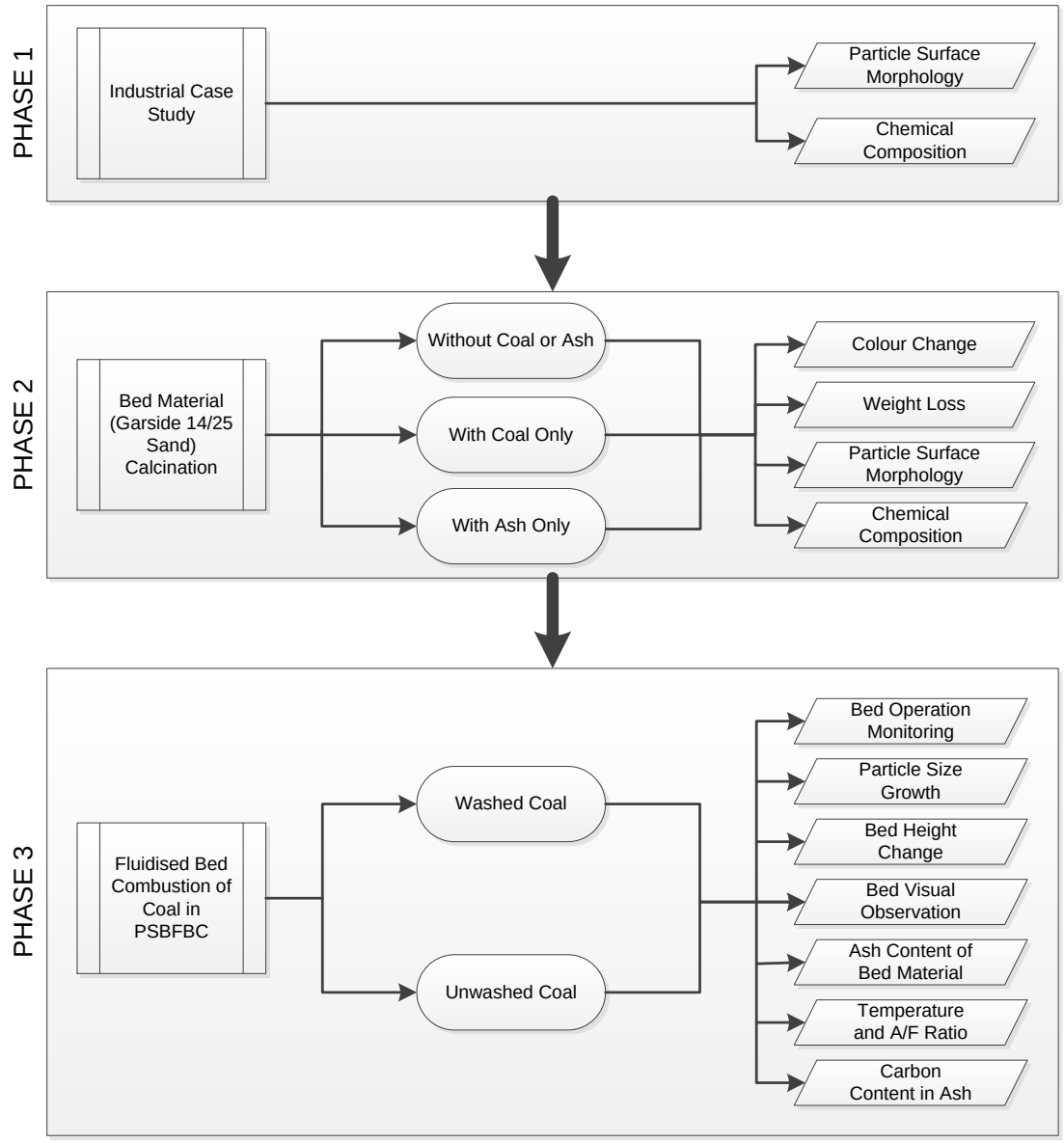

Figure 4-1: Overall experimental flow sheet

The experimental methods including sample preparation methods, procedures and characterisation techniques used during this research were formed based on the knowledge acquired from the literature survey detailed in chapter 2 and operation experience shared by the operators of the industrial scale FBC system based at AB Sugar.

4.2. Materials Specification

4.2.1. Bed Material

Garside 14/25 sand, used as bed material in the industrial FBC system at AB Sugar, was selected as bed material of choice in the operation of the PSBFBC system. This was done in order to meet criteria VI of the pre-design decision specification given in section 3.2. The physical and chemical analysis of Garside 14/25 sand supplied by the manufacturer is given in Table 4-1 (Garside Sands 2011). Comparison between the particle size distribution data supplied by the manufacturer of Garside 14/25 sand bed material and those measured during this investigation on as received basis (a.r) is shown in Appendix C.

Table 4-1: Physical and chemical analysis of Garside 14/25 sand

PHYSICAL PROPERTIES	**Size Range (mm)**		0.6 to 1.18
	Grain Shape		Sub angular to Rounded
	Colour		Yellowish Brown
	Specific Gravity		2.65
	Un-compacted Bulk Density (kg/m^3)		1560
	Nominal Effective Size (mm)		0.63 – 0.85
	Uniformity Co-efficient (mm)		<1.4
CHEMICAL PROPERTIES	**Name**	**Molecular Formula**	**Weight %**
	Silica	SiO_2	96.67
	Alumina	Al_2O_3	0.33
	Titania	TiO_2	0.03
	Iron	Fe_2O_3	2.4
	Magnesium	MgO	<0.01
	Calcium	CaO	0.01
	Sodium	Na_2O	0.03
	Potassium	K_2O	0.01
	Phosphate	P_2O_5	<0.01
	Manganese	MnO_2	<0.005
	Chromium	Cr_2O_3	0.02

4.2.2. Coal Samples

Bituminous coal from three different mines / location was used during the course of this research work. Two of the coals used were washed (gone through the cleaning process to remove the mud/shale stones present in them during the coal processing), while the third one is unwashed (did not go through the cleaning process and contains large amount of mud/shale stones). All the coals used were supplied by AB Sugar in particle size range of 12 – 25mm as received from the coal supplier. The thermal and chemical properties as well as the ash composition analysis of these coals are presented in Table 4-2.

Table 4-2: Coal sources and their chemical, thermal and ash composition analyses

MINE / LOCATION		Thoresby Washed *	Blyth Washed *	Blyth Unwashed *
PROXIMATE ANALYSIS	Moisture (wt.% ar)	4.2	12	10.5
	Volatiles (wt.% ar)	36.5	31.6	30.2
	Fixed carbon (wt.% ar)	54.9	52.5	53.1
	Ash (wt.% ar)	4.4	3.9	6.2
ULTIMATE ANALYSIS	Carbon (% ar)	72.9	66.5	67.8
	Hydrogen (% ar)	5.1	4.6	4.6
	Nitrogen (% ar)	1.7	2.1	1.6
	Sulphur (% ar)	1.9	0.9	1.1
ENERGY CONTENT - LHV (MJ/kg)		28.5	27.5	27.8
ASH ANALYSIS (% in Ash)	SiO_2	25.85	41.67	33.94
	Al_2O_3	29.34	24.93	25.70
	Fe_2O_3	19.67	9.94	17.17
	TiO_2	2.55	1.02	1.21
	K_2O	0.07	1.32	1.01
	MgO	1.28	1.97	1.44
	Na_2O	1.81	1.47	0.39
	CaO	11.02	12.42	12.22
	SO_3	8.41	5.26	6.93

** Values were obtained from coal characterisation analysis performed in the laboratory as part of this study*

4.3. Bed Material Calcination

Bed material calcination experiments were conducted to investigate the characteristic agglomeration behaviour of Garside 14/25 sand material at high temperature fixed bed conditions using an electrically heated high temperature furnace (Vecstar VF1) with a maximum furnace operating temperature of 1500°C. The furnace is connected to a continuous air supply for combustion purposes and exhaust ventilation to remove flue gas from the system. The furnace temperature was set to an investigating temperature of choice (800, 1000 or 1200°C) and allowed to reach the set temperature after which the sample in a high temperature ceramic crucible was placed in the furnace for a known duration of time.

At the end of the experimental run, the ceramic crucible containing the Garside 14/25 sand or mixture was removed from the furnace and allowed to cool down (to room temperature in a glass desiccator containing silica gel desiccant) before carrying out visual inspection, weight change measurements and particle surface morphology characterisation. The particle surface morphology characterisation was completed using a scanning electron microscope (SEM) equipped with energy dispersed x-ray (EDX) (see section 4.6.2 and 4.6.3). The weight of Garside 14/25 sand, coal and coal ash, both before and after the investigation were measured using Precisa 165 (BJ 410C) weighing scale, which has a readability and repeatability of 0.01g.

4.3.1. Sample Preparation

4.3.1.1. Garside 14/25 Sieving

A 25kg bag of Garside 14/25 sand bed material supplied from AB Sugar was divided into two halve fractions (primary sample: two parts of 12.5kg each) using

a riffle splitter. One half of the primary sample was further subdivided into eight fractions to obtain eight representative samples (eight parts of 1.56kg each). One portion of the eight representative samples of the Garside 14/25 sand was sieved using sieve pans and a sieve shaker into four different size fractions as follow: <212µm, 212µm - 599µm, 600µm - 999µm and >1000µm denoted as pan, 212µm, 600µm and 1000µm respectively. The pan fraction was discarded and the remaining three different size fractions were placed in plastic sample bags, labelled and stored. A second portion of the eight representative samples was stored in a plastic sample bag and labelled as raw (un-sieved).

4.3.1.2. Coal Preparation

Each coal type was supplied in 20kg bags from AB Sugar with particle size range of 12 – 25mm and was divided into two halve fractions (primary sample: two part of 10kg each) using a riffle splitter. One half of the primary sample was further subdivided into eight fractions to obtain eight representative samples (eight parts of 1.25kg each). One portion of the eight representative samples was crushed using a jaw crusher to obtain particle size less than 6mm (< 6mm). This was further milled to less than 1mm (< 1mm) particle size using Humboldt pulveriser mill. The pulverised coal of <1mm particle size was sieved into three size fractions as follows <212µm, 212µm – 599µm and >600µm denoted as pan, 212µm and 600µm respectively. The pan and 600µm fractions were discarded while the 212µm size fraction was stored in a plastic sample bag and labelled.

4.3.1.3. Ash Preparation

A second portion of Thoresby washed coal eight representative samples prepared earlier in section 4.3.1.2 was taken and processed following the crushing, pulverising, sieving and storing approach detailed in the section. 10g of the 212µm size fraction of the coal was measured into a high temperature

ceramic crucible. The ceramic crucible containing the coal was placed in a high temperature furnace connected to a continuous air supply of flow rate 15 litres/minute operating at 815°C and was left inside for 1 hour to generate ash. The ceramic crucible containing the ash was removed from the furnace after 1 hour and allowed to cool down to room temperature in a glass desiccator containing silica gel desiccant. After cooling, the coal ash was poured into a plastic sample bag, labelled and stored. The ashing process was repeated until 10g of coal ash was generated.

4.3.2. Calcination Procedure

Figure 4-2 shows the picture of the electrically heated high temperature furnace used for the calcination process. The electrically heated high temperature furnace was turned on using the power switch and the furnace temperature was set using the temperature heating controller to a ramp rate of 20°C/minute and a set point of 800°C, 1000°C or 1200°C depending on the temperature requirement for the investigation.

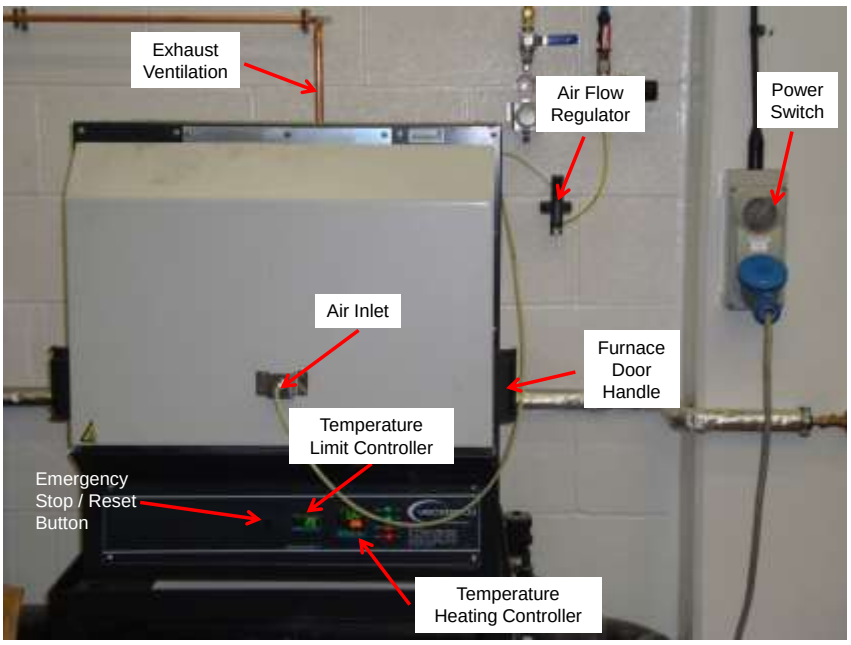

Figure 4-2: High Temperature Furnace (Vecstar VF1) used for calcination

The limit or over temp controller was set to 50°C above the set point temperature of the furnace. Air flow rate supply into the furnace was set at 15litres/minute using the air flow regulator to allow continuous supply of air into the furnace.

4.3.2.1. Pure Garside 14/25 Sand Calcination

10g of each size fraction collected and stored discussed in section 4.3.1.1, as well as a representative sample of the raw (un-sieved) Garside 14/25 sand, were measured and placed in different uncovered high temperature ceramic crucibles. The high temperature furnace was allowed to reach the set temperature of 800°C, 1000°C or 1200°C after which the ceramic crucibles containing the Garside 14/25 sand of different size fractions were placed in the furnace and left inside for 1 hour. After 1 hour, the ceramic crucibles were taken out of the furnace and placed in a glass desiccator containing silica gel desiccant and allowed to cool down to room temperature. On cooling, the samples were visually inspected to observe colour change and weighed to determine the weight loss during calcination before being stored in 7ml glass vials and labelled prior to SEM – EDX sample preparation. A second set of calcination tests were also carried out at 1000°C and 1200°C for a longer heating period of 4 hours using fresh Garside 14/25 sand each time following the procedures detailed above.

4.3.2.2. Garside 14/25 Sand and Coal or Ash Mix Calcination

9g of the un-sieved Garside 14/25 sand and 1g of the sieved 212µm coal size fraction prepared in section 4.3.1.2 were measured to make Garside 14/25 sand to coal mixture of 90% to 10% (ratio 9:1). The measured Garside 14/25 sand and coal were thoroughly mixed and poured into a high temperature ceramic crucible and place into the high temperature furnace after it has reached the set temperature and left inside for 4 hours. The ceramic crucible was taken out of the furnace after 4 hours and placed in a glass desiccator containing silica gel

desiccant and allowed to cool down to room temperature. After cooling down, the sample was visually inspected before been stored in a 7ml glass vial and labelled prior to SEM – EDX sample preparation and analysis (see section 4.6). Procedures detailed above was repeated for the calcination of Garside 14/25 sand to coal mix of 80% to 20% (ratio 8:2) and Garside 14/25 sand to ash mix of 90% to 10% (ratio 9:1) using coal ash prepared in section 4.3.1.3.

4.3.3. Percentage Weight Loss

The percentage weight loss that occurred during calcination of pure Garside 14/25 sand bed material was determined using equation 4.1.

$$\%\ \text{weight loss} = \frac{w_i - w_o}{w_i} \times 100 \tag{4.1}$$

where w_i is the initial weight before calcination and w_o is the final weight after calcination.

4.4. Industrial Scale FBC Combustor

The industrial FBC system is a 23MW lump coal combustor system used to generate hot gas required for drying pressed pulp from sugar beet processing. A schematic diagram and bed floor plan of the industrial FBC system are given in Figure 1-1 and Figure 4-3 respectively. As shown in Figure 4-3, the industrial FBC consists of a sand top-up addition port, 2 “flicker feeder” coal feeders, 4 LFO light-up burners, 2100 pieces of (1” sized) distribution nozzles and 4 multipoint thermocouple housings (A, B, C and D). Each thermocouple housing consists of two type N thermocouples (one to measure the upper bed temperature, while the other measures the lower bed temperature) with a gap of 125mm apart from each other as shown in Figure 4-4.

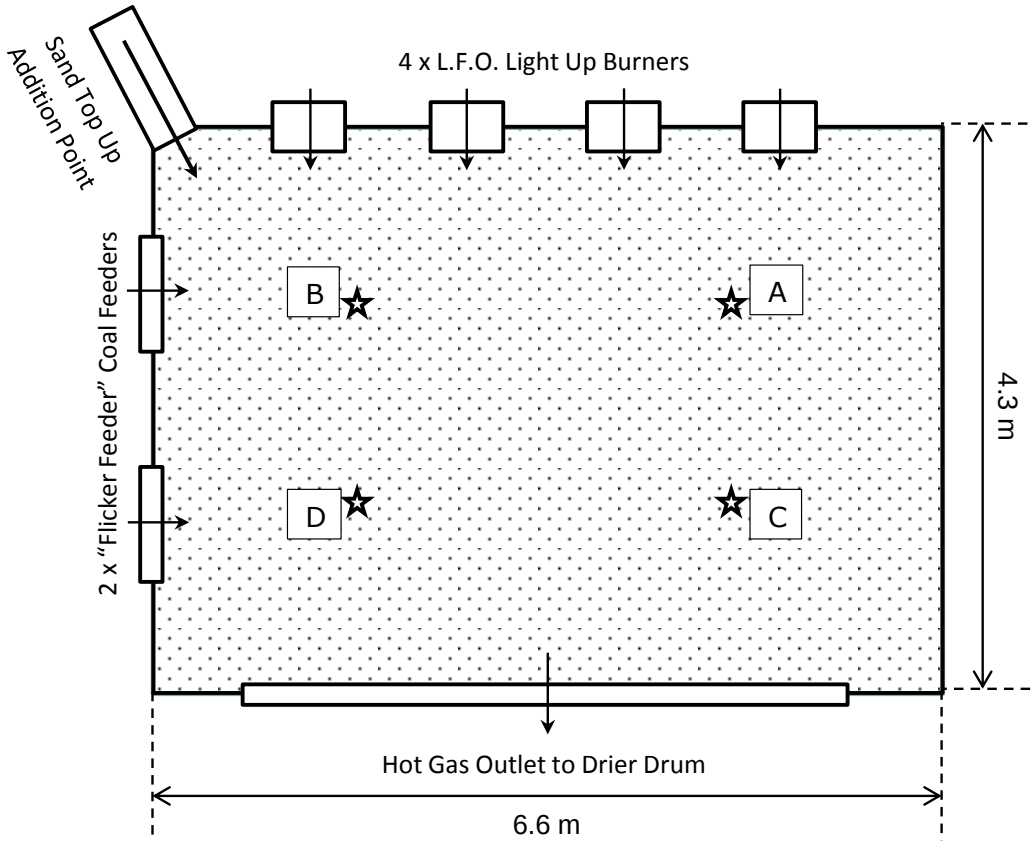

Figure 4-3: Schematic diagram of the floor mapping of the industrial FBC showing the positions of its various components

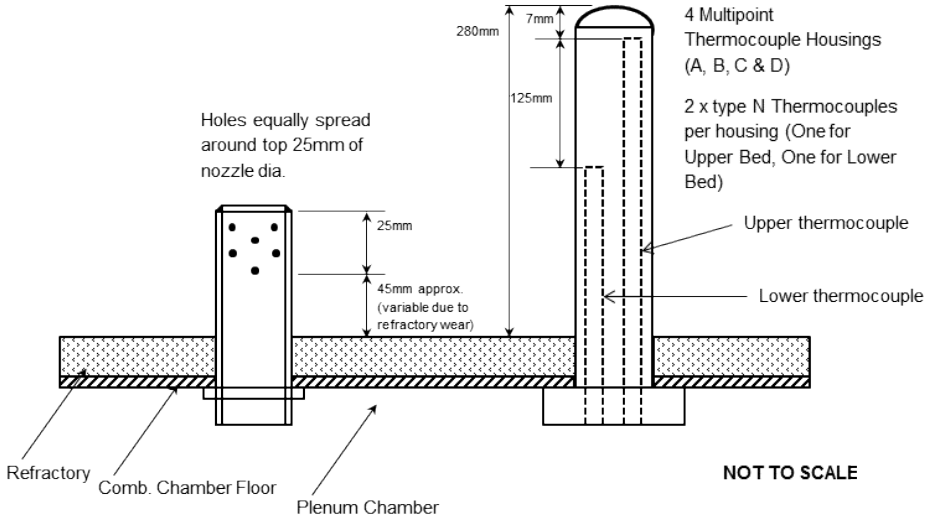

Figure 4-4: Schematic diagram showing the details of a thermocouple housing

At start-up, 12 tons of Garside 14/25 sand bed material is poured into the FBC to attain a static bed height of approximately 25cm. The FBC bed is then heated by burning LFO using the four LFO burners. During this same period, about

50,000kg/h of fluidising was gradually introduced into the bed. The heating of the bed is continued until a bed temperature of 900°C is attained at fully fluidised condition (expanded bed height of 50cm) after which, the LFO burner are turned off and the coal feeder is switched on at an average coal feeding rate of 2.5 tph to continuously supply lump coal of particle size 12 – 25mm. In order to maintain the bed temperature between 900 and 950°C.

Due to the shattering of Garside 14/25 sand bed material particles into smaller fragments when the bed material particles collides with each other at high temperature combined with the high operating fluidising air velocity of the FBC, a lot of the bed material particles get entrained and carried away via the hot gas outlet into the drier drum. In order to maintain the bed height in the industrial FBC, Garside 14/25 sand bed material is continuously added to bed via the sand top up addition port at an approximate rate of 1 tpd throughout the course of FBC operation. The industrial FBC is continuously operated at these condition until sintering and agglomerate formation and defluidisation of the bed occurs which typically happens between 6 and 8 weeks of continuous operation.

At this point, the industrial FBC is shut-down and allowed to cool down to room temperature after which it is opened up to dig out the agglomerated bed. Typically, it takes about 5 working days from the beginning of the shutdown of the FBC to restarting back up again. Samples of the removed agglomerated bed materials from the industrial FBC was obtained from the combustion of unwashed Blyth coal and washed Thoresby coal and analysed as part of this study using SEM, EDX and XRF characterisation techniques.

4.5. PSBFBC Coal Combustion

Experiments were conducted to investigate sintering and agglomerate formation during lump coal combustion in the PSBFBC system earlier designed and

described in chapter 3 using Blyth washed and unwashed coals. The PSBFBC start-up was initiated with the use of Watlow electrical heaters to attain a fluidised Garside 14/25 sand bed temperature of 600°C after which lump coal was continuously fed into the BFBR until a bed temperature of between 900 – 950°C was achieved. This temperature was maintained throughout the duration of each experimental run by varying the lump coal feed-rate and / or fluidising air flowrate.

During the investigation, attention was given to the combustion and bed temperature in the BFBR, temperature and pressure profile across the BFBR, fluidising air flowrate and composition of flue gas produced. All of these data were measured and logged every 10 seconds on the PSBFBC computer. At the end of each experimental run after the PSBFBC system has cooled down to room temperature, the flange at the top of the BFBR was removed in-order to carry out visual inspection of the bed, measure the bed height and collect some bed material sample for characterisation and analysis. Other measurements taken include the amount of lump coal used for each experimental run and the amount of cyclone reject collected. The coal preparation procedure and bed material inventory methodology are described in Appendix D.

4.5.1. Normal Combustion Procedure

The combustion of lump coal was performed at a bed temperature of between 900 and 950°C in the PSBFBC at atmospheric pressure. Pictures of the PSBFBC combustion rig used for this investigation are presented in Appendix E highlighting various component and parts of the system. The procedure implemented during the combustion process has been divided into five stages namely: pre start-up preparation, start-up, coal combustion, shut-down and emergency stop or shutdown.

4.5.1.1. Pre Start-up Preparation

The measured and sieved 6kg of Garside 14/25 sand described in Appendix D-2 was poured into the BFBR section of the PSBFBC to attain a static bed height of 20cm. This was done by removing the flange located at the top end of the BFBR freeboard zone and was sealed back using appropriate bolt, nuts, washers and high temperature thermiculite 815 gasket for a standard 6 inches flange. A known amount of the chosen coal of particle size range 10 – 19mm prepared by following the procedures detailed in Appendix D-1 was measured using a Kern and Shon GMBH weighing scale (model: ECB 20K20) with a readability and repeatability of 20g. The measured coal was poured into the coal hopper which has a holding capacity of up to 17kg and was sealed with the hopper cover using appropriate bolts, nuts, washers and rubber O-ring. A pre start-up checklist given in Appendix F was completed and signed off as part of the pre start-up preparation.

4.5.1.2. Start-up

The fluidised bed heater control system was activated by using the main switch and the heating temperature controller was set to a temperature ramp rate of 400°C/hour and a set-point of 850°C. The temperature limit controller was set to 890°C which is 40°C above the set-point of the heating controller and the “on” button for the BFBR heater control system was pressed to start the heating cycle for the BFBR heaters. After 20 minutes of operation, the fluidising fan was turned on and ramped up to a speed of 2500rpm using the Super Drive G2 software installed on the PSBFBC computer. Manual ball valve 2 was opened and regulated to a fluidising air flowrate of 200 litres/minute measured using the variable area flowmeter, and was allowed to operate at this condition for another 20 minutes after which the fluidising air flowrate was further increased by 60

litres/minute to 260 litres/minute at a time interval of 40 minutes from the beginning of the heating cycle.

This procedure was repeated at 60, 80,100, and 120 minutes from the beginning of the heating cycle and the fluidising air flowrate was increased by 60 litres/minute each time to 320, 380, 440 and 500 litres/minute respectively at each time interval. After 120 minutes (2 hours) of continuous operation from the beginning of heating cycle at 500 litres/minute fluidising air flowrate, the PSBFBC was further allowed to continue operating at this conditions until a bed temperature of 600°C was achieved in the BFBR. This normally takes between 140 and 150 minutes from the beginning of the heating cycle. During this period, all the PSBFBC temperatures, pressure and fluidising air flowrate data were monitored, collected and logged on the PSBFBC computer.

4.5.1.3. Coal Combustion

After a bed temperature of 600°C has been reached in the BFBR, lump coal was fed into the BFBR. The coal feeder inverter frequency was set to 4Hz, which equates to a coal feeding rate of about 2.2kg/hour (for more information on the coal feeder calibration which shows comparison between coal feeder frequency and coal feeding rate, see Appendix A). As soon as the lump coal starts entering the BFBR, the temperature measured across the six thermocouples in the BFBR starts to increase, which was observed in the displayed BFBR temperature chart on the PSBFBC computer.

The bed temperature was left to continue increasing at this condition until a bed temperature of 900°C was achieved after which the fluidising air flowrate into the BFBR was increased to 640 litres/minute using manual valve 1. The BFBR was left to continue operating at this condition and stabilise to a bed temperature between 900 and 950°C. As it is very important to maintain the bed temperature

between 900 and 950°C, the bed temperature was continuously monitored and maintained throughout the duration of each experimental run by varying the lump coal feed-rate and / or fluidising air flowrate using the operating chart given in Appendix G running between 70 and 90% excess air conditions.

In addition to the temperature and pressure data continually collected and logged every 10 seconds on the DT80 series data logger, the flue gas composition which can be used to predict the state of coal combustion in the PSBFBC was also measured and logged. This was done using the flue gas sampling probe cooled with water connected to a gas conditioning unit for the condensation and removal of vapour and ash particles before entering into to the gas analyser to measure the amount of oxygen (O_2), carbon dioxide (CO_2), carbon monoxide (CO) and oxides of nitrogen (NO_x) present in the flue gas.

The side of the coal hopper was regularly tapped at 15 minutes time interval during each experimental run and / or as seen fit using a rubber mallet to clear any coal bridging or blockage that might occur in the system. The need for additional tapping was identified by a sudden progressive decrease in bed temperature and the compositions of CO_2 and NO_x measurement in the flue gas stream.

4.5.1.4. Shut-down

At the end of the combustion run, the coal feeder inverter was turned off and the fluidising fan speed was reduced to 1500rpm and allowed to continue operating at this condition until the BFBR bed temperature drops below 200°C after which a shutdown checklist given in Appendix F was completed and signed off as part of the shutdown procedure.

4.5.2. Crash-stop Combustion Procedure

The pre start-up preparation and start-up methodologies for this setup are the same as those for the normal combustion procedure detailed in sections 4.4.1.1 and 4.4.1.2 respectively. The only difference is the additional method to the previously described combustion procedures detailed in section 4.4.1.3 in order to attain the crash stop phenomenon.

The earlier described combustion procedures detailed in section 4.4.1.3 is followed to attain a bed temperature of between 900°C and 950°C and maintained for 1 hour. After which, the fluidising air and coal feeder are shut off for a period of 25 minutes. After the 25 minutes time interval, the fluidising fan was re-started to the same fan speed (air flowrate) and the coal feeder to the same motor speed (frequency) before it was shut off. The PSBFBC bed was then allowed to reach a temperature of between 900 and 950°C. This bed temperature was maintained for 1 hour after which the fluidising air and coal feeder shut off procedure was repeated. These procedures were repeated about two to four times during the course of the combustion run during which all the process parameters were collected and logged. At the end of the experimental run, the shutdown methodology detailed in section 4.4.1.4 was followed.

4.5.3. PSBFBC Bed Material Sampling and Other Measurements

Discussion in this section covers the procedures implemented for the visual inspection of the BFBR bed, bed height measurements, bed material sampling, cyclone reject collection and coal usage determination in the PSBFBC system. The BFBR bed visual inspection, bed height measurement and bed material sampling were completed in this order after the removal of BFBR flange at the top of the BFBR freeboard zone. The bed material samples and cyclone rejects collected were measured using Precisa 165 (BJ 410C) weighing scale which has

a readability and repeatability of 0.01g. All the procedures outlined and discussed in this section were carried out and repeated for every experimental run after the PSBFBC system had cooled down to room temperature.

4.5.3.1. Visual Inspection

The flange located at the top end of the BFBR freeboard zone was removed and with the use of a flashlight, the BFBR bed was visually inspected for signs of sintering or agglomeration. Pictures of the bed were also taken for a closer observation of the bed surface in order to identify sign of sintering or agglomerate formation that might have occurred in the bed during the combustion run.

4.5.3.2. Bed Height

A 2.5m long probe with a flat square plate of dimension 20mm by 20mm at one end was inserted into the BFBR until the flat plate end touches the surface of the bed. The length at which the plate touches the bed surfaces was marked on the probe against the flange and this was repeated at six other random locations across the surface of the bed. After this, the probe was removed from the BFBR and the length (height) from the end of the flat plate to each marked point on the probe was measured using a measuring tape and recorded. This measured length equates to the height of the free space above the bed. An average of the measured lengths was found and the bed height was calculated using equation 4.2.

$$\text{Bed height (mm)} = 1800 - L_{B(av)} \quad (4.2)$$

where 1800 is the total length of the fluidising and freeboard zone of the BFBR in mm and $L_{B(av)}$ is the average of the measured height of the free space above the bed in mm.

4.5.3.3. Bed Material Sampling

The bed material sample was collected using the bed material sampling probe designed and described in section 3.6.8. The sampling probe was lowered into the BFBR, via the top flange opening, and manoeuvred into the bed until the sample collector is filled after which it was removed from the BFBR. The collected sample was weighed, placed in a plastic sample bag, labelled and stored prior to the SEM-EDX and XRF sample preparation and analysis (see section 4.6). The above procedure was repeated to collect a second sample. A measured amount of fresh Garside 14/25 sand bed material equal to the total amount of bed material samples taken (typically ≤ 166g) was measured and poured back into the BFBR after which the flange was sealed.

4.5.3.4. Cyclone Reject

During lump coal combustion in the PSBFBC system, the solid (ash, char and or bed material) particles entrained in the updraft flue gas from the BFBR carried into the gas-solid cyclone are separated into a solid (cyclone reject) stream. The flue gas stream was removed by extraction fan via the exhaust and the solids were collected in the cyclone reject container shown in Appendix E (Figure E-1). The collected reject was measured, placed in a plastic sample bag, labelled and stored.

4.5.3.5. Carbon in Ash

This was done by following the laid out procedures in BS 1016-104.4:1998 (ISO 1171:1997) for the determination of ash in coal and coke.

4.5.3.6. Coal Used

The top cover of the coal hopper was removed and using the same coal type as the one currently in the hopper prepared in Appendix D, the coal hopper was

filled back to the top. The amount of coal poured into the coal hopper to fill it back was measured using Kern and Shon GMBH weighing scale (model: ECB 20K20) with a readability and repeatability of 20g and recorded. This value is assumed to equate to the amount of coal used for the experimental run.

4.5.4. Particle Size Distribution of PSBFBC Bed Material

The particle size distribution analysis of the Garside 14/25 sand bed material was carried out at two stages. The first stage was carried out during the bed inventory prior to the combustion procedure (detailed in section Appendix D) while the second stage which is described here was carried at the end of the experimental investigation.

4.5.4.1. Bed Material Removal from the PSBFBC

After the PSBFBC system has been switched off and allowed to cool down to room temperature, the fluidising air duct connected to the plenum chamber shown in Appendix E (Figure E-1) was removed. This was followed by the removal of the bars supporting the PSBFBC frame running through the base of the plenum chamber flange. A rectangular cardboard paper of size 1400mm by 1200mm was laid on the floor onto which a plastic sheet of at least the same size as the cardboard paper was also laid to collect the sand. The bolts, nuts and washers attaching the plenum chamber and distribution plate to the fluidising zone were removed and the sand was allowed to flow out and pour onto the laid cardboard paper and plastic sheet. The collected bed material was visually inspected for signs of sintering and agglomeration after which it was packed into a sample bucket, labelled and stored.

4.5.4.2. Particle Size Distribution Analysis Procedure

The collected and stored used bed material described in section 4.5.4.1 or fresh bed material described in Appendix D was sieved using sieve pans and a sieve shaker. The sample/s were sieved into nine different size fractions as follow: <212µm, 212µm – 424µm, 425µm – 599µm, 600µm – 849µm, 850µm – 1179µm, 1180µm – 1669µm, 1770µm – 2359µm, 2360µm – 3349µm and >3350µm denoted as pan, 212µm, 425µm, 600µm, 850µm, 1180µm, 1770µm, 2360µm and 3350µm respectively. Each collected size fraction was weighed and recorded using Precisa 165 (BJ 410C) weighing scale, which has a readability and repeatability of 0.01g. The different size fraction were mixed back together for use in the pre start-up preparation detailed in Appendix D for the fresh Garside 14/25 sand bed material or stored away back in the sample bucket for the case of the old bed material.

4.6. Bed Material Characterisation

Characterisation of the loose bed material, agglomerated bed material and calcinated bed material were undertaken using x-ray florescence (XRF), scanning electron microscopy (SEM) and energy dispersed x-ray (EDX. The selection of these characterisation techniques were based on the findings and conclusions drawn from the literature survey (chapter 2) based on their suitability for sintering and agglomerate formation investigation. The XRF analysis was carried out using a Bruker S8 Tiger high end wavelength dispersed XRF spectrometer equipped with Spectra plus software version 2.0 and Quant-express software for data analysis. SEM and EDX analysis were done using an SEM Quanta 600 equipped with EDX Genesis 4000i X-ray analyser. Details of the sample preparation, methods and analysis of results generated from these characterisation techniques are outlined in this section.

4.6.1. X-Ray Fluorescence (XRF)

4.6.1.1. Introduction

X-ray fluorescence (XRF) works by bombarding the prepared sample being analysed with high energy x-ray causing the ejection of electrons from the inner shells (typically K and L) surrounding the nucleus of the atoms present in the sample. The ejection of this electron renders the atom unstable and in order to attain a stable nature, an electron from the outer shell is released to replace the ejected one. This transition causes the release of excess energy in the form of photon referred to as x-ray fluorescence (XRF) as shown in Figure 4-5. The energy of the photons emitted has a characteristic nature distinctive to individual elements present in the sample, which is detected and measured to identify and quantify the element/s present in the sample. XRF analytical technique can be used to characterise inorganic samples existing in various forms namely liquids; solids and powders (prepared as pressed pellets or fused beads).

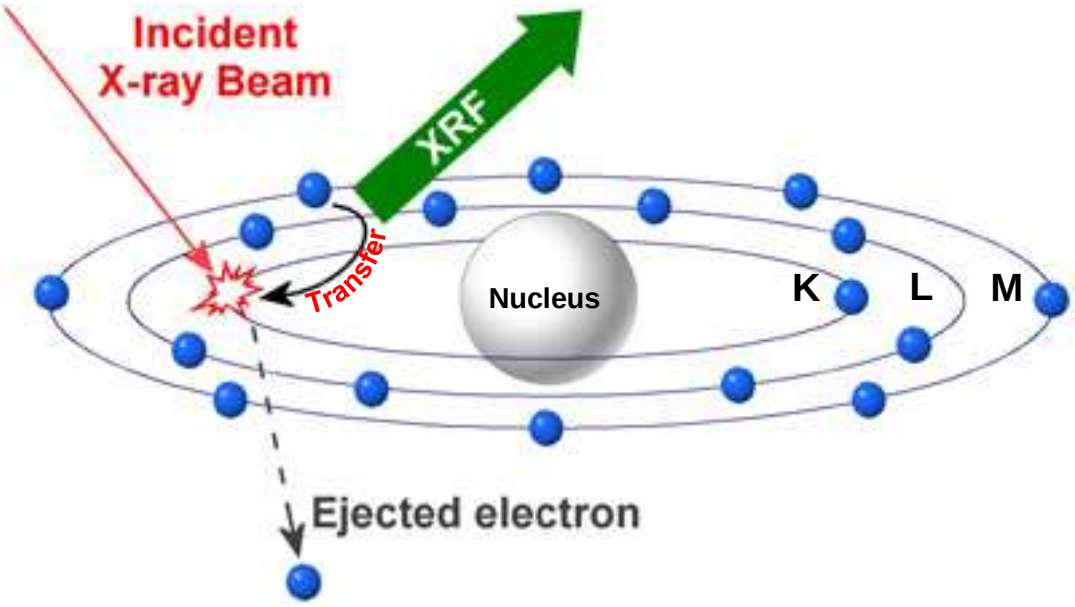

Figure 4-5: Principle of a typical XRF operation

4.6.1.2. Sample Preparation and Method

XRF characterisation was done using powder samples prepared in the form of 10mm diameter pressed pellets. The pressed pellet was prepared by milling the sample to be characterised into powder (particle size ≤355µm) using Humboldt pulveriser mill. The finer or smaller the particle size of the powder is, the firmer it holds together when pelletised. The milled powder sample was thoroughly mix after which 500mg (0.5g) of the sample was measured and mixed with 100mg (0.1g) of inert wax binder in the proportion of (5:1) sample to wax binder ratio before been pelletized using a Graseby Specac pellet press.

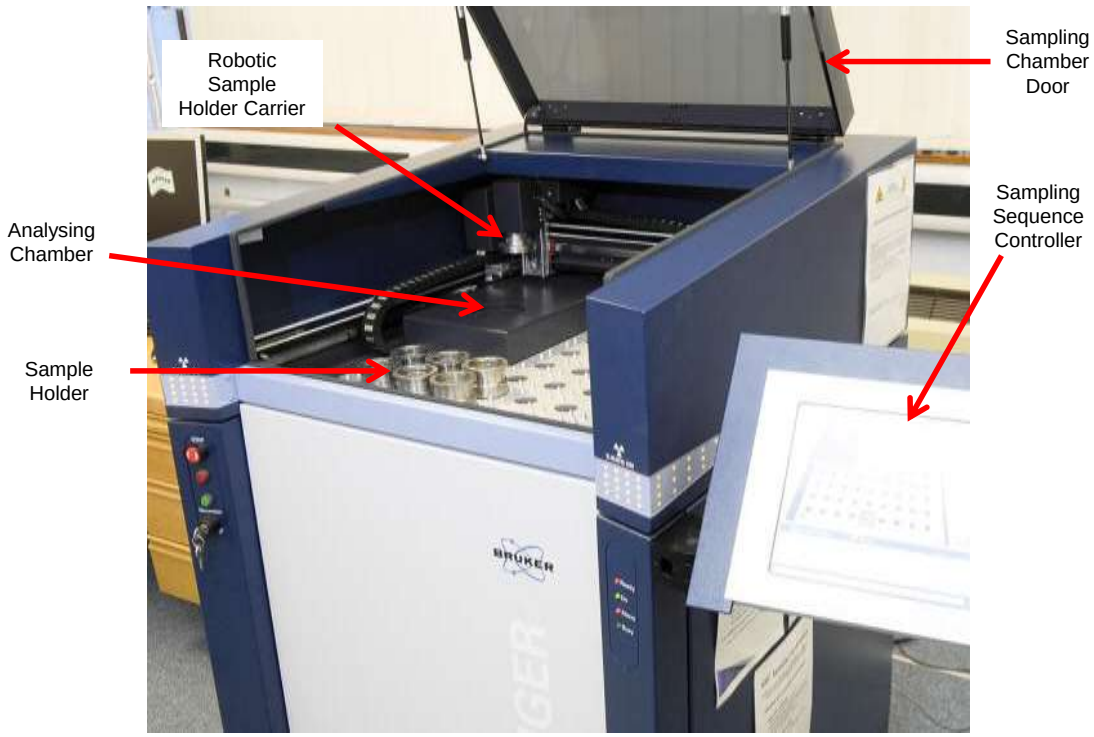

Figure 4-6: Bruker S8 Tiger high end wavelength dispersive XRF

The made pressed pellet was placed and tightly secured in an 8mm aperture size sample holder before been loaded into the sampling chamber of the XRF analyser as shown in Figure 4-6. The door to the sampling chamber was closed and with the use of the XRF sampling sequence controller, XRF analysis was initiated. The analysis requires the exact measured weight of the pellet, the

selection of the type of analysis (element or elemental oxide) and the detection routine of the analysis (duration). For the case of this work, best detection routine which has analysis duration of seven minutes was used.

Results generated from the XRF analysis were processed using the Spectra plus software version 2.0 and Quant-express software loaded on the XRF computer system. The results were presented in a quantitative format with details of the elemental oxides identified to be present in the sample with their respective quantities in weight percentages and an accuracy and precision of ±5% and ±0.5% respectively for a measured weight percentage composition above 1wt%. The results were stored as excel format and processed to be presented either in the form of charts or tables.

4.6.2. Scanning Electron Microscopy (SEM)

4.6.2.1. Introduction

A typical column of a SEM is shown in Figure 4-7. SEM works based on the generation of monochromatic electron beams by the electron gun under vacuum. These electron beams are collimated by magnetic condenser lenses and apertures, which are then focused onto a selected region of the sample by a final objective lens (Reed 2005). When the beam of electrons interacts with the atoms present on the sample surface, various signals are produced such as back-scattered electron (BSE), secondary electron (SE), characteristic X-rays, transmitted electrons and specimen current. These signals are collected depending on the detector on the equipment and then processed. The BSE electrons, which are formed from the elastic scattering of reflected electrons from the surface of the sample, are often used for SEM imaging as also in the case of this study.

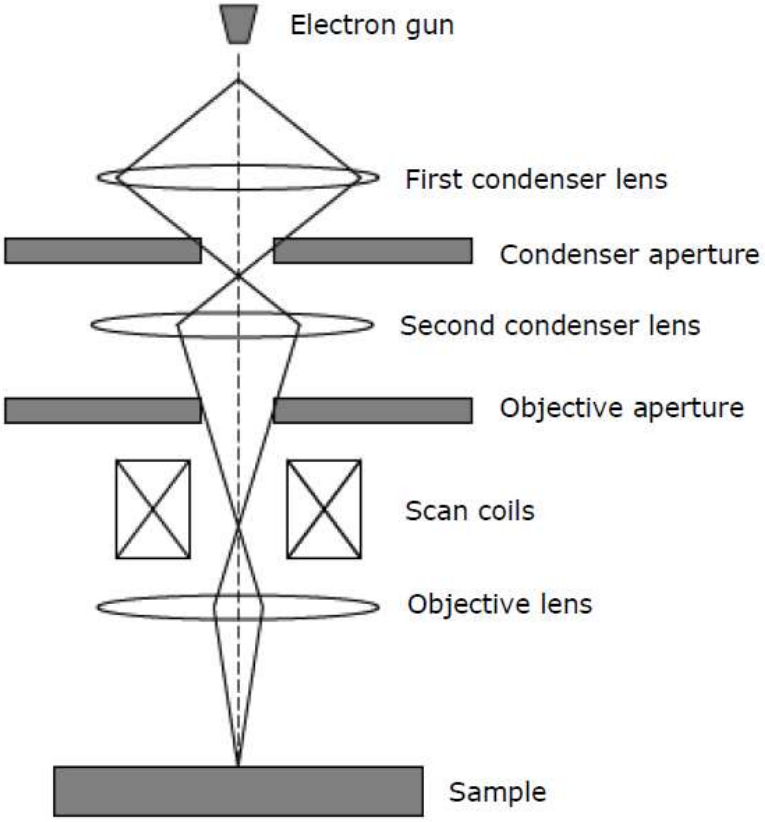

Figure 4-7: Typical electron-optical column of an SEM (Kobusheshe 2010)

4.6.2.2. Sample Preparation and Method

Two different types of SEM sample preparation techniques were used during this investigation namely resin blocks and carbon tabs. The resin block sample preparation was used for agglomerated bed material collected from the industrial operated FBC system in the PSBFBC and loose bed material sample collected from the PSBFBC. Resin block sample preparation is time consuming as it takes about three days on average to complete from start to finish. However, embedding the sample in resin block provides good quality images with high resolution because the analysis is carried out under high vacuum operation.

The carbon sticky tab sample preparation was used for the calcinated pure Garside 14/25 sand and mix with coal and coal ash produced from the calcination process as well as the loose Garside 14/25 bed material collected from the PSBFBC described in section 4.4.4.3. This sample preparation

technique takes about two hours to complete and can only be used for SEM analysis at low vacuum operation. Resin blocks manufacturing and carbon tabs making methodology are described in Appendix H-1 and Appendix H-2 respectively.

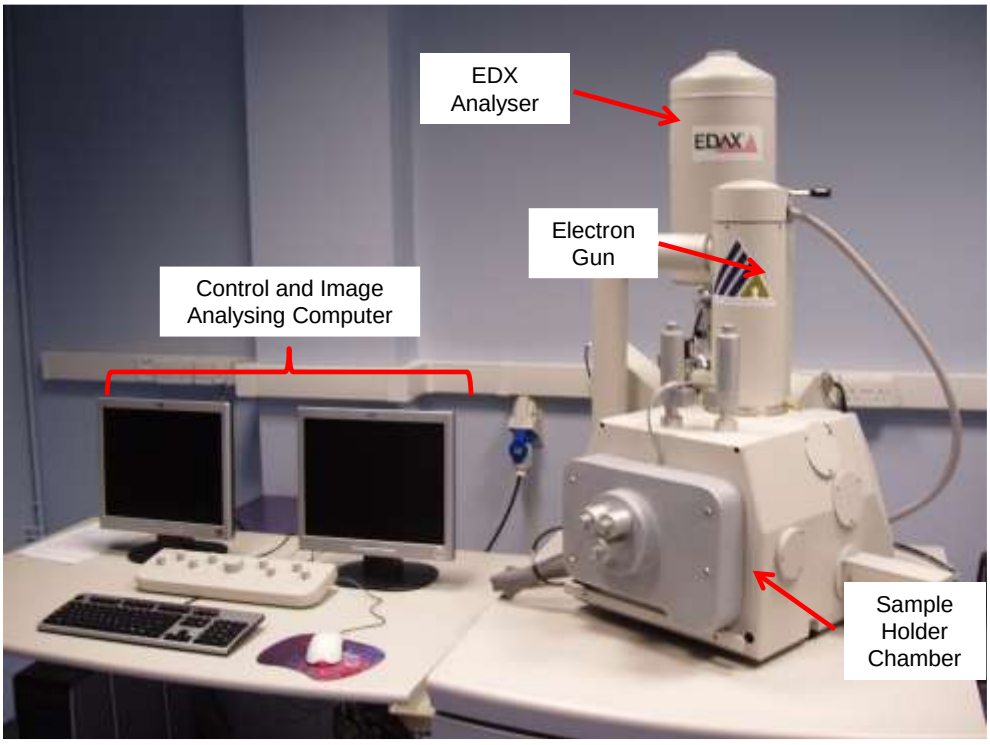

Figure 4-8: Quanta 600 SEM equipped with EDX Genesis 4000i X-ray Analyser

The prepared sample is mounted on the sample holder in the SEM sample holder chamber shown in Figure 4-8, which allows automated measurements of up to eighteen samples to be done. The SEM analysis was done using the backscattered electron (BSE) type detector, accelerated voltage 25kV operated under low vacuum mode for carbon tabs and high vacuum for resin blocks. Images of samples were taken at different magnifications of 50, 100, 150 and 300 times.

SEM characterisation results are shown in the form of micrograph images given in Figure 4-9 which shows typical SEM micrograph images from a resin block and carbon sticky tab analysis at different magnifications. The SEM micrographs

produced from a resin block analysis as shown in Figure 4-9a. provides a two-dimensional (2D) visual representation of the inter-particle interaction that occurs between particles present in the agglomerated sample. The presence of the binder responsible for this occurrence is also clearly shown. On the other hand, the SEM image generated from a carbon tab analysis shown in Figure 4-9b and c provides a three-dimensional (3D) visual representation of the samples been analysed. The carbon tab analysis also shows the surface morphology of the analysed sample as opposed to the resin block analysis which shows the smooth internal structure of the sample been analysed.

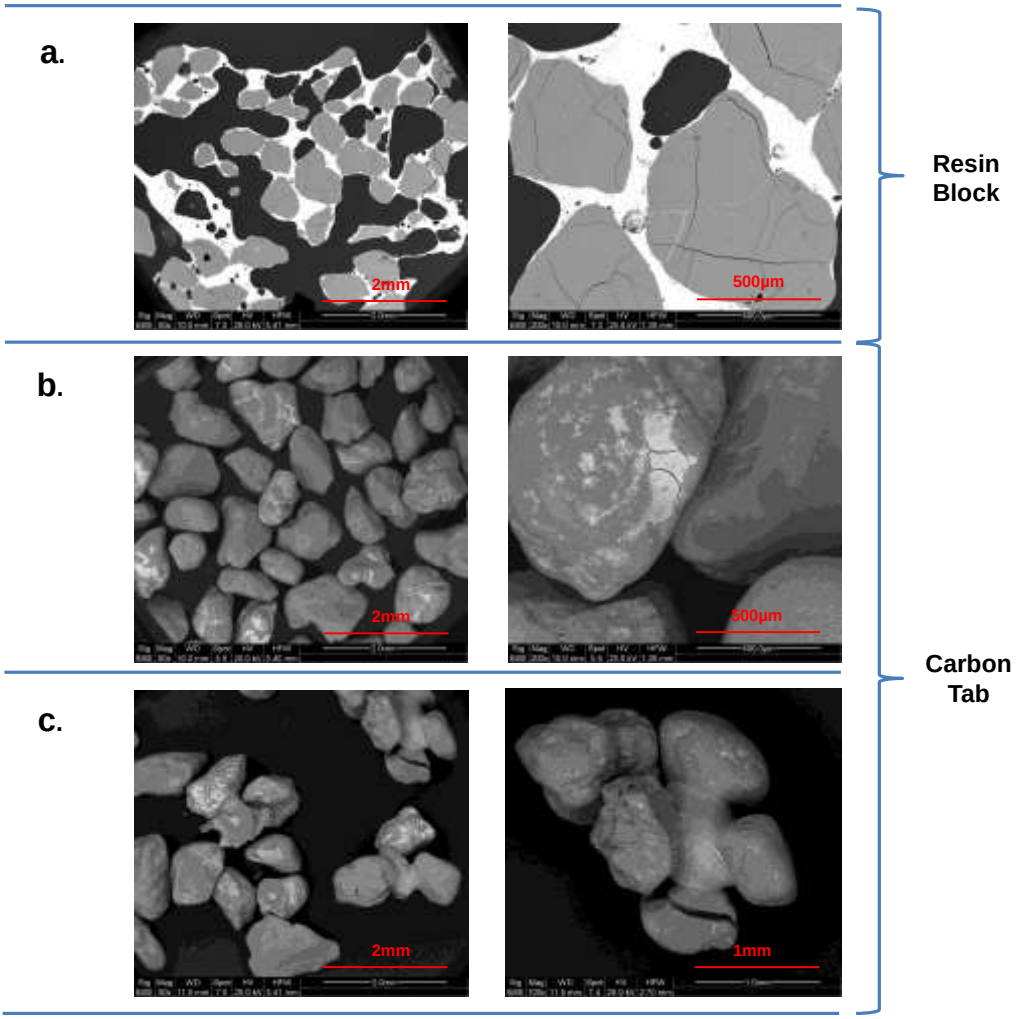

Figure 4-9: Typical SEM micrograph images from a resin block and carbon tab analysis at different magnifications. (a) Internal structure of agglomerated bed material. (b) Loose Garside 14/25 sand bed material. (c) Agglomerated calcinated pure Garside 14/25 sand

4.6.3. Energy Dispersed X-ray (EDX) Analysis

4.6.3.1. Introduction

Energy dispersed x-ray (EDX) is an elemental or chemical characterisation technique used in combination with SEM. One of the signals produced during the interactions between electrons beam and the atom present on the surface of the sample mentioned earlier is characteristic X-ray and continuum X-rays (Reed 2005). X-ray is formed when the electron beam removes an inner shell electron from the sample, causing a higher-energy electron to fill the shell and release energy. This causes an inelastic scattering of the reflected electrons from the surface of the sample. The characterisation abilities of X-ray are due to the unique atomic structure possessed by each element, which allows the formation of distinctive peaks based on the abundance of the element in the sample. The ability to identify the elemental composition of an agglomerated bed sample helps in understanding its formation mechanism.

4.6.3.2. Sample Preparation and Method

The sample preparation and method for EDX analysis are the same as discussed for SEM in section 4.6.2.2. In addition to the earlier discussed method, two forms of EDX analysis were utilised during this investigation namely EDX elemental spot analysis, and EDX elemental surface mapping. EDX elemental spot analysis is a semi - quantitative approach that measures and provides an estimate of the abundance of each element present in a particular spot of the sample.

EDX result for elemental spot analysis contains a SEM micrograph image, semi - quantitative elemental composition table and elemental composition spectrum as shown in Figure 4-10. The spot been analysed is denoted by the red “+” sign on the grey particle in the image and the elemental composition at this spot has

been identified and quantified by the EDX software which is summarised in the composition table.

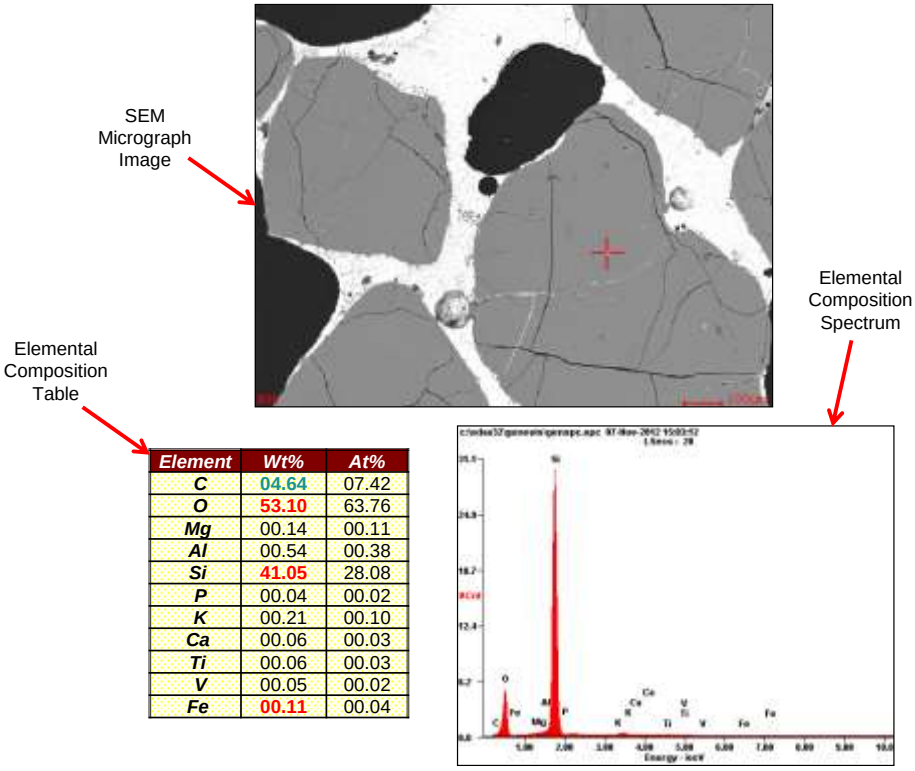

Element	Wt%	At%
C	04.64	07.42
O	53.10	63.76
Mg	00.14	00.11
Al	00.54	00.38
Si	41.05	28.08
P	00.04	00.02
K	00.21	00.10
Ca	00.06	00.03
Ti	00.06	00.03
V	00.05	00.02
Fe	00.11	00.04

Figure 4-10: Typical EDX elemental spot analysis of an agglomerated Garside 14/25 sand bed material sample and its elemental spectrum.

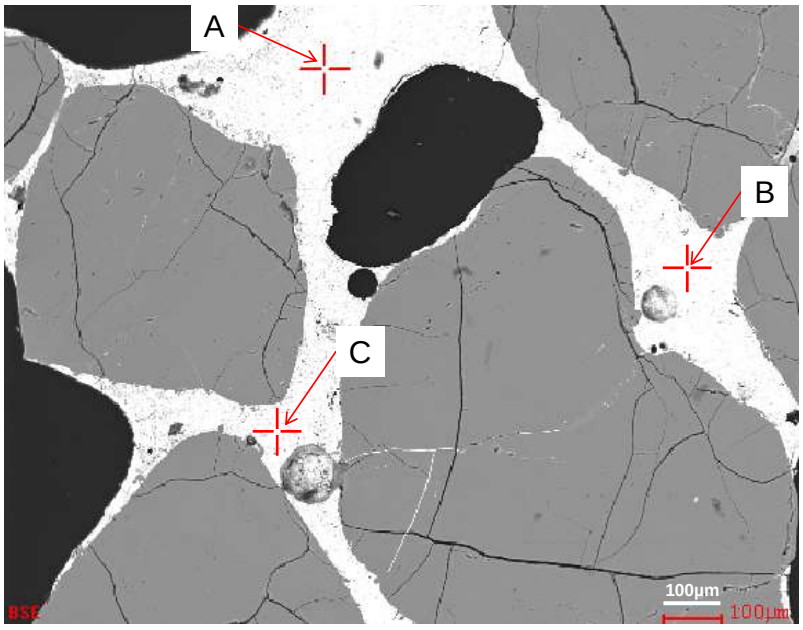

Figure 4-11: EDX micrograph showing the various spots within the same coloured /shade area in a sample frame where EDX elemental spot analysis was carried out

A viable assumption was made with the use of EDX elemental spot analysis technique during this study. This assumption is that the elemental composition of a single analysed spot within a sample frame exhibits a similar composition with identical areas with same colour / shade. This assumption is supported by the EDX analysis results obtained for spot A, B and C shown in Figure 4-11 which are presented in Table 4-3.

Table 4-3: Comparison of the elemental composition data obtained from various spots within the same coloured /shade area in sample frame using EDX elemental spot analysis technique

Spots	Weight Percentage (wt.%)										
	C	O	Mg	Al	Si	P	K	Ca	Ti	V	Fe
A	3.78	42.23	0.15	3.46	14.91	0.05	0.27	0.32	0.13	0.09	34.61
B	3.8	40.9	0.23	2.89	15.03	0.02	0.15	0.34	0.08	0.02	36.54
C	3.72	42.13	0.19	3.31	14.96	0.03	0.19	0.35	0.09	0.05	34.98
Average	3.77	41.75	0.19	3.22	14.97	0.03	0.20	0.34	0.10	0.05	35.38
STDEV	0.04	0.74	0.04	0.30	0.06	0.02	0.06	0.02	0.03	0.04	1.02
Variance	0.002	0.549	0.002	0.087	0.004	0.000	0.004	0.000	0.001	0.001	1.049

The EDX elemental surface mapping analysis is a qualitative approach, which produces a comprehensive visual representation of the elemental abundance across the surface of the sample. EDX elemental mapping of iron (Fe), silica (Si), aluminium (Al), potassium (K), and calcium (Ca) or vanadium (V), which has been identified from literature survey to cause sintering and agglomeration formation, were done as well as that of oxygen (O).

Figure 4-12a shows the distribution of Fe, Si, O, K, Al and V across the surface of the samples previously analysed in Figure 4-10 using EDX elemental spot analysis. From this analysis, the elemental composition of the particles present in the analysed sample can easily be identified as predominantly Si and O while the binder region shows the abundant presence of Fe, K, Al, V and O.

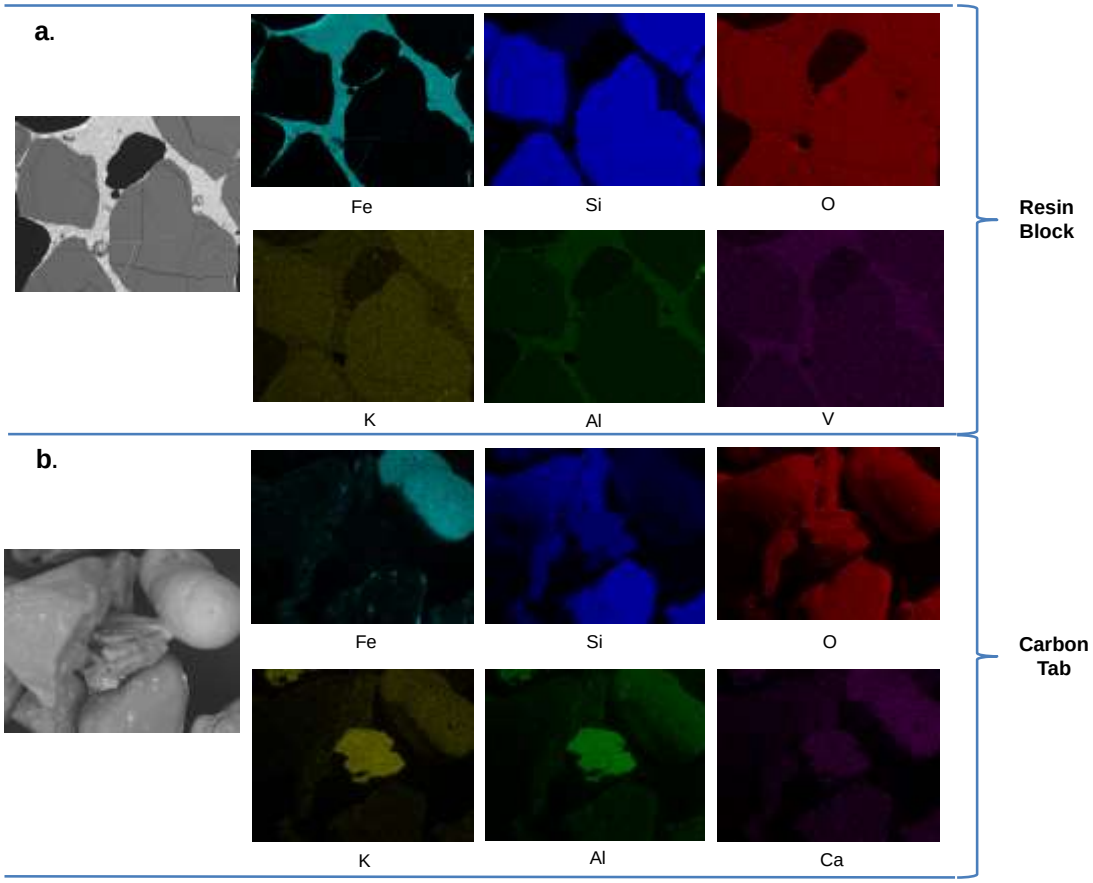

Figure 4-12: Typical EDX elemental surface mapping. (a) Internal structure of agglomerated bed material. (b) Agglomerated calcinated pure Garside 14/25 sand

The presence of large abundance of oxygen distributed across the surface of the samples shows that the elements identified exist as a compound in their oxide forms. The spread and overlay of this element also shows that there is a chemical interaction between them, which might suggest they possibly exist as a complex mineral compound. On comparing the EDX elemental surface mapping for a sample prepared on a carbon sticky tab shown in Figure 4-12b, it can be seen that the quality of the image generated from this analysis is of a lower resolution to that of a resin block. This observation is associated with the smooth analytical surface possessed by the resin block as opposed to the curved or natural surface exhibited by the carbon sticky tab sample.

CHAPTER FIVE

AGGLOMERATION BEHAVIOUR OF FLUDISED SAND DURING CALCINATION

5.1. Introduction

As identified from the literature survey detailed in chapter 2 that sintering and agglomerate formation in FB systems is a widely studied phenomenon in gasification and combustion processes especially for biomass and low rank coal fuels, with few research interest of this problem in high ranked coal applications, which needs to increase. Also, as part of the discussion in the same chapter, mechanisms responsible for sintering and agglomerate formation suggested by various scholars were identified which led to proposing a comprehensive sintering and agglomerate formation mechanism for lump coal combustion in a FB system given in section 2.5.4 as part of this studies. In order to study the applicability of this proposed mechanism, various fundamental aspects of this mechanism needs to be studied, which have been identified, investigated and discussed in this chapter.

The first fundamental aspect of the proposed mechanism that was identified, is based on the well-established fact in literature that sintering and agglomerate formation is an ash related problem which develops between the bed material and ash particles present in the FB system (Unsworth et al. 1991; Teixeira et al. 2012). Previous researchers into this subject area have focused on this bed material and ash relationship either in the form of chemical reactions or bed

material and ash particle interactions. They have however ignored the inter-particle interaction that may occur between the bed material particles at high temperatures in the form of strong sintered bridges. As previously suggested in section 2.8, it might be possible for sintering to occur between the bed material particles when exposed to high temperature in the absence of fuel ash following solid state sintering phenomenon which exist in ceramic processing (Rajput 2007; Tanaka et al. 2012). Hence, the possibility of this occurring has been investigated using FB bed material Garside14/25 sand earlier described in section 4.2.1.

Secondly, during the combustion of coal as described in section 2.3, it was identified that coal undergoes three stages namely heating and drying, devolatilisation and volatile combustion, and char combustion during which heat, flue gases and ash are produced as by-product (Basu 2006; Liu 2011a). Ash which has been identified by previous scholars as the cause of sintering is only one of the by-product produced from the combustion process. It is therefore seen as very important to establish the sole contributory effect of ash to sintering and agglomerate formation in the absence of other factors present during the combustion process. The ability to do this will either support or oppose the proposed notion of the localised temperature influence of the burning char particle to sintering and agglomerate formation in the FB system during lump coal combustion as proposed in section 2.4.2.1 and 2.5.4.

Thirdly, sintering and agglomerate formation has been identified to be associated with the inorganic constituents of the fuel mainly the alkali and alkaline elements present in them, which influence the type/s of alkaline-silicate formed (Schairer & Yagi 1952; Olanders & Steenari 1995). Various scholars have identified many of these elements or oxides in relation to different fuel types that have been investigated (Wu et al. 2009; Datta et al. 2015; Namkung et al. 2015). With

limited reported investigations on sintering and agglomerate formation in high ranked coal and varying differences in the coal composition based on the location where they are formed, it is vital to establish the identity of the particular alkali and alkaline earth elements responsible for sintering and agglomerate in this system.

All these three fundamental aspects identified, investigated and discussed in this chapter covers the phase 1 and 2 of the overall experimental flow sheet given in section 4.1. This serve as a precursor to phase 3 experimental work, which is discussed in chapter 6. More details about the findings from these investigations is reported and discussed in this chapter. Discussions in this chapter also covers observations made during these investigations, which includes colour change of the bed material during calcination, measured weight loss and surface morphology characteristics of the bed material particles.

5.2. Methodology

Material specifications of the Garside 14/25 sand bed material and coals used in this investigation are detailed in section 4.2 while the experimental methodology approaches implemented are detailed in section 4.3. Characterisation techniques used in this study are SEM and EDX analysis, which have been described in section 4.6.2 and 4.6.3 respectively.

5.3. Pure Garside 14/25 Sand Calcination

Discussions covered in this section are based on the first fundamental aspect of the proposed sintering and agglomerate formation mechanism identified and described in section 5.1. As described earlier, previous researchers into the subject area of sintering and agglomerate formation have ignored to investigate or failed to report on the inter-particle interactions that might occur between the

bed material particles at high temperatures in the absence of fuel ash. The prospect of this interaction occurring has been suggested to possibly contribute to the overall sintering and agglomerate formation observed in the FBC system. Hence, the need to investigate this occurrence was seen as vital to provide more understanding into sintering and agglomeration phenomena. Findings made from this investigation are discussed in this section covering topics, which includes colour change, weight loss due to calcination, particle surface characteristics and sintering and agglomeration types observed.

5.3.1. Colour Change

From the visual observation carried out on Garside 14/25 sand bed material before and after the calcination process at various temperatures, it was observed that the appearance of the bed material changes from its natural yellowish brown colour when in the raw form to a brick red colour as shown in Figure 5-1. This brick red colouration appears to intensify as the calcination temperature increases from 800 to 1200°C. These colouration change pattern was observed to be the same even with different particle size fractions of Garside 14/25 sand bed material investigated.

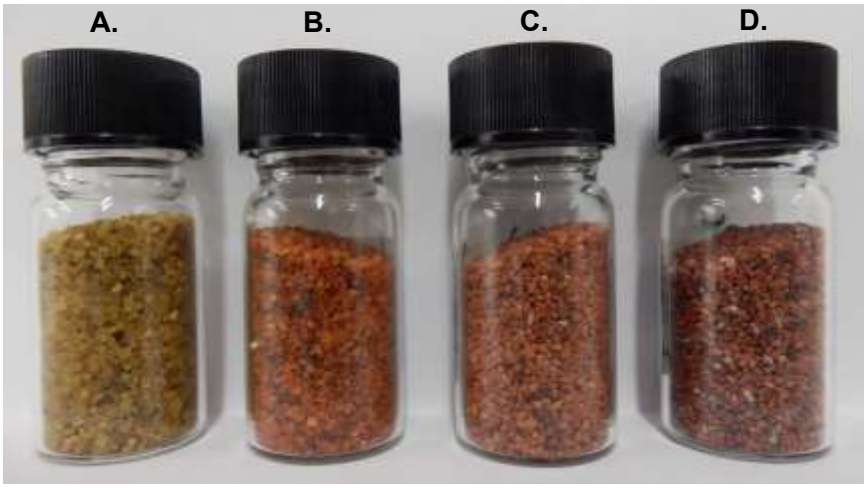

Figure 5-1: Colour change for un-sieved Garside 14/25 sand bed material at various conditions: (A) raw (B) calcinated at 800°C (C) calcinated at 1000°C (D) calcinated at 1200°C (for 1 hour)

The observed colour change is suspected to be associated with the thermal decomposition of Fe_2O_3 identified to be present in the fresh Garside 14/25 sand bed material given in Table 4.1. This hypothesis can be supported by findings of Vujtek and colleagues (2003) who identified the phase transition of Fe_2O_3 that occurs at a temperature above 500°C from βFe_2O_3 usually yellow in colour to αFe_2O_3 which is red in colour (Vujtek et al. 2003). From this, it can be concluded that the colour change of Garside 14/25 sand bed material during calcination is dependent on the calcination temperature.

5.3.2. Weight Loss Due to Calcination

Recorded values of the initial measured weight and final weight (wt.) as well as the calculated percentage weight loss (% wt. loss) determined using equation 4.1 for each Garside 14/25 sand bed material particle size fractions at different calcination temperatures and time periods are presented in Tables 5-1 and 5-2. From the percentage weight loss comparison of the Garside 14/25 sand bed material samples before and after calcination, for different particle size fractions, calcination temperatures and calcination time, a weight loss was observed in each case.

Table 5-1: Weight loss of Garside 14/25 sand bed material for different size fraction after 1 hour of calcination at different calcinated temperatures

Temperature (°C)	Initial Weight (g)	Final Weight							
		212µm		600µm		1000µm		Un-sieved	
		Wt. (g)	% Wt. loss	Wt. (g)	% Wt. loss	Wt. (g)	% Wt. loss	Wt. (g)	% Wt. loss
800	**10.00**	9.94	0.6	9.93	0.7	9.92	0.8	9.93	0.7
1000	**10.00**	9.91	0.9	9.95	0.5	9.91	0.9	9.94	0.6
1200	**10.00**	9.92	0.8	9.94	0.6	9.92	0.8	9.93	0.7

This observed percentage weight loss is proposed to be caused by two activities, which is suspected to occur during the calcination process. The first activity is the

drying phase during which moisture is removed from the bed material and the weight of the bed material is reduced by the fraction of the moisture present in the initial sample which occurs at a temperature of up to 140°C supported by the findings of Venkataraman (Venkataraman 1996).

Table 5-2: Weight loss of Garside 14/25 sand bed material for different size fraction after 4 hours of calcination at different calcinated temperatures

Temperature (°C)	Initial Weight (g)	Final Weight (g)							
		212µm		600µm		1000µm		Un-sieved	
		Wt. (g)	% Wt. loss	Wt. (g)	% Wt. loss	Wt. (g)	% Wt. loss	Wt. (g)	% Wt. loss
1000	**10.00**	9.92	0.8	9.93	0.7	9.93	0.7	9.94	0.6
1200	**10.00**	9.92	0.8	9.92	0.8	9.95	0.5	9.92	0.8

The percentage moisture value of the Garside 14/25 sand bed material was measured in a separate test and an average value of 0.19% of the original mass was obtained to account for the moisture content of the bed material which was indifferent of the particle size fraction at a test temperature of 140°C. The second phase is the thermal decomposition phase of the compounds present in the raw Garside 14/25 sand bed material especially of Fe_2O_3.

Thermal decomposition activities are suspected to occur at various stages during the calcination process (Venkataraman 1996; Dejoie et al. 2014). The thermal decomposition activity is expected to lead to decrease in weight of the bed material due to the reduction of Fe_2O_3 or other compounds present in the bed material. From the data presented in Tables 5-1 and 5-2, it can be seen that the calculated percentage weight loss for the Garside 14/25 sand bed material is between 0.5 and 0.9% across the various particle sizes, calcination temperatures and calcination time periods. Also no pattern or trend can be found between the weight loss and any of these variables. In the absence of moisture in the bed material, the corrected percentage weight loss is between 0.31 and 0.71%, which

can be solely attributed to the thermal decomposition activities that occurs during the calcination process. The percentage weight loss of 0.48% reported by the supplier of Garside 14/25 sand bed material obtained at a temperature of 1000°C (Garside Sands 2011) is within the range measured from this investigation.

5.3.3. Particle Surface Characteristics

In addition to the earlier reported colour change and weight loss that occurred during the calcination of Garside 14/25 sand bed material, a change in the surface characteristics of the bed material particles was also observed. Figure 5-2 shows the SEM micrographs comparing the surface characteristics of the raw (unheated) un-sieved Garside 14/25 sand particles with those calcinated at 800°C, 1000°C and 1200°C respectively. The particle surface of the raw form of un-sieved Garside 14/25 sand bed material shown in Figure 5-2A appears to be smooth with no visible fracture or crack on its surface.

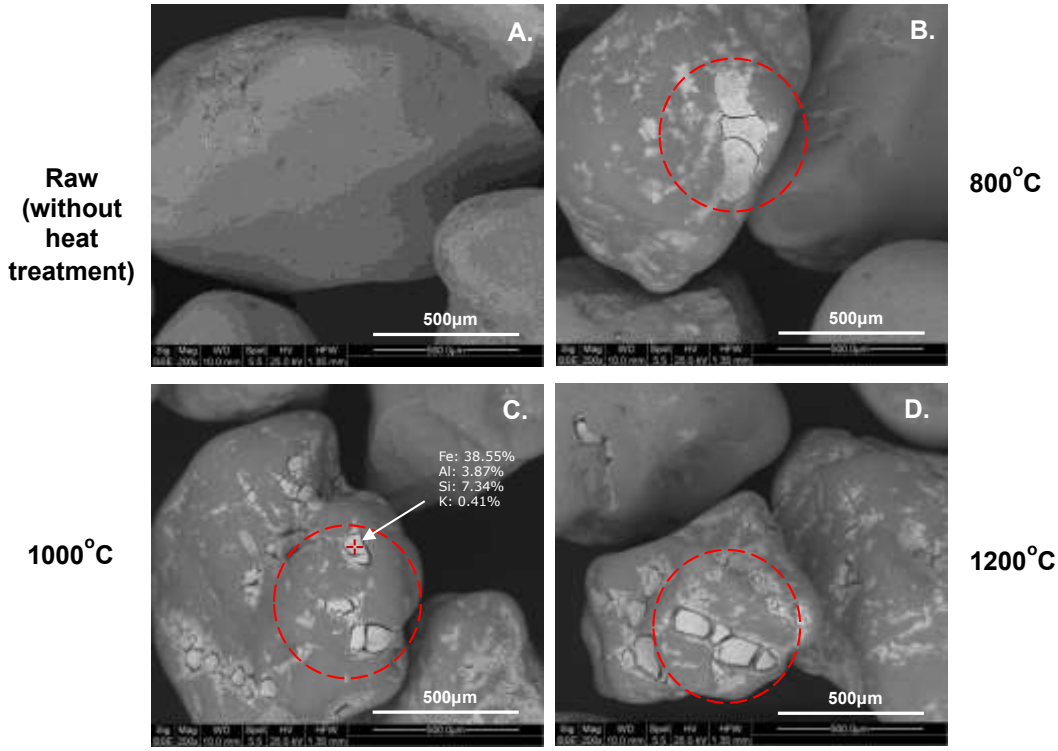

Figure 5-2: SEM micrograph showing the surface morphology of the un-sieved Garside 14/25 sand bed material particles at different conditions: (A) raw (without heat treatment) (B) 800°C (C) 1000°C (D) 1200°C

It was however observed that at calcination temperature of 800°C, the iron-rich regions on the surface of the bed material particles begin to fracture and crack as shown in Figure 5-2B. The intensity of the fractures and cracks of the iron-rich region observed on the surface of the bed materials appears to increase for the bed material calcinated at 1000°C and even higher in those calcinated at 1200°C where the cracks became more obvious with the iron-rich regions forming distinctive separate units as shown in Figure 5-2C and Figure 5-2D respectively. These observation shows that the structure of the iron-rich surface on the Garside 14/25 sand bed material particles is greatly affected by the calcination temperature.

Further SEM analyses of the surface morphology of the different size fractions of Garside 14/25 sand bed material calcinated at different temperatures and durations presented in Figure 5-3 and Figure 5-4 were done which shows a similar pattern of increase in the intensity of fractures and cracks observed on the surface of the bed material particles with increasing calcination temperature as summarised in Table 5-3.

It was also noticed that the intensity of the fractures and cracks in the iron-rich regions on the surface of the bed material sand particles was not significantly affected by particle size. It was however noticed that during calcination of the bed material of particle size 600µm and 1000µm at calcination temperature of 1000°C for 1 hour shown in Figure 5-3(F, G) and particle size 212µm, 600µm and un-sieved at 1000°C for 4 hours shown in Figure 5-4(A, B, D) the cracked iron rich regions on the bed particles was found to have exfoliated away from the bed material particles surface.

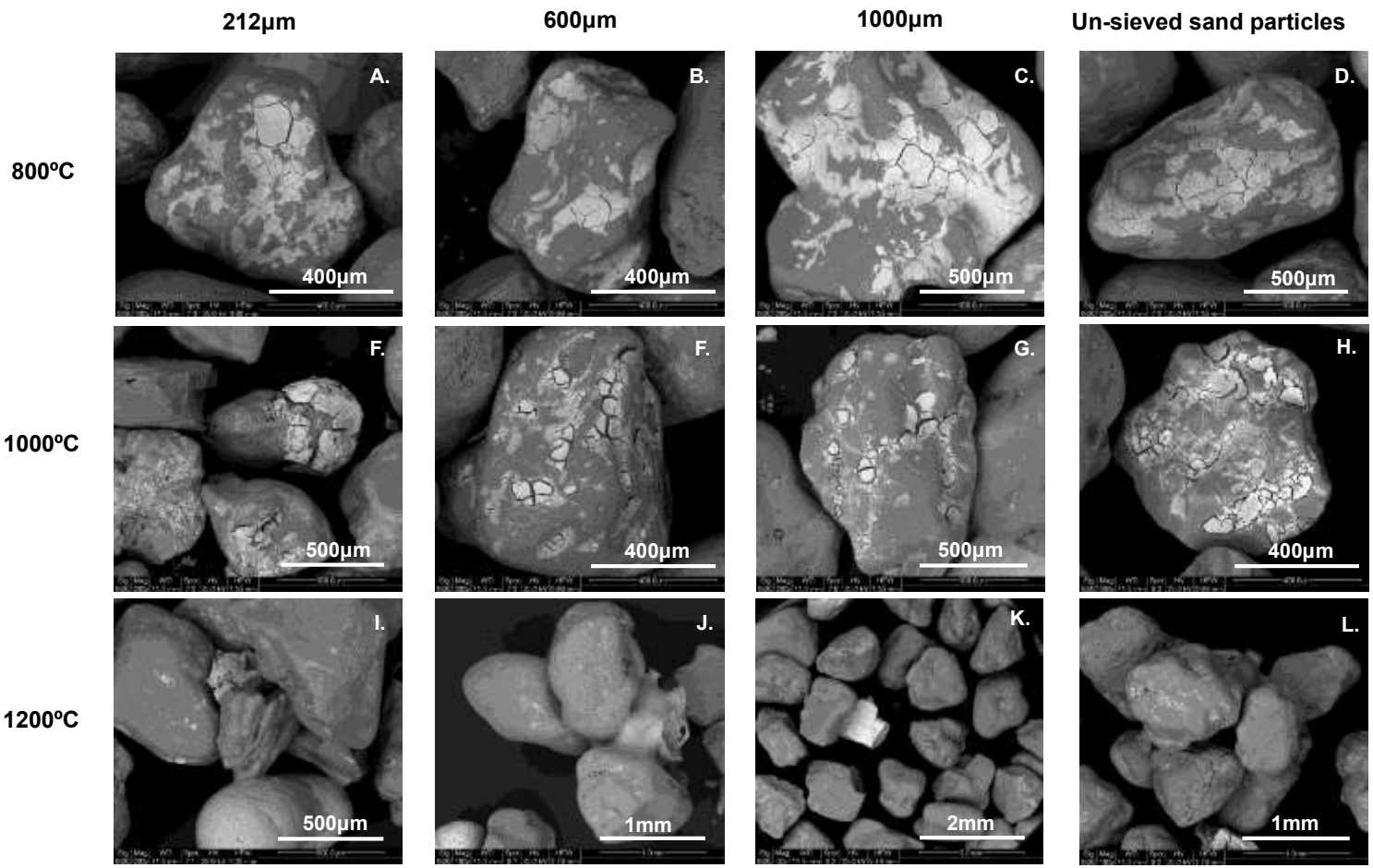

Figure 5-3: SEM micrographs showing the surface morphology of the calcinated Garside 14/25 sand bed materials of different particle sizes held at noted temperatures for 1 hour

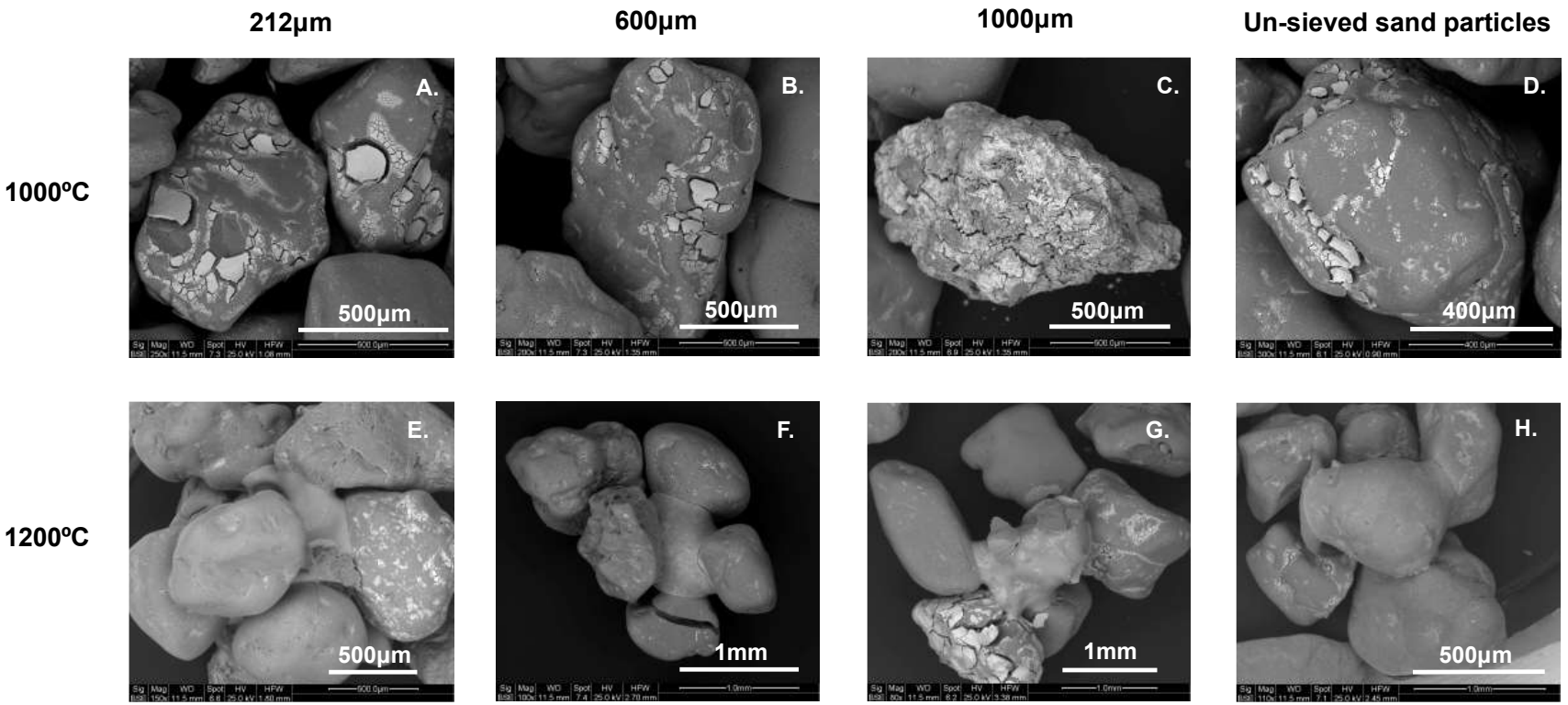

Figure 5-4: SEM micrographs showing the surface morphology of the calcinated Garside 14/25 sand bed materials of different particle sizes held at noted temperatures for 4 hours

Table 5-3: Garside 14/25 sand bed material calcination test conditions and observations

Sample Number	Bed Material Particle Size Fraction	Percentage Weight of Mix (wt. %)		Duration (h)	Furnace Temperature (°C)	Number of Agglomerated Samples	Average Numbers of Particles Per Agglomerated Sample	Comments on Particle Surface Characteristics	Comments on the State of Sintering and Agglomeration
		Coal	Bed Material						
1	212µm	0	100	1	800	0	0	Fracturing / cracking of the iron-rich deposit on the bed material surface	No sintering / agglomeration
2	600µm	0	100	1	800	0	0		
3	1000µm	0	100	1	800	0	0		
4	Un-sieved	0	100	1	800	0	0		
5	212µm	0	100	1	1000	0	0	Increase in intensity of fracturing / cracking and some exfoliation of iron-rich deposit on the bed material surface	No sintering / agglomeration
6	600µm	0	100	1	1000	0	0		
7	1000µm	0	100	1	1000	0	0		
8	Un-sieved	0	100	1	1000	0	0		
9	212µm	0	100	1	1200	7	5.2	Formation of distinctive and separated iron-rich units with more particle surface exfoliation	Sintering / agglomeration of the bed material
10	600µm	0	100	1	1200	4	4.8		
11	1000µm	0	100	1	1200	0	0		No sintering / agglomeration
12	Un-sieved	0	100	1	1200	7	7.3		Sintering / agglomeration of the bed material
13	212µm	0	100	4	1000	0	0	Increase in intensity of fracturing / cracking and some exfoliation of iron-rich deposit on the bed material surface	No sintering / agglomeration
14	600µm	0	100	4	1000	0	0		
15	1000µm	0	100	4	1000	0	0		
16	Un-sieved	0	100	4	1000	0	0		
17	212µm	0	100	4	1200	7	5.4	Formation of distinctive and separated iron-rich units with more particle surface exfoliation	Sintering / agglomeration of the bed material
18	600µm	0	100	4	1200	5	4.7		
19	1000µm	0	100	4	1200	5	4.2		
20	Un-sieved	0	100	4	1200	8	6.4		

The observed exfoliated surface suggests that if the intensity of the cracks of the iron rich region is high enough, distinctive separate flakes can fall off from the surfaces of the particles, which can potentially be deposited in the FB bed. With the presence of high temperature, this exfoliated iron particles might melt to form a concentrated liquid iron oxide based binder or interphase between the bed material particles. In a fluidising environment, the rate of exfoliation of the iron-rich surface can possibly be achieved at a lower between 800°C and 1000°C due to the collision that occurs between the bed material particles, which might enhance mechanical breakage. Another observation made which is explained later in section 5.3.4 is the agglomeration of the Garside 14/25 sand bed materials which occurred at a calcination temperature of 1200°C.

5.3.4. Sintering and Agglomeration Types / Mechanism

At a calcination temperature of 1200°C from visual observation, it was noticed that the Garside 14/25 sand bed material sintered / agglomerated across the different particle size investigated except for 1000µm particle size fraction calcinated at temperature of 1200°C for 1 hour as summarised in Table 5-3. The reason why the bed material of particle size 1000µm calcinated for 1 hour did not agglomerate at this condition could not be established as the same particle sized fraction sintered / agglomerated at the same temperature at a longer calcination time of 4 hours. As the only variable between these two scenarios is the difference in calcination time, it can be proposed that large particle sized fractions required longer calcination time to sinter or agglomerate in fixed bed conditions.

Also as part of the visual observation, the numbers of agglomerated sample of Garside 14/25 sand bed material obtained at calcination temperature of 1200°C for each particles size fraction and calcination time was physically counted. In addition to this, the numbers of Garside 14/25 bed material particles present in each

agglomerated sample was also counted using a magnifying lens. Both of which are detailed in Table 5-3. A summary of the estimated number of Garside 14/25 sand particle agglomerated at different conditions during the calcination of pure Garside 14/25 sand is presented in Table 5-4.

Table 5-4: Estimated number of Garside 14/25 sand particles agglomerated at different conditions during the calcination of pure Garside 14/25 sand particles

Bed Material Particle Size Fraction	Duration of Calcination (h)	Estimated Number of Particles
212µm	1	36.4
600µm	1	19.2
1000µm	1	0
NM	1	51.1
212µm	4	37.8
600µm	4	23.5
1000µm	4	21
NM	4	51.2

It can be seen from this comparison that the total number of agglomerated particles was highest in the un-sieved particle size fraction which was followed by the particle size fraction 212µm for both calcination period of 1 hour and 4 hours. A deceasing trend in the number of agglomerated particles with increase in size fraction can be also be observed and based on this, it can be argued that larger sized particles have a lower agglomeration formation tendencies than smaller sized ones.

On further analysing the sintered / agglomerated Garside 14/25 sand bed material formed at the calcination temperature of 1200°C using SEM as shown in Figure 5-3(I, J, L) and Figure 5-4(E – H), two types of sintering processes which can be described as transient liquid phase sintering and solid state sintering were identified to be present.

5.3.4.1. Transient Liquid Phase Sintering

The transient liquid phase sintering was only observed in the Garside 14/25 sand bed material particle size 212µm fractions calcinated at 1200°C for both 1 hour and 4 hours' time duration as shown in Figure 5-5. Within Figure 5-5, the bed material particle, which is attached to many other particles, have been identified in this text as a binder. This is because they form the base for sintering and agglomerate formation to occur. The binder in this case appears as a strong inter-particle bridge formed from a solidified molten liquid which have being characterised by the presence of bubble pores and ridges / contours on its surface. The morphology of the binder appears not be identical to those of the Garside 14/25 bed material particles. Hence, it can be said to have been formed from a liquid melt. Some of this characteristic property matches the description of transient liquid phase sintering given in literature (Kang 2005; German 1996; German et al. 2009).

In order to have a better understanding of the chemical composition of the binder and formed agglomerate of calcinated Garside 14/25 sand bed material particles, an EDX elemental spot analysis and elemental mapping were done on the agglomerated particles. The focus of this analysis was to identify the presence of K, Al, Si and Fe which have been previously identified to be responsible for sintering and agglomerate formation. Results from this analysis are presented in Figure 5-5 and Figure 5-6 respectively. Within Figure 5-5, the cross sign highlighted by the arrow identifies the precise location of the spot been analysed as shown in each image. The elemental analyses of the binders presented in Figure 5-5(A, B, D, E) identifies the major chemical composition of the binder as K, Al and Si which are typically present in their oxide form as K_2O, Al_2O_3 and SiO_2 respectively. Si was identified as the most abundant element in the binder region accounting for between 23.40 and 29.33%, which is lower than a composition of 96.67% measured in the bulk fresh sample of Garside 14/25 sand.

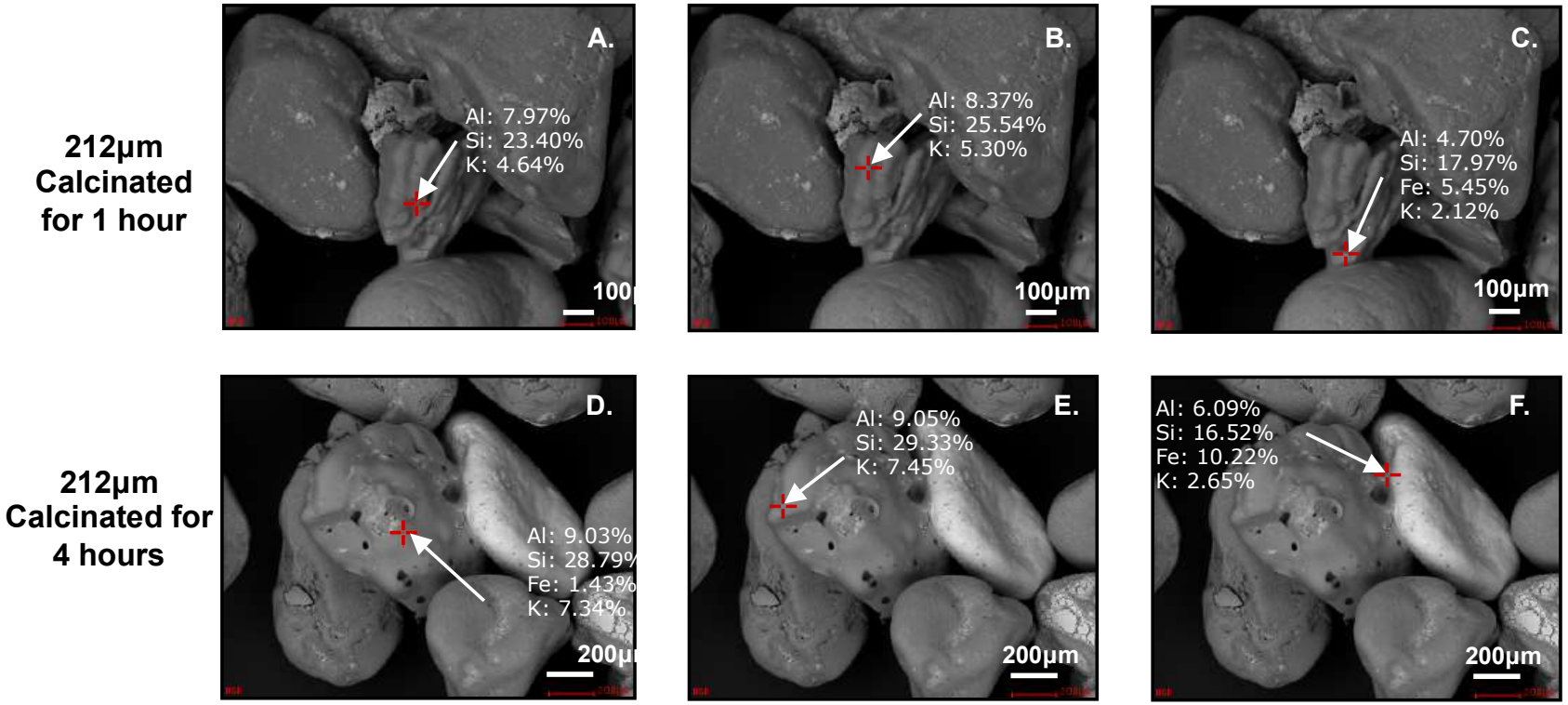

Figure 5-5: SEM / EDX micrographs showing the elemental spot analysis of calcinated Garside 14/25 sand bed material agglomerates showing the transient liquid phase sintering process at 1200°C

Compositions of Al and K measured in the binder region were between 7.97 and 9.05%, and 4.64 and 7.45% respectively. Both of which were found to be higher their compositions of 0.33% and 0.01% measured in the bulk fresh sample of Garside 14/25 sand respectively. The maximum amount of Fe typically identified as Fe_2O_3 measured on the surface of the binders was 1.43% which was also found to be higher than the composition of 2.4% measured in the bulk fresh Garside 14/25 sample. A composition of between 5.45% and 10.22% was measured in the joint section between the binders and the Garside 14/25 sand bed material particles as shown in Figure 5-5(C, F). The result from the EDX elemental mapping presented in Figure 5-6 provides a detailed visual representation of the distribution / spread of the Fe, Si, Al and K. across the surface of the formed agglomerate of calcinated Garside 14/25 sand bed material particles.

Within Figure 5-6 a circle has been highlighted in each image to allow the reader to link the SEM and EDX mapping images of two different agglomerated particles. The original image at the top is the SEM micrograph of the agglomerated particles with each having four other images below them highlighting the presence of earlier identified elements (elemental oxide). The results show that Si, Al and K are the major components of the binder while the Fe is only sparsely present. This supports the earlier findings of the EDX elemental spot analysis.

On the strength of this, it can be argued that the heavy presence of Si, Al and K in the binder possibly suggest that the strong inter-particle liquid bridge formed between the bed material particles can be identified as chemical reaction melting mechanism from a combination of species within the K_2O – Al_2O_3 – SiO_2 phase equilibrium system typically formed in a K and Al rich environment (Schairer & Bowen 1947) the identity of the species could not be established due to availability of limited resources on the subject area of equilibrium phase system, hence more work need to be done on this.

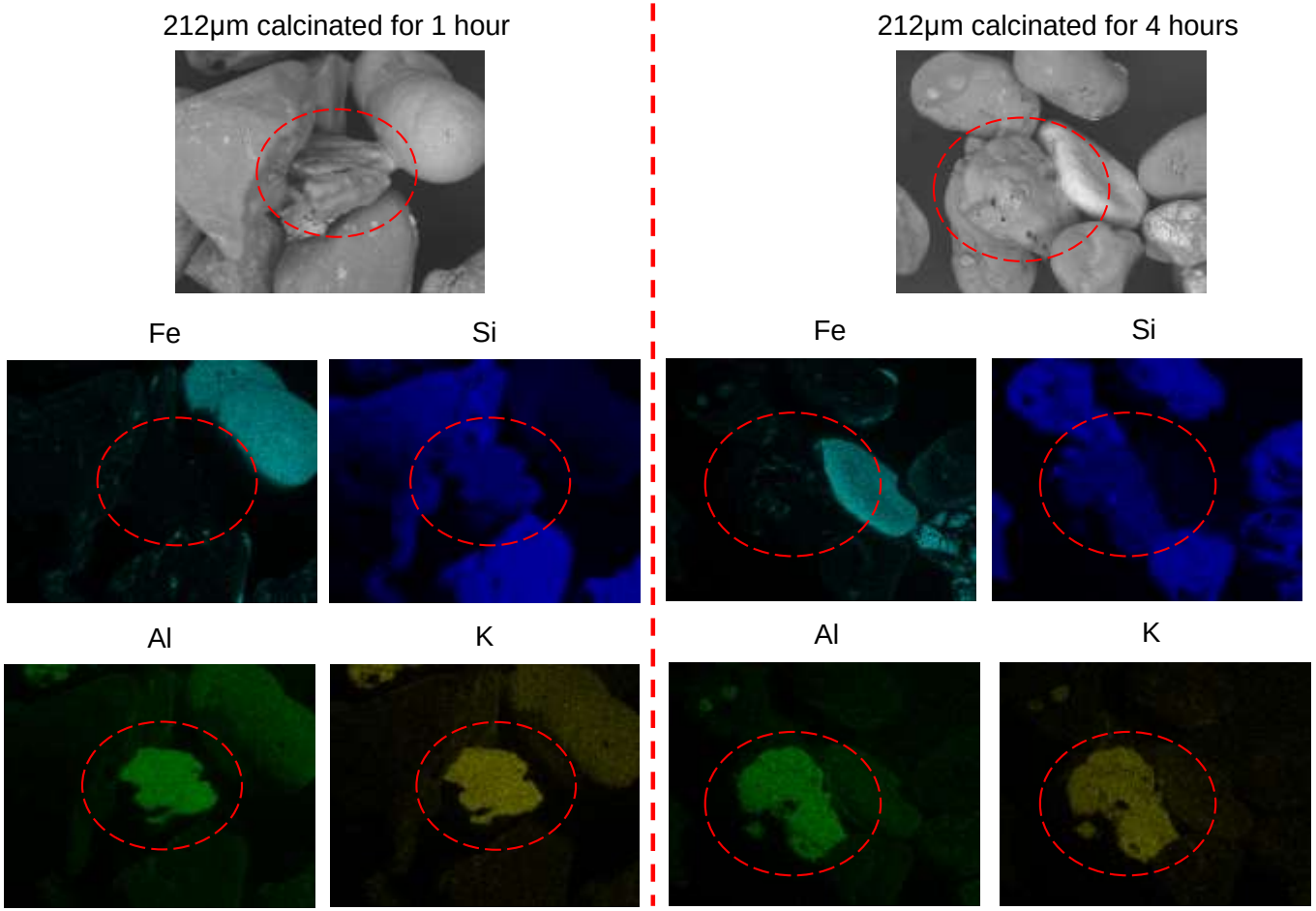

Figure 5-6: EDX elemental mapping of calcinated Garside 14/25 sand bed material agglomerate showing the distribution of identified elements in transient liquid phase sintering process after at 1200°C

Although fuel ash is not present in this investigation, but as earlier identified in section 4.2.1 that fresh Garside 14/25 sand bed material contains SiO_2, Fe_2O_3, Al_2O_3, K_2O and CaO which are also found in biomass and coal ash (Unsworth et al. 1991; Carpenter et al. 2007) all of which have been also been earlier identified to be responsible for sintering and agglomerate formation in section 2.5.3. Bearing this in mind, it can be concluded that the presence of elements or elemental oxides identified to be responsible for sintering formation in a system can promote agglomerate formation even in an ash free environment hence contributing to the total sinter or agglomerate formed within the system alongside other sintering and agglomerate formation mechanisms.

5.3.4.2. Solid State Sintering

Solid state sintering was observed in all the Garside 14/25 sand bed material particle size fractions calcinated at 1200°C including those of 212µm particle size fraction as shown in Figure 5-7 and Figure 5-8 for calcination time 1hour and 4hours respectively. As described by Tanaka and colleagues (2012) that during solid state sintering formation, particles are wholly densified in the solid state causing a distortion in the shape of the particle and decrease in the inter-particle distance (Tanaka et al. 2012) as illustrated in Figure 2.5A. From the SEM micrographs presented in Figure 5-7 and Figure 5-8, the surface morphology of the binder in this case appears to be identical to those of the Garside 14/25 bed material particles.

Using EDX analytical technique with focus of identifying the presence of Fe, Al, Si and K the chemical composition of the binder linking the Garside 14/25 sand bed material particles together was analysed and presented in Figure 5-7 and Figure 5-8 for calcination time of 1hour and 4hours respectively. It was discovered that the binder predominately contained Fe and Si with similar

quantities of Al and K. The elemental analysis of the binder present in Figure 5-7(A, E, I) and Figure 5-8(A, E, I, M), the amount of Fe was found to vary between 12.47 and 44.67% which is higher than the composition of 2.4% amount measured in the bulk fresh sample of Garside 14/25 sand. Composition of Si was found to be between 12.61 and 26.14% which is considerably lower than the composition of 96.4% measured in the bulk fresh sample of Garside 14/25 sand.

The composition of Si in the binder and was also noticed to be higher than that of Fe in most of the cases except in Figure 5-7A, and Figure 5-8E. Composition of Al and K were found to vary between 3.87 and 4.90% and between 2.51 and 3.48% respectively. Both of which are higher than a composition of 0.33% and 0.01% measured in the bulk fresh sample of Garside 14/25 sand respectively.

EDX elemental spot analysis of the joint section between the binder and the bed material particles shown in Figure 5-7(B, F, G, J, K) and Figure 5-8(B – D, F – H, J – L, N – P) clearly indicated that Fe was present in far greater quantity than those of Al and K. Based on this findings, it can be proposed that solid state sintering formed during the calcination of pure Garside 14/25 sand occurs on the surface of the particle which is predominately iron rich due to the high Fe measure in the binder. The EDX elemental mapping analysis shown in Figure 5-9 clearly demonstrates that Si, Al and Fe are the major compounds heavily present in the binder regions and responsible for the agglomeration formation. The results also show that there is an even spread of K compound across the surfaces of the binders.

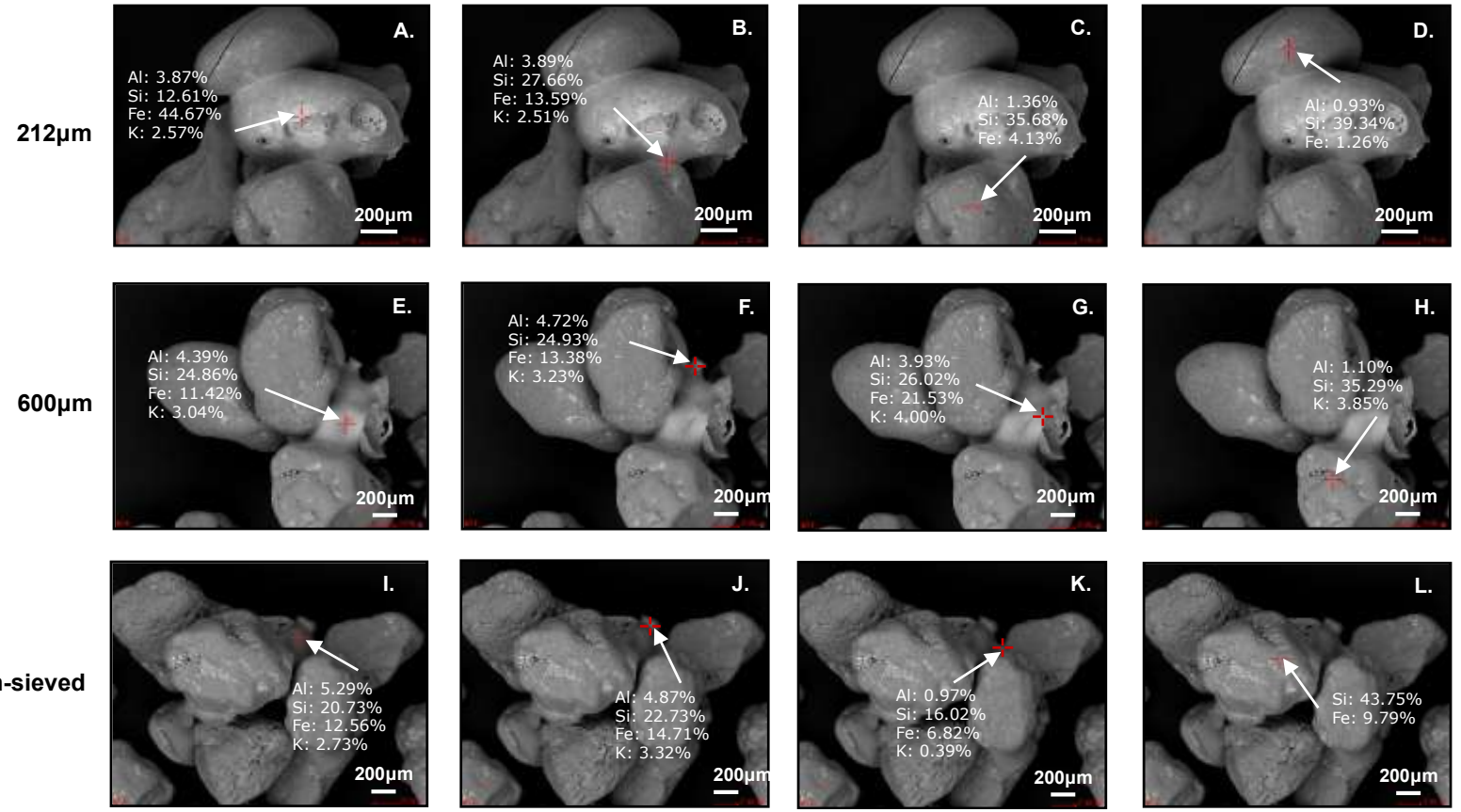

Figure 5-7: SEM / EDX micrographs showing the elemental spot analysis of calcinated Garside 14/25 sand bed material agglomerates showing the solid stage sintering process after 1 hour of calcination at 1200°C

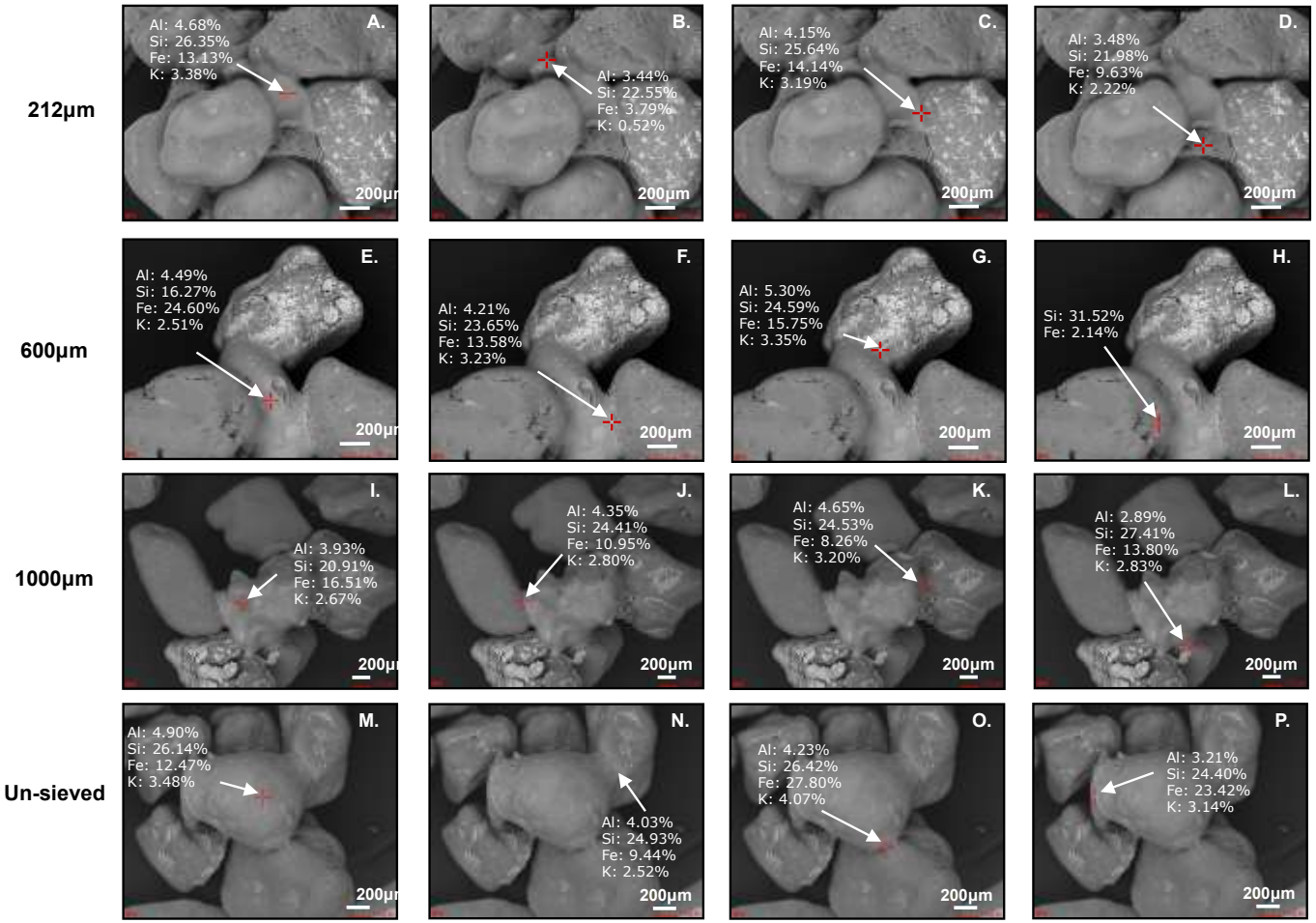

Figure 5-8: SEM / EDX micrographs showing the elemental spot analysis of calcinated Garside 14/25 sand bed material agglomerates showing the solid stage sintering process after 4 hours of calcination at 1200°C

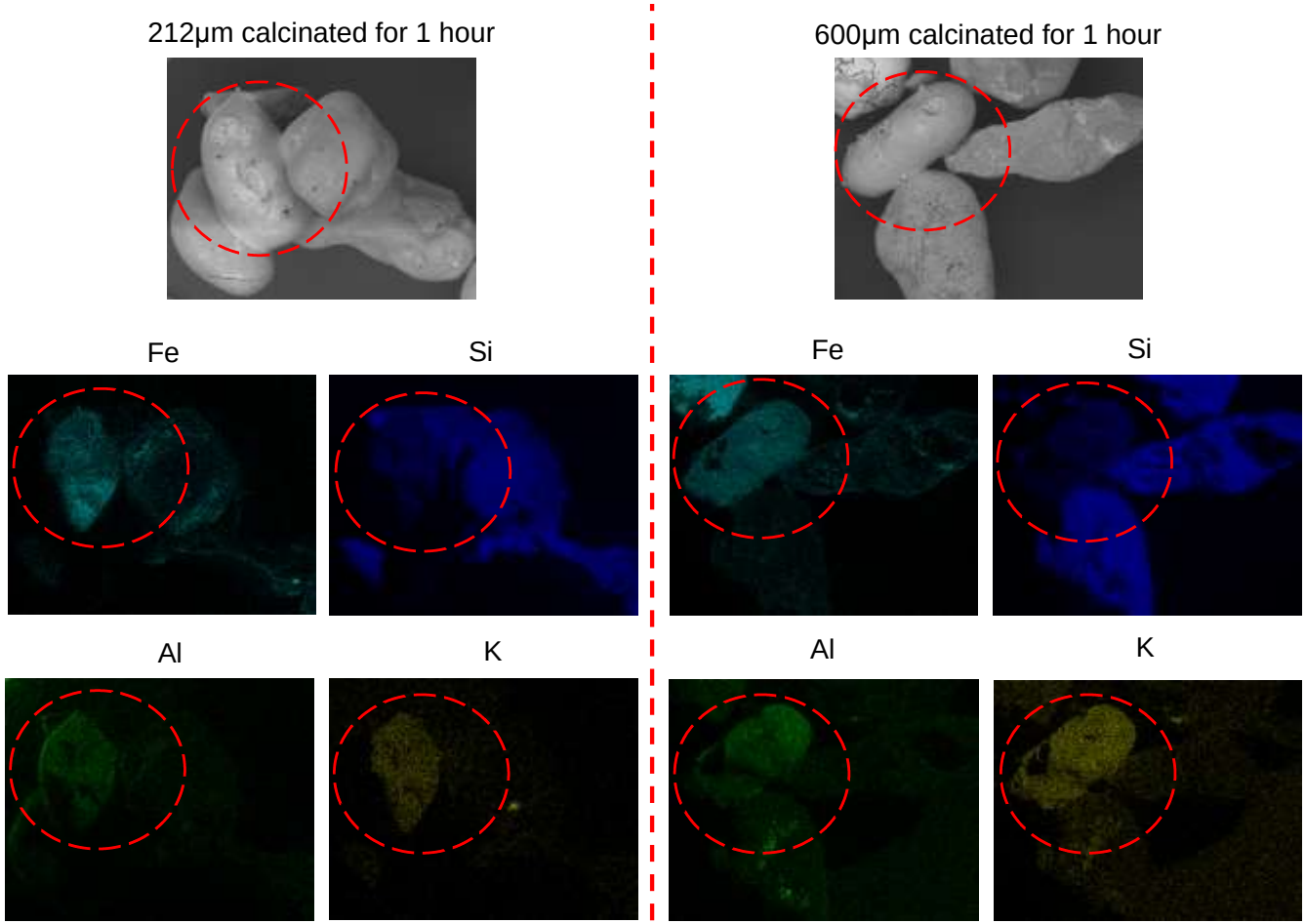

Figure 5-9: EDX elemental mapping of calcinated Garside 14/25 sand bed material agglomerate showing the distribution of identified elements in solid state sintering process after at 1200°C

Although it might be debateable to say that solid state sintering is formed due to alkali-silicate melt especially with the absence of liquid binder / ash, but with heavy presence of Fe and Si in the binder alongside with relative amount of Al and K, it can be argued that the formation of solid state sintering at a calcination temperature of 1200°C is promoted by the relative composition of these four elements in their elemental oxide states as pointed out by Kang that one of the parameters that influenced sintering formation is the chemical composition of the material (Kang 2005). Hence, the melt in this case is proposed to be from the species of Fe_2O_3 – Al_2O_3 – SiO_2 phase equilibrium system identified in iron-rich environments (Schairer & Yagi 1952). However more work needs to be done to identify the identity of the species. This finding also support earlier stated argument that it is possible to form a sinter / agglomerate if the elemental oxides identified to be responsible for agglomerate formation are present in the system and the condition (concentration and temperature) is right (Huggins et al. 1981).

5.3.5. Summary

The agglomeration properties of Garside 14/25 sand used as bed material in the industrial scale FBC have been investigated through calcination in air and fuel ash free environment at a temperature of 800 - 1200°C at calcination time of 1 hour and 4 hours and was observed that at a calcination temperature of about 1200°C, agglomeration of the bed material sand particles occurs.

Transient liquid phase sintering and solid state sintering were the two types of sintering processes observed to be present during the calcination of Garside 14/25 sand bed material. Form all the observations made in this investigation, it was concluded that the presence of elements or elemental oxides identified to be responsible for sintering formation in a system can promote agglomerate formation even in an ash free environment provided the conditions are right (concentrations and temperature). This may not be the sole process responsible

for sintering and agglomerate formation during coal combustion in a FBC due to its reliance of sticky impact. However, it can contribute to the total amount of formed sinter or agglomerate within the FBC system by acting as the initial step for sintering and agglomerate formation especially in the blank region of the FBC nozzles where fixed bed like conditions occurs.

With increasing calcination temperature, it was observed that the iron-rich areas on the surface Garside 14/25 sand bed material particle fractures / crack. The intensity of the observed fractures / cracks increases as the calcination temperature increases causing exfoliation of this iron-rich surface at a calcination temperature of 1000°C. The extent of the crack and exfoliation of the iron-rich regions was however found to be independent on the particle size, calcination temperature or calcination time.

Garside 14/25 sand bed material was also observed to undergo colour change, from the yellowish brown colour appearance to red due to the phase change of Fe_2O_3 from βFe_2O_3 to αFe_2O_3. The depth of colour observed increases with the calcination temperature. Intensity of agglomerate formed was also found to be dependent on particle size. In addition, Garside 14/25 sand was also observed to experience a weight loss of between 0.5 and 0.9% which accounts for both moisture loss and the thermal decomposition process and between 0.31 and 0.79% weight loss which account for the thermal decomposition process alone.

5.4. Calcination of Garside 14/25 Sand Mix with Coal or Coal Ash

As described earlier as part of the second fundamental that previous researchers into this subject area have suggested that sintering and agglomerate formation is an ash related problem during the combustion of coal. It is also a well-established fact that combustion of coal undergoes three stages leading to the

formation of three main by-products of which ash is just one of them. The need to clearly establish the sole contributory effect of ash to sintering and agglomerate formation in the absence and presence of the combustion stages and other by-products is seen as important to better understand sintering and agglomerate formation and also in identifying effect of ash alone to agglomerate formation.

5.4.1. Visual Inspection of Agglomerates

Table 5-5 provides a detailed description of the test conditions for the calcination investigation of Garside 14/25 sand bed material mix with coal or coal ash carried out and the observations made on the agglomerated bed samples produced and collected from this investigation after it has cooled down to room temperature. It was evident that in every case investigated, sintering / agglomeration of the Garside 14/15 sand bed material occurred. However the strength of the agglomerated bed material formed was observed to vary depending on the calcination temperature, the use of coal or coal ash and percentage composition of the coal present in the sample mix.

At calcination temperature of 1000°C and bed material to coal mix of 80%: 20%, sintered bridge appeared only to have been formed between few particles of Garside 14/45 sand bed material. This sintering bridge or agglomerate formed were also observed to be very weak and in most cases broken and this is suspected to be caused by the fact that the ash generated from the coal appears to be in the initial stages of melting which can be described as the initial deformation temperature stage in ash fusibility temperature studies (Teixeira et al. 2012). At higher calcination temperature of 1200°C, for the same bed material to coal mix ratio a very strong sintered agglomerate was observed to have been formed between the particles. This signifies the importance of temperature to ash melting and behaviour, which have earlier been reported by many scholars (Manzoori & Agarwal 1992; Olanders & Steenari 1995; Ohman et al. 2000).

Table 5-5: Garside 14/25 sand bed material with coal / coal ash calcination test conditions and observations

Sample Number	Coal Type	Percentage Weight of Mix (Wt. %)		Duration (h)	Furnace Temperature (°C)	Number of Agglomerated Samples	Average Numbers of Particles Per Agglomerated Sample	Comments on the State of Sintering and Agglomeration
		Coal	Bed Material					
1	**Thoresby Washed**	20	80	4	1000	5	3.6	Very weak sintering of the bed material particles
2	**Blyth Washed**	20	80	4	1000	4	2	
3	**Blyth Unwashed**	20	80	4	1000	6	2	
4	**Thoresby Washed**	5	95	4	1200	7	6.5	Weak / strong sintering / agglomeration of the bed material particles
5	**Blyth Washed**	5	95	4	1200	6	6.7	
6	**Blyth Unwashed**	5	95	4	1200	7	8.3	
7	**Thoresby Washed**	10	90	4	1200	10	9.2	Strong sintering / agglomeration of the bed material particles
8	**Blyth Washed**	10	90	4	1200	6	6.8	
9	**Blyth Unwashed**	10	90	4	1200	9	10.7	
10	**Thoresby Washed**	20	80	4	1200	12	11.1	Very strong sintering / agglomeration of the bed material particles
11	**Blyth Washed**	20	80	4	1200	8	9	
12	**Blyth Unwashed**	20	80	4	1200	11	12.7	
13	**Thoresby Washed Coal Ash**	10	90	4	1200	2	4	Loose and weak sintering of bed material particles

On comparing the agglomerated bed material sample formed in the industrial FBC while burning Thoresby washed coal to those formed during calcination of Garside 14/25 sand in the absence and presence of coal (Thoresby washed coal) and / or coal ash (Thoresby washed coal ash) presented in Figure 5-10. It can be seen that physical appearance of the agglomerated sample formed in the industrial FBC presented in Figure 5-10A resembles those formed during the calcination of Garside 14/25 sand mix with coal presented on Figure 5-10 (C - E) due to the presence of the white binding layer.

The physical appearance of the agglomerates formed during the calcination of bed material and coal ash mix appears to be very different from those observed in the coal environment as presented in Figure 5-10F. The sintering bridge looks like a very porous structure, which is different from the solid and rigid appearance of those formed in the coal mix environment. The pure Garside 14/25 sand agglomerate presented in Figure 5-10B appears to be solid and rigid as those formed during the calcination of Garside 14/25 sand mix with coal and in the industrial FBC. However, the absence of the white binding layer around the binder joints clearly highlight the different between their physical appearances. On the strength of this, it can be argued that sintering and agglomeration formation may be an ash related problem during combustion process but its formation is also heavily influenced by the stages of combustions and localized temperature effect created by the burning char particles of the fuel.

Also as part of the visual observation, the number of agglomerated samples of Garside 14/25 sand bed material and the number of particles present in each agglomerated sample obtained for each bed material to coal mix was physically counted Both of which are detailed in Table 5-5. A summary of the estimated number of Garside 14/25 sand particle agglomerated at different conditions during the calcination of pure Garside 14/25 sand is presented in Table 5-6.

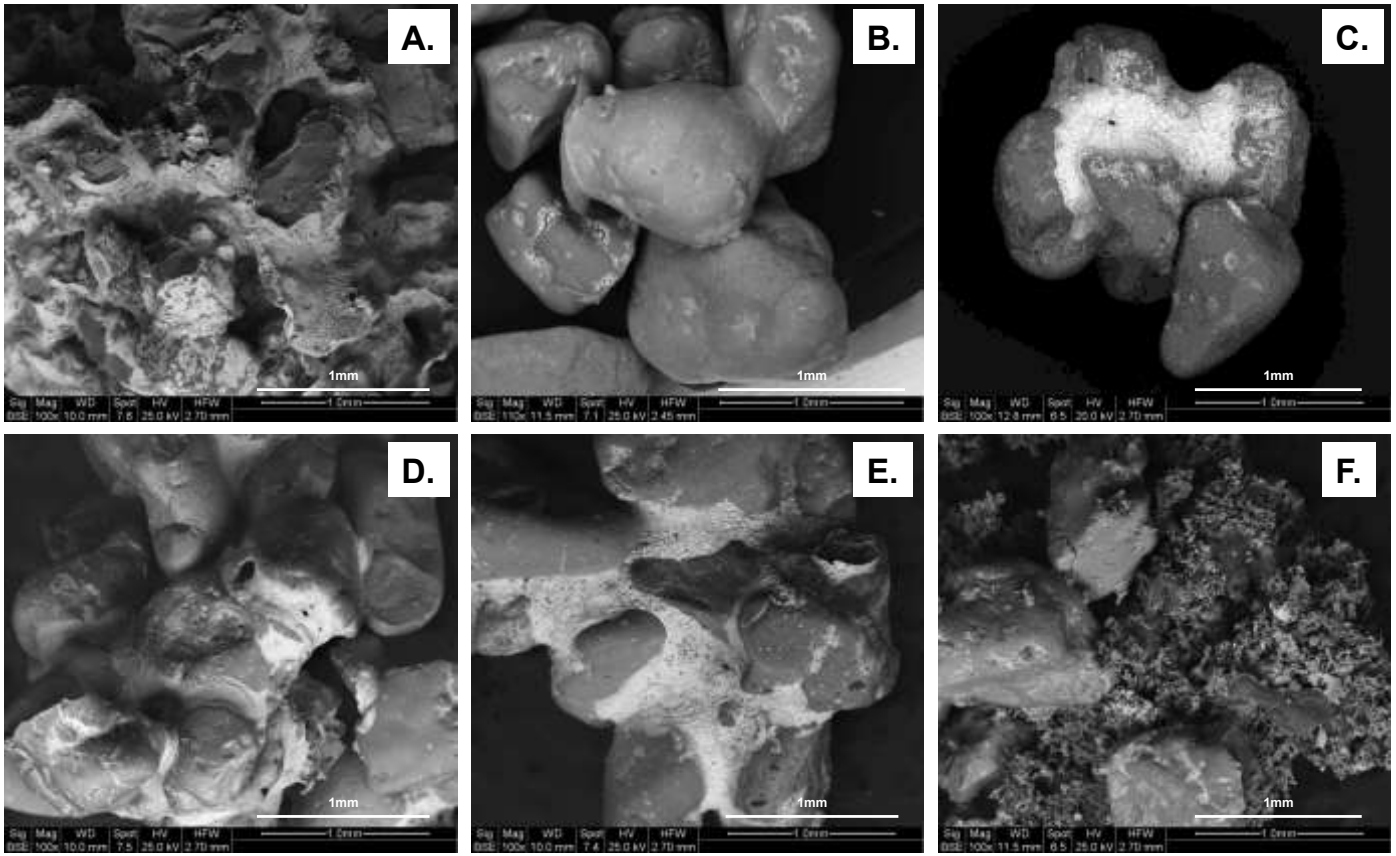

Figure 5-10: SEM micrographs comparing the surface morphological characteristics of different agglomerated Garside 14/25 sand bed materials from: (A) Industrial FB system at AB Sugar, (B) calcination of pure Garside sand bed material at 1200°C for 4 hours, (C) bed material to coal mix of 95%: 5% calcination at 1200°C for 4 hours, (D) bed material to coal mix of 90%: 10% calcination at 1200°C for 4 hours, (E) bed material to coal mix of 80%: 20% calcination at 1200°C for 4 hours, (F) bed material to coal ash mix of 90%: 10% calcination at 1200°C for 4 hours

Table 5-6: Estimated number of Garside 14/25 sand particles agglomerated at different conditions during the calcination of Garside 14/25 sand particles mix with coal or coal ash

Furnace Temperature (°C)	Percentage Weight Mix (Coal : Bed Material)	Estimated Number of Agglomerated Particles		
		Thoresby Washed	Blyth Washed	Blyth Unwashed
1000	20 : 80	18	8	12
1200	5 : 95	45.5	40.2	58.1
	10 : 90	92	40.8	96.3
	20 : 80	133.2	72	139.7

It can be seen from Table 5-6 that the total number of particles agglomerated together was higher in the unwashed Blyth coal followed by Thoresby washed coal while washed Blyth coal has the least. This finding can be related to the industrial FBC operation where the bed agglomerated after occurred after 10 days of continuous operation using washed Blyth coal and Thoresby coal lasted 42 days. Blyth washed coal on the other hand lasted over 63 days without any visible sintering or bed agglomeration.

The ash analysis of the coal presented in Table 4-2 also shows that both Thoresby washed coal and Blyth unwashed coal have a higher composition of Fe_2O_3 than Blyth washed while their SiO_2 compositions are lower than that of Blyth washed coal. This may explain the reason why the amount of agglomerate formed in Thoresby was and Blyth unwashed are higher than that of Blyth washed.

In addition, the estimated numbers of agglomerated particles was also found to increase as the composition of coal ash in the Garside 14/25 sand mix with coal increases at a calcination temperature of 1200°C. This observation shows that the higher the coal composition of a bed, the greater the tendency of the bed agglomerating.

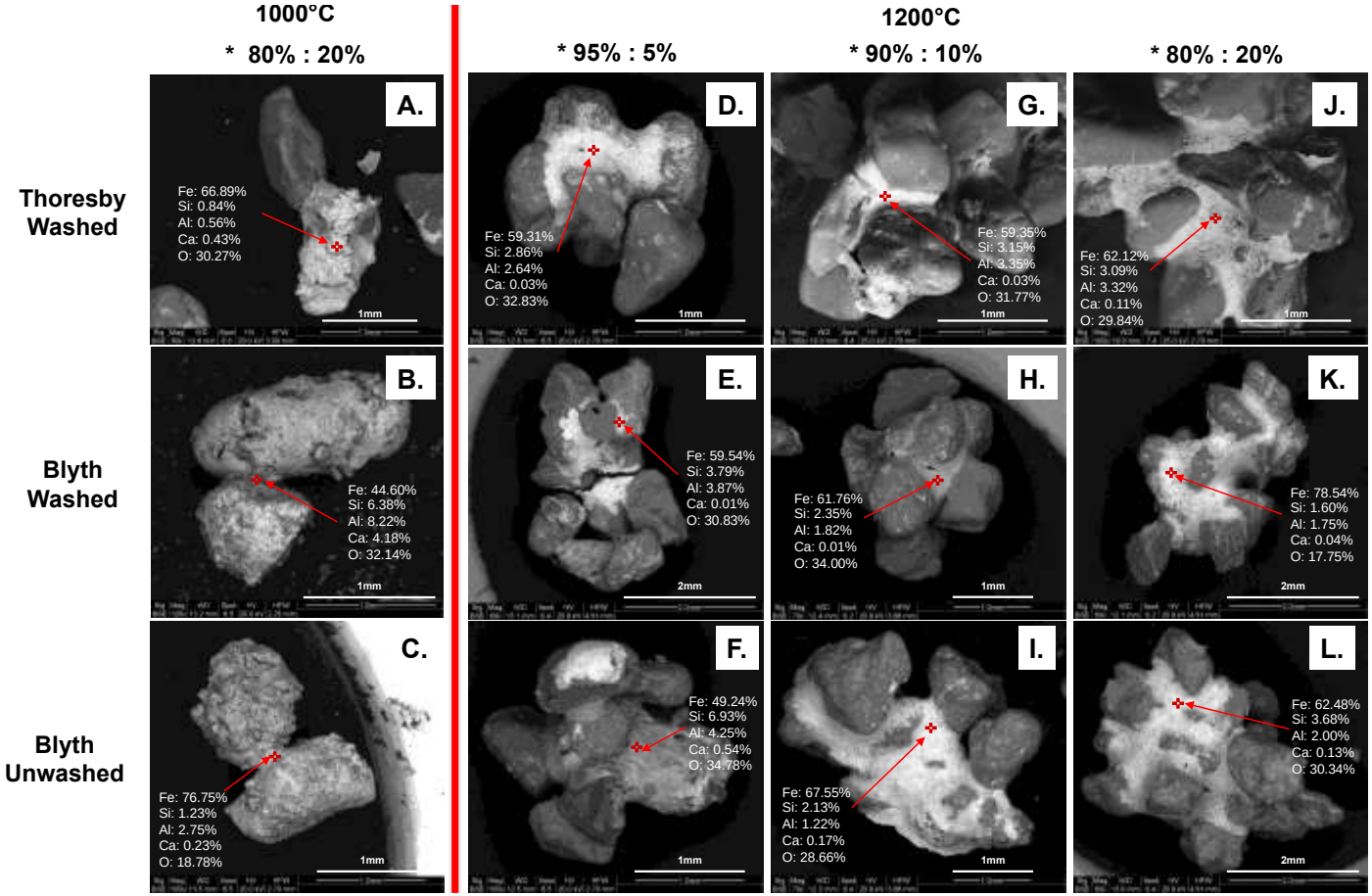

Figure 5-11: SEM / EDX micrographs showing the elemental spot analysis of calcinated Garside 14/25 sand bed material agglomerates showing the liquid phase sintering process after 4 hours of calcination at the identified temperatures and bed material to coal mix for different coal types (* percentage mix of bed material: coal)

5.4.2. Sintering and Agglomeration Type / Mechanism

As reported during the visual inspection carried out on the calcinated Garside 14/25 sand bed materials and coal mix, that agglomeration was observed for each investigated sample irrespective of the coal type. The strength and appearance of the sintering bridge that exist between the Garside 14/25 bed material particles earlier discussed in the section 5.4.1 during the visual inspections of the formed agglomerated bed material is supported by the SEM micrograph images presented in the Figure 5-11.

From the SEM micrograph images, it can be seen that the sintering bridge that occurs in the agglomerated bed material formed from Garside14/25 sand bed material with coal mix calcinated at 1000°C given in Figure 5-11(A – C) appears to be weak / thin and cracked in one of the case as shown in Figure 5-11A for Thoresby washed coal. The strength of the sintered bridge in this investigation was described by the thickness of the binder and intensity of deposition present between the bed material particles.

With increased calcination temperature to 1200°C for a mix of Garside 14/25 sand bed material with coal in the ratio of 95% to 5%, the strength of the sintered bridge between the bed material particles appears to be stronger as shown in Figure 5-11(D – F) than those formed at 1000°C for higher composition of coal due to the presence of more deposition in the binder. As the composition of coal in the mix was further increased to 10% and 20% presented in Figure 5-11(G – I) and Figure 5-11(J – L) respectively for the different coal types, the amount of deposition in the binder of the formed agglomerated Garside 14/25 sand bed materials appears to increase, hence the strength of the agglomeration formed increases. Based on these findings, it can be said that the strength of agglomerated Garside14/25 sand bed material formed at calcination temperature

of 1200°C increases as the coal composition in the mix increases. This supports the earlier reported observation from the visual inspection carried out which is detailed in Table 5-5.

Also from the SEM micrographs presented in Figure 5-11, the type of sintering mechanism present between the Garside 14/25 sand bed material particles was identified as liquid phase sintering due to the unchanged inter-particle distance and structure of the bed material particles during grain densification (Kang 2005). In order to identify the element / elemental oxides responsible for this liquid phase sintering mechanism, an EDX spot analysis was carried on the binder region between the Garside 14/25 sand bed material particles which is presented in Figure 5-11.

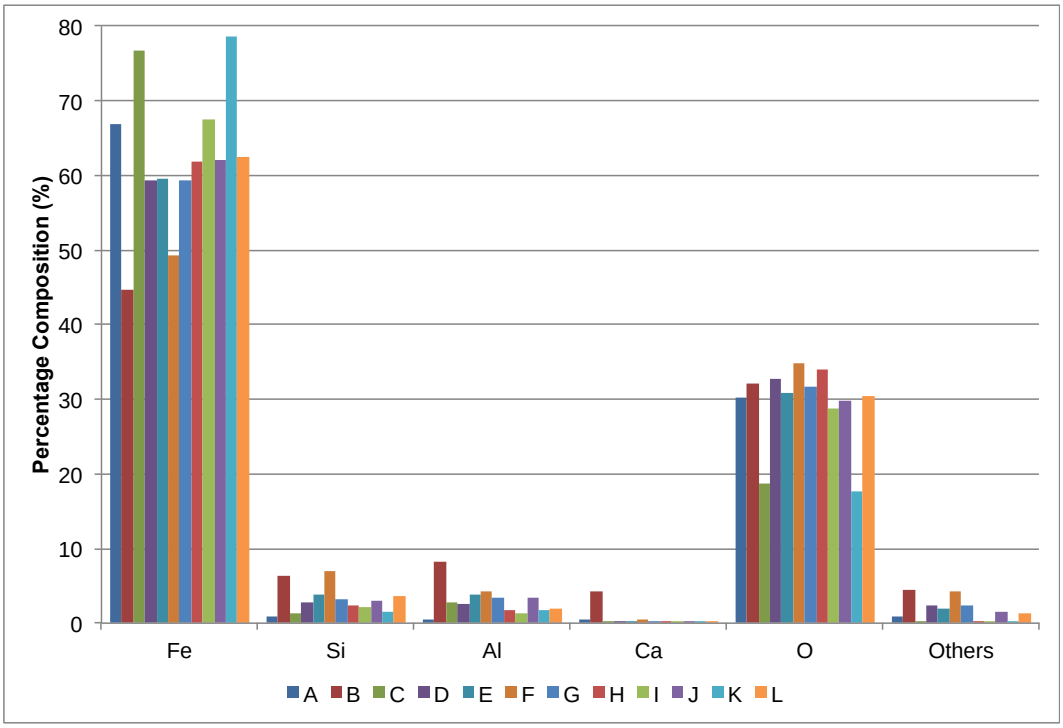

Figure 5-12: Manually performed EDX spot analysis of the sintering bridge (binder region) between the agglomerated Garside 14/25 sand particles from the calcination of Garside 14/25 sand bed material and coal mix at various compositions

It was discovered that the binder predominately contains Fe with a varying composition of between 44.46 and 78.54% followed by O (oxygen) with a

composition of between 17.75 and 34.78%. The presence of oxygen supports the arguments that all the identified elemental identified to be present in the binder are in their oxide states (elemental oxides). Si and Al were the next major element identified to be present in the binder with composition of between 0.84 and 6.93% for Si and 0.56% and 8.22% for Al. This is followed by Ca with a composition of 0.01 to 4.18% while elements such as Na, K, Mg also identified to be present in the binder are categorised as others measuring between 0.06% and 4.48%. The elemental composition of the binder is plotted in Figure 5-12 to show a visual comparison between the measured quantities. No pattern or trend could be identified between the ratio of Al, Si and Fe present in the binder.

Based on the identified composition of the binder between the bed material particles, it is proposed that the liquid melt present as a binder within the agglomerated particle is formed from Fe, Si and Al due to their high abundance in this region. Hence, the melt in this case is believed to be from species of Fe_2O_3 – Al_2O_3 – SiO_2 phase equilibrium system identified to be present in iron-rich environments (Schairer & Yagi 1952) and during the studies on coal ash behaviours (Huffman et al. 1981; Wu et al. 2009). The identity of these species could not be identified due to limited resources in plotting equilibrium phase system for this interaction. More work needs to be done to identify the identity of these species.

5.4.3. Summary

From this investigation, it was evident that the surface morphology of the agglomerated bed material formed from the calcination of Garside 14/25 sand bed material with coal (Thoresby coal) mix of various compositions at 1200°C resembles the one formed in the industrial operated FBC system during

Thoresby coal combustion. This emphasises the contributory effect of combustion stages to ash melting behaviour and agglomeration formation.

The strength of the sintering bridge or agglomerate formed has been identified to increase with increase in calcination temperature and composition of coal present in the sample mixture irrespective of the coal type. The number of agglomerated particle formed was also found to be higher in the Thoresby washed and Blyth unwashed than in Blyth washed. In addition, increasing concentration of coal in the Garside 14/25 sand bed mix with coal was found to increase its agglomeration tendencies for each coal type investigated.

Liquid phase sintering type was identified as the sintering process responsible for agglomerate formation in the type of system resulting in the melts formed from the species of Fe_2O_3 – Al_2O_3 - SiO_2 phase equilibrium system. However, more work needs to be done to establish the identity of these species.

CHAPTER SIX

EFFECT OF WASHED AND UNWASHED COAL ON FLUIDISED BED OPERATION AND SINTERING AND AGGLOMERATE FORMATION

6.1. Introduction

From the earlier calcination investigation detailed and discussed in chapter 5, the contributory effect of the combustion stages to sintering and agglomeration formation during coal combustion was made evident. However these tests were carried out under conditions which can be described as fixed bed coal combustion setup. The findings and conclusions drawn from that investigation cannot be used as a universal basis to justify the reason for sintering and agglomerate formation during lump coal combustion in a fluidised bed system. Hence, more investigation needs to be done to establish if any of the earlier identified sintering processes in chapter 5 is applicable to sintering and agglomerate formation in real FB lump coal combustion systems.

In order to do this, a FB lump coal combustion investigation was carried out using the PSBFBC system designed and discussed in chapter 3 of this work. The investigations carried out in this study are divided into two broad parts. The first part which is described as the prolonged normal operation runs of the PSBFBC was done using two different coals classified as washed or unwashed from the same mine (Blyth typically referred to as Blyth coals). Each coal type was fed

and combusted in the PSBFBC for a total number of 10 runs and a total combustion time of approximately 52 hours. For each coal type investigated, a new batch of fresh Garside 14/25 sand bed material was introduced into the PSBFBC and continuously used for the entire duration of the 10 runs or 52 hours of combustion operation. After each experimental run, samples of the bed material were taken and analysed. Other measurements which were taken during or after each runs includes bed height, coal usage, bed temperature, pressure drop across the system, cyclone reject, flue gas composition and so on.

From this investigation, the effect of mud/shale stone left in the bed on bed temperature and sintering and agglomerate formation, as well as the deposition of ash on the surface bed material particles, which is part of the bed material and ash interaction mechanisms were observed. The observations made from this investigation enhanced the understanding of the change in hydrodynamic profile which causes an increase in the mean particle size of the bed, and poor heat transfer. This eventually was found to lead to increase in localised temperature in the bed earlier identified and discussed as part of the proposed sintering and agglomerate formation mechanisms for lump coal combustion given in section 2.5.4.

The second part of this investigation described as the crashed stop combustion runs of the PSBFBC system involves the troubleshooting of a typical fluidisation combustion run by stopping fluidisation of the bed material in the PSBFBC. This was done in order to further establish the localised temperature build-up effect in the FBC responsible for promoting sintering and agglomerate formation. For this investigation, the same washed and unwashed Blyth coals as those used in the part one of these studies were used. The old Garside 14/25 sand bed material obtained at the end of each of the 10 coal type runs or approximately 52 hours of combustion operation in phase 1 was re-used for this investigation. The findings

and observation made from this investigation emphasises the contributory effect of temperature increase attained from stopping fluidisation to sintering and agglomerate formation.

The two investigation parts discussed in this chapter covers phase 3 of the overall experimental flow sheet given in section 4.1.

6.2. Methodology

Material specifications of the Garside 14/25 sand bed material and coals used in this investigation are detailed in section 4.2 while the experimental methodology approaches implemented including sampling techniques and measurements are detailed in section 4.4 and 4.5. Characterisation techniques used in this study are XRF, SEM and EDX analyses, which have been described in section 4.6.1, 4.6.2 and 4.6.3 respectively.

6.3. Normal Combustion Runs

As earlier stated that in order to achieve better understanding of sintering and agglomerate formation mechanism/s during lump coal combustion in a FBC, a prolonged normal combustion operation run is required. Based on this, a prolong normal combustion operation was setup using two coal types (washed and unwashed Blyth coals) which were fed and combusted in the PSBFBC for a total number of 10 runs within a total accumulated combustion time of approximately 52 hours. For each coal type investigated, a new batch of fresh Garside 14/25 sand bed material was introduced into the PSBFBC and continuously used for the entire duration of the whole set of 10 runs or 52 hours of combustion operation. After each experimental run, samples of the bed material were taken and analysed as well as other measurements, which were taken during or after the each run. Findings made from this investigation are discussed in this section

covering topics, which includes monitoring of bed operation, visual observation of agglomeration, agglomerated bed material chemistry, ash coated bed material properties, bed height, particle size growth and carbon in ash.

6.3.1. Monitoring of Bed Operation

The condition of the bed fluidisation and operation of the PSBFBC system was primarily monitored using the bed temperature (T1 to T6), pressure drop and flue gas composition measurements. This was done throughout the operation of the PSBFBC from start-up until shutdown. The temperature profile of the bed marked from T1 to T6 identifies various temperature measuring positions across the PSBFBC reactor section previously described in section 3.8.1 as TC-1 to TC-6. Discussion in this section has been structured to cover two parts namely start-up operating condition and lump coal combustion condition.

6.3.1.1. Start-up Operating Condition

During the start-up operation of the PSBFBC system, the temperature profiles (T1 to T6) and pressure drop profile are the only variables monitored to understand the operating conditions of the bed. Typical examples of some cases specific data to illustrate this measured variable are presented in Figure 6-1 to Figure 6-6 respectively. As shown in these figures, the broken red coloured vertical lines labelled from A to H identifies various operating conditions of the PSBFBC system. Lines marked A to G identifies the changes that occurs in the bed PSBFBC conditions as fluidising air volumetric flowrate is increased as noted where A: 0, B: 200, C: 260, D: 320, E: 380, F: 440 and G: 500 (all measured in litres/minute at room temperature). Line marked H identifies the point when coal injection into the PSBFBC bed starts after a temperature of 600°C has been reached by temperature point T3 or T2.

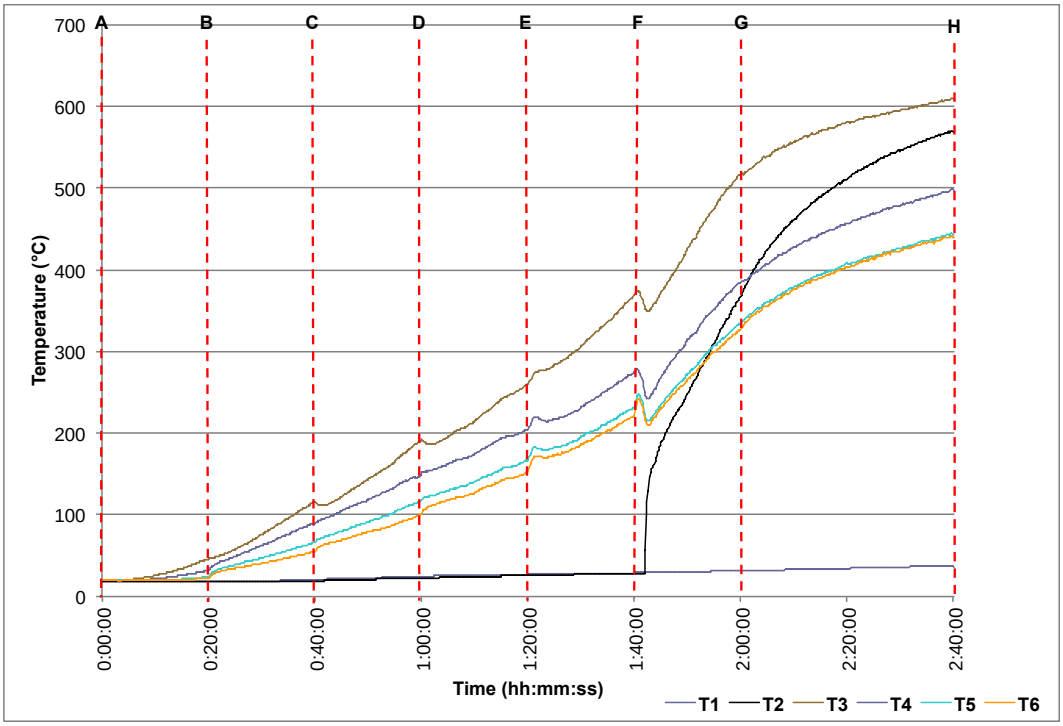

Figure 6-1: Typical PSBFBC bed temperature profile at start-up before coal injection for washed Blyth coal experimental run 1 to 10 and unwashed Blyth coal run 1 to 7

The bed measured temperature profile presented in Figure 6-1, shows a typical example of the PSBFBC bed temperature profile observed at start-up for washed Blyth coal experimental run 1 to 10 and unwashed Blyth coal experimental run 1 to 7. From Figure 6-1, it can be seen that temperature measured inside the PSBFBC reactor section increases as time increases. The measured temperatures (T1 to T6) was observed to slightly decrease at point B, C, D and F when volumetric air flow rate was increased. This initial dip in temperature at these points is known to be due to the increase in the flow of low temperature air into the PSBFBC, which creates an initial temperature cooling effect. Over time, the introduced low temperature air mixes with hot air in the system to attain a stable temperature after which the air temperature begins to rise again by absorbing heat from the bed materials that was heated by the PSBFBC heaters.

The highest temperature measured in the system prior to the introduction of coal into the PSBFBC is at temperature point T3, which is located in the fluidising

zone of the PSBFBC bed above the heaters. While the lowest temperature measured is at point T1, which is located in the plenum chamber. Temperature measuring point T2, which is located in the fluidising zone of the PSBFBC bed, placed to measure the bed temperature can be observed to experience a rapid increase after line F as shown in Figure 6-1. Line marked F signifies the point when the fluidising air flowrate has been increased to 440 litres/minute. The occurrence of this sharp increase in temperature has been identified as the point where bed fluidisation begins. This phenomenon can be supported by the pressure drop profile data presented in Figure 6-2.

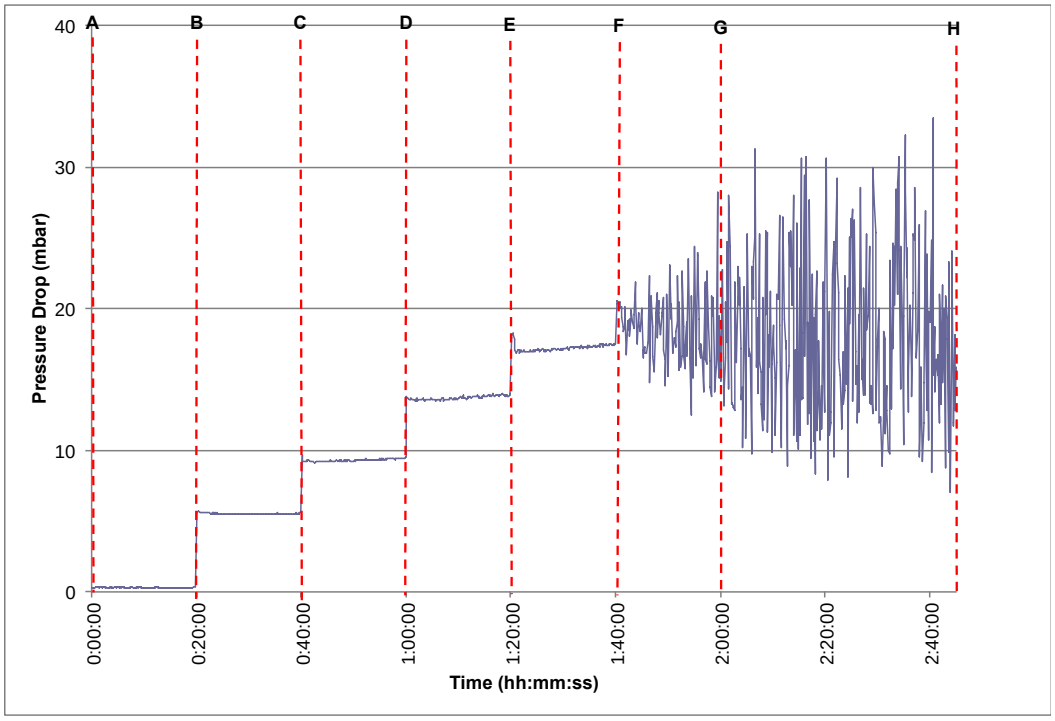

Figure 6-2: Typical PSBFBC bed pressure profile at start-up before coal injection for washed Blyth coal experimental run 1 to 10 and unwashed Blyth coal run 1 to 7

The bed pressure profile presented in Figure 6-2, shows a typical example of the PSBFBC bed pressure profile observed at start-up for washed Blyth coal experimental run 1 to 10 and unwashed Blyth coal experimental run 1 to 7. it can be observed in Figure 6-2, that the measured pressure drop of the PSBFBC bed begins to fluctuate after line marked F, which signifies fluidisation. The quality of

the bed fluidisation can be judged by the height of the pressure drop fluctuation (Bartels et al. 2010b), which appears to be increasing as temperature and fluidising air flowrate increases. The pressure drop profile also shows the occurrence of a step change increase in the measured bed pressure drop as the volumetric airflow rate was increased until line marked F.

During the start-up for unwashed Blyth coal experimental run 8, a change in the measured temperature and pressure drop profile of the PSBFBC system was observed which are presented in Figure 6-3 and Figure 6-4 respectively.

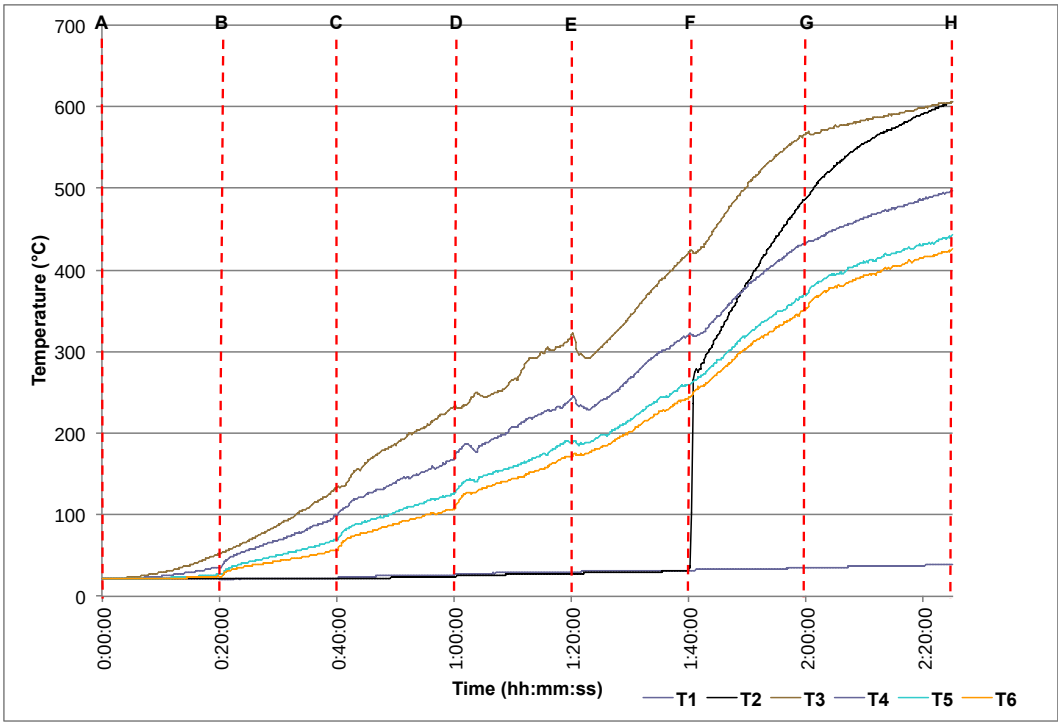

Figure 6-3: PSBFBC bed temperature profile at start-up before coal injection for unwashed Blyth coal run 8

The measured temperature at T2 was observed to be as high as the measured temperature at T3. The occurrence of this is surprising and might be argued to have being influenced by various factors such as ambient air temperature and ignition of left over coal in the PSBFBC bed from the previous experimental run. However, the pressure drop profile presented in Figure 6-4 over the same period

provides an insight into the possible cause of this occurrence, which was not so visible from the temperature profile.

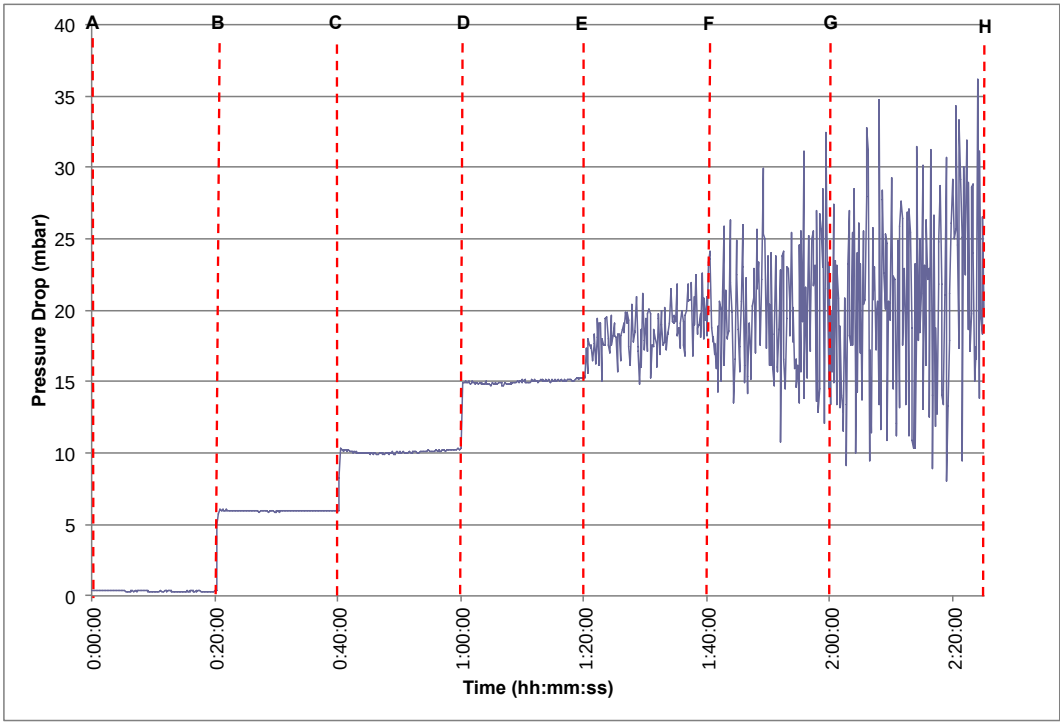

Figure 6-4: PSBFBC bed pressure profile at start-up before coal injection for unwashed Blyth coal run 8

As shown in Figure 6-4, PSBFBC bed fluidisation was observed to start after line marked E, which equates to an air flowrate of 380 litres/minute as opposed to 440 litres/minute reported earlier. The reason for this change in fluidisation profile is believed to have being caused by the high amount of mud/shale stones deposition in the PSBFBC bed, which is explained later in section 6.3.2. This change in fluidisation profile, which causes early fluidisation of the bed, is proposed to have caused the rapid rise in measured temperature T2. These same observations were made for the temperature and pressure drop profiles of the PSBFBC system presented in Figure 6-5 and Figure 6-6 respectively during experimental run 9 and 10 for the unwashed Blyth coal.

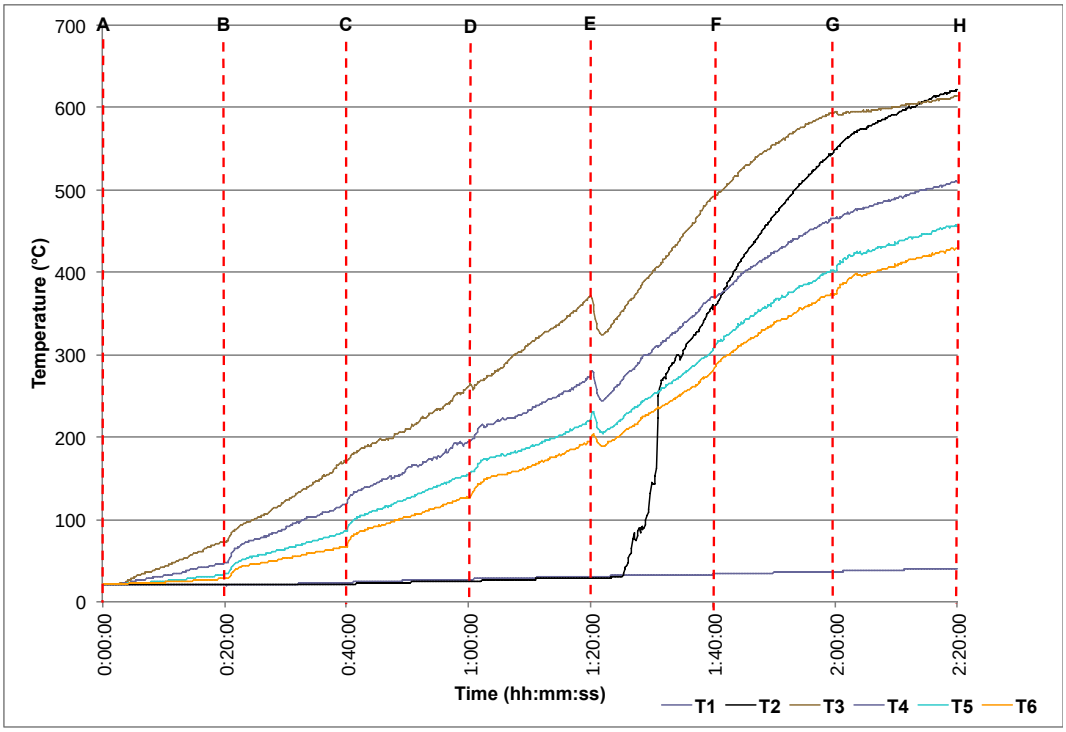

Figure 6-5: PSBFBC bed temperature profile at start-up before coal injection for unwashed Blyth coal run 9 and 10

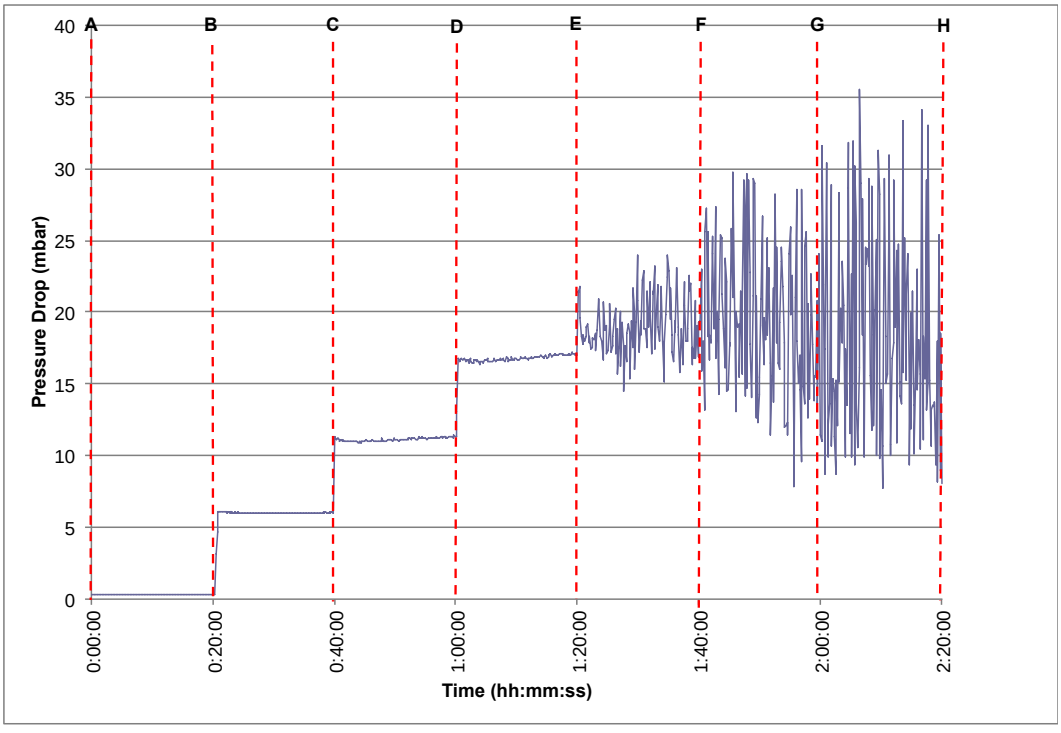

Figure 6-6: PSBFBC bed pressure profile at start-up before coal injection for unwashed Blyth coal run 9 and 10

6.3.1.2. Lump Coal Combustion Conditions

During lump coal combustion, vertical temperature, linear pressure drop and flue gas composition were all measured to monitor the fluidisation quality and operating condition of the PSBFBC system. Comprehensive summaries of the experimental operating conditions for each experimental run for both washed and unwashed Blyth coal are presented in Table 6-1 and Table 6-2 respectively. The bed temperature, furnace temperature, pressure drop, air flowrate and flue gas composition data presented in Table 6-1 and Table 6-2 are all average values obtained for each experimental run.

Temperature Profile

For each experimental run, the vertical temperature data obtained throughout the combustion process for a typical experimental run is presented in Figure 6-7. After coal injection into the PSBFBC to initiate the combustion process, temperature T2, which indicates the bed temperature increases and becomes the hottest point in the PSBFBC system, as this is where combustion takes place.

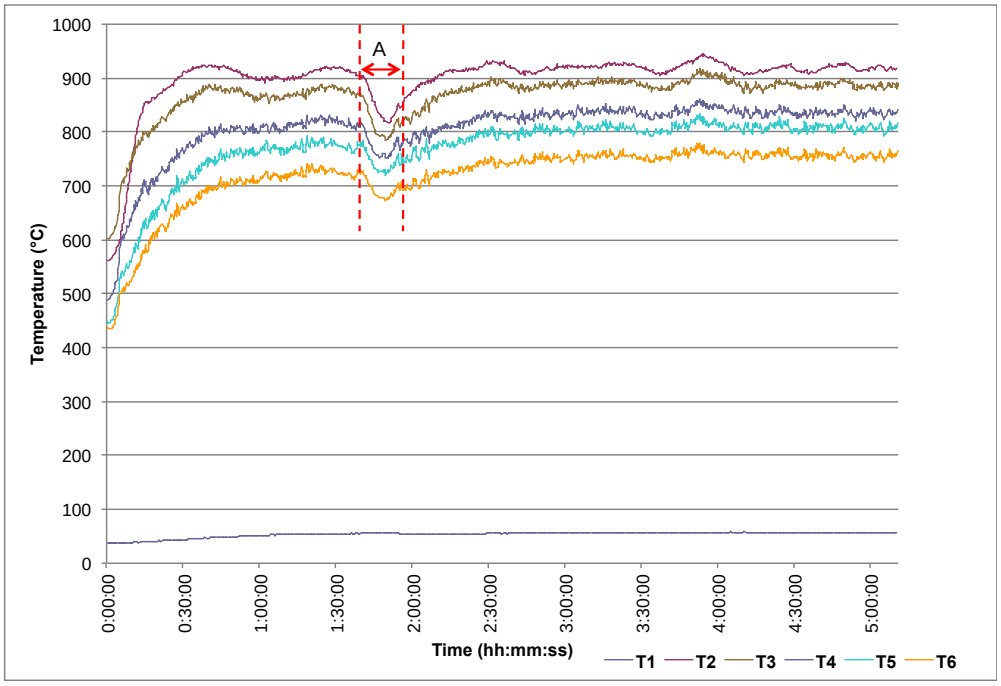

Figure 6-7: Typical PSBFBC bed temperature profile during combustion of lump washed and unwashed Blyth coals

Table 6-1: Experimental operating conditions for evaluating sintering and agglomerate formation during PSBFBC of washed Blyth coal

Run	Run Time (h)	Bed Temp. (°C)	Furnace Temp. (°C)	Max. Bed Temp. (°C)	Pressure Drop (mbar)	Air Flowrate (l/min)	Coal Feedrate (kg/h)	Bed Height (cm)	Ash Collected (g)	Flue gas Composition			
										O_2 (% Vol.)	CO_2 (% Vol.)	NO_x (ppm)	CO (% Vol.)
1	5.13	887	856	985	19.31	619	1.9	18.7	550	14.39	5.35	169.27	0.03
2	5.17	893	870	950	19.63	632	2.4	19.3	509	11.05	9.13	387.61	0.02
3	5.18	899	880	935	19.44	629	1.8	19.9	769	10.75	9.39	371.53	0.03
4	5.18	895	877	939	19.71	640	2.4	20.1	800	10.96	9.17	382.29	0.03
5	5.18	899	883	945	20.33	636	2.4	20.2	800	10.86	9.31	400.68	0.03
6	5.18	902	886	939	20.16	633	2.1	21.2	755	10.69	9.41	409.08	0.02
7	5.18	908	893	949	20.53	654	2.1	21.8	747	10.76	9.37	383.12	0.02
8	5.18	913	899	940	21.1	692	2.2	21.8	786	10.68	9.39	386.34	0.02
9	5.18	912	897	943	21.18	695	2.2	21.8	775	10.79	9.29	385.8	0.02
10	5.18	908	894	952	21.07	712	2.0	21.6	809	10.87	9.15	383.6	0.02

Table 6-2: Experimental operating conditions for evaluating sintering and agglomerate formation during PSBFBC of unwashed Blyth coal

Run	Run Time (h)	Bed Temp. (°C)	Furnace Temp. (°C)	Max. Bed Temp. (°C)	Pressure Drop (mbar)	Air Flowrate (l/min)	Coal Feedrate (kg/h)	Bed Height (cm)	Ash Collected (g)	Flue gas Composition			
										O_2 (% Vol.)	CO_2 (% Vol.)	NO_x (ppm)	CO (% Vol.)
1	5.18	918	889	959	19.85	709	2.3	20.8	703	11.16	8.8	380.14	0.02
2	5.18	906	889	945	19.71	682	2.1	21.8	685	11.12	8.9	397.66	0.02
3	5.18	917	903	948	20.78	712	2.3	22.0	703	10.83	9.21	397.11	0.02
4	5.18	916	901	950	20.7	707	2.1	22.2	802	10.90	9.14	404.47	0.02
5	5.18	917	905	948	20.82	695	2.1	22.8	701	10.78	9.27	406.04	0.02
6	5.18	917	908	953	21.15	701	2.3	23.0	748	10.72	9.31	403.21	0.02
7	5.18	922	914	958	20.73	708	2.2	23.1	809	10.64	9.37	394.47	0.02
8	5.18	918	909	960	21.53	702	2.2	23.2	828	10.77	9.26	397.67	0.02
9	5.18	910	898	940	21.08	688	2.1	23.4	826	11.05	8.99	414.37	0.02
10	5.18	919	907	966	21.61	688	2.2	23.8	807	10.70	9.26	411.35	0.02

The next highest temperature measuring point in the PSBFBC is T3, which measures the temperature above the bed in the PSBFBC fluidising zone. This is followed by temperature point T4, T5, T6 and T1 respectively in their measured temperature decreasing order from hottest to coldest. This same pattern or order was observed to be constant in every experimental run for both washed and unwashed Blyth coal. Overall, the temperature profile of the PSBFBC system was found to be quite stable except for cases where blockage occurred in the coal feeder with an example marked by "A" in Figure 6-7. During this period, a drop in temperature was observed across the six temperature measuring points in the PSBFBC due to the lack of fuel to sustain the combustion process. This shows that the vertical temperature measuring approach is very sensitive to change in combustion temperature, which makes it a very suitable technique to detect any change in the combustion characteristics of the bed.

The practical effectiveness and applicability of using vertical temperature measurement approach earlier described in section 2.6.2.2 as a suitable sintering and agglomeration detection technique from literature (Scala & Chirone 2006; Zhong et al. 2013; Gatternig & Karl 2014; Duan et al. 2015) could not be fully established in this work. Although a small amount of agglomerated bed was material (later discussed in section 6.3.2) formed in the unwashed Blyth coal bed but did not show any visible alteration to the PSBFBC temperature profile. Hence, it can be argued that larger amount of agglomerated bed material is required to be formed in order for this technique to be effective.

Pressure Drop Profile

A typical linear pressure drop measured across the PSBFBC system is shown in Figure 6-8. It can be seen from the large fluctuations in the pressure drop data profile that the PSBFBC bed is well fluidised throughout the combustion cycle.

This pattern was observed to be similar in all experimental runs for both the washed and unwashed Blyth coal investigations. This might be due to the fact that full agglomeration and defluidisation of the PSBFBC bed did not occur over the 52 hours investigation period in each coal type case. The coal feeder blockage clearly identified in the temperature profile was also slightly visible in linear pressure drop profile as shown by region marked “A” in Figure 6-8.

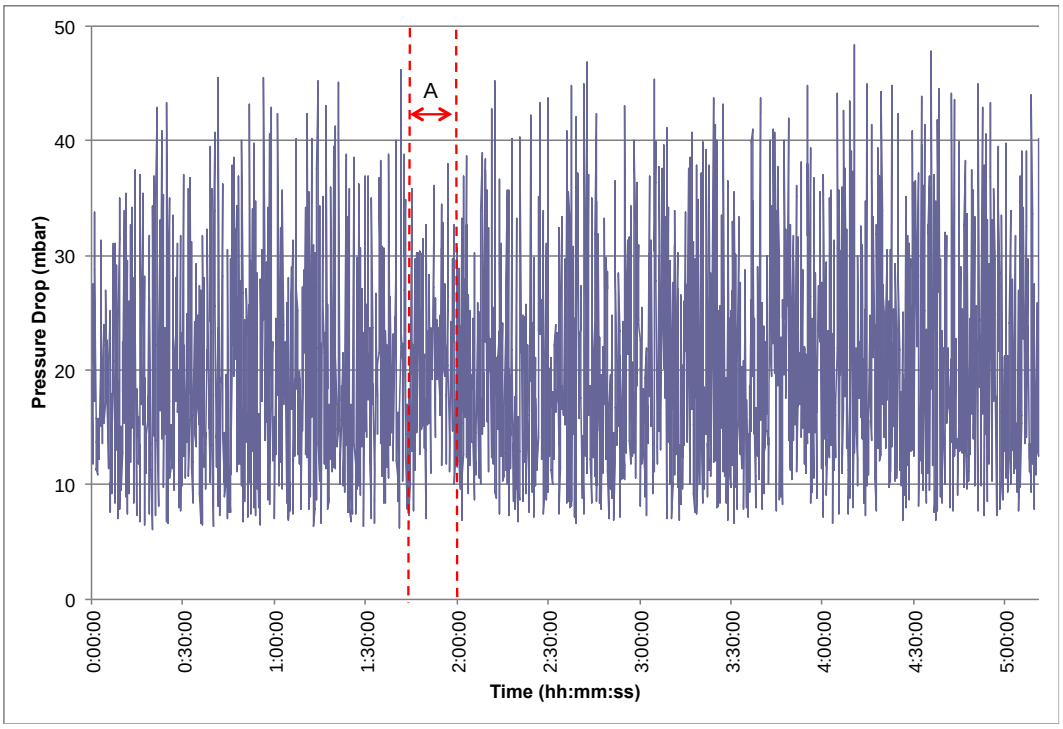

Figure 6-8: Typical PSBFBC bed pressure profile during combustion of lump washed and unwashed Blyth coals

The average linear pressure drop data obtained for every experimental run using washed and unwashed Blyth coals is presented in Figure 6-9. Overall, it can be seen that the average pressure drop increases as the experimental run (operation time) increases. The reason for this observed increased is proposed to be caused by the increase in the measured bed height to be further discussed in section 6.3.5.

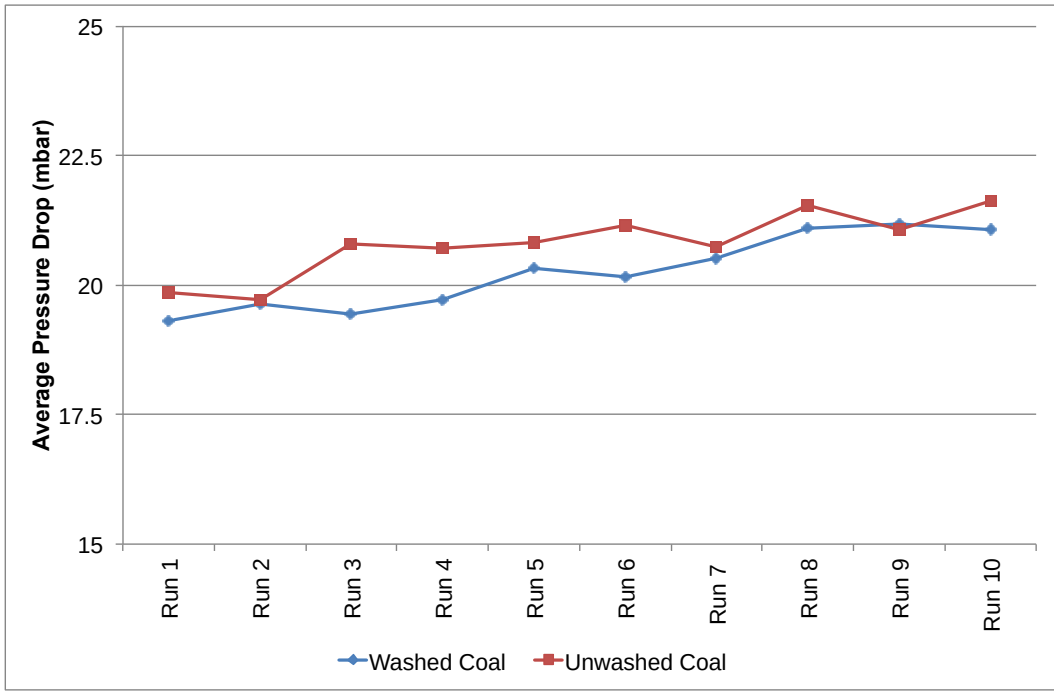

Figure 6-9: Average pressure drop profile for the operation of PSBFBC for each experimental run during the evaluation of sintering and agglomerate formation using washed and unwashed Blyth coal

Flue Gas Composition Profile

A typical profile of the flue gas composition data measured over the course of a combustion run is presented in Figure 6-10. The composition of CO_2, CO and O_2 are measured in volume percentage (Vol.%) while that of NO_x was measured in part per million (ppm).

The percentage composition of CO in the flue gas stream was observed to be very low which shows the efficiency of the combustion process. The relatively high percentage composition of O_2 in the flue gas stream was caused by the high amount of excess air used (90 to 100%), which was needed in order to maintain the bed temperature in the PSBFBC.

The coal feeder blockage effect identified in the vertical bed temperature profile marked as “A” was also identified in the flue gas composition profile as presented in Figure 6-10. The percentage concentrations of NO_x and CO_2 were observed to decrease while that of O_2 increased in the flue gas stream as a result of the

blockage in the coal feeder due to the lack of fuel to continue the combustion process in the PSBFBC bed.

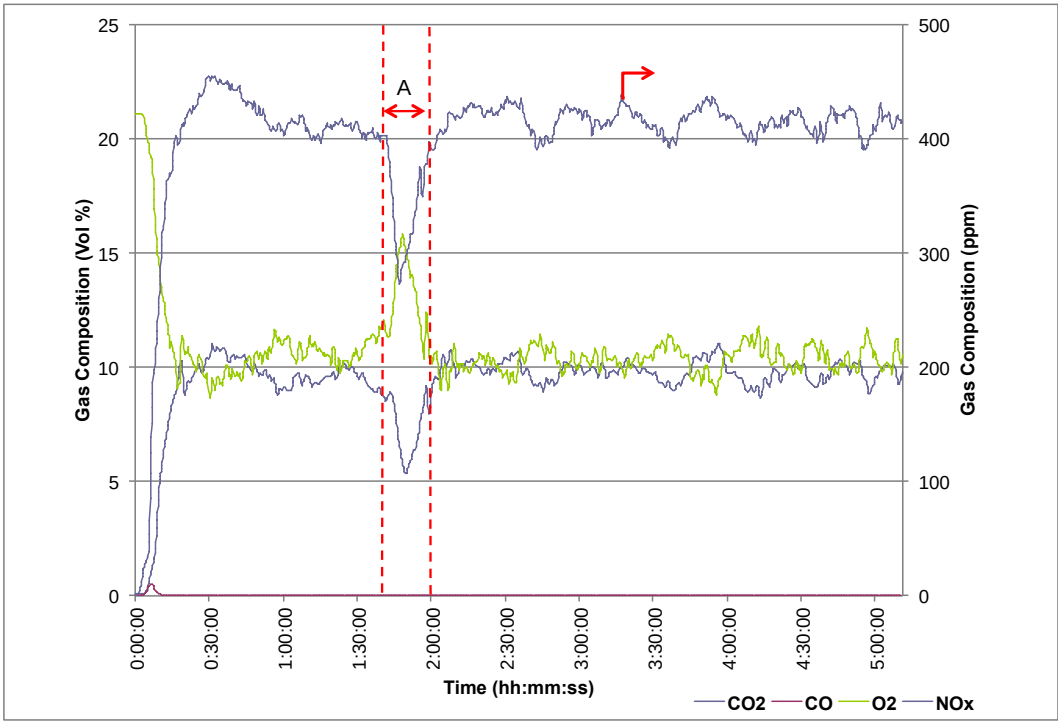

Figure 6-10: Typical PSBFBC flue gas composition during combustion of lump washed and unwashed Blyth coals

6.3.2. Visual Observation of Agglomeration

Following the visual inspection procedure earlier detailed in section 4.4.1, after the 10 runs or approximately 52 hours of combustion operation with washed and unwashed Blyth coal, the PSBFBC bed from each coal was removed after cooling down to room temperature and visually inspected. Photographs showing the representation of the observed difference during the visual inspection of the PSBFBC bed material obtained after the combustion of washed and unwashed Blyth coals are presented in Figure 6-11. As shown in Figure 6-11, five distinctive items were marked labelled A – E. Item marked A identifies the Garside 14/25 sand bed material which have been coated with ash generated from the coal combustion process. These ash coated bed materials were discovered in the

PSBFBC bed for both the washed and unwashed Blyth coal in the fluidising section of the bed where coal combustion and ash deposition occurs.

The second type of items marked as B, which identifies the mud/shale stones present in the PSBFBC bed. It can be seen that deposition of mud/shale stones in the PSBFBC bed was clearly observed in both cases of washed and unwashed Blyth coal PSBFBC beds. This shows that the washing process is not 100% efficient in removing all the mud/shale stones present in the coal but helps in reducing it composition as evident from the comparison between the two beds which shows a larger quantity of mud/shale stones in the unwashed Blyth coal PSBFBC bed than that of the washed PSBFBC bed. The mud/shale stones were also noticed to be predominant at the base of the bed as shown in the “bottom of bed” images for both washed and unwashed Blyth coals PSBFBC beds given in Figure 6-11. The occurrence of this is due to the larger weight and larger particle bulk density of the mud/shale stone, which causes them to sink to the base of the PSBFBC bed.

Items marked as C, which identifies the uncoated Garside 14/25 sand bed materials was observed to be present in the PSBFBC beds of the washed and unwashed Blyth coal setup. The uncoated bed materials were found at the base of PSBFBC bed in the blank region (dead zone) of the nozzle in the PSBFBC rig shown Figure 6-12 where no fluidisation or combustion is expected to occur. The Garside 14/25 sand bed material however found in this zone were observed to have gone through the colour change phase similar to what was earlier reported and discussed during the calcination of fresh Garside 14/25 sand bed material in section 5.3.1. This colour is suspected to have occurred based on the radiation or conduction of heat that might have occurred from the combustion of coal above this region and from the electrical heater used during start-up.

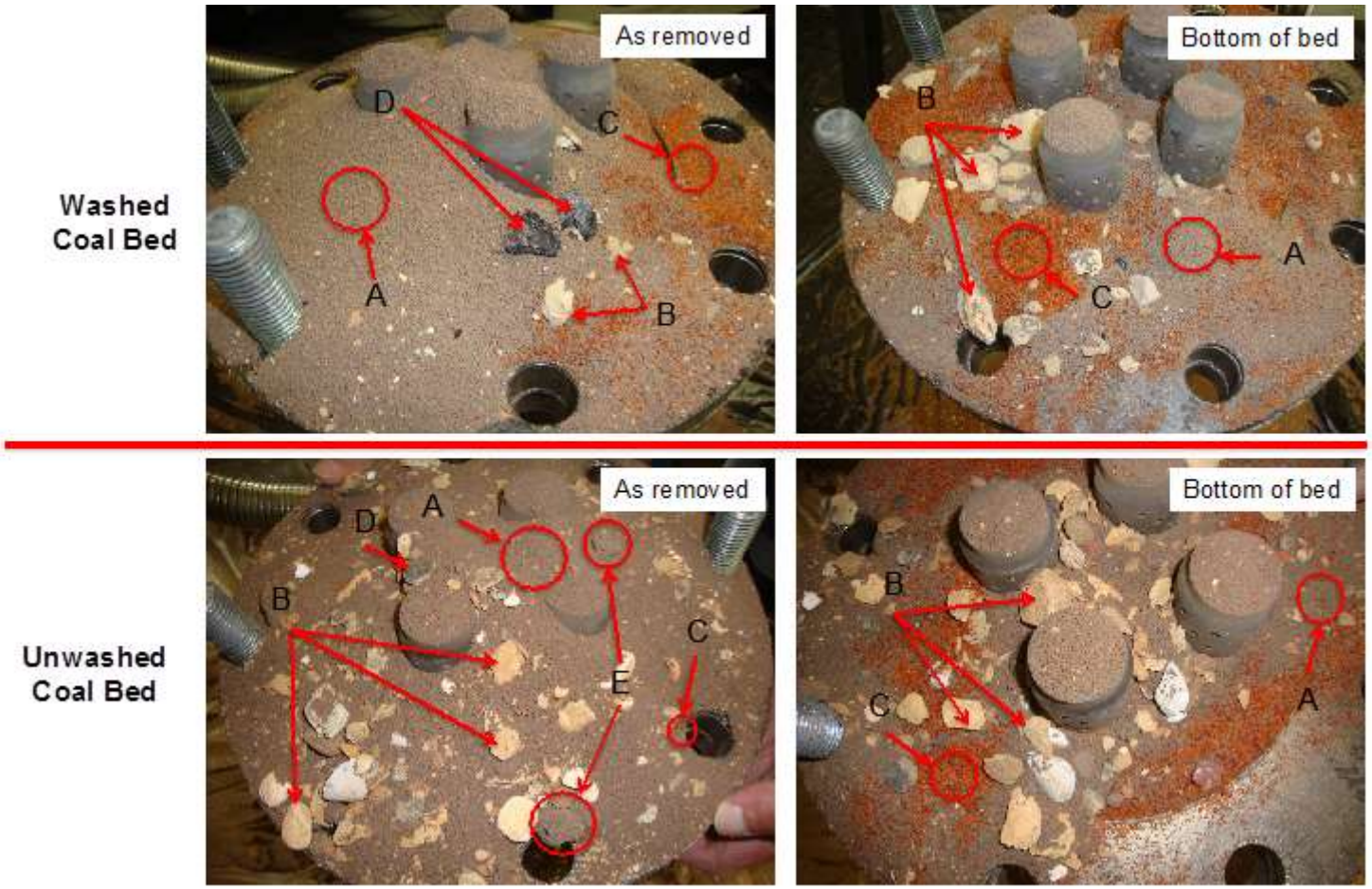

Figure 6-11: Photograph of the PSBFBC bed after 10 runs (52 hours) of combustion operation during the evaluation of sintering and agglomerate formation using washed and unwashed Blyth coal:(A) Garside 14/25 sand bed material with ash coating, (B) mud/shale stones, (C) Garside 14/25 sand bed material without ash coating (D) un-burn coal, (E) agglomerated bed material

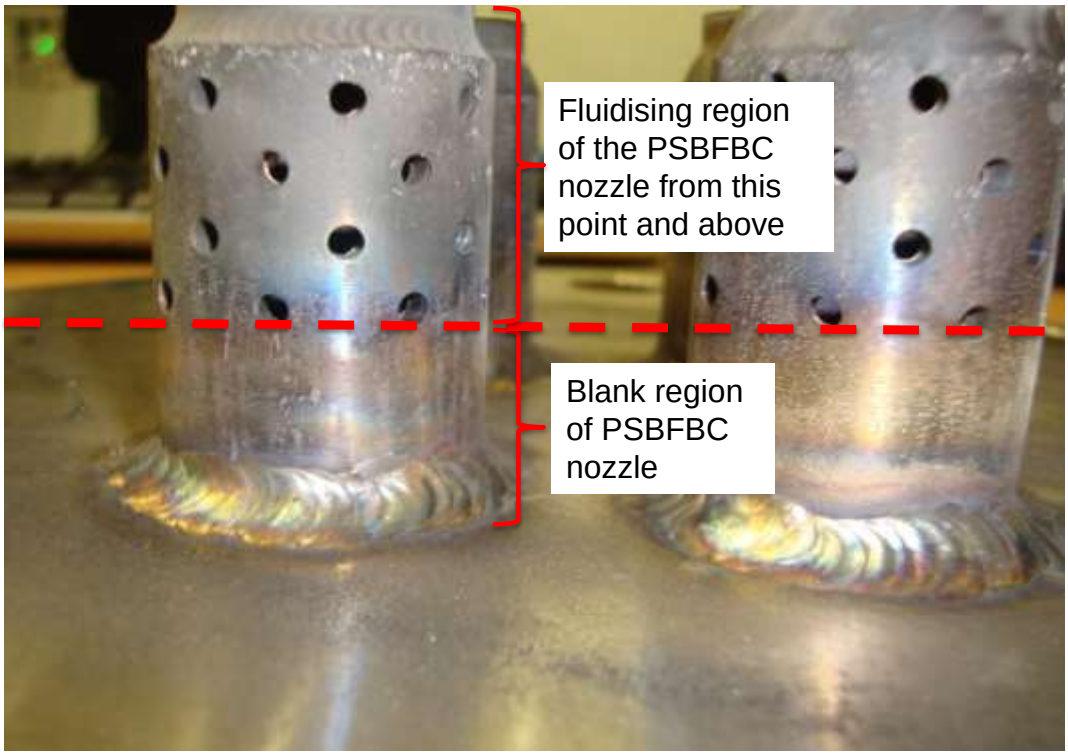

Figure 6-12: Sections of the zones identified on the PSBFBC nozzle influencing Garside 14/25 sand bed material coating with ash or not

Unburnt coals were the fourth set of items marked as D, which were found to be present in the PSBFBC bed of both the washed and unwashed Blyth coals. The presence of the unburnt coal shows that not all the coals injected into PSBFBC bed has been combusted when the experiment was stopped.

The final set of items identified in the PSBFBC bed are agglomerated bed materials marked as E in Figure 6-11. Agglomerated bed material samples were only found to be present in the PSBFBC bed of the unwashed Blyth coal. From this observation, it can be argued that the formation of agglomerated bed material during the combustion of lump coal in a FB is possibly caused by a major characteristic difference between the two fuel beds in this case which has been identified as varying amount of deposited mud/shale stones in the PSBFBC bed. It is been proposed at this stage that the higher deposition of mud/shale stone observed in the PSBFBC bed of the unwashed Blyth coal creates a change

in the hydrodynamics of the bed, causing a higher localised temperature build-up and possibly initiating ash melting.

6.3.3. Bed Height

The bed height measurement data collected for each run is presented in Figure 6-13. From the collected data, it can be seen that the bed height measured at the start of the washed Blyth coal investigation was 19cm and over the course of the 10 combustion runs, the bed height progressively increased to a measured height of 21.6cm at the end of run 10 which accounts for a total bed height increase of 2.6cm. In the case of unwashed Blyth coal, the measured bed height at the start before run 1 was 19.8cm, which progressively increased to a measured bed height of 23.8cm at the end of run 10 giving a total bed height increase of 4cm.

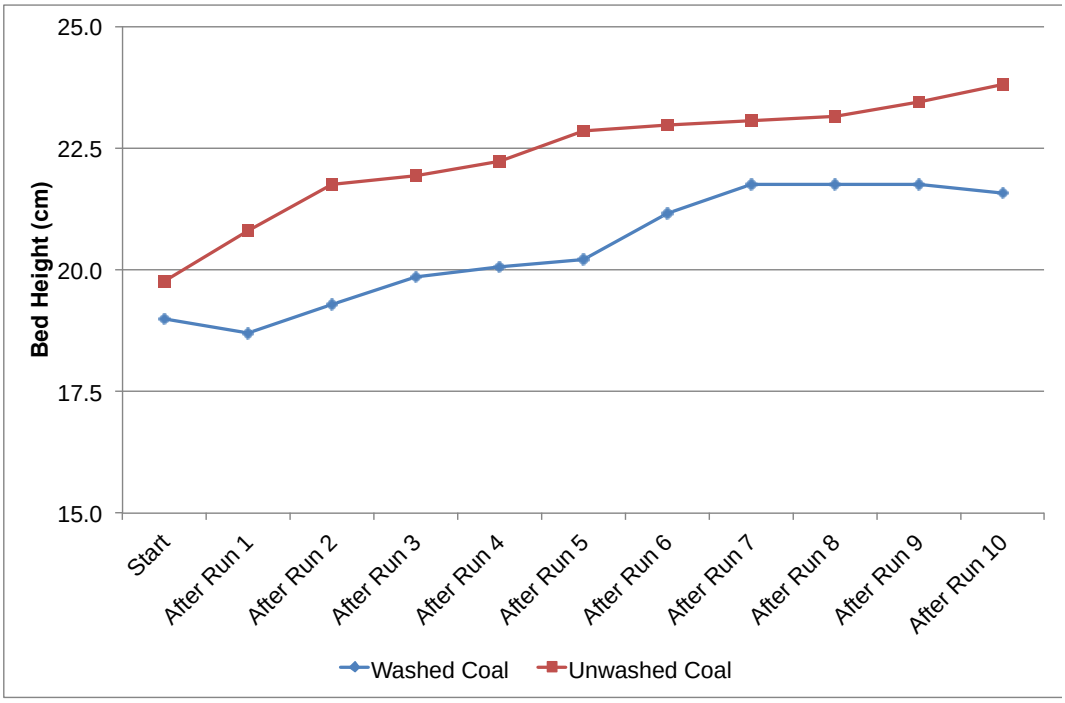

Figure 6-13: Average PSBFBC bed height measurement obtained after each experimental run during the evaluation of sintering and agglomerate formation using washed and unwashed Blyth coal

Hence, it can be seen that measured bed height increase in the unwashed Blyth coal investigation after 52 hours of combustion is about 1.5 times that observed

in the washed Blyth coal investigation. This bed height increase is due to the deposition of shale/mud stone in the PSBFBC bed, which was observed to be greater in bed of unwashed Blyth coal investigation earlier discussed in section 6.3.2. Other factors that are suspected to have contributed to this difference in measured bed heights includes higher deposition of ash in the PSBFBC bed (7.4% deposition for washed Blyth coal and 31% for unwashed Blyth coal) and presence of agglomerated bed material in the unwashed Blyth coal investigation when compared with washed coal investigation.

6.3.4. Particle Size Growth

Sieving analysis was performed on the entire Garside 14/25 sand bed material prior to introducing it into the PSBFBC and after the 10 combustion runs for each of the washed and unwashed Blyth coal investigated after it has cooled down to room temperature to determine the particle size of growth of the bed material. The particle size fraction data obtained from sieving of the bed materials are presented in Figure 6-14. From this figure, it can be clearly seen that a wide variation occurs between the particle size fractions of the fresh Garside 14/25 sand bed material when compared with those obtained from the PSBFBC after the 52 hours combustion of washed or unwashed Blyth coals.

A general trend of lower particle sized fraction was observed for the unwashed Blyth coal PSBFBC bed when compared with that of the washed Blyth coal bed and fresh bed materials. This occurred until a particle size of about 1050μm after which, larger particle sized fractions than that of the washed Blyth coal bed and fresh bed materials were obtained for the same percentage composition.

From Figure 6-14, three main zones have been highlighted for discussions. The first zone is the large particle sized fractions (≥1180μm), which are marked A and B Figure 6-14 for washed and unwashed Blyth coal PSBFBC bed respectively.

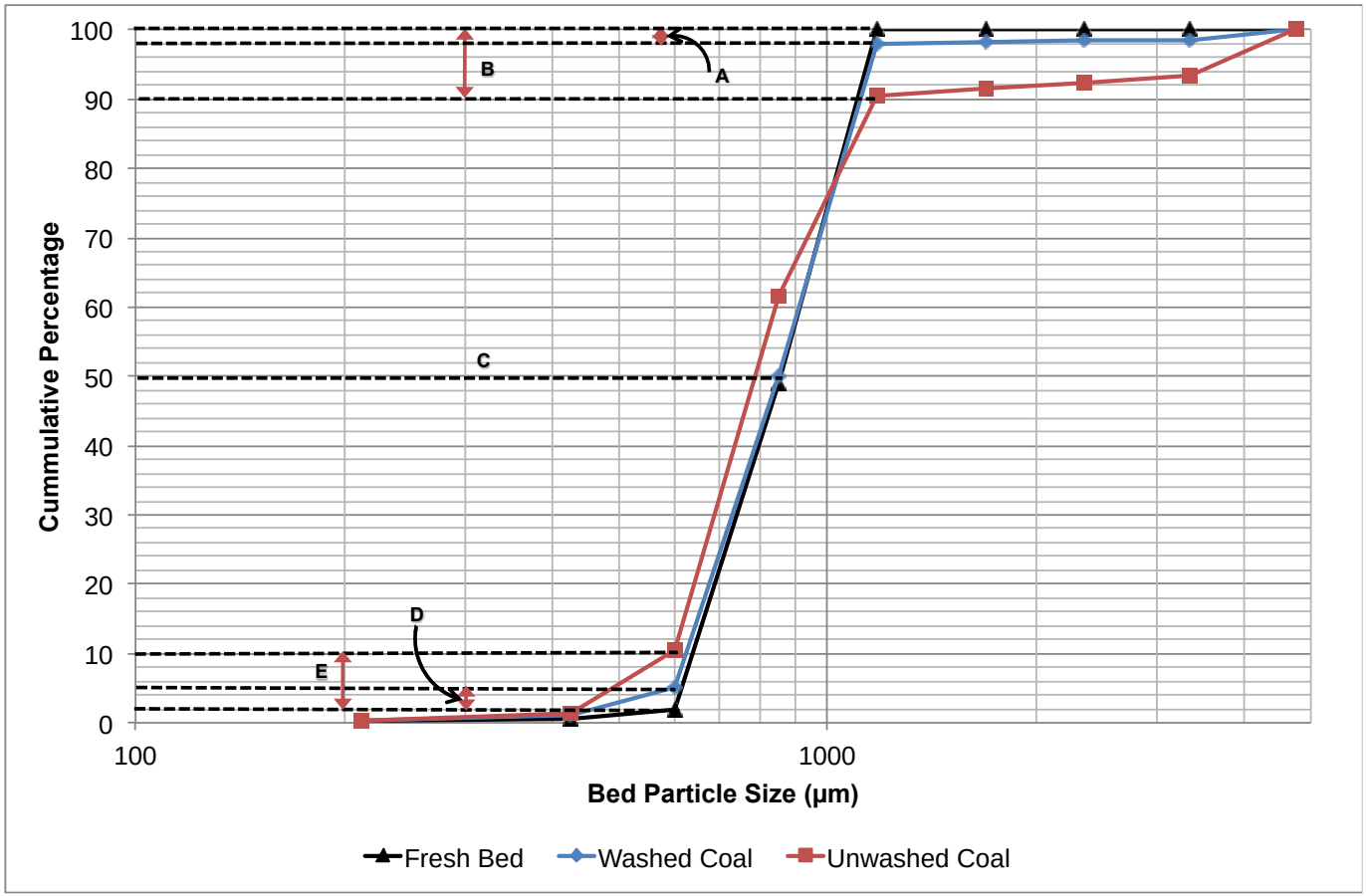

Figure 6-14: Comparison of Garside 14/25 sand bed material particle size distribution of the PSBFBC bed obtained after 10 runs (52 hours) of combustion operation during the evaluation of sintering and agglomerate formation using washed and unwashed Blyth coal to that of the fresh bed material

For this particle size fraction range, a percentage composition of 0.01% was measured for the fresh Garside 14/25 sand bed material, which increased to 2.05% for the washed coal bed and 9.44% for the unwashed coal bed obtained after 52 hours of combustion runs in the PSBFBC system. This observed increase in the fraction of larger sized particles for both cases of washed and unwashed Blyth coal PSBFBC bed when compared to that of the fresh bed can be attributed to the deposition of mud/shale in the bed, unburned coal and bed material particle coating with ash which were all identified during the visual inspection discussed in section 6.3.2. The greater increase observed between the washed and unwashed Blyth coal PSBFBC bed is due to the higher deposition of mud/shale stones and formed of agglomerated Garside 14/25 sand bed material in the unwashed Blyth PSBFBC bed as identified and discussed in section 6.3.2.

The second zone is change in the mean particle size diameter marked by C in Figure 6-14. A mean particle size diameter of 850μm was measured for the fresh Garside bed material which is identical to that of the washed Blyth coal PSBFBC bed with small negligible change. However for the case of the unwashed Blyth coal PSBFBC bed, the mean particle size diameter was observed to have decreased to 790μm.

The third zone is the small particle size fractions (≤600μm) marked D and E in Figure 6-14 for washed and unwashed Blyth coal PSBFBC bed respectively. The percentage composition of this size fraction measured in the fresh Garside 14/25 sand bed material was 1.84% which increased to 5.03% and 10.48% for the washed and unwashed Blyth coal PSBFBC bed respectively. The increase in the small size fraction is suspected to be due to ash deposition in the bed and shattering effects of the Garside 14/25 sand bed material discussed later in section 6.3.7. For the case of Blyth unwashed coal PSBFBC bed, a higher rate of

ash deposition is expected to occurs in the bed due to the high composition of ash in the Blyth unwashed coal. This can be supported by the estimated higher rate of ash deposition in the bed of the unwashed Blyth coal than that of the washed Blyth coal bed.

All this observed changes in the bed material particle size fractions is expected to widen the size distribution of the bed causing a change in the hydrodynamics of the bed. This is expected to negatively affect (reduce) the fluidisation quality of the bed (Ninduangdee & Kuprianov 2015). The findings here also supports those earlier discussed in section 6.3.2, which will later be used as the basis to support the argument on increased in localised bed temperature.

6.3.5. Carbon in Ash

Carbon content of cyclone ash reject can be used to access the efficiency of the combustion process (McCullough et al. 2011). The measured percentage weight composition of the carbon present in the cyclone reject ash is plotted against the average bed temperature of the PSBFBC as function of each experimental run for the washed and unwashed Blyth coal presented in Figure 6-15 and Figure 6-16 respectively.

The carbon content in ash measured for the washed Blyth coal is between 49 to 53% and 44 to 54% for the unwashed Blyth coal respectively across 10 experimental run for each coal type. From Figure 6-15, which represents the washed Blyth coal setup, it can be seen that a coherent relationship occurs between the carbon content in ash and the average bed temperature measured for each experimental run.

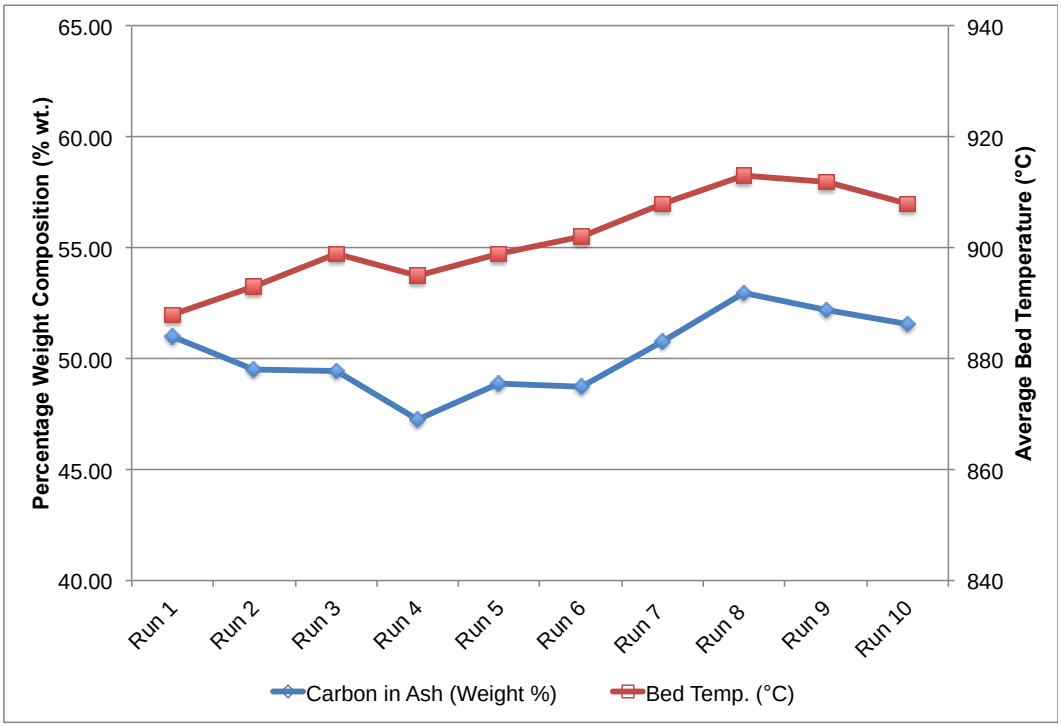

Figure 6-15: Percentage weight composition of carbon in the cyclone-reject ash and average bed temperature of the PSBFBC as a function of each experimental run during the evaluation of sintering and agglomerate formation using washed Blyth coal

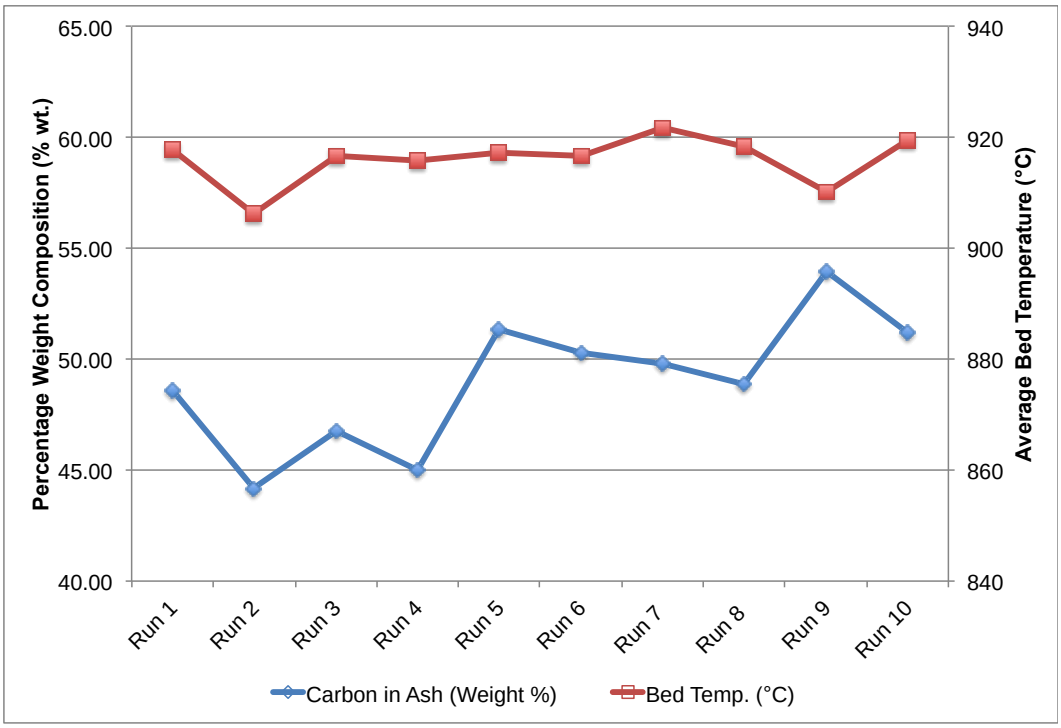

Figure 6-16: Percentage weight composition of carbon in the cyclone-reject ash and average bed temperature of the PSBFBC as a function of each experimental run during the evaluation of sintering and agglomerate formation using unwashed Blyth coal

In the case of the unwashed Blyth coal setup presented in Figure 6-16, a clear similar trend between carbon content in ash and average bed temperature as seen in the case of the washed Blyth coal could not be observed in this case. The reason for this is unknown but it is however suspected that the change in the hydrodynamic profile of the bed due to the deposition of mud/shale stone might have contributed to the further loss in combustion efficiency in PSBFBC system resulting in high carbon content in ash even at a higher bed temperature.

6.3.6. Agglomerated Bed Material Chemistry

As reported earlier, agglomeration of Garside 14/25 sand bed material occurred during the combustion of unwashed Blyth coal in the PSBFBC at the operating bed temperature of between 906°C and 922°C after 10 runs equating to 52 hours of operation. Similarly, agglomeration of Garside 14/25 sand bed material was also observed to occur in the industrial FBC during the combustion of same unwashed Blyth coal at an operating bed temperature of between 900°C and 950°C after 240 hours of continuous operation.

Making a comparison between these two agglomerated bed material samples formed from the same coal types, bed material and similar operating temperatures may not be straight forward. This is due to the fact they are formed in two different systems where refractory, flue gas recycle stream and continuous operating combustion condition is present in one (industrial FBC) and not the other (PSBFBC). Detailed conditions such as the flue gas compositions, bed pressure-drop measurements and air to fuel ratios over which the industrial FBC system was operating before the formation of the agglomerated bed material could not be fully established. Also in addition, the amount of ash reject collected from the industrial FBC cyclone which might be used to determine the ash composition in the bed is not known. The argument for this comparison

presented in this case is to determine if there is any difference / similarities in the chemistry and surface morphology of the agglomerated bed material produced from the same coal type, bed material and similar operating temperatures using best estimates where applicable even with all the unknowns in the system.

6.3.6.1. Comparison of the Surface Morphology of Industrial and PSBFBC formed Agglomerated Bed Material

A visual comparison between the two agglomerated bed material samples are presented in Figure 6-17. From the presented image, it is evident that the surface morphology of the two agglomerated bed material samples are different. The agglomerated bed material produced from the industrial operated FBC presented in Figure 6-17A shows the individual bed material particles joined together by what appears like a shiny glassy liquid melt which can be identified as the inter-particle liquid bridge.

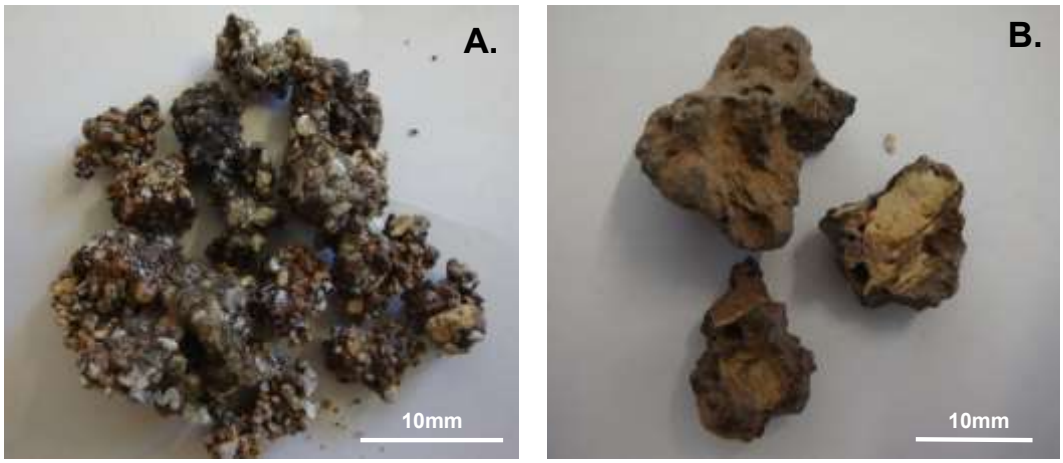

Figure 6-17: Agglomerated Garside 14/25 sand bed material obtained from the combustion of unwashed Blyth coal: (A) Industrial operated FBC after 240 hours of operation, (B) PSBFBC after 52 hours of operation

In the case of the agglomerated bed material produced from the PSBFBC shown in Figure 6-17B, the agglomerated particle appears very dirty and completely fused together with some pore like structures and some mud/shale stones within the fused melt. The structure appears to have been formed from heavy

deposition and melt because the bed material particles and the inter-particle liquid bridges existing between them are not visible. These early findings suggests that their formation mechanisms are totally different.

6.3.6.2. Sintering and Agglomerate Type / Mechanism

In order to better understand the mechanism responsible for sintering and agglomerate formation in these samples, SEM analysis was done on the two agglomerated bed material samples, which are presented in Figure 6-18. From Figure 6-18A, it can be seen that the agglomerated bed material formed from the industrial FBC during the combustion of lump Blyth unwashed coal shows the presence of liquid bridge binder in-between the Si (bed material) particles. In the case of the agglomerated bed material formed during the combustion of lump Blyth unwashed coal in the PSBFBC system which is presented in Figure 6-18B, it can be observed that a dense liquid melt or liquid bridge binder appears around the Si particle.

From direct comparison between the SEM micrographs of the two agglomerated bed material samples presented in Figure 6-18, it can be noticed that the number of Si particles present in the industrial agglomerated bed material sample is far higher than that observed in the PSBFBC agglomerated sample even though the two micrograph image are of the same magnification (x 100) and scale (1mm).

The proposed reasons for this difference can be attributed to the difference in their formation mechanism. As earlier pointed out in the visual observation discussion detailed in section 6.3.3.1 that a difference was seen in the surface morphology appearance of the two agglomerated bed material samples. It is possible that this difference in physical appearance corresponds to this observed difference, which might suggest that the industrial agglomerated bed material sample was formed from a melting induced pathway (low viscous binder)

(Teixeira et al. 2012; Mac an Bhaird et al. 2014; Namkung et al. 2015) whereas the PSBFBC agglomerated bed material was formed from coating induced pathway due to the heavy presence of the liquid binder (high viscous binder) (Visser 1989; Bartels et al. 2008; Teixeira et al. 2012).

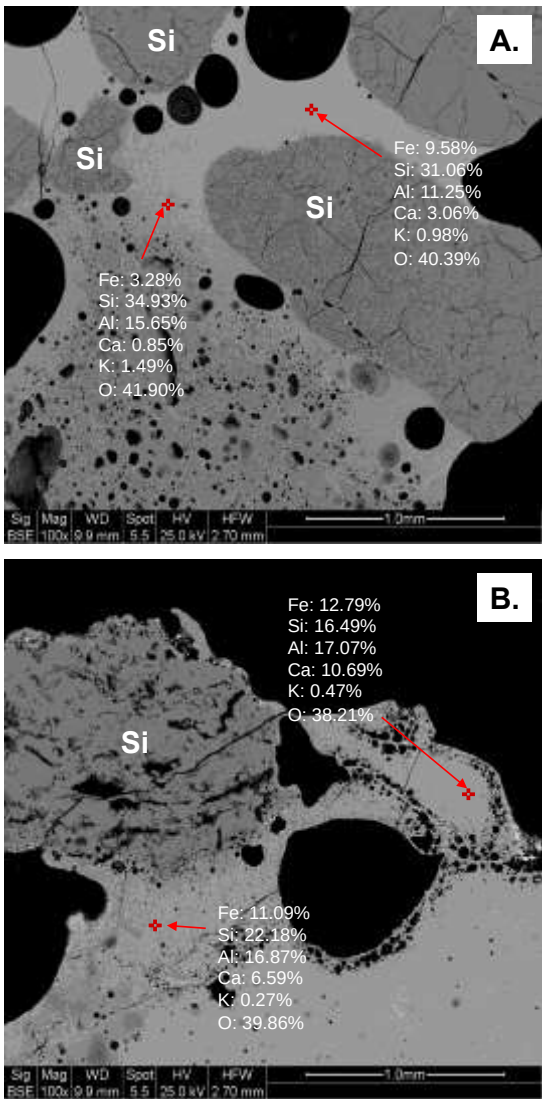

Figure 6-18: SEM / EDX micrograph showing the cross-sectional surface as well as the elemental spot analysis of the binder region of agglomerated Garside 14/25 sand bed material obtained from the combustion of unwashed Blyth coal (A) Industrial operated FBC after 240 hours of operation, (B) PSBFBC after 52 hours of operation

To verify this theory, the amount of ash deposited in the bed of the PSBFBC and industrial FBC were estimated as presented in Appendix I. Although most of the parameters around the operation of the industrial FBC required to be able to determine the ash content left over in the bed were not available. The best

estimated guess was done based on the limited data available. From this calculation, the ash composition of PSBFBC was estimated as 31% while that of the industrial FBC was estimated as 15% of the bed mass during the combustion of unwashed Blyth coal. It is evident from this comparison that the ash composition in the PSBFBC bed is higher than that of the industrial FBC, which may explain why the agglomerate formed in the PSBFBC shows a high fusing characteristics with less Si particles when compared to that of the industrial FBC. Both melting and coating induced pathways are types of bed material and ash particles interaction mechanism as described in section 2.5.2.

This concept was further supported by the result generated from the EDX analytical technique setup to determine the chemical composition of the binder linking the Si bed material particles together presented in Figure 6-18(A and B) for both the industrial agglomerated and PSBFBC agglomerated samples. Within Figure 6-18, the cross sign highlighted by the arrow identifies the precise location of the spot been analysed as shown in each image. It was discovered that the binder is predominately containing Fe, Si and Al with lower quantities of Ca and K. The elemental analysis of the binder in the industrial formed agglomerated bed material in Figure 6-18A shows that the amount of Fe was found to vary between 3.28 and 9.58%, Si was found to be between 31.06 and 34.93%, Al was found to be between 11.25 and 15.65%, amount of Ca was between 0.85 and 3.06% while that of K was between 0.98 and 1.49%.

For the agglomerated bed material produced from the PSBFBC shown in Figure 6-18B, the percentage weight (wt. %) of Fe was found to vary between 11.09 and 12.79%, Si was found to be between 16.49 and 22.18%, Al was found to be between 16.87 and 17.07%, amount of Ca was between 6.59 and 10.69% while that of K was between 0.27 and 0.47%. From the direct comparison of the composition of the binder region of the two agglomerated bed material samples,

it can be seen that PSBFBC agglomerated sample contains higher proportions of Fe, Al and Ca than those of the industrial formed agglomerated sample which exhibits higher amounts of Si and K. This composition variation is different from the findings of van Eyk and colleagues (2016) who reported a higher composition of Si in the binder region followed by Ca, Al, Fe and K during the gasification of south Australian low ranked coal (van Eyk et al. 2016). The findings of Luan and colleagues (2014) during their studies of combustion and sintering characteristics of ash from co-firing of coal and biomass ash shows a different composition trend to the reported pattern in this study and that of van Eyk and colleagues.

The result obtained from the XRF analysis presented in Figure 6-19 for the bulk analysis of agglomerated bed material obtained from the industrial FBC and PSBFBC correlates with the trend observed from the EDX analysis except for the composition K which was higher in PSBFBC agglomerated sample when compared with the industrial agglomerated sample.

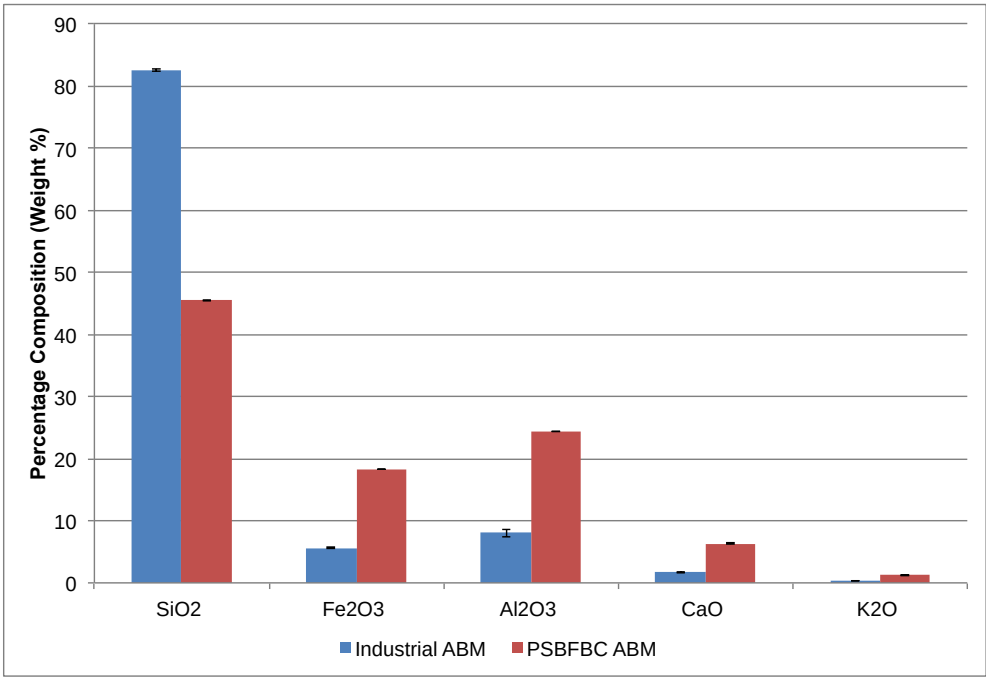

Figure 6-19: Comparison between the elemental oxide composition of agglomerated Garside 14/25 sand bed material (ABM) obtained from the combustion of unwashed Blyth coal in industrial operated FBC after 240 hours and PSBFBC after 52 hours of operation

On further analysing the agglomerated bed material samples using EDX elemental mapping, the distribution / spread of Si (silica), Fe (iron), Al (aluminium), Ca (calcium), K (potassium) and O (oxygen) across the surface of the agglomerated bed material samples was identified as presented in Figure 6-20 and Figure 6-21. In Figure 6-20 and Figure 6-21 which represent the industrial agglomerated bed material and PSBFBC agglomerated bed material respectively, the original images at the very left hand side are the SEM micrographs of the agglomerated bed material samples with each having six other images beside them highlighting the presence of earlier identified elements. For each image, the intensity of the colour across a particular area signifies the relative abundance of the element in that region. The spread of oxygen across the entire surface of agglomerated bed material samples shows that the identified elements are present in their elemental oxide forms.

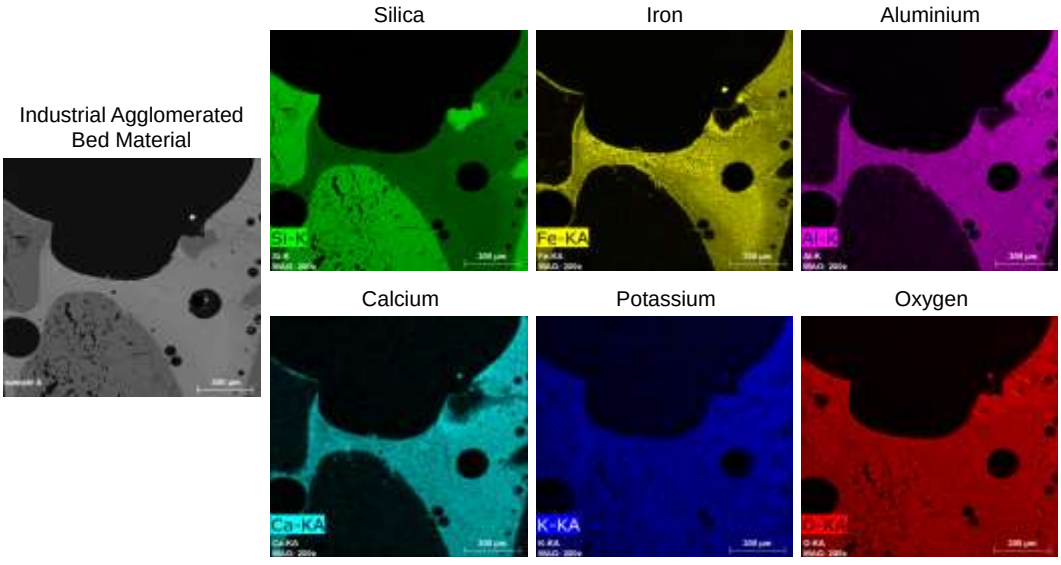

Figure 6-20: EDX elemental mapping of agglomerated Garside 14/25 sand bed material obtained after 240 hours of industrial FBC operation using unwashed Blyth coal showing the cross sectional surface distribution of identified elements in the melting induced sintering process

The EDX elemental mapping results clearly demonstrates the presence of Si, Fe, Al, Ca, K and O in the binder region of the agglomerated bed material samples in both cases. This supports the earlier findings reported from the EDX elemental

spot analysis measurement. It can be argued that the heavy presence of Si, Fe, Al, Ca and K in the binder possibly suggests that various types of strong alkaline-silicate inter-particle liquid bridge can be formed between the bed material particles.

Some of the possible alkaline-silicate melt that might have been responsible for this binder formation have been identified as a K_2O – Al_2O_3– SiO_2 which melts at temperature of 770°C typically formed in a K and Al rich environment (Schairer & Bowen 1947; Chaivatamaset et al. 2013), K_2O – CaO – SiO_2 which melts at a temperature of 790°C previously identified during the studies of agglomeration characteristics in fluidised bed combustion of biomass fuel (Brus et al. 2005; Llorente & Garcia 2005; Wang et al. 2012), Fe_2O_3 – Al_2O_3 – SiO_2 which melts at a temperature of 1073°C from the studies on coal ash agglomeration behavior (Schairer & Yagi 1952; Huffman et al. 1981; Wu et al. 2009; Datta et al. 2015) and CaO – SiO_2 – Al_2O_3 which melts at a temperature of 1093°C formed during the studies of coal melting behaviours (Huggins et al. 1981; Wu et al. 2009).

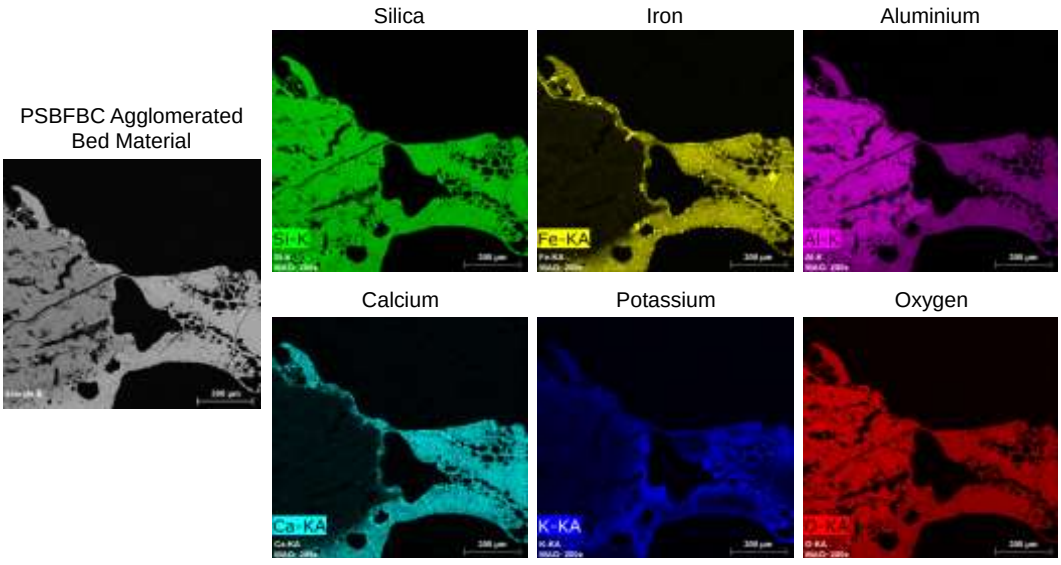

Figure 6-21: EDX elemental mapping of agglomerated Garside 14/25 sand bed material obtained after 52 hours of PSBFBC operation using unwashed Blyth coal showing the cross sectional surface distribution of identified elements in the coating phase sintering process

The decision on the type of melt/s responsible for this liquid bridge formation is dependent on abundance of the elemental composition of the identified elemental oxide present in the agglomerated bed material especially in the binder region (Huggins et al. 1981; Wu et al. 2009; Teixeira et al. 2012) as well as temperature. On comparing the EDX elemental spot analysis, XRF bulk analysis and surface mapping results with the possible options of alkaline-silicate salts responsible for the binder melts, it can be concluded that a $Fe_2O_3 – Al_2O_3 – SiO_2$ and $CaO – SiO_2 – Al_2O_3$ are the most possible melts based on the abundance of the elemental composition in the binder. In addition, it can also be said that the difference in appearance observed between the agglomerated samples from the visual inspection and SEM micrograph are more related to difference in mechanism due to the variation in the chemical composition based on the differences in the bed ash composition of the two agglomerated samples.

6.3.7. Ash Coated Bed Materials Properties

As reported earlier in section 6.3.2 that one of the major observation made in PSBFBC bed of both washed and unwashed Blyth coal is the ash coating of the bed material. The occurrence of this during combustion of solid fuel was expected as reported by previous scholars into this subject area (Lin et al. 2003; Lundholm et al. 2005; Luan et al. 2014). In order to study this phenomenon, during the investigation of sintering and agglomeration in the PSBFBC using the two coal types, samples of the bed materials were obtained after each run and analysed to create a coherent trend of the ash deposition properties on the bed material particles surface.

6.3.7.1. Surface Morphology

On analysing the surface morphology of bed material particles obtained after run 1, 5 and 10 respectively for the washed and unwashed Blyth coal shown in

Figure 6-22 using SEM, the deposition of ash on the surface of the bed material particles can be clearly seen. In Figure 6-22, the SEM micrograph image on the left side hand represents that of the fresh bed material before being introduced into the PSBFBC system. It can be clearly seen, that as the run (operating time) increases, the deposition of ash on the surface of the bed material particle also increased.

The deposition and attachment of ash on the surface of the bed material particles is proposed to be a chemical reaction rather than a physical reaction as the ash appears to have fully adhered to the surface of the bed material particle. This observation supports the findings of Ohman and colleagues (Ohman et al. 2000) who suggested chemical reactions of gaseous alkali on to the surface of the bed material particle as part sintering and agglomeration formation mechanism.

To further study the ash deposition phenomenon on the surface of the bed material particles, a cross sectional SEM analysis of the bed material particles was done which is presented in Figure 6-23. The amount / intensity of ash coating on the surface of the bed material particle is characterised by the thickness of the white layer around the external surface of each bed material particle.

In Figure 6-23, the SEM micrograph image on the left hand side represents that of the fresh bed material before being introduced into the PSBFBC system. It can be seen that the intensity of white layer appearing on the outer surface of the bed material particles increases as the combustion run (operating time) increases for both coal types. This supports the earlier findings from the SEM surface morphology micrograph images discussed earlier and those reported by other scholars who carried out during sintering and agglomerate formation studies (Lundholm et al. 2005; Brus et al. 2005; Coda Zabetta et al. 2013; Chaivatamaset et al. 2013).

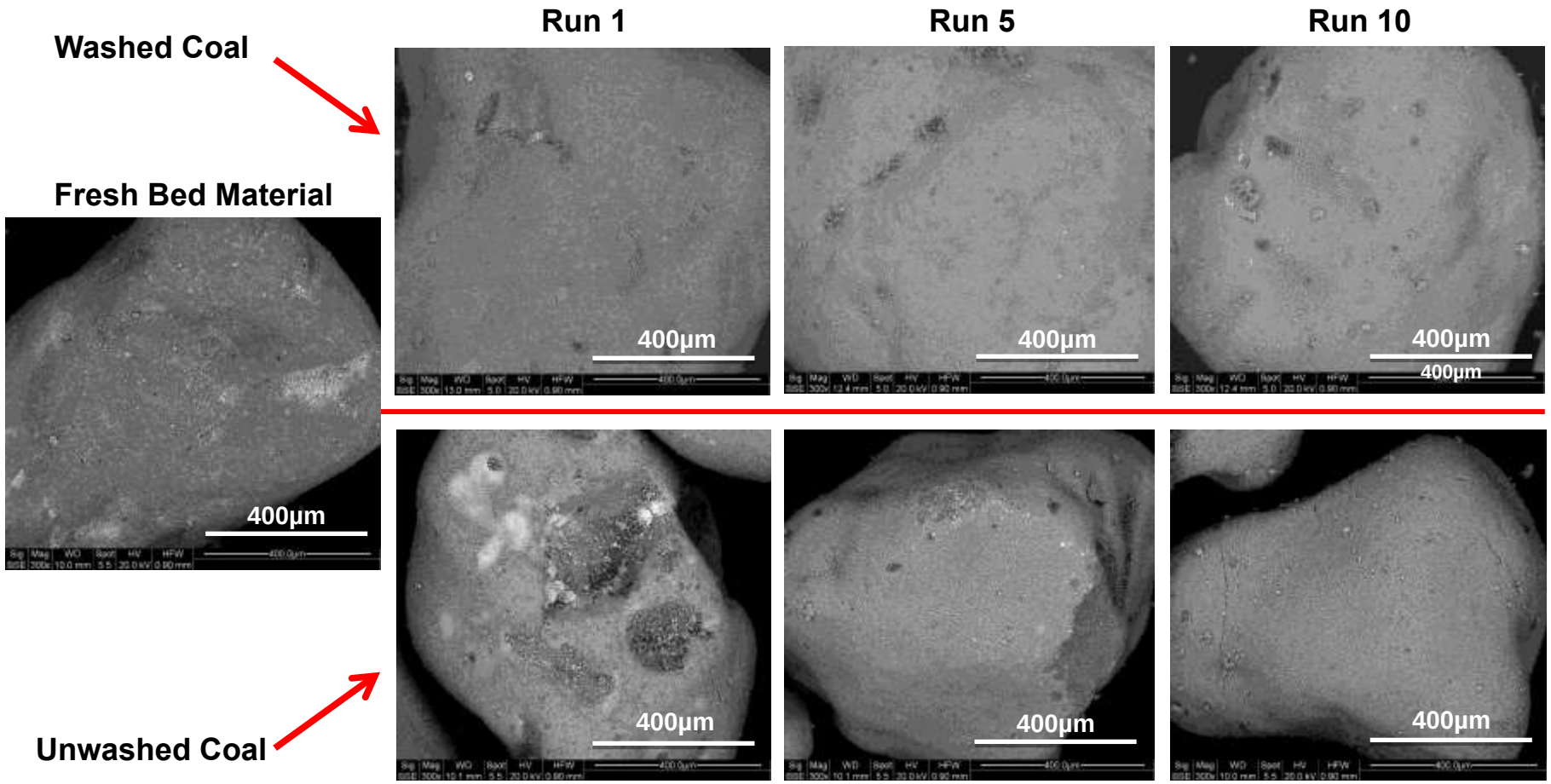

Figure 6-22: SEM micrograph showing the surface morphology of PSBFBC Garside 14/25 sand bed material obtained after the highlighted run during the evaluation of sintering and agglomerate formation using washed and unwashed Blyth coal

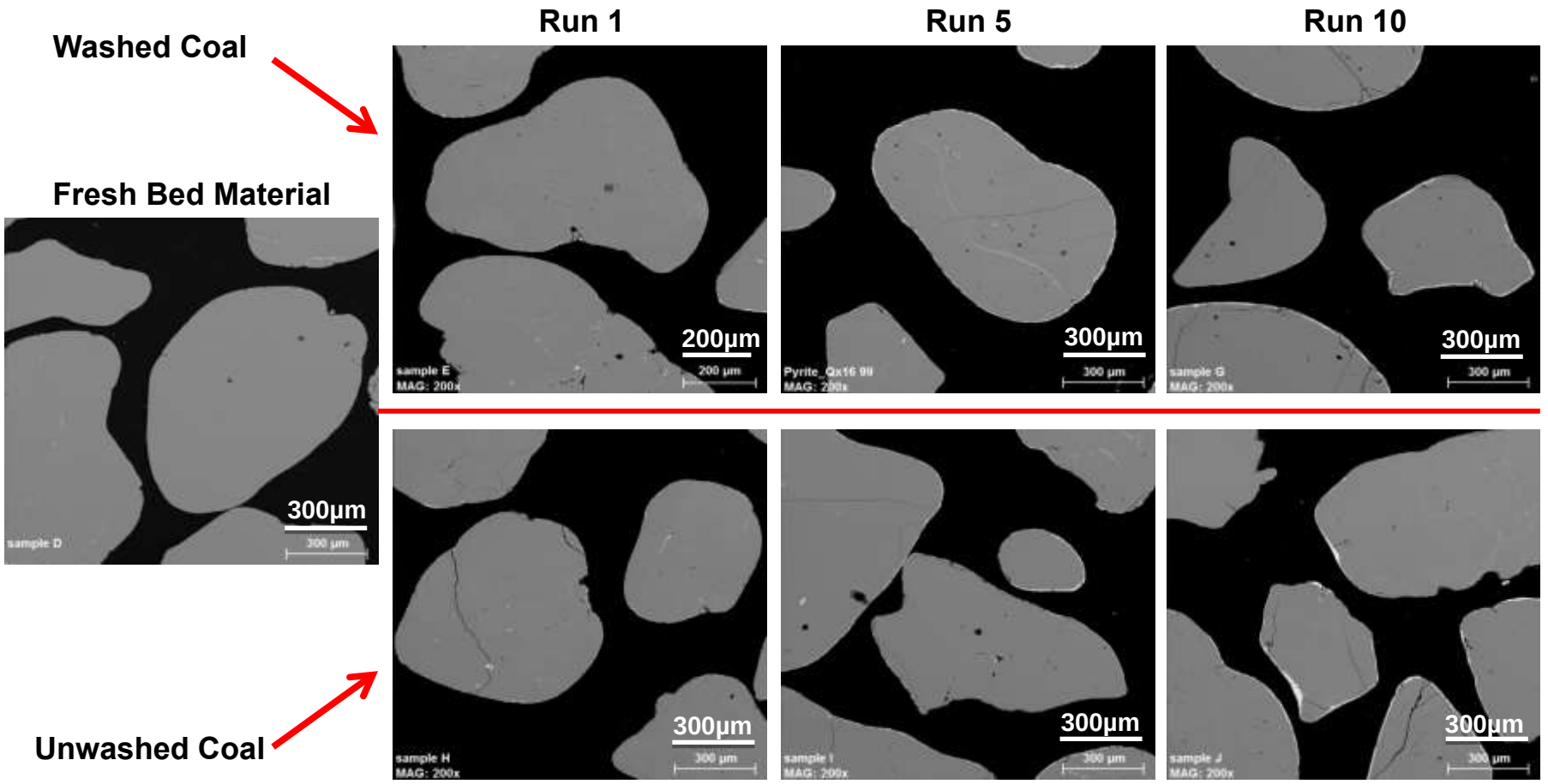

Figure 6-23: SEM micrograph showing the cross-sectional surface of PSBFBC Garside 14/25 sand bed material obtained after the highlighted run during the evaluation of sintering and agglomerate formation using washed and unwashed Blyth coal

6.3.7.2. Elemental Distribution on the Bed Material Particle Surface

To better understand the ash deposition / coating chemistry, EDX elemental surface mapping and XRF bulk analysis were done on the ash coated bed material samples obtained from the PSBFBC bed. The EDX elemental surface mapping was carried out on the same bed material particles, which cross sectional SEM micrograph are presented in Figure 6-23 for experimental runs 1, 5 and 10 respectively. Element identified in this analysis are Si, Fe, Al, Ca and K, which corresponds to SiO_2, Fe_2O_3, Al_2O_3, CaO and K_2O respectively from the XRF bulk analysis. The XRF analysis was carried out on bulk bed material samples obtained from the PSBFBC rig after each experimental combustion run (start to end of run 10).

In addition, O (oxygen) distribution across the cross sectional surface of the ash coated bed material particle was also done using EDX elemental mapping to support the argument that the identified elements (Si, Fe, Al, Ca and K) occurs in their elemental oxide forms, which corresponds to the XRF analysis result. Each identified element (elemental oxide) in the coated bed material sample is individual discussed in this section.

Composition of Si (SiO_2)

From the EDX elemental mapping of Si (SiO_2) distribution across the cross sectional surface of the ash coated bed material particles, is presented in Figure 6-24, the even spread of SiO_2 across the surface can be clearly seen in both cases. The intensity of colour signifies the abundance level of the identified element across the surface of each sample frame. Little / or no visual difference in the intensity of SiO_2 can be observed between the bed material particles and the coating layer around the edges of the particle.

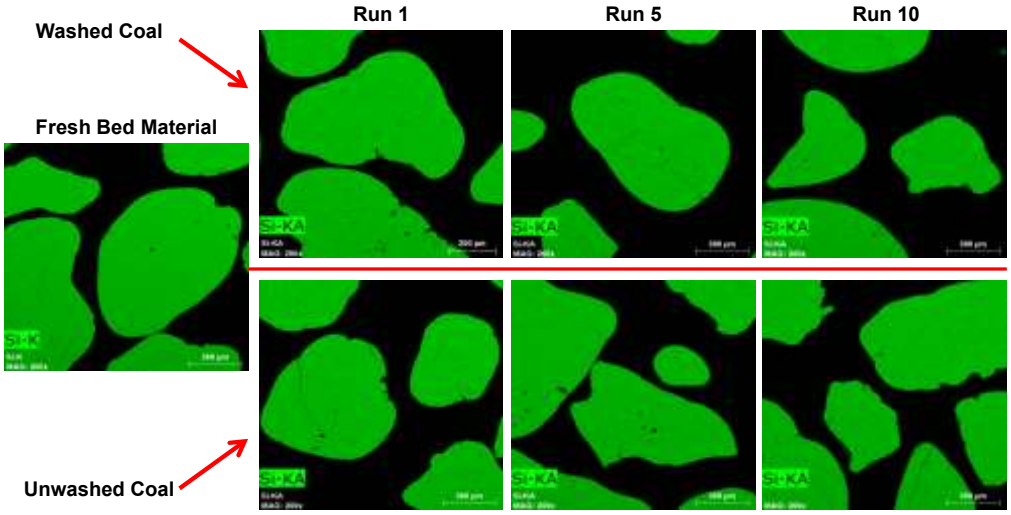

Figure 6-24: EDX elemental mapping showing the distribution of Si (SiO_2) across the cross sectional surface of PSBFBC Garside 14/25 sand bed material obtained after the highlighted run during the evaluation of sintering and agglomerate formation using washed and unwashed Blyth coal

The XRF result of the bulk ash coated bed material samples presented in Figure 6-25 shows that the amount of SiO_2 present in the bulk samples of the bed material decreases as the experimental run (operation time) increases from the start to the end of 10 in both cases. The measured average composition of SiO_2 in the bulk sample of the PSBFBC bed material at the start of the investigation compared to the end of run 10 is 96.7 to 94.9% for the washed Blyth coal and 95.7 to 86.8% for unwashed Blyth coal bed. This observed decreasing trend in SiO_2 composition of the bed material can be linked to the increasing trend as operating time increases ash coating.

The observed decreasing trend in the composition of SiO_2 was observed to be far greater in the unwashed Blyth coal bed than that of the washed Blyth coal bed. The reason for this can be associated with the expected higher ash content of unwashed coal when compared to that of the washed Blyth coal. Hence, more ash deposition and coating on the bed material particles surface occurs in the unwashed coal setup than that of washed coal.

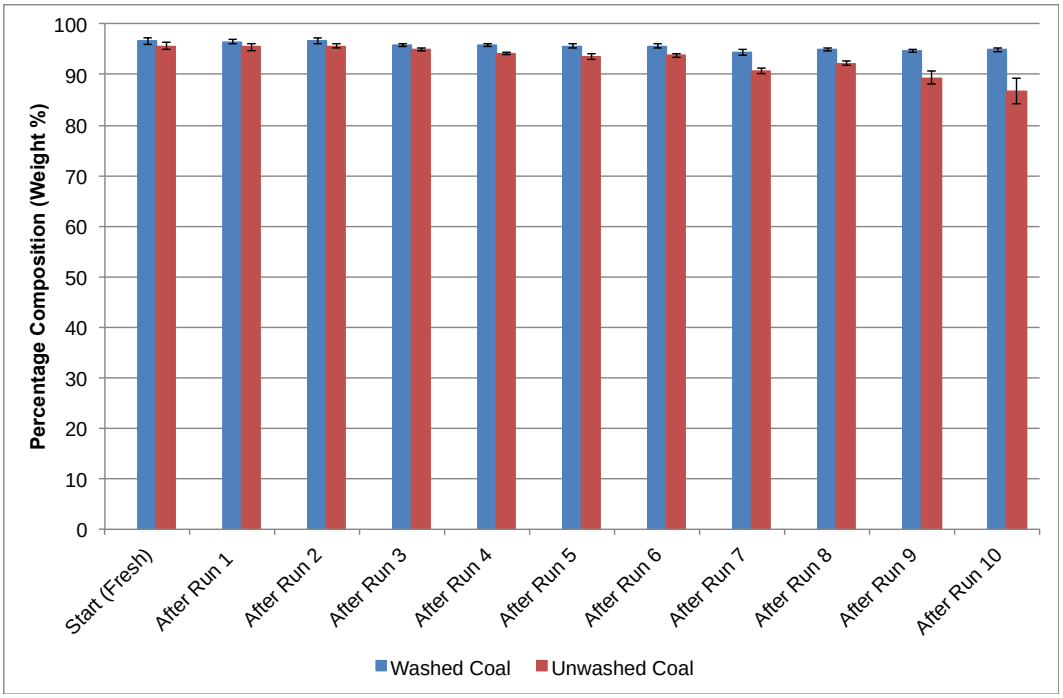

Figure 6-25: XRF analysis of Garside 14/25 sand bed material showing the changes in its SiO_2 composition from the fresh state to those obtained from the PSBFBC after the each run during the evaluation of sintering and agglomerate formation using washed and unwashed Blyth coal

Composition of Fe (Fe_2O_3)

For the composition of Fe (Fe_2O_3) deposited on the surface of the bed material particles determined using EDX elemental surface mapping presented in Figure 6-26, the amount of Fe deposited on the outer layer of the bed material can be seen to increase as the experimental run (operation time) increases. The intensity of the coating colour clearly shows this increasing trend especially when compared to the Fe deposition across the surface of fresh bed material shown on the left side of Figure 6-26.

The trend observed from the performed XRF analysis to measure the composition of Fe_2O_3 in the bulk ash coated bed material samples is presented in Figure 6-27 shows an initial decrease in the composition of Fe_2O_3 between the start of the investigation until after run 2 for both coal types. This decrease was followed by an increasing trend in the composition of Fe_2O_3 due to the increase in the ash coating as the experimental run (operation time) increases.

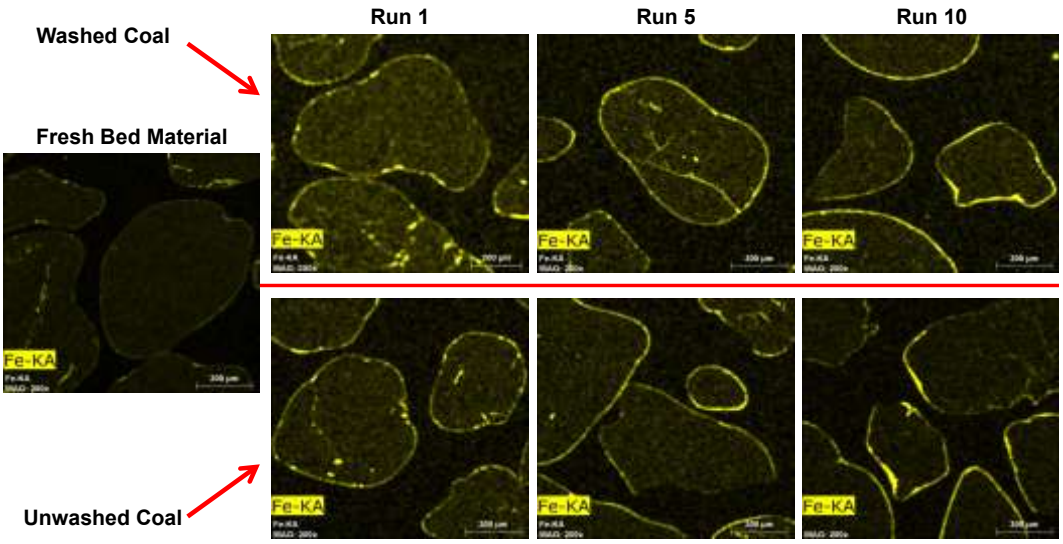

Figure 6-26: EDX elemental mapping showing the distribution of Fe (Fe_2O_3) across the cross sectional surface of PSBFBC Garside 14/25 sand bed material obtained after the highlighted run during the evaluation of sintering and agglomerate formation using washed and unwashed Blyth coal

The initial observed decrease in the Fe_2O_3 composition of the PSBFBC bed material between the start and end of run 2 is believed to have been caused by the cracking / fracturing and exfoliation of the Fe rich surface earlier observed during the calcination of pure Garside 14/25 sand bed material particles at high temperatures explained in section 5.3.3, which might have being partly entrained by the flue gases to the cyclone and exhaust. As experimental run (operating time) increases, the deposition of ash in the PSBFBC bed is expected to increase the composition of Fe_2O_3 in the bed, which nullifies the reported loss by the exfoliation effects.

The measured average composition of Fe_2O_3 in the bulk sample of the PSBFBC bed material at the start of the investigation compared to the end of run 10 is 2.4 to 1.9% for the washed Blyth coal and 3.0 to 2.7% for unwashed Blyth coal bed. An overall decrease in the composition of Fe_2O_3 in the ash coated bed materials from the PSBFBC is observed which contradicts the early reported Fe_2O_3 composition increase from the EDX elemental mapping. It may be fair to say that even though there is an evidence of increasing Fe_2O_3 on the surface of the bed

material particles as shown in Figure 6-26, the rate of exfoliation of the Fe region from the surface of the bed material particle is far higher than the rate of coating / deposition on to the surface which account for the overall decrease in the composition of Fe_2O_3 in the bed material in both cases. With prolonged operating time of the PSBFBC, which equates to more ash deposition, the composition of Fe_2O_3 is expected to increase further to overcome the initial high rate of cracking and exfoliation of the iron rich region experienced between the start and end of run 2.

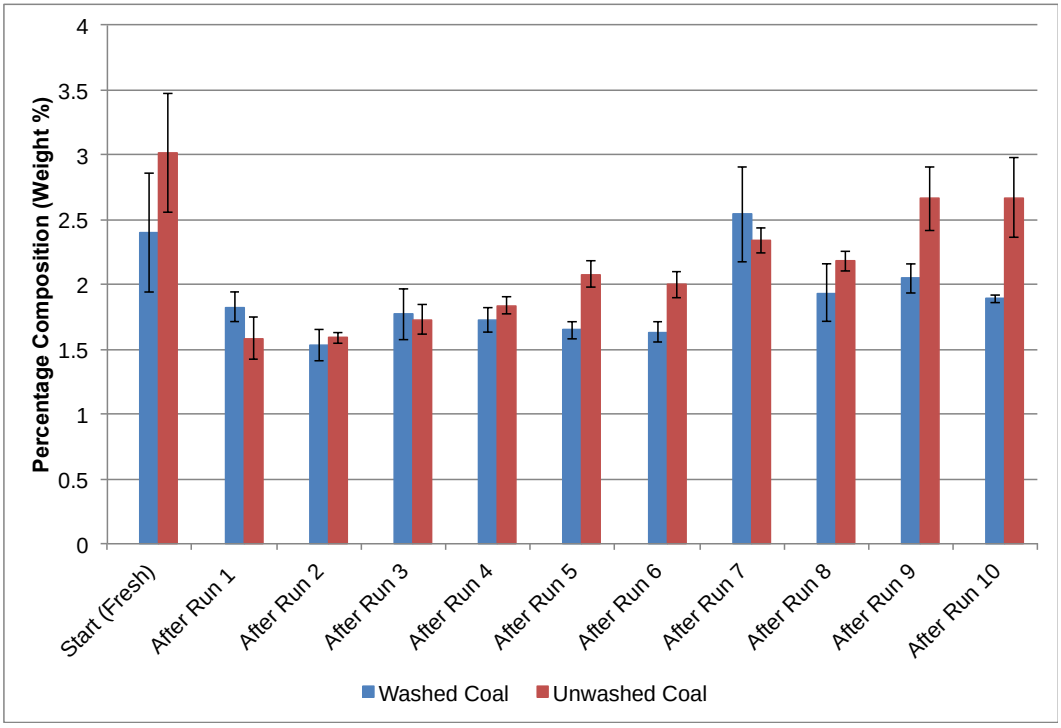

Figure 6-27: XRF analysis of Garside 14/25 sand bed material showing the changes in its Fe_2O_3 composition from the fresh state to those obtained from the PSBFBC after the each run during the evaluation of sintering and agglomerate formation using washed and unwashed Blyth coal

Composition of Al (Al_2O_3)

The distribution of Al (Al_2O_3) across the cross sectional surface of the ash coated bed material particles shown in Figure 6-28, clearly identifies the increasing composition of Al_2O_3 in the coating layer of the bed material particles in both coal types. This increasing trend again supports the argument on the increasing ash

deposition on the surface of the bed material particles as experimental run (operating time) increases.

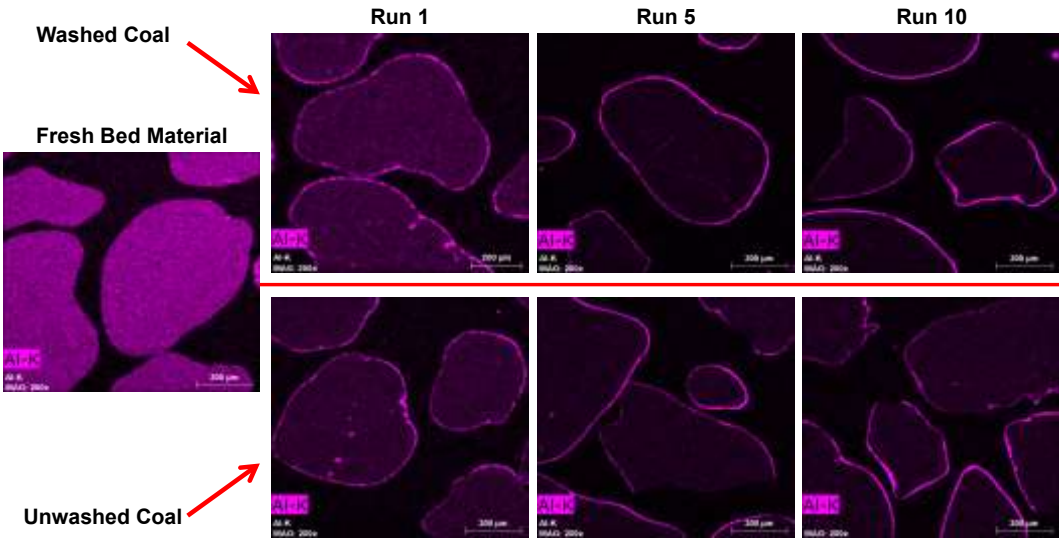

Figure 6-28: EDX elemental mapping showing the distribution of Al (Al_2O_3) across the cross sectional surface of PSBFBC Garside 14/25 sand bed material obtained after the highlighted run during the evaluation of sintering and agglomerate formation using washed and unwashed Blyth coal

The increasing trend of the composition of Al_2O_3 in the ash coated bed material samples can be supported by the findings from the XRF analysis on the bulk ash coated bed material samples presented in Figure 6-29 for both coal types. The measured average composition of Al_2O_3 in the bulk sample of the PSBFBC bed material at the start of the investigation compared to the end of run 10 is 0.4 to 1.9% for the washed Blyth coal and 0.5 to 5.6% for unwashed Blyth coal bed. The increasing trend in the amount of Al_2O_3 in the ash coated bed material was observed to be higher in the unwashed Blyth coal bed when compared to that of the washed Blyth coal. The reason for this difference again can be associated with the higher deposition of ash expected to be presented in unwashed Blyth coal compared to the washed Blyth coal as well as the higher composition of Al_2O_3 identified to be present in the unwashed than the washed Blyth coals earlier shown in Table 4-2.

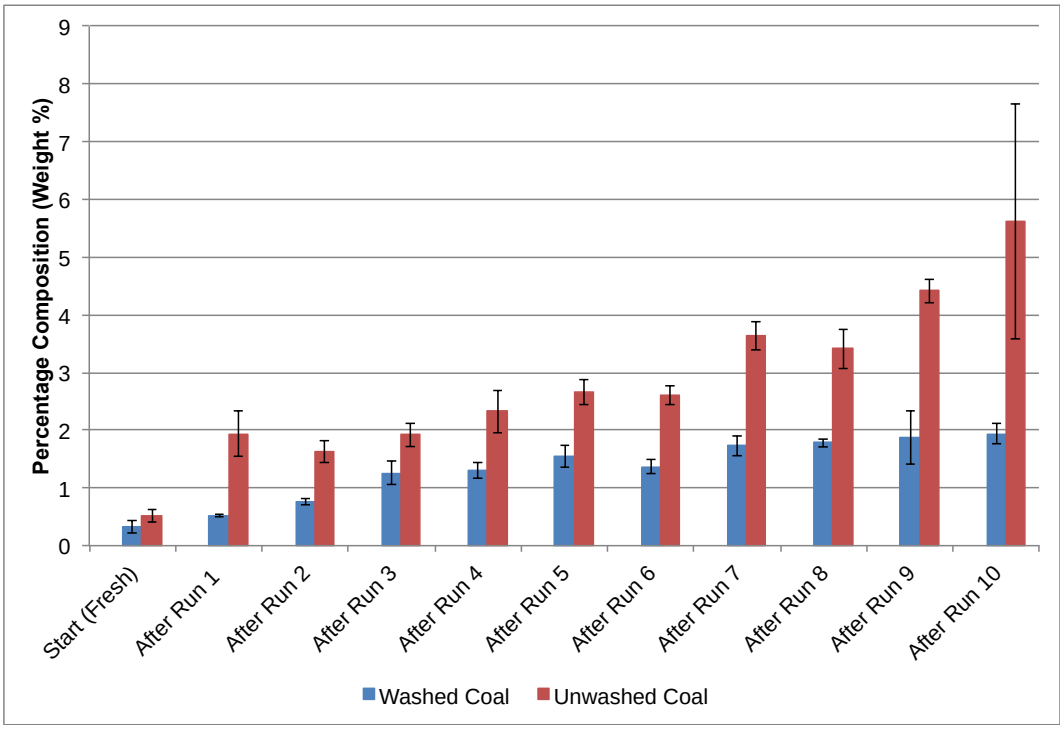

Figure 6-29: XRF analysis of Garside 14/25 sand bed material showing the changes in its Al_2O_3 composition from the fresh state to those obtained from the PSBFBC after the each run during the evaluation of sintering and agglomerate formation using washed and unwashed Blyth coal

Composition of Ca (CaO)

For the distribution of Ca (CaO) across the cross sectional surface area of ash coated bed material particles shown in Figure 6-30, the increasing trend of CaO can be seen in the coating layer of the bed material particles as the experimental run (operating time) increases for both coal types. This increasing trend can be identified with the increase in the intensity of the colour around the external surface of the bed material particles, which signifies the abundance of CaO in the region.

The observed increasing trend in the composition of CaO in the ash coated bed material samples can be supported by the findings from the XRF analysis on the bulk ash coated bed material samples presented in Figure 6-31 for both coal types. The measured average composition of CaO in the bulk sample of the PSBFBC bed material at the start of the investigation compared to the end of run

10 is 0.1 to 0.6% for the washed Blyth coal and 0 to 3.3% for unwashed Blyth coal bed. The increasing trend in the amount of CaO in the ash coated bed material was observed to be higher in the unwashed Blyth coal bed when compared to that of the washed Blyth coal, which is the same as the trend observed for the composition of Al_2O_3. This difference again supports the argument on the higher composition of ash expected to be presented in unwashed Blyth coal compared to the washed Blyth coal.

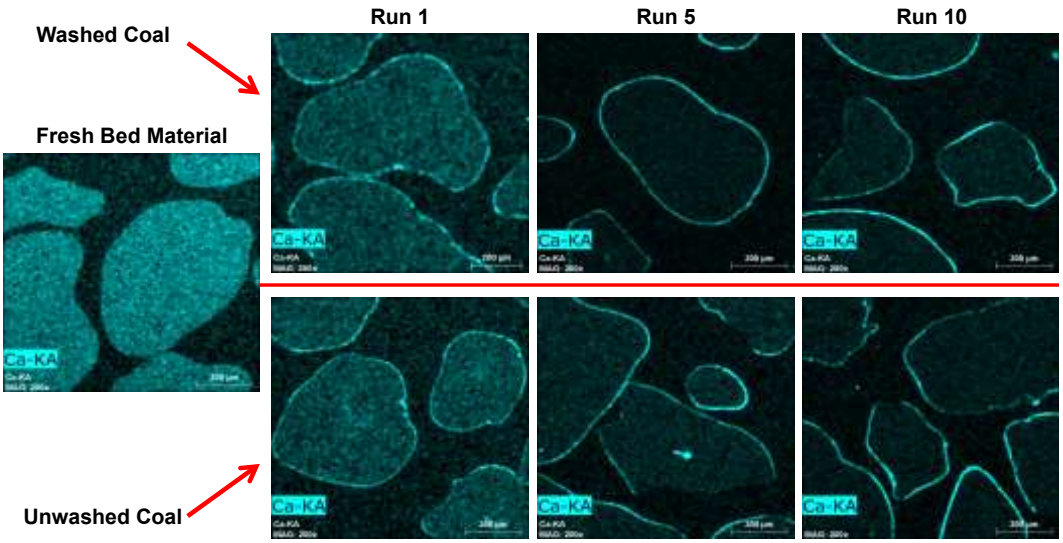

Figure 6-30: EDX elemental mapping showing the distribution of Ca (CaO) across the cross sectional surface of PSBFBC Garside 14/25 sand bed material obtained after the highlighted run during the evaluation of sintering and agglomerate formation using washed and unwashed Blyth coal

Composition of K (K_2O)

The distribution of K (K_2O) across the cross sectional surface of the ash coated bed material particles is shown in Figure 6-32. As shown in Figure 6-32, a slightly higher intensity or deposition of K_2O in the coating layer on the bed material particles was observed around the external surface of the bed material particles for both cases. Overall trend shows that higher deposition of K_2O was observed across the external surface of the bed material particles as operating time increases from start to the investigation to the end of run 10.

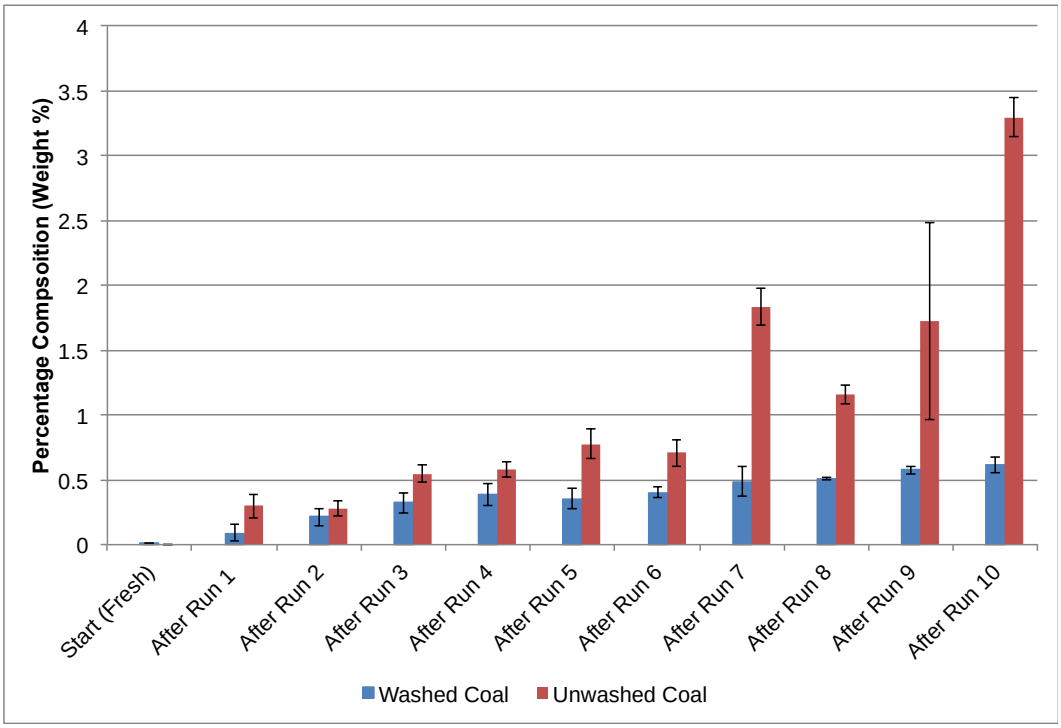

Figure 6-31: XRF analysis of Garside 14/25 sand bed material showing the changes in its CaO composition from the fresh state to those obtained from the PSBFBC after the each run during the evaluation of sintering and agglomerate formation using washed and unwashed Blyth coal

Findings from the XRF analysis to identify the K_2O composition in the bulk sample of the ash coated bed material presented in Figure 6-33 supports the reported observation from the EDX elemental surface mapping. The measured average composition of K_2O in the bulk sample of the PSBFBC bed material at the start of the investigation compared to the end of run 10 is 0.01 to 0.06% for the washed Blyth coal and 0 to 0.31% for unwashed Blyth coal bed. The low composition of K_2O is consistent with that of the unwashed and washed coal ash earlier described in section 4.2.2. In both cases, an overall increasing trend was observed for the composition of K_2O in their respective bed materials which supports the ash coating / deposition theory. The increasing trend in the amount of K_2O in the unwashed Blyth coal ash coated bed material was observed to be higher when compared to that of the washed Blyth coal. This observed trend is the same as those earlier reported for the composition of Al_2O_3 and CaO.

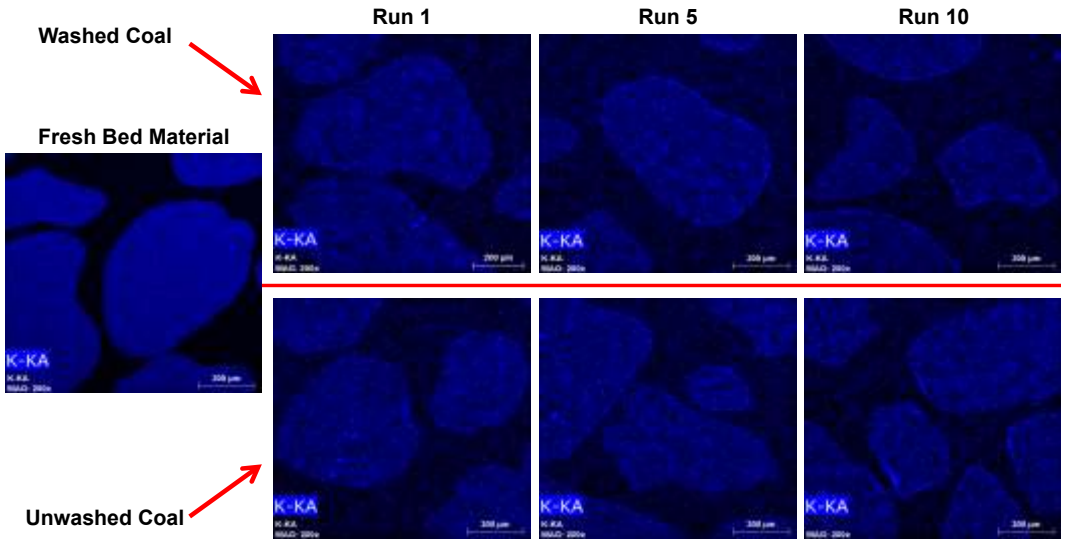

Figure 6-32: EDX elemental mapping showing the distribution of K (K_2O) across the cross sectional surface of PSBFBC Garside 14/25 sand bed material obtained after the highlighted run during the evaluation of sintering and agglomerate formation using washed and unwashed Blyth coal

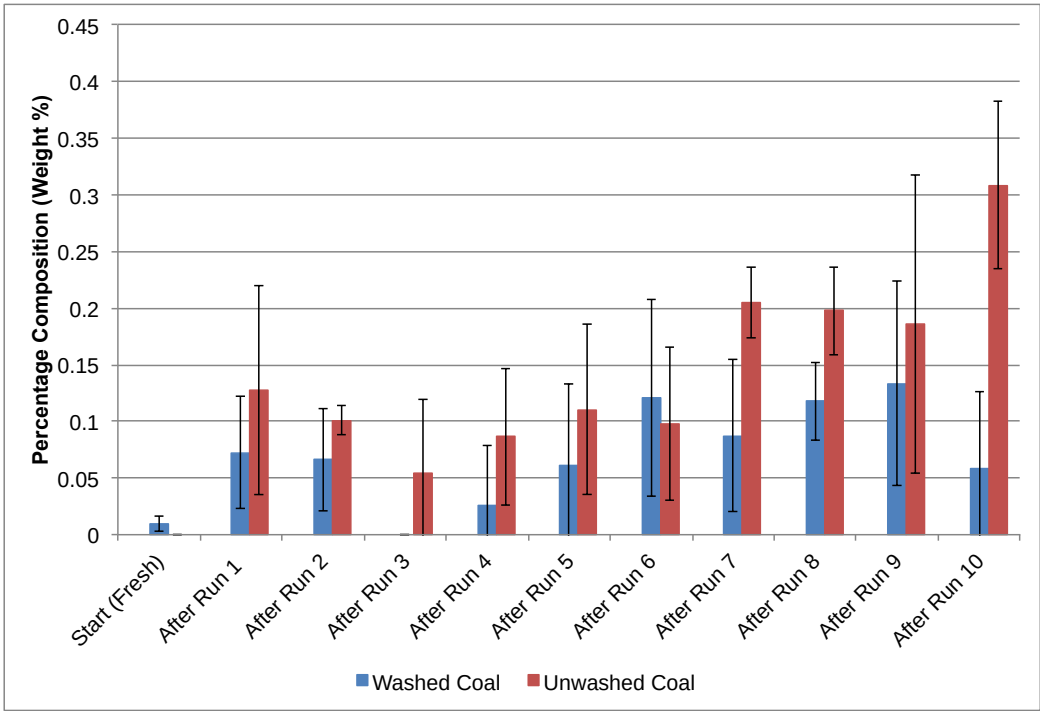

Figure 6-33: XRF analysis of Garside 14/25 sand bed material showing the changes in its K_2O composition from the fresh state to those obtained from the PSBFBC after the each run during the evaluation of sintering and agglomerate formation using washed and unwashed Blyth coal

Composition of O (Oxygen)

The distribution of O (oxygen) across the cross sectional surface of the bed material particles presented in Figure 6-34 was carried out using EDX elemental

surface mapping to support the argument that all identified elements exist in their oxide forms. The intensity of colour signifies the abundance level of the identified element in the particular spot. As shown in Figure 6-34, the even distribution of O elements can clearly be observed across the surface of the cross sectional area of the bed material particles. No difference in the intensity of O can be observed between the bed material particles and the coating layer around the edges of the particle.

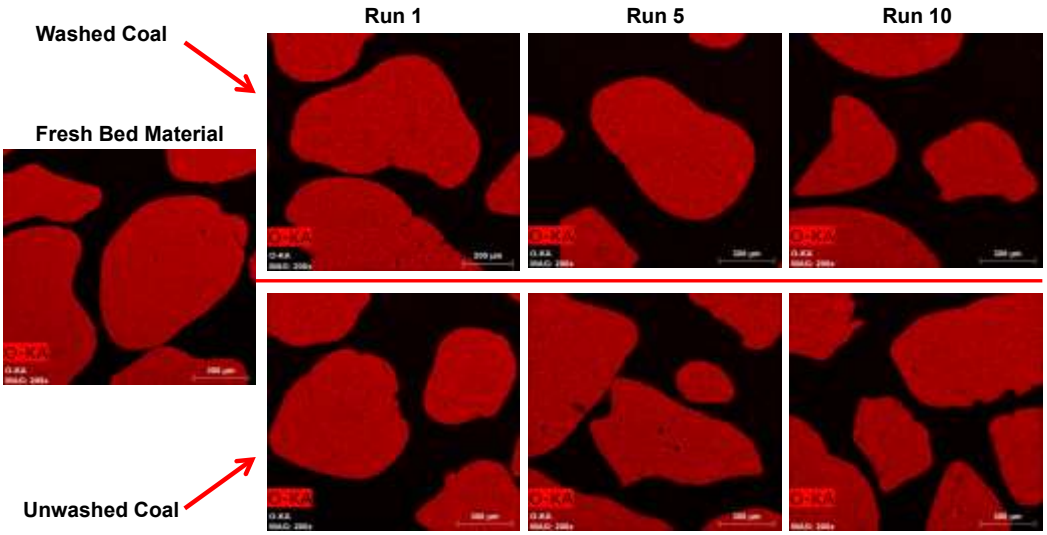

Figure 6-34: EDX elemental mapping showing the distribution of oxygen (O) across the cross sectional surface of PSBFBC Garside 14/25 sand bed material obtained after the highlighted run during the evaluation of sintering and agglomerate formation using washed and unwashed Blyth coal

6.3.8. Summary

Vertical bed temperature, linear average pressure drop and flue gas composition measurements techniques were not found to be effective for small quantities of sintering and agglomerate formation detection over a 52 hours combustion-operating period. Hence, more operating time is required in order for the PSBFBC bed to fully agglomerate so as to further certify the suitability of these techniques for sintering and agglomerate formation detection.

Sintering and agglomerate formation is an ash related problem whose formation tendencies is increased by the use of lump unwashed Blyth coal. The use of

unwashed Blyth coal causes a higher increase in the amount of mud/shale stone deposited in the PSBFBC bed when compared with washed Blyth coal. The greater the amount of mud/shale stones deposited in the bed, the greater the sintering and agglomerate formation tendency.

Increasing mud/shale stone deposition also causes an increase in the bed pressure drop and bed height. Measured bed height for unwashed Blyth coal bed was found to be about 1.5 times that of the washed Blyth coal after a combustion period of 52 hours at similar coal feeding rate. In addition the increase in the mud/shale stone composition in the PSBFBC bed also causes the bed to get fluidised at a lower volumetric air flowrate.

Coating and deposition of ash on the surface of the bed material particles increases as operating time increases. This also results in the increase of the composition of Al_2O_3, CaO and K_2O deposited onto the surface of the bed material particles and decrease in the SiO_2 composition of the bed.

The average particle size of the bed material was found to vary largely in the unwashed Blyth coal bed than the washed Blyth coal bed when compared to the original bed sample. The mean particle size of the bed material was found to reduce to 790µm for unwashed coal bed from 850µm.

6.4. Crash Stop Combustion Run

The discussion covered in this section is based on the second part of the investigation in this study identified and described earlier in section 6.1. As a follow-up from the normal PSBFBC combustion operation investigation and in-order to further establish the localized bed temperature build-up effect prompting sintering and agglomerate formation, the crashed stop combustion runs of the PSBFBC system was setup. This was done using the old Garside 14/25 sand bed material obtained at the end of the each coal type 10 runs or approximately

52 hours of combustion operation. Findings made from this investigation are discussed in this section covering topics, which includes monitoring of bed operation, visual observation of the bed material and chemical composition of the agglomerated bed material formed.

6.4.1. Monitoring of Bed Operation

The condition of the bed fluidisation and operation of the PSBFBC system was primarily monitored during the crash stop combustion investigation using the bed temperature (T1 to T6), pressure drop and flue gas composition measurements same as described in section 6.3.1. Discussion in this section has been structured to cover two parts namely start-up operating condition and lump coal combustion condition.

6.4.1.1. Start-up Operating Condition

The reported start-up condition profiles for the bed temperature and pressure drop are the same as those discussed earlier in section 6.3.1.1. Fluidisation of the unwashed Blyth coal PSBFBC bed was achieved at a fluidising air flowrate of 380 litres/minute same as what was reported for experimental run 8, 9 and 10 for the same unwashed Blyth coal type during the normal combustion run. The washed Blyth coal bed fluidisation on the other hand was achieved at an air flowrate of 440 litres/minute same as described in section 6.3.1.1 for experimental runs 1 – 10 for washed Blyth coal.

6.4.1.2. Lump Coal Crash Stop Combustion Conditions

During the lump coal crash stop combustion runs, vertical temperature, linear pressure drop and flue gas composition were all measured to monitor the fluidisation quality and operation condition of the PSBFBC system. Summary of the experimental operating condition for both washed and unwashed Blyth coal are presented in Table 6-3.

Table 6-3: Experimental operating conditions for evaluating sintering and agglomerate formation during PSBFBC crash stop operation using washed and unwashed Blyth coal (* This accounts for time from the beginning of coal injection into the PSBFBC to shut down only and does not account for start-up and cooling down time)

TEST CONDITIONS	Washed Coal	Unwashed Coal
Total No of Experimental Runs	3	1
***Time for Each Run (hours)**	4.45	5
***Total Run Time (~hours)**	13.35	5
Total Number of Stops	7	3
Duration per Stop (Minutes)	25	25
Air Flowrate (l/min)	640 - 700	640 - 700
Coal Feedrate (kg/h)	2.2	2.2

Temperature Profile

The vertical temperature data obtained throughout the combustion process for a typical washed and unwashed coal experimental run are presented in Figure 6-35 and Figure 6-36 respectively. From these figures, it can be seen that the temperature profile of the PSBFBC system is in the same decreasing order of T2, T3, T4, T5, T6 and T1 from hottest to coldest as discussed earlier in section 6.3.1.2 irrespective of the coal type.

The vertical temperature profile presented in Figure 6-35 for washed coal crash stop identifies 3 stops. It can be seen from the figure on stopping the fluidising air and coal feeding, the measured bed temperature T2 and plenum chamber temperature T1 was increased by a factor of 30 to 50°C. At the same time, temperature point T3, T4, T5 and T6 deceases 100 to 150°C. At this stage, the PSBFBC heaters are off. On re-starting the fluidising air after 25 minutes with the PSBFBC heaters still off, the measured temperature at T3, T4, T5 and T6 was increased by 100 to 150°C while that of T1 decreased by 50°C. This observed changes were also noticed in the unwashed Blyth coal crash stop combustion run temperature profile given in Figure 6-36.

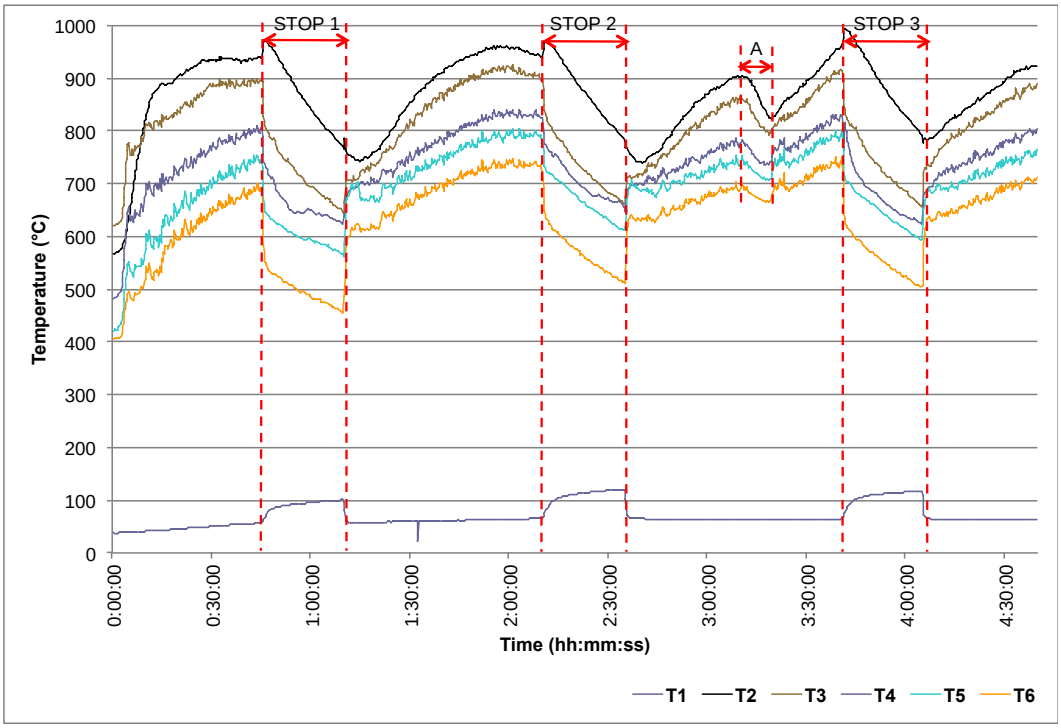

Figure 6-35: Typical PSBFBC bed temperature profile during crash stop combustion of lump washed Blyth coals showing 3 stops

At restart the fluidising air and coal feeder, the measured temperatures across the PSBFBC gradually increase until a bed temperature of between 900°C and 950°C was attained before stabilising. The ability to be able to get the bed temperature back to what it was shows no large amount of agglomerate was formed in the bed (Bartels et al. 2009). No evidence of agglomeration formation or defluidisation of the bed was observed from the temperature profile

The measured temperature drop due to coal feeder blockage marked as “A” in Figure 6-35 occurred during the unwashed coal crash stop combustion run. During this period, a drop in temperature was observed across the six temperature measuring point in the PSBFBC similar to what was described earlier in section 6.3.2 (Figure 6-7) due to the lack of fuel to sustain the combustion process.

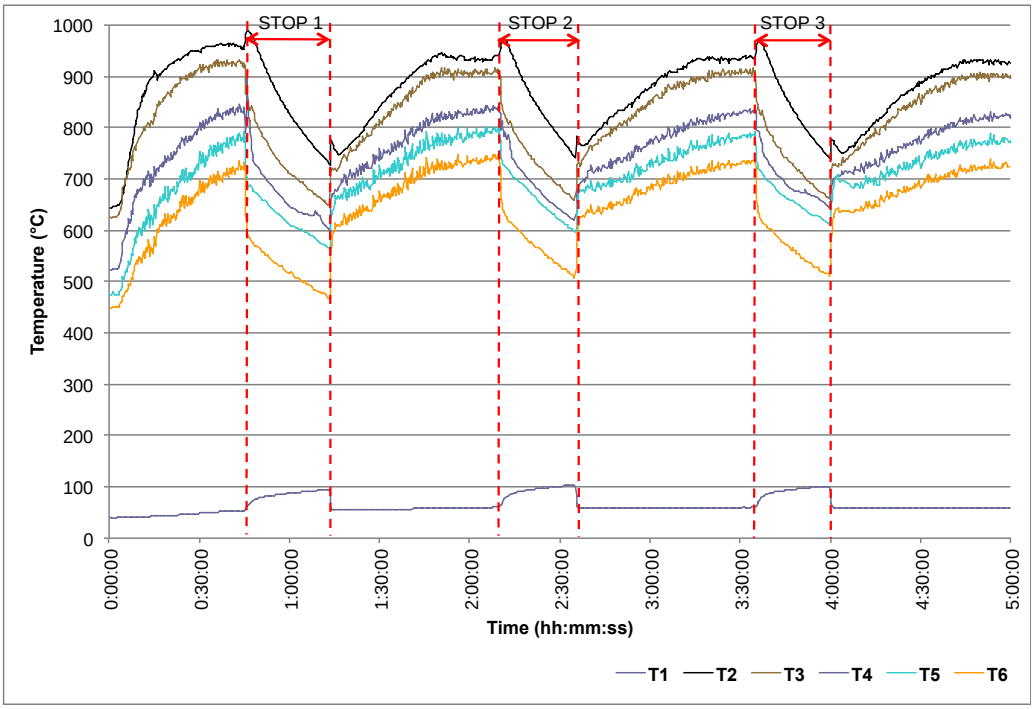

Figure 6-36: Typical PSBFBC bed temperature profile during crash stop combustion of lump unwashed Blyth coals showing 3 stops

Pressure Drop

Typical linear pressure drop measured across the PSBFBC system during the crash stop investigation for the washed and unwashed Blyth coals are presented in Figures 6-37 and 6-38. It can be seen in both cases that when the fluidising air and coal feeding were turned off, the measured pressure drop drops down to 0 until re-start when fluidisation of the bed begins again. It can also be seen from the large fluctuations in the pressure data profile reported in both cases that after restart, the PSBFBC bed get re-fluidised very well which means no evidence of the formation of large agglomerate that might have led to defluidisation. Also the coal feeder blockage identified in the temperature profile for the washed coal in Figure 6-35 was not easily visible in linear pressure drop profile shown Figure 6-37.

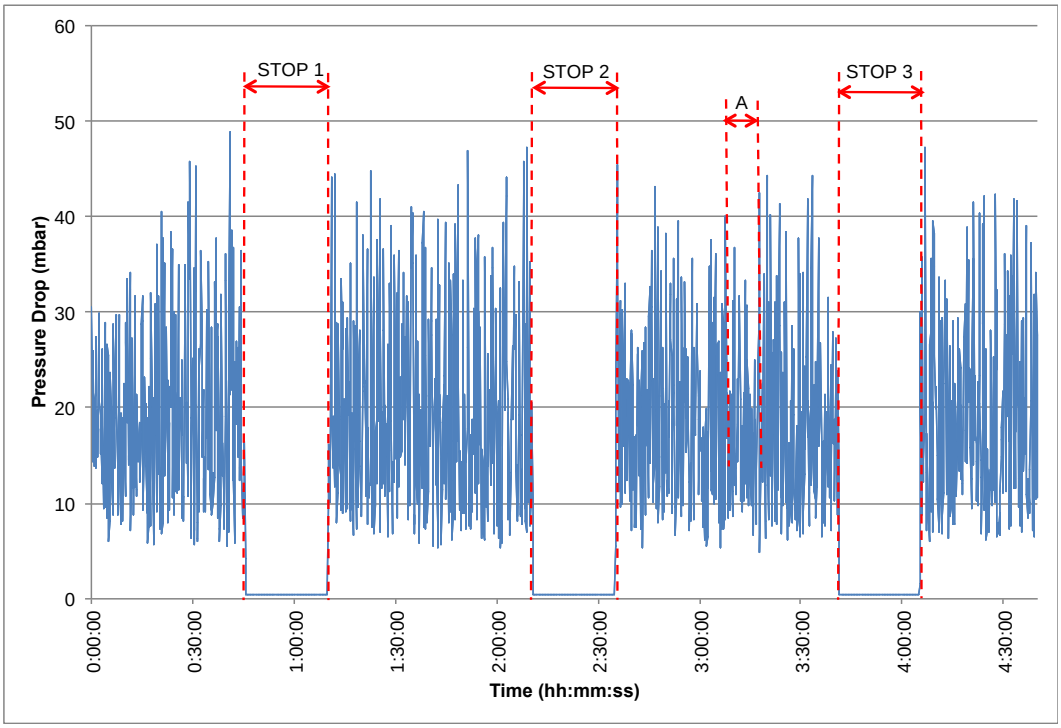

Figure 6-37: Typical PSBFBC pressure drop profile during crash stop combustion of lump washed Blyth coals showing 3 stops

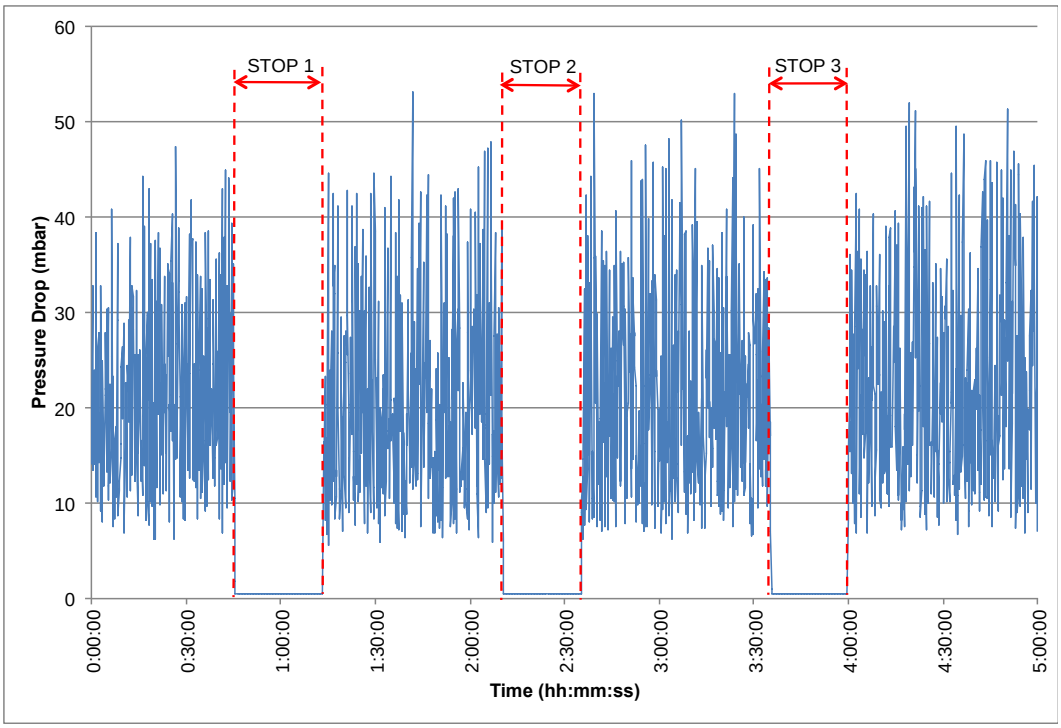

Figure 6-38: Typical PSBFBC pressure drop profile during crash stop combustion of lump unwashed Blyth coals showing 3 stops

Flue Gas Composition

The flue gas composition data measured over the course of a crash stop combustion run is presented in Figures 6-39 and 6-40 for washed and unwashed Blyth coal respectively. The composition of CO_2, CO and O_2 are measured in volume percentage (Vol.%) while that of NO_x was measured in part per million (ppm).

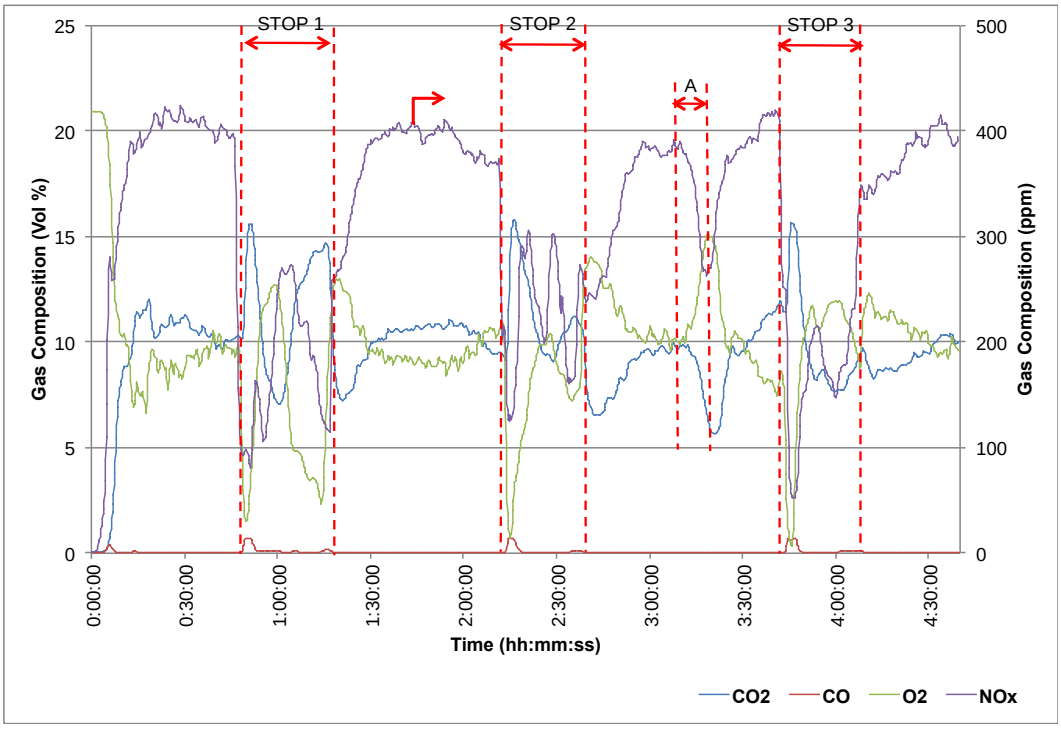

Figure 6-39: Typical PSBFBC flue gas composition profile during crash stop combustion of lump washed Blyth coals showing 3 stops

At the crash stop, it can be seen in both cases that when the fluidising air and coal feeding were turned off, the composition of CO and CO_2 increases while that of NO_x and O_2 decreases. At restart after turning on the fluidising air and coal feeder, the composition of NO_x and O_2 increases while that of CO and CO_2 decreases.

Also, the measured percentage composition of NO_x and CO_2 decreases while that of O_2 increased due to coal feeder blockage marked as “A” in Figure 6-39

occurred during the unwashed coal crash stop combustion run. This observed trend is similar to what was described earlier in section 6.3.2 (Figure 6-10) due to the lack of fuel to sustain the combustion process.

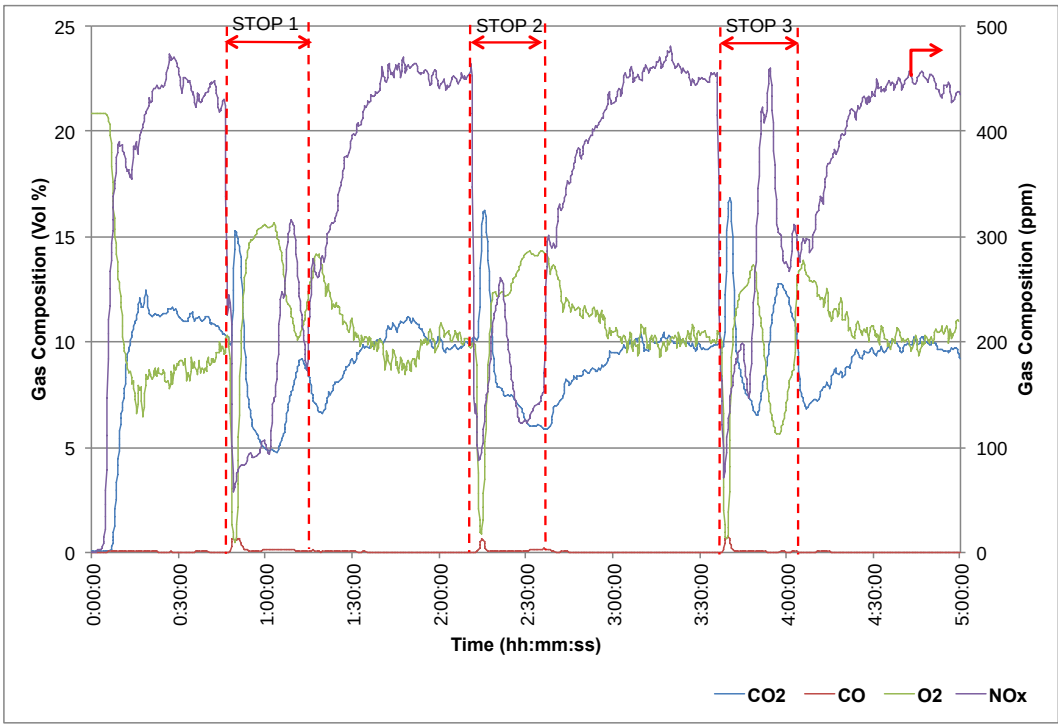

Figure 6-40: Typical PSBFBC flue gas composition profile during crash stop combustion of lump unwashed Blyth coals showing 3 stops

6.4.2. Agglomerated Bed Material Chemistry

Sintering and agglomerate formation of Garside 14/25 sand bed material occurred during the crash stop combustion investigation of washed and unwashed Blyth coal in the PSBFBC after 13.35 hours and 5 hours of operating times respectively. During normal operation of the PSBFBC rig, it is worth remembering that no sintering and agglomeration of the bed material was observed with the use of washed Blyth coal but in the case of unwashed Blyth coal, it was reported after 52 hours of operation (see section 6.3.2). The fact that sintering and agglomeration is now observed in the PSBFBC bed using both coal types over additional combustion time (13.35 hours and 5 hours as opposed to 52 hours each) is worth investigating. Making this direct comparison between

these two agglomerated bed material samples formed from the two coal types under this operating condition in the PSBFBC will provide further understanding into sintering and agglomerate formation phenomenon.

6.4.2.1. Comparison of the Surface Morphology of Agglomerated Bed Material Formed from Washed and Unwashed Blyth Coal

A visual comparison between the two agglomerated bed material samples are presented in Figure 6-41. From the presented image, it is evident that the surface morphology of the two agglomerated bed material samples are different. The agglomerated bed material produced from the washed Blyth coal presented in Figure 6-41A shows a fused structure with smooth surface. In the case of the unwashed Blyth coal agglomerated bed material shown in Figure 6-41B, the agglomerated particles appears very identical to those observed during the normal combustion run of unwashed Blyth earlier discussed in section 6.3.2.

6.4.2.2. Sintering and Agglomeration Types/ Mechanism

In order to better understand the mechanism responsible for sintering and agglomerate formed in the case of washed and unwashed Blyth coal, SEM analysis was done, which are presented in Figure 6-42. From Figure 6-42A, it can be seen that the agglomerated bed material formed from the washed Blyth coal during crash stop combustion investigation shows a solid sintering or fusing together of particles without visible presence of any liquid bridge and Si (bed material) particles. In the case of the agglomerated bed material formed unwashed Blyth coal crash stop combustion investigation which is presented in Figure 6-18B, tiny bed material particles can be observed linked together with a dense (viscous) liquid melt or liquid bridge binder.

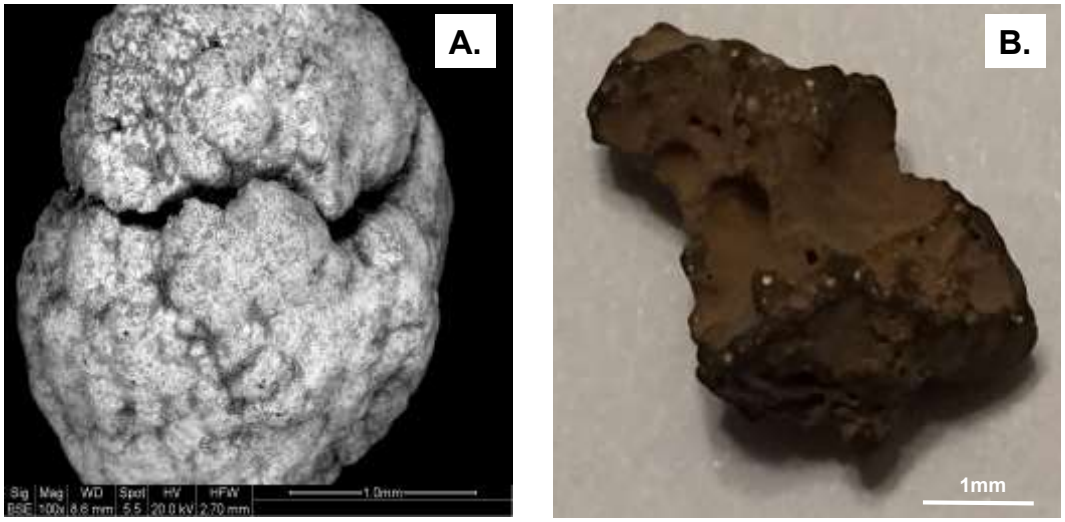

Surface Morphology Cross Section Image

Figure 6-41: Agglomerated Garside 14/25 sand bed material obtained from the crash stop combustion runs in the PSBFBC: (A) washed Blyth coal after additional 13.35 hours of operation, (B) unwashed Blyth coal after additional 5 hours of operation

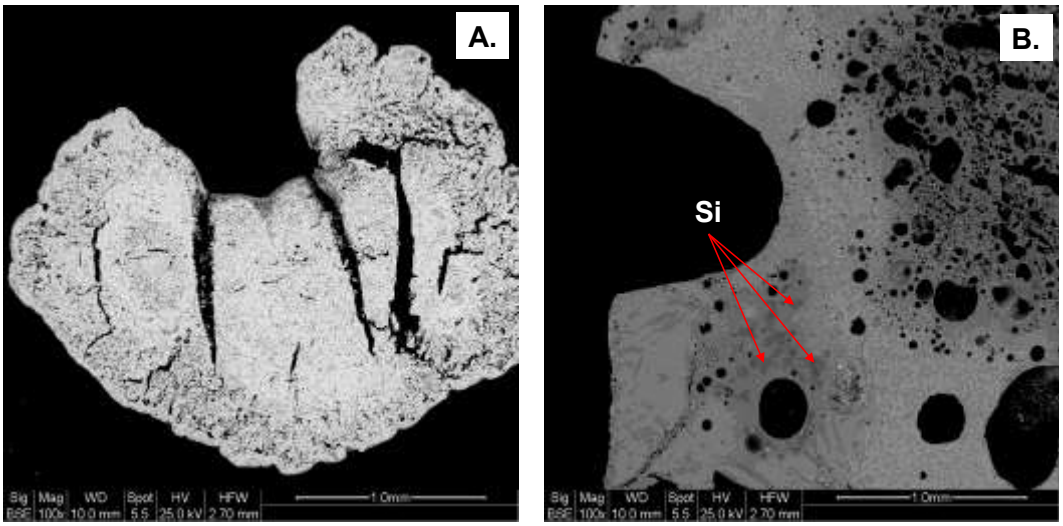

Figure 6-42: SEM showing the cross-sectional surface of agglomerated Garside 14/25 sand bed material obtained from the crash stop combustion runs in the PSBFBC: (A) washed Blyth coal after additional 13.35 hours of operation, (B) unwashed Blyth coal after additional 5 hours of operation

To have a better understanding of the chemical composition of the agglomerated bed materials, EDX elemental mapping was done to determine the distribution / spread of Si (silica), Fe (iron), Al (aluminium), Ca (calcium), K (potassium) and O (oxygen) across the cross sectional surface of the agglomerated bed material

samples which are presented in Figures 6-43 and 6-44. In both in Figure 6-43 and 6-44, which represents the washed and unwashed Blyth coal agglomerated bed material samples respectively, the original image at the left side is the SEM micrographs of the agglomerated bed material samples with each having six other images beside them highlighting the presence of earlier identified elements.

For each image, the intensity of the colour across a particular area signifies the relative abundance of the element in that region. The spread of oxygen across the entire surface of the agglomerated bed material samples shows that the identified elements are present in their elemental oxide forms.

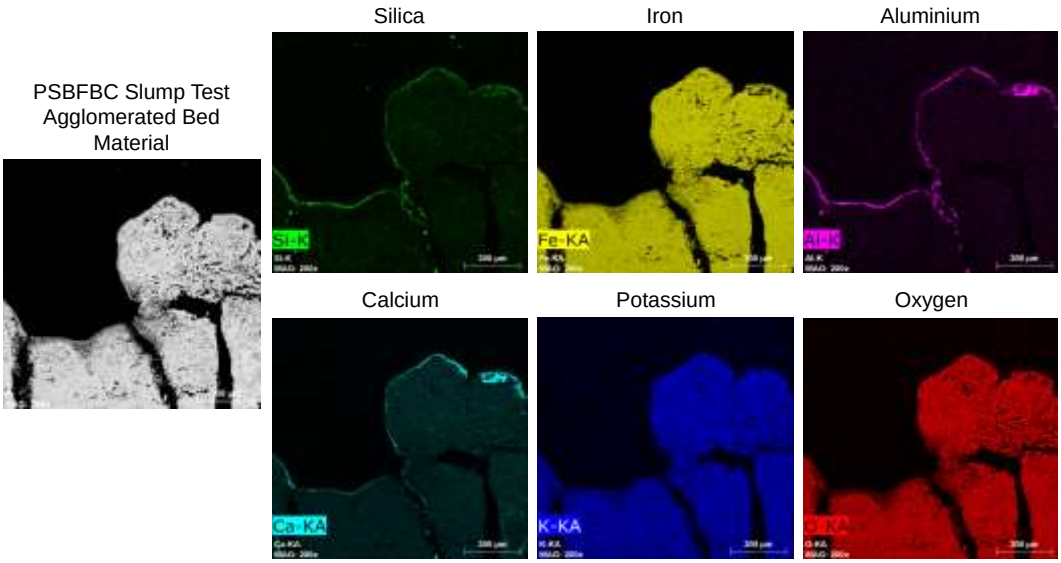

Figure 6-43: EDX elemental mapping of agglomerated Garside 14/25 sand bed material obtained after additional 13.35 hours of PSBFBC crash stop combustion run using washed Blyth coal showing the cross sectional surface distribution of identified elements in solid phase sintering process

The EDX elemental mapping results clearly demonstrates that the agglomerated bed material produced from the washed Blyth coal setup given in Figure 6-43 is predominantly made up of Fe, K and O with coating of Si, Al and Ca around the external surface of the agglomerated particle. The high intensity of Fe in this agglomerated bed material structure and fusing together of various small segmented particles lead to the proposed suggestion that this agglomerated structure might have been formed from the exfoliated Fe rich region off the

surface of the bed material particles.

The exfoliation of the Fe rich region off the surface of the Garside sand 14/25 sand bed material has earlier been explained in section 5.3.3 as a phenomenon that occurs at high temperature of between 800 and 1200°C. With the absence of a liquid binder and bed material particles in the agglomerated structure, it can be argued that the exfoliated Fe rich surface off the bed material particle sinters together by solid state sintering to form the agglomerate during washed coal crash stop earlier described in section 2.5 and 5.3.4.2.

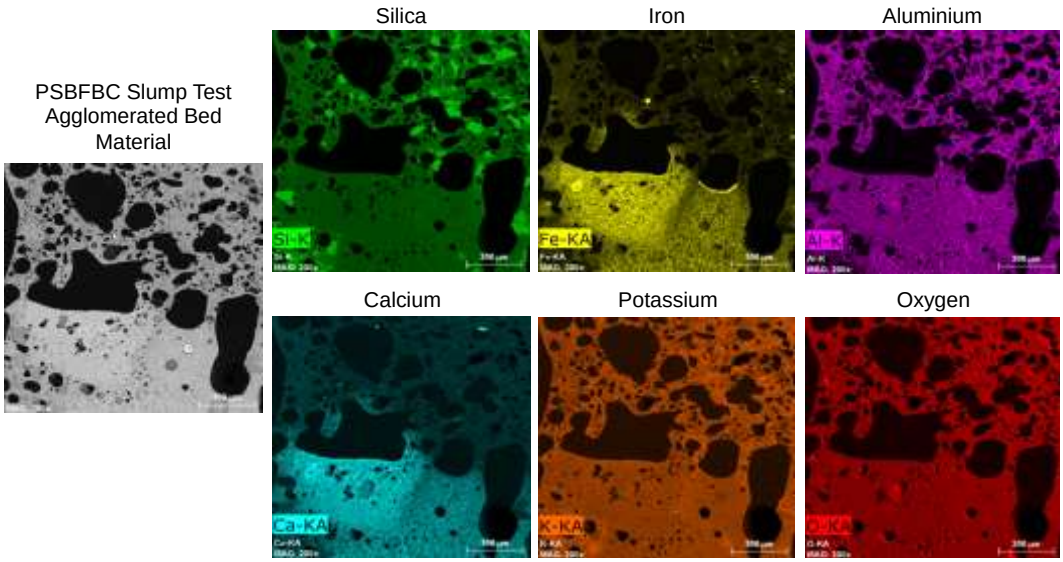

Figure 6-44: EDX elemental mapping of agglomerated Garside 14/25 sand bed material obtained after additional 5 hours of PSBFBC crash stop combustion run using unwashed Blyth coal showing the cross sectional surface distribution of identified elements in solid phase sintering process

For the agglomerated bed material made from crash stop combustion run of unwashed Blyth coal presented in Figure 6-44, it can be seen that Si, Fe, Al, Ca, K and O are distributed across the cross section surface area of the agglomerated bed material and the binder region. With the small presence of Si particles overpowered by heavy (viscous) binder containing Si, Fe, Al, Ca and K. It can be argued that various types of strong alkaline-silicate inter-particle liquid bridge can be formed between the bed material particles similar to those earlier identified and discussed in section 6.3.3.2.

To further clarify and quantify the chemical composition of the agglomerated bed material samples, an XRF analysis was done on the bulk agglomerated bed material samples results, which is presented in Figure 6-45. It can be observed from Figure 6-45 that the chemical composition of washed Blyth coal agglomerated bed material in descending order is Fe_2O_3, SiO_2, Al_2O_3, CaO and K_2O. The measured amount of Fe_2O_3 was found to vary between 50.6% and 55.1%. Composition of SiO_2 was found to be between 18.7 and 23.2% while that of Al_2O_3 was found to vary between 13.4 and 13.6%, CaO was found to be between 6.3 and 7.7% and K_2O present was between 0 and 0.2%.

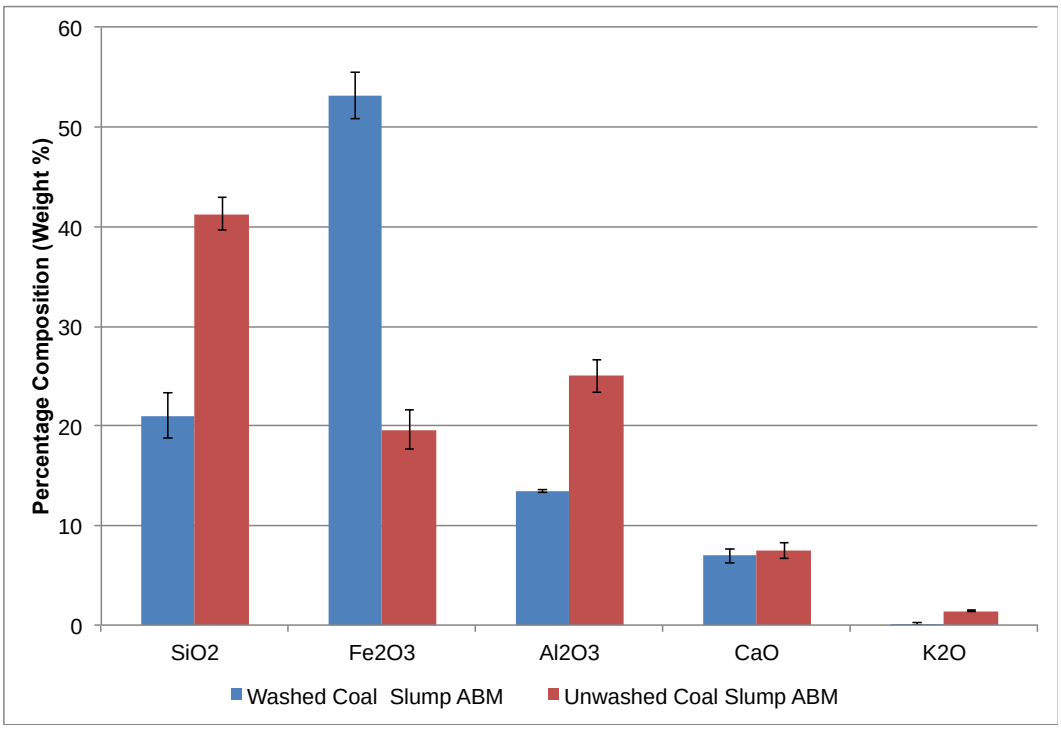

Figure 6-45: Comparison between the elemental oxide composition of agglomerated Garside 14/25 sand bed material (ABM) obtained from the crash stop combustion run of washed and unwashed Blyth coal after additional 13.35 and 5 hours of operations respectively in the PSBFBC

In the case of unwashed Blyth coal agglomerated bed material, the chemical composition was found to vary between 16.8 and 21.3% for Fe_2O_3, 39.6 and 43.4% for SiO_2, 23.3 and 27.2% for Al_2O_3, 6.5 and 8.4% for CaO and 1.4 and 1.5% for K_2O. With clear differences between the morphology, and chemical composition of the agglomerated bed materials formed from the washed and

unwashed Blyth coal, it can be concluded that different species of Fe_2O_3 – Al_2O_3 – SiO_2 and / or CaO – SiO_2 – Al_2O_3 melts are responsible for sintering and agglomerate formation in both cases based on the large differences in the percentage composition of the elemental oxide in the agglomerated samples or in the binder region.

6.4.3. Summary

A measured bed temperature rise of between 30 and 50°C occurs in the PSBFBC system, which is suspected to promote the melt responsible for sintering and agglomerate formation in both washed and unwashed Blyth coal crash stop combustion investigation.

The possibility of forming agglomerated bed material from the crash stop combustion of washed Blyth coal in the PSBFBC over an operating time of 13.34 hours suggests that the crash stop promotes sintering and agglomeration formation possibly due to the bed temperature increase effect which occurs after the fluidising air is turned off. This causes the exfoliated iron rich region from the surface of the bed material to fuse together exhibiting a solid state sintering.

The mechanisms responsible for sintering and agglomerate formation in the washed and unwashed Blyth coal crash stop combustion runs are different from each other. This difference can be seen in their surface morphology characterisation and elemental oxide composition.

The agglomerated bed material formed from the unwashed Blyth coal crash stop combustion process has a similar chemistry to those formed from the same coal type during normal combustion operation.

CHAPTER SEVEN

CONCLUSIONS, FUTURE WORK AND RECOMMENDATIONS

7.1. Introduction

Mechanisms responsible for sintering and agglomerate formation during combustion of lump washed and unwashed Blyth coals with particle sizes between 9 and 19 mm in a PSBFBC system were investigated. Sintering and agglomerate formation properties of Garside 14/25 sand bed materials were also investigated in the absence and presence of coal or coal ash.

Conclusions drawn from these investigations are summarised in section 7.2. Recommendations for future works based on these findings are presented in section 7.3, and recommendations for industrial FBC system are discussed in section 7.4.

7.2. Conclusions

Findings both address project objectives and add to the body of knowledge on sintering and agglomerate formation. Niche areas of this study suitable for publications are:

1. Sintering and agglomerate formation tendencies of Garside 14/25 sand bed material during calcination at high temperature in the presence and absence of coal or coal ash.

2. Sintering and agglomerate formation mechanism (detailed and described in section 2.5.4 for lump coal combustion in a fluidised bed combustion BFB system without ash removal capability) developed and investigated herein regarding its viability.
3. Impact of mud/shale stone deposition in the bed on localised temperature, coating induced and melting induced pathways, strong inter-particle bridge formation, and their effect on increasing mean particle size diameter of bed material when using washed and unwashed Blyth coals.
4. In-depth use of EDX/SEM and XRF analytical techniques for detailed studies of sintering and agglomerate formation and properties of ash deposited on the surface of bed material particles.

Conclusion details are presented in four subcategories. The first two subcategories (sections 7.2.1 and 7.2.2) are based on the calcination test investigation discussed in chapter 5. Conclusions detailed in section 7.2.3 and 7.2.4 are based on the PSBFBC investigations discussed in chapter 6.

7.2.1. Characteristic Behaviour of Garside 14/25 Sand Bed Material at High Temperature (Calcination Test)

The agglomeration of Garside 14/25 sand used as the bed material in the industrial scale FBCs occurs at a calcination temperature of about 1200°C irrespective of particle size in the absence of coal and coal ash. Two types of sintering processes (transient liquid phase and solid state sintering) are responsible for agglomeration formation under this condition. Agglomeration formation under this condition is dependent on the presence of elements or elemental oxides (Fe_2O_3, SiO, K_2O and Al_2O_3), traditionally identified as responsible for sintering and agglomerate formation. Although this type of agglomeration formation process may not be the sole process responsible for

sintering and agglomerate formation during coal combustion in a FBC, it does contribute to the overall formed sinter or agglomerate formed within the system.

With increasing calcination temperature, iron-rich areas on the Garside 14/25 sand bed material particle surfaces fractures / crack. The intensity of the fractures and cracks increases as the calcination temperature increases, causing exfoliation of this iron-rich surface at a calcination temperature of about 1000°C. The extent of the crack and exfoliation of the iron-rich regions is independent of particle size, calcination temperature or calcination time, whereas the intensity of cracking was found to be dependent on calcination temperature.

Garside 14/25 sand bed material was also observed to undergo colour change, from yellowish brown in its fresh state to red due to the phase change from βFe_2O_3 to αFe_2O_3. The hue of colour increases with the calcination temperature. Garside 14/25 sand bed material also experienced a weight loss between 0.5% and 0.9% which accounts for both moisture loss and the thermal decomposition process, and between 0.31 and 0.79% weight loss which accounts for the thermal decomposition process alone

7.2.2. Impact of Coal Combustion Stages on Sintering and Agglomerate Formation Surface Morphology and Chemistry (Calcination Test)

Surface morphology of agglomerated bed material formed from calcination of Garside 14/25 sand bed material with coal mix of various compositions at about 1200°C resembles that formed in the industrial operated FBC system during lump coal combustion. This shows the contributory effect of combustion stages to ash melting behaviour and agglomerate formation.

Liquid phase sintering is the sintering process responsible for agglomeration formation in this type of system that results in formation of Fe_2O_3 – Al_2O_3 - SiO_2 alkali – silicate melt. This sintering process is also proposed as the major cause of sintering bridge / agglomerate formation during coal combustion. The strength of the sintering bridge or agglomerate formed increases with increased calcination temperature and the amount of coal present in the sample mixture irrespective of coal type

7.2.3. Sintering and Agglomerate Formation Mechanism during Normal Combustion Runs of Washed and Unwashed Blyth Coal (PSBFBC Test)

Sintering and agglomerate formation is an ash related problem whose formation tendencies are increased by the use of lump unwashed Blyth coal. Use of unwashed Blyth coal causes a more pronounced increase in the amount of mud/shale stone deposited in the PSBFBC bed when compared with washed Blyth coal. The greater the amount of mud/shale stones deposited in the bed, the greater the sintering and agglomerate formation tendency. Increasing mass of mud/shale stone deposited in the bed also causes an increase in the bed pressure drop and bed height, and also causes the bed to become fluidised at a lower volumetric air flowrate.

Coating and deposition of ash on the surface of bed material particle above the fluidising nozzle increases as operation time increases. This also results in increased composition of Al_2O_3, CaO and K_2O deposited onto the surface of the bed material particles and the decrease in the SiO_2.

Vertical bed temperature, linear average pressure drop and flue gas composition measurements techniques were not effective for small quantities of sintering and agglomerate formation detection over a 52 hours combustion-operating period.

More operating time is required for the PSBFBC bed to fully agglomerate to establish the suitability of these techniques for sintering and agglomerate formation detection.

7.2.4. Effect of Loss of Fluidising Air during Combustion Runs on Sintering and Agglomerate Formation (PSBFBC Test)

Sintering and agglomerate formation are more pronounced during the crash-stop combustion runs of washed and unwashed Blyth lump coal using aged Garside 14/25 sand bed. This simulates a fan trip scenario that might occur in the industrial scale FBC system. A fan trip occurrence is suspected to have been caused by the 30 to 50°C rise in bed temperature.

The agglomerated bed material formed from the crash stop combustion runs of washed and unwashed Blyth coals can be associated with alkaline-silicate melts of $Fe_2O_3 – Al_2O_3 – SiO_2$ and / or $CaO – SiO_2 – Al_2O_3$. However due to the large differences in the percentage composition of the elemental oxide in the agglomerated samples or in the binder region, the mechanisms responsible for sintering and agglomerate formation in the washed and unwashed Blyth coal crash stop combustion runs are believed to be different. This difference is also observed in their surface morphology characterisation based on their physical appearance. The agglomerated bed material formed from the unwashed Blyth coal crash stop combustion process has a similar chemistry and physical appearance to those formed from the same coal type during normal combustion operation.

7.3. Future Work

Opportunities for further research based on avoiding sintering and agglomerate formation in a lump coal fired BFB study are highlighted below.

- Investigate the impact of continuous operation of the PSBFBC rig for a prolonged period similar to operating practice in the industrial scale FBC system on sintering and agglomerate formation.

- As identified agglomeration formation is more pronounced during crash stop combustion of coal using aged bed material due to temperature rise, which is similar to fan trip condition in the industrial scale FBC system, investigate the practicability of injecting a form of flame retardant (e.g., nitrogen) during this period to create an inert environment in the bed that could mitigate this effect.

- Investigate the impact of lump coal particle size on sintering and agglomerate formation (e.g., by using smaller particle sized coal in the range of 5 to 12mm in the PSBFBC) to determine the effect it has on particle size growth of the bed and sintering and agglomerate formation.

- Investigate the maximum amount of mud/shale stone deposition that the bed can accommodate before negatively influencing their fluidisation quality and hydrodynamic properties.

- Investigate methods of continual removal of mud/shale stone deposited in the bed during normal combustion runs to reduce the impact on agglomeration formation.

- Investigate and identify the species of $CaO – Al_2O_3 – SiO_2$ and $Fe_2O_3 – Al_2O_3 – SiO_2$ in the phase equilibrium system that might be responsible for sintering and agglomerate formation during the combustion of unwashed Blyth coal.

- With the aim of reducing green house gas emission, investigate co-firing of biomass (bagasse and / or sugar beet pulps) with washed Blyth coal or

other types of washed bituminous coals to determine the impact on agglomeration formation.

- Based on preliminary analysis, no obvious pattern has been detected from linear pressure, vertical temperature and flue-gas measurements to suggest their suitability for sintering and agglomerate formation detection. Hence, more studies are required to determine their suitability for this purpose in a fully agglomerated bed situation.

7.4. Recommendations for Industrial FBC

Based on this study on avoiding sintering and agglomerate formation in a lump coal fired bubbling fluidised bed, recommendations for industrial FBC systems, are provided below.

- Investment in a continuous ash / bed material particularly deposited mud/shale stone removal technology, will be very advantageous for stabilising the hydrodynamic properties of the bed, especially in unwashed coal applications. This will help reduce the occurrence of sintering and agglomerate formation in the bed.

- Periodically and significantly increasing the fluidizing air flow rate and stopping the coal feeder for a short period of time so that fine coal ash particles can be removed from the industrial FBC bed, should reduce ash deposits on bed materials thus reducing the chance of sintering and agglomerate formation that might later cause defluidisation of the FBC bed.

- Better placed and more thermocouples in the industrial FBC is required to provide clearer understanding of the bed during operation. A better temperature control approach is also needed to prevent ash melting

- Due to the low composition of mud/shale stone in washed coals, continual use of high quality washed coal is recommended to mitigate mud/shale stone deposition in the bed.

References

ANSYS., 2006. *FLUENT Software 6.3 User's Guide*, Lebanon, NH, USA: Fluent Inc.

Anthony, E.J., Iribarne, A.P. & Iribarne, J.V, 1997. A New Mechanism for FBC Agglomeration and Fouling in 100 Percent Firing of Petroleum Coke. *Journal of Energy Resources Technology*, 119(1), pp. 55–61.

Anthony, E.J., Preto, F., Jia, L. & Iribarne, J.V, 1998. Agglomeration and Fouling in Petroleum Coke-Fired FBC Boilers. *Journal of Energy Resources Technology*, 120(4), pp. 285–292.

Atakul, H. & Ekinci, E., 1990. Agglomeration in lignite ash flotsam- and jetsam-rich systems. *Powder Technology*, 60(2), pp. 77–82.

Bartels, M., Lin, W.G., Nijenhuis, J., Kapteijn, F. & van Ommen, J.R., 2008. Agglomeration in fluidized beds at high temperatures: Mechanisms, detection and prevention. *Progress in Energy and Combustion Science*, 34(5), pp. 633–666.

Bartels, M., Nijenhuis, J., Lensselink, J., Siedlecki, M., De Long, W., Kapteijn, F, & van Ommen, J.R., 2009. Detecting and Counteracting Agglomeration in Fluidized Bed Biomass Combustion. *Energy & Fuels*, 23(1), pp. 157–169.

Bartels, M., Nijenhuis, J., Kapteijn, F, & van Ommen, J.R., 2010a. Case studies for selective agglomeration detection in fluidized beds: Application of a new screening methodology. *Powder Technology*, 203(2), pp. 148–166.

Bartels, M., Nijenhuis, J., Kapteijn, F, & van Ommen, J.R., 2010b. Detection of agglomeration and gradual particle size changes in circulating fluidized beds. *Powder Technology*, 202(1-3), pp. 24–38.

Basu, P., 2006. *Combustion and Gasification in Fluidized Beds*, Taylor & Francis Group.

Benson, S.A., Jones, M.L. & Harb, J.N., 1993. Ash Formation and Deposition. In L. D. Smoot, ed. *Fundamentals of coal combustion: for clean and efficient use*. London: Elsevier, pp. 299–373.

Benson, S.A., Sondreal, E.A. & Hurley, J.P., 1995. Status of coal ash behavior research. *Fuel Processing Technology*, 44(1-3), pp. 1–12.

Mac an Bhaird, S.T., Walsh, E., Hemmingway, P., Maglinao, A.L., Capareda, S.C & McDonnell, K.P., 2014. Analysis of bed agglomeration during gasification of wheat straw in a bubbling fluidised bed gasifier using mullite as bed material. *Powder Technology*, 254, pp. 448–459.

Brus, E., Ohman, M. & Nordin, A., 2005. Mechanisms of bed agglomeration during fluidized-bed combustion of biomass fuels. *Energy & Fuels*, 19(3), pp. 825–832.

Carpenter, A., Niksa, S., Scott, D.H., Wu, Z. & SRI International, 2007. *Fundamentals of Coal Combustion*, IEA Clean Coal Centre,.

Chaivatamaset, P., Sricharoon, P., Tia, S. & Bilitewski,B., 2013. A prediction of defluidization time in biomass fired fluidized bed combustion. *Applied Thermal Engineering*, 50, pp. 722–731.

Chirone, R., Miccio, F. & Scala, F., 2006. Mechanism and prediction of bed agglomeration during fluidized bed combustion of a biomass fuel: Effect of the reactor scale. *Chemical Engineering Journal*, 123(3), pp. 71–80.

Coda Zabetta, E., Barisic, V., Peltola, K., Sarkki, J. & Jantti, T., 2013. Advanced technology to co-fire large shares of agricultural residues with biomass in utility CFBs. In *Fuel Processing Technology*. pp. 2–10.

Dahlin, R.S., Dorminey, J.R., Peng, W.W., Leonard, R.F. & Vimalchand, P., 2009. Preventing Ash Agglomeration during Gasification of High-Sodium Lignite. *Energy & Fuels*, 23(1), pp. 785–793.

Dainton, A.D., 1979. The Combustion of Coal. In G. J. Pitt & G. R. Millward, eds. *Coal and Modern Coal Processing: An Introduction*. London: Academic Press, pp. 109–131.

Datta, S., Sarkar, P., Chavan, P.D., Saha, S., Sahu, G., Sinha, A.K. & Saxena, V.K., 2015. Agglomeration behaviour of high ash Indian coals in fluidized bed gasification pilot plant. *Applied Thermal Engineering*, 86, pp. 222–228.

Daw, C.S., Finney, C.E.A., Nguyen, K. & Halow, J.S., 1998. Symbol statistics: a new tool for understanding multiphase flow phenomena. In R. A. Nelson Jr, T. Chopin, & S. T. Thynell, eds. *Proceedings of the ASME Heat Transfer Division*. pp. 221–229.

Daw, C.S. & Hawk, J.A., 1995. Fluidisation quality analyser for fluidised beds in fluidised bed reactor—uses fast response pressure transducer to measure overall or part bed pressure drop and processes pressure drop signal to produce output voltage which changes with degree of fluidis U. S. D. E. (USAT), ed.

Dejoie, C., Sciau, P., Li, W., Noe, L., Mehta, A., Chen, K., Luo, H., Kunz, M., Tamura, N. & Liu, Z., 2014. Learning from the past: rare ε-Fe_2O_3 in the ancient black-glazed Jian (Tenmoku) wares. *Scientific reports*, 4, p. 4941.

van der Drift, A. & Olsen, A., 1999. *Conversion of biomass, Prediction and Solution Methods for Ash Agglomeration and Related Problems*, European Commission .

Duan, F., Chyang, C.S., Zhang, L. & Yin, S.F., 2015. Bed agglomeration characteristics of rice straw combustion in a vortexing fluidized-bed combustor. *Bioresource technology*, 183, pp. 195–202.

Ergudenler, A. & Ghaly, A.E., 1993. Agglomeration of silica sand in a fluidized bed gasifier operating on wheat straw. *Biomass and Bioenergy*, 4(2), pp. 135–147.

van Eyk, P.J., Kosminski, A., Mullinger, P.J. & Ashman, P.J., 2016. Control of agglomeration during circulating fluidized bed gasification of a south australian low-rank coal: pilot scale testing. *Energy and Fuel*, 30, pp. 1771 - 1782.

Fonseca, A.G., 1995. The Challenges of coal preparation. In S. K. Kawatra, ed. *High Efficiency Coal Preparation*. Littleton: Society for Mining, Metallurgy, and Exploration.

Fueyo, N. & Dopazo, C., 1995. Fluidization fundamentals. In M. A. Cuenca & E. J. Anthony, eds. *Pressurized Fluidized Bed Combustion*. Springer Netherlands, pp. 38–79.

Fuller, T.A., Flynn, T.J., Daw, C.S. & Halow, J.S., 1993. *Interpretation of pilot-scale, fluidized bed behavior using chaotic time series analysis*,

Garside Sands, 2011. Data Sheet for Garside Leighton Buzzard 14/25 Garside Sands, ed.

Gatternig, B. & Karl, J., 2014. The influence of particle size, fluidization velocity and fuel type on ash-induced agglomeration in biomass combustion. *Frontiers in Energy Research*, 2.

Geldart, D., 1973. Types of gas fluidization. *Powder Technology*, 7(5), pp.285–292.

German, R., Suri, P. & Park, S., 2009. Review: liquid phase sintering. *Journal of Materials Science*, 44(1), pp. 1–39.

German, R.M., 1996. Sintering theory and practice. *Sintering Theory and Practice, by Randall M. German, pp. 568. ISBN 0-471-05786-X. Wiley-VCH, January 1996.*, 1.

Gheorghiu, S., van Ommen, J.R. & Coppens, M.O., 2004. Monitoring fluidized bed hydrodynamics using power-law statistics of pressure fluctuations . In U. Arena et al., eds. *Fluidization XI. Engineering conferences international*. pp. 403–410.

Glazer, M.P., Khan, N.A., de Jong, W., Spliethoff, H., Schurmann, H. & Monkhouse, P., 2005. Alkali Metals in Circulating Fluidized Bed Combustion of Biomass and Coal: Measurements and Chemical Equilibrium Analysis. *Energy & Fuels*, 19(5), pp. 1889–1897.

Grubor, B.G., Oka, S.N., Ilic, M.S., Dakic, D.V. & Arsic, B.T., 1995. Biomass FBC Combustion - Bed Agglomeration Problems. In K. J. Heinschel, ed. *Proceedings of the 13th international conference on fluidised bed combustion*. Orlando, USA, pp. 515–522.

Hamidi, M., Briens, C. & Berruti, F., 2015. *Development And Study Of Measurement Methods For Jets And Bogging In A Fluidized Bed*. Electronic Thesis and Dissertation Repository Paper 2679: University of Western Ontario.

Hayrinen, V., Hernberg, R. & Aho, M., 2004. Demonstration of plasma excited atomic resonance line spectroscopy for on-line measurement of alkali metals in a 20kW bubbling fluidized bed. *Fuel*, 83(7-8), pp. 791–797.

Holdich, R.G., 2002. *Fundamentals of Particle Technology*, Midland Information Technology and Publishing.

Huffman, G.P., Huggins, F.E. & Dunmyre, G.R., 1981. Investigation of the high-temperature behaviour of coal ash in reducing and oxidizing atmospheres. *Fuel*, 60(7), pp. 585–597.

Huggins, F.E., Kosmack, D.A. & Huffman, G.P., 1981. Correlation between ash-fusion temperatures and ternary equilibrium phase diagrams. *Fuel*, 60(7), pp. 577–584.

Jinsheng, G., 2009. *Coal, Oil Shale, Natural Bitumen, Heavy Oil and Peat*, Eolss Publishers Company Limited.

Kai, T. & Furusaki, S., 1987. Methanation of carbon dioxide and fluidization quality in a fluid bed reactor - the influence of a decrease in gas volume. *Chemical Engineering Science*, 42(2), pp. 335–339.

Kang, S.J.L., 2005. *Sintering: Densification, Grain Growth and Microstructure*, Oxford: Elsevier Science. *ISBN-10 0750663855.*

Khan, A.A., de Jong, W., Jansens, P.J. & Spliethoff, H., 2009. Biomass combustion in fluidized bed boilers: Potential problems and remedies. *Fuel Processing Technology*, 90(1), pp. 21–50.

Kobusheshe, J., 2010. *Microwave Enhanced Processing of Ores*. University of Nottingham.

Koppejan, J. & van Loo, S., 2003. *The Handbook of Biomass Combustion and Co-firing*, Earthscan.

Kyi, S. & Chadwick, B.L., 1999. Screening of potential mineral additives for use as fouling preventatives in Victorian brown coal combustion. *Fuel*, 78(7), pp. 845–855.

Lau, I.T. & Whalley, B.J.P., 1981. A differential thermal probe for anticipation of defluidization of caking coals. *Fuel Processing Technology*, 4(2-3), pp. 101–115.

Leach, M.F., Rubin, G.A. & Williams, J.C., 1978. Analysis of gaussian size distribution of rigid particles from their acoustic emission. *Powder Technology*, 19(2), pp. 189–195.

Leach, M.F., Rubin, G.A. & Williams, J.C., 1977. Particle size determination from acoustic emissions. *Powder Technology*, 16(2), pp. 153–158.

Levenspiel, O., 1999. *Chemical Reaction Engineering*, New York, USA: John Wiley & Sons, Inc. ISBN 978-0-471-25424-9.

Levine, D.G., Schlosberg, R.H. & Silbernagel, B.G., 1982. Understanding the Chemistry and Physics of Coal Structure (A Review). *Proceedings of National Academy of Science*, 70(10), pp. 3365–3370.

Lin, W., Dam-Johansen, K. & Frandsen, F., 2003. Agglomeration in bio-fuel fired fluidized bed combustors. *Chemical Engineering Journal*, 96(1), pp. 171–185.

Liu, H., 2011a. Combustion and Thermochemistry University Of Nottingham, ed. *Combustion and Pollution Control*.

Liu, H., 2011b. Combustion of Solid Fuels University Of Nottingham, ed. *Combustion and Pollution Control*.

Liu, Y., Gupta, R., Sharma, A., Wall, T., Butcher, A., Miller, G., Gottlieb, P. & French, D., 2005. Mineral matter–organic matter association characterisation by QEMSCAN and applications in coal utilisation. *Fuel*, 84(10), pp. 1259–1267.

Llorente, M.J.F. & Garcia, J.E.C., 2005. Comparing methods for predicting the sintering of biomass ash in combustion. *Fuel*, 84(14-15), pp. 1893–1900.

van Loo, S. & Koppejan, J., 2008. *The Handbook of Biomass Combustion and Co-Firing*, Earthscan.

Lowry, H.H., 1945. *The Chemistry of Coal Utilization*, New York: John Wiley & Sons Inc.

Luan, C., You, C. & Zhang, D., 2014. Composition and sintering characteristics of ashes from co-firing of coal and biomass in a laboratory-scale drop tube furnace. *Energy*, 69, pp. 562–570.

Lundholm, K., Nordin, A., Ohman, M. & Bostrom, D., 2005. Reduced bed agglomeration by co-combustion biomass with peat fuels in a fluidized bed. *Energy & Fuels*, 19(6), pp. 2273–2278.

Manzoori, A.R. & Agarwal, P.K., 1992. The fate of organically bound inorganic elements and sodium chloride during fluidized bed combustion of high sodium, high sulphur low rank coals. *Fuel*, 71(5), pp. 513–522.

Matthews, V., 2005. *Colorado Coal: energy security for the future*,

McCullough, D.P., van Eyk, P.J., Ashman, P.J. & Mullinger, P.J., 2011. Investigation of Agglomeration and Defluidization during Spouted-Bed Gasification of High-Sodium, High-Sulfur South Australian Lignite. *Energy & Fuels*, 25(7), pp. 2772–2781.

McDougall, S., Saberian, M., Briens, C., Berruti, F. & Chan, E., 2005. Using dynamic pressure signals to assess the effects of injected liquid on fluidized bed properties. *Chemical Engineering and Processing: Process Intensification*, 44(7), pp. 701–708.

Meyers, R.A., 1981. Coal Handbook P. N. Power & W. Meier, eds. *Energy, Power, and Environment*, 11, *ISBN-10 0824712706.*

Molerus, O., 1982. Interpretation of Geldart's type A, B, C and D powders by taking into account interparticle cohesion forces. *Powder Technology*, 33(1), pp. 81–87.

Namkung, H., Kim, C.H., Kim. D., Yuan, X., Kang, T.J. & Kim, H.T., 2015. Effect of bed agglomeration by mineral component with different coal types. *Journal of the Energy Institute*.

National Coal Board, 1980. *Fluidised Bed Combustion of Coal*, London.

Ninduangdee, P. & Kuprianov, V.I., 2015. Combustion of an oil palm residue with elevated potassium content in a fluidized-bed combustor using alternative bed materials for preventing bed agglomeration. *Bioresource technology*, 182, pp. 272–81.

Ohman, M., Nordin, A., Skrifvars, B.J., Backman, R. & Hupa, M., 2000. Bed agglomeration characteristics during fluidized bed combustion of biomass fuels. *Energy & Fuels*, 14(1), pp. 169–178.

Oka, S., 2010. *Fluidized Bed Combustion*, CRC Press. *ISBN 9780824746995.*

Olanders, B. & Steenari, B.M., 1995. Characterization of ashes from wood and straw. *Biomass and Bioenergy*, 8(2), pp.105–115.

van Ommen, J.R., Coppens, M.O., van den Bleek, C.M. & Schouten, J.C., 2000. Early warning of agglomeration in fluidized beds by attractor comparison. *AIChE Journal*, 46(11), pp. 2183–2197.

Park, D., 1989. Estimation of temperature difference between char particles and the fluidized bed in char combustion. *Fuel*, 68(10), pp. 1320–1324.

Qureshi, A.E. & Creasy, D.E., 1979. Fluidised bed gas distributors. *Powder Technology*, 22(1), pp. 113–119.

Rajput, R.K., 2007. *A Textbook of Manufacturing Technology: Manufacturing Processes*, Laxmi. *ISBN 8131802442.*

Reed, S.J.B., 2005. *Electron Microprobe Analysis and Scanning Electron Microscopy in Geology.*, Cambridge University Press. *ISBN 9780521848756.*

Richardson, J.F., Harker, J.H. & Backhurst, J.R., 2002. *Coulson and Richardson's Chemical Engineering Volume 2 - Particle Technology and Separation Processes (5th Edition)*, Elsevier. *ISBN 0750644451.*

Saberi, S., Saberi, B., Shakourzadeh, K. & Guigon, P., 1995. Comparative study of tuyere designs for fluidized beds. *The Chemical Engineering Journal and the Biochemical Engineering Journal*, 60(1–3), pp. 75–79.

Sánchez-Prieto, J., Soria-Verdugo, A., Briongos, J.V. & Santana, D., 2014. The effect of temperature on the distributor design in bubbling fluidized beds. *Powder Technology*, 261, pp. 176–184.

Scala, F. & Chirone, R., 2006. Characterization and Early Detection of Bed Agglomeration during the Fluidized Bed Combustion of Olive Husk. *Energy & Fuels*, 20(1), pp. 120–132.

Schairer, J.F. & Bowen, N.L., 1947. Melting relations in the systems Na_2O - Al_2O_3 - SiO_2 and K_2O - Al_2O_3 - SiO_2. *American Journal of Science*, 245, pp. 193–204.

Schairer, J.F. & Yagi, K., 1952. The System FeO - Al_2O_3 - SiO_2. *American Journal of Science*, Bowen Volu, pp. 471–512.

Schobert, H.H., 1990. Chapter 10 - Coal combustion. In H. H. Schobert, ed. *The Chemistry of Hydrocarbon Fuels*. Butterworth-Heinemann, pp. 255–270. *ISBN 9780408038256.*

Schobert, H.H., 1987. *Coal: The Energy Source of the Past and Future*, Washington D.C.: America Chemical Society. *ISBN 0841211728*

Seville, J.P.K. & Clift, R., 1984. The effect of thin liquid layers on fluidisation characteristics. *Powder Technology*, 37(1), pp. 117–129.

Seville, J.P.K., Willett, C.D. & Knight, P.C., 2000. Interparticle forces in fluidisation: a review. *Powder Technology*, 113(3), pp. 261–268.

Simpson, J., 2009. Oxford English Dictionary, Second Edition on CD-ROM Version 4.0.

Sinnott, R.K., 2005. Coulson and Richardson's Chemical Engineering Volume 6 - Chemical Engineering Design (4th Edition). *ISBN 9780080418667*

Skrifvars, B.J., Backman, R. & Hupa, M., 1998. Characterization of the sintering tendency of ten biomass ashes in FBC conditions by a laboratory test and by phase equilibrium calculations. *Fuel Processing Technology*, 56(1-2), pp. 55–67.

Skrifvars, B.J., Hupa, M. & Hiltunen, M., 1992. Sintering of ash during fluidized bed combustion. *Industrial & Engineering Chemistry Research*, 31(4), pp. 1026–1030.

Skrifvars, B.J., Ohman, M., Nordin, A. & Hupa, M., 1999. Predicting Bed Agglomeration Tendencies for Biomass Fuels Fired in FBC Boilers: A Comparison of Three Different Prediction Methods. *Energy & Fuels*, 13(2), pp. 359–363.

Takens, F., 1981. Detecting strange attractors in turbulence. In D. Rand & L.-S. Young, eds. *Dynamical Systems and Turbulence, Warwick 1980*. Springer Berlin Heidelberg, pp. 366–381.

Tanaka, H., Yamamoto, A., Shimoyama, J., Ogino, H. & Kishio, K., 2012. Strongly connected ex situ MgB 2 polycrystalline bulks fabricated by solid-state self-sintering. *Superconductor Science and Technology*, 25(11), pp.115022.

Tardos, G. & Pfeffer, R., 1995. Chemical reaction induced agglomeration and defluidization of fluidized beds. *Powder Technology*, 85(1), pp. 29–35.

Teixeira, P., Lopes, H., Gulyurtlu, I., Lapa, N. & Abelha. P., 2012. Evaluation of slagging and fouling tendency during biomass co-firing with coal in a fluidized bed. *Biomass and Bioenergy*, pp. 1–12.

Unsworth, J.F., Barratt, D.J. & Roberts, P.T., 1991. *Coal Quality and Combustion Performance: An international Perspective*, Amsterdam: Elsevier. *ISBN-10 0444887032.*

Vassilev, S. V, Vassileva, C.G. & Vassilev, V.S., 2015. Advantages and disadvantages of composition and properties of biomass in comparison with coal: An overview. *Fuel*, 158(0), pp. 330–350.

Vassileva, C.G. & Vassilev, S. V, 2005. Behaviour of inorganic matter during heating of Bulgarian coals: 1. Lignites. *Fuel Processing Technology*, 86(12–13), pp. 1297–1333.

Venkataraman, A., 1996. Studies on hydrogen ferrite phase in γ-Fe_2O_3 synthesised from ferrous fumarate half hydrate precursor. *Journal of Thermal Analysis*, 46(1), pp. 219–224.

Visser, J., 1989. Van der Waals and other cohesive forces affecting powder fluidization. *Powder Technology*, 58(1), pp. 1–10.

Vujtek, M., Zboril, R., Kubinek, R. & Mashlan, M., 2003. Ultrafine Particles of Iron(III) Oxides by View of AFM – Novel Route for Study of Polymorphism in Nano-world. *Science, technology and education of microscopy: an overview, Microscopy Book Series*, 1.

Vuthaluru, H.B., Zhang, D.K. & Linjewile, T.M., 2000. Behaviour of inorganic constituents and ash characteristics during fluidised-bed combustion of several Australian low-rank coals. *Fuel Processing Technology*, 67(3), pp. 165–176.

Wall, T.F., Creelman, R.A., Gupta, R.P., Gupta, S., Colin, C. & Lowe, A., 1996. Coal Ash Fusion Temperatures — New Characterisation Techniques, and Associations with Phase Equilibria. In L. Baxter & R. DeSollar, eds. *Applications of Advanced Technology to Ash-Related Problems in Boilers*. Springer US, pp. 541–556.

Wang, J., Cao,Y., Jiang, X. & Yang, Y., 2009. Agglomeration Detection by Acoustic Emission (AE) Sensors in Fluidized Beds. *Industrial & Engineering Chemistry Research*, 48(7), pp. 3466–3473.

Wang, L., Hustad, J.E., Skreiberg, O., Skjevrak, G. & Gronli, M., 2012. A Critical Review on Additives to Reduce Ash Related Operation Problems in Biomass Combustion Applications. *Energy Procedia*, 20, pp. 20–29.

Wen, C.Y. & Yu, Y.H., 1966. A generalized method for predicting the minimum fluidization velocity. *AIChE Journal*, 12(3), pp. 610–612.

Wu, X., Zhang, Z., Piao, G., He, X., Chen, Y., Kobayashi, N., Mori, S. & Itaya, Y., 2009. Behavior of Mineral Matters in Chinese Coal Ash Melting during char-CO_2/H_2O Gasification Reaction. *Energy & Fuels*, 23(5), pp. 2420–2428.

Zenz, F.A., 1981. Elements of Grid Design. In *Gas Particle Industrial Symposium, Engineering Society*. Western PA, Pittsburgh, USA.

Zhang, W., Liu, H., Sun, C., Drage, T.C. & Snape, C.E., 2014. Performance of polyethyleneimine–silica adsorbent for post-combustion CO_2 capture in a bubbling fluidized bed. *Chemical Engineering Journal*, 251, pp. 293–303.

Zhong, Y., Wang, Z., Guo, Z. & Tang, Q., 2013. Prevention of agglomeration/defluidization in fluidized bed reduction of Fe_2O_3 by CO: The role of magnesium and calcium oxide. *Powder Technology*, 241, pp. 142–148.

Zukowski, W.A., 1999. Acoustic effects during the combustion of gaseous fuels in a bubbling fluidized bed. *Combustion and Flame*, 117(3), pp. 629–635.

Appendix A: Coal Feeder Calibration

Calibration of the coal feeder was done by setting the speed of the coal feeder screw auger using item marked D in Figure E-3 coal feeders, collecting the coal conveyed through the feeder system and weighting it constantly over a fixed period of time (every 1 minute). The coal particle size used during the calibration is 9 to 19mm which is the same as those proposed to be used in during combustion run investigation in the PSBFBC system. Results obtained from the coal feeder calibration setup are presented Figure A-1 and Table A-1.

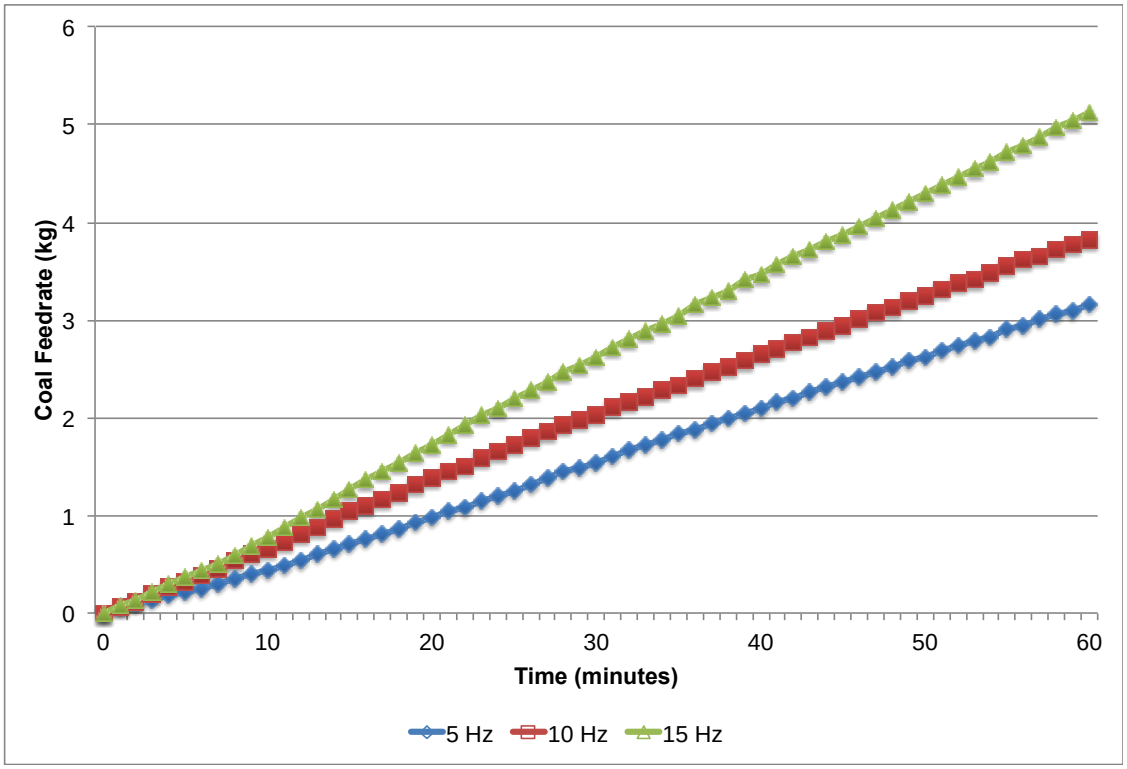

Figure A-1: Coal feeder calibration chart

Table A-1: Coal feedrate raw data taken at every time interval

Frequency (Hz)	5	7.5	10
Motor Speed (rpm)	1.25	1.75	2.25
Time (minute)	Weight (kg)		
0	0.00	0.00	0.00
1	0.06	0.07	0.08
2	0.09	0.12	0.13
3	0.13	0.20	0.21
4	0.18	0.26	0.30
5	0.21	0.32	0.36
6	0.25	0.39	0.44
7	0.30	0.46	0.50
8	0.35	0.53	0.58
9	0.40	0.60	0.69
10	0.44	0.66	0.77
11	0.49	0.72	0.87
12	0.54	0.81	0.97
13	0.60	0.88	1.07
14	0.65	0.96	1.17
15	0.71	1.04	1.27
16	0.75	1.10	1.37
17	0.81	1.17	1.46
18	0.86	1.24	1.54
19	0.92	1.32	1.64
20	0.98	1.39	1.73
21	1.04	1.45	1.83
22	1.08	1.51	1.92
23	1.14	1.59	2.02
24	1.20	1.65	2.10
25	1.25	1.72	2.20
26	1.31	1.79	2.28
27	1.39	1.85	2.37
28	1.45	1.92	2.47
29	1.49	1.97	2.54
30	1.54	2.02	2.62
31	1.61	2.11	2.72
32	1.67	2.16	2.80
33	1.72	2.22	2.89
34	1.78	2.28	2.96
35	1.84	2.33	3.05
36	1.88	2.40	3.16
37	1.94	2.46	3.23
38	2.00	2.52	3.30
39	2.04	2.58	3.41
40	2.10	2.66	3.47
41	2.16	2.70	3.57
42	2.20	2.77	3.65
43	2.26	2.82	3.72
44	2.32	2.89	3.80
45	2.36	2.95	3.88
46	2.42	3.01	3.96
47	2.47	3.07	4.05
48	2.52	3.13	4.12
49	2.58	3.20	4.21
50	2.62	3.25	4.30
51	2.68	3.31	4.38
52	2.74	3.38	4.46
53	2.79	3.42	4.55
54	2.83	3.48	4.62
55	2.90	3.55	4.72
56	2.95	3.62	4.79
57	3.01	3.66	4.88
58	3.06	3.72	4.97
59	3.10	3.77	5.05
60	3.16	3.83	5.13

Total coal collected at the end of each motor frequency is plotted against each other to interpolate for missing data point are presented in Table A-2 and Figure A-2

Table A-2: Coal feedrate at specific motor frequency

Frequency (Hz)	0	5	7.5	10
Coal Feedrate (kg)	0	3.16	3.83	5.13

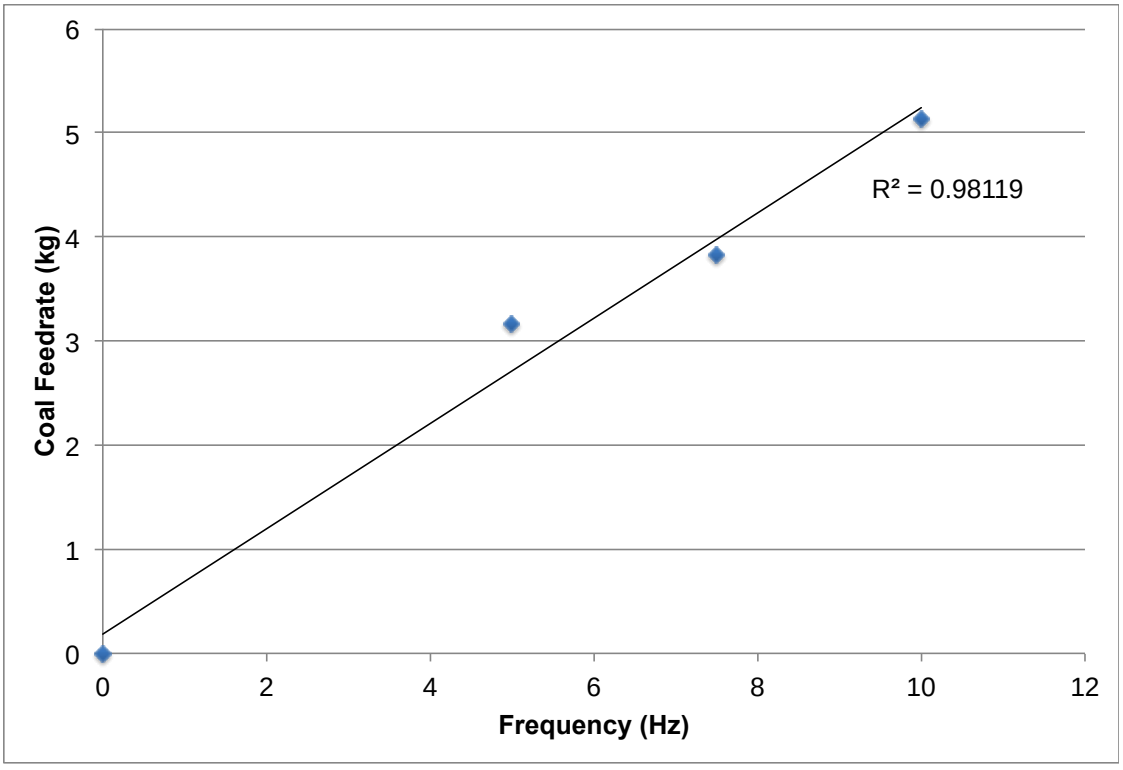

Figure A-2: Interpolation of coal feeding rate for other feeder motor frequency

Appendix B: PSBFBC Fluidising Fan Schematics

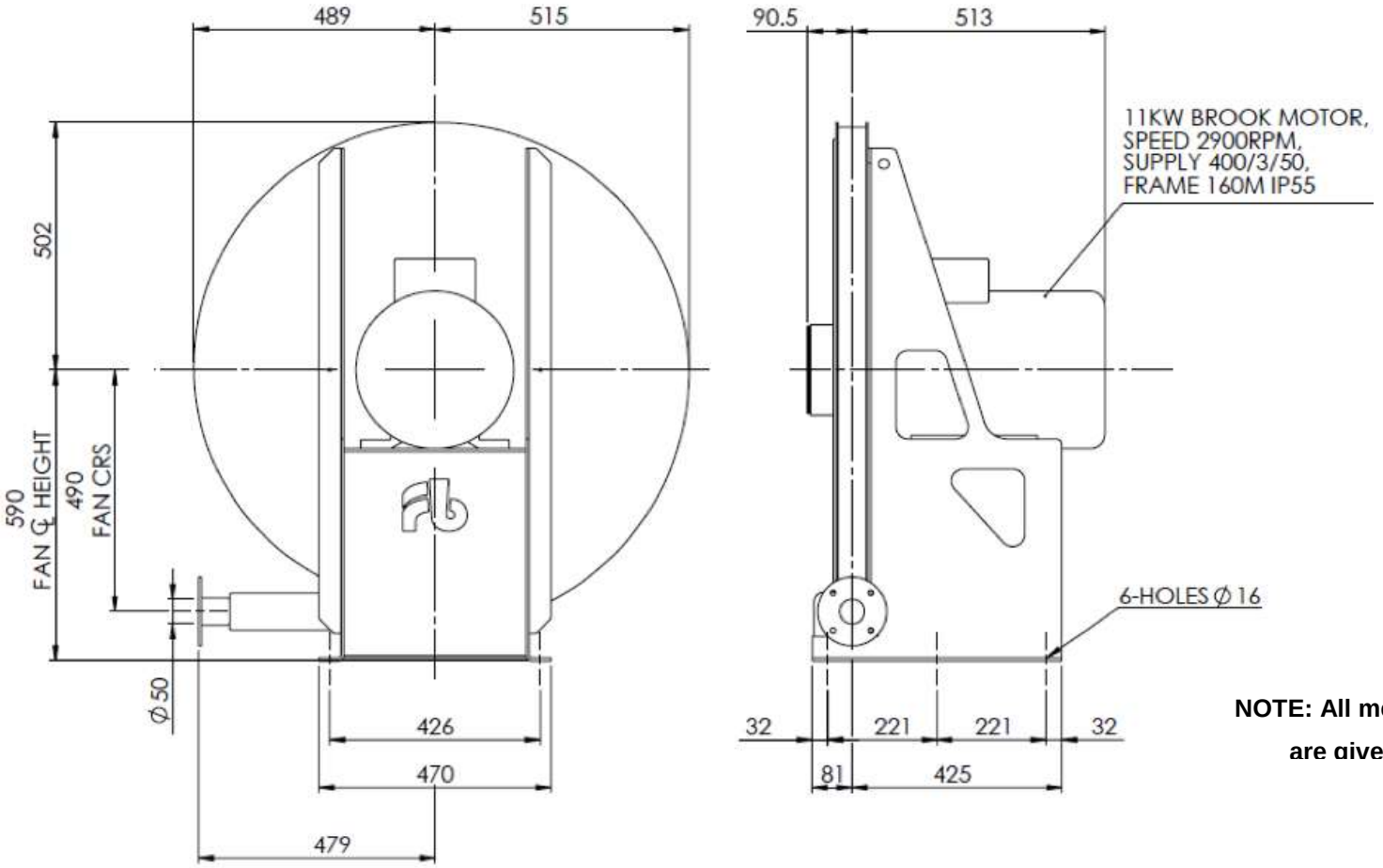

Figure B-1: Schematic diagram and dimensions of the BFBR fan showing the back and right hand view

Appendix C: Sieving Analysis Data Comparison for Garside 14/25 Sand Bed Material

Sieving analysis was performed on the Garside 14/25 sand bed material on as received basis using a different set of sieve arrangement of pan, 212µm, 425µm, 600µm, 850µm, 1180µm, 1700µm, 2360µm, 3350µm and 4750µm as opposed to the sieve arrangement of pan, 500µm, 600µm, 710µm, 850µm, 1000µm, 1180µm and 1400µm. A comparison between the percentage retained quantity in each sieve size of the measured particle size fraction distribution and those supplied in the data sheet is shown in Figure C-1.

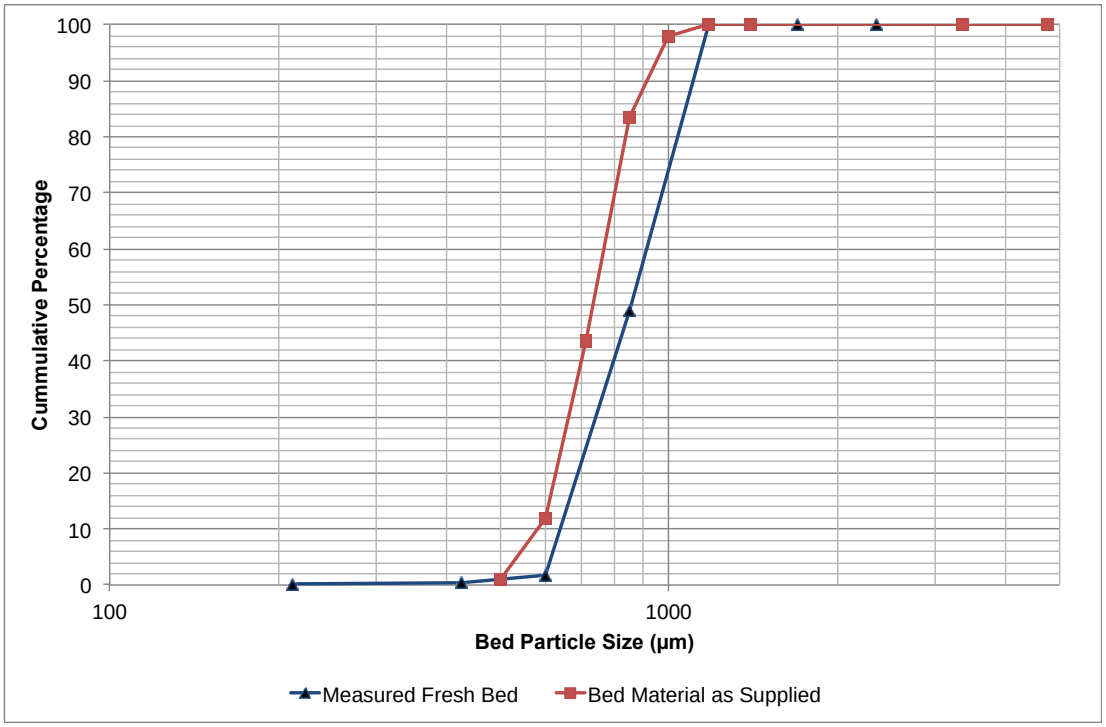

Figure C-1: Sieve analysis data comparison between for measured and as supplied Garside 14/25 sand bed material

The measured fresh bed identifies that measured in the laboratory on delivery while bed material as supplied identifies value given on the data sheet provided by the Garside 14/25 sand bed material supplier

Appendix D: Coal Preparation and Bed Material Inventory

D-1: Coal Preparation

Two sorts of Blyth bituminous coal (washed and unwashed) was used for this investigation. The coals were supplied in 20 kg bags from AB Sugar in particle size range of 12 – 25 mm. Upon arrival, the coal of choice depending on the experimental run was crushed using a jaw crusher to obtain particle size range of 10 – 19mm. The crushed coal was then sieved using 800mm by 800mm square hand sieves with a bottom and top mesh with aperture size of 10mm and 19mm respectively. The small particle sized fraction that goes through the bottom sieve (<10mm) were discarded and the large sized fractions retained in the top sieve (>19mm) were reprocessed in the jaw crusher. The particle size fraction retained in the 10mm aperture size sieves which are greater or equal to 10mm (≥10mm) but less than 19mm (<19mm) in particle size were collected and stored for use in the PSBFBC operation. This coal processing procedure was repeated for every coal bag supplied by AB Sugar to be used in the PSBFBC.

D-2: Bed Material Inventory

The 25 kg bag of Garside 14/25 sand supplied from AB Sugar was thoroughly mixed and 6kg of the sand was measured using a Kern and Shon GMBH weighing scale (model: ECB 20K20) with a readability and repeatability of 20g. The measured 6kg of sand was sieved using sieve pans and sieve shaker to determine the particle size distribution following procedures detailed in section 4.4.5. This procedure was repeated prior to the introduction of fresh Garside 14/25 sand of quantity >1kg into the BFBR.

Appendix E: Pictures of the PSBFBC Rig

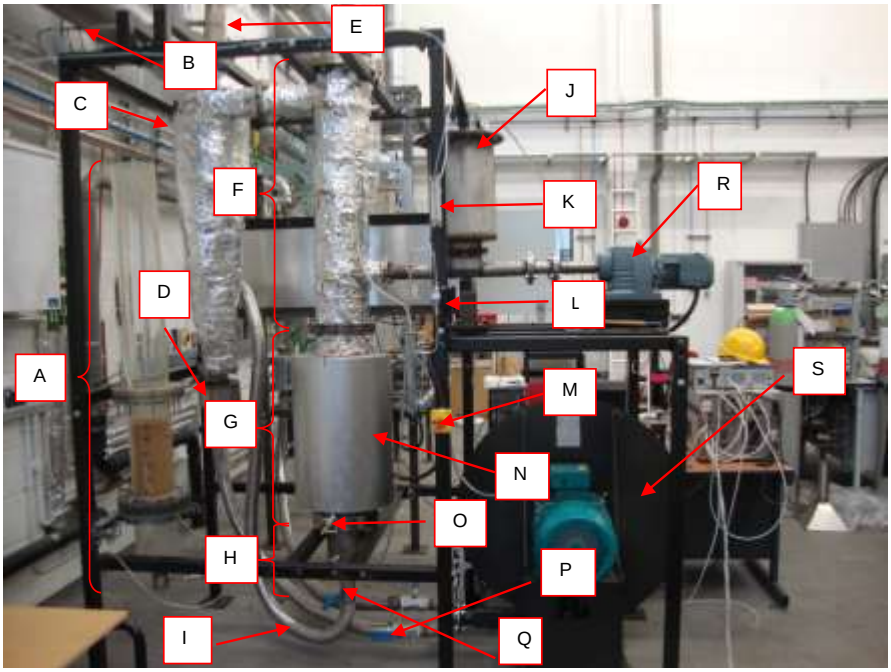

Figure E-1: Photograph of PSBFBC rig showing the BFBR, cyclone and coal feeder system: (A) transparent BFBR prototype rig, (B) cooling water flue gas sampling probe, (C) gas-solid cyclone, (D) cyclone reject container, (E) cyclone exhaust to extraction duct, (F) freeboard zone, (G) fluidising chamber, (H) plenum chamber, (I) fluidising air duct, (J) coal hopper, (K) nitrogen / air flowmeter for coal hopper, (L) pressure transducer, (M) emergency stop button 1, (N) BFBR heater, (O) pressure probe, (P) manual ball valve 1, (Q) manual ball valve 2 (R) coal feeder motor, (S) fluidising fan

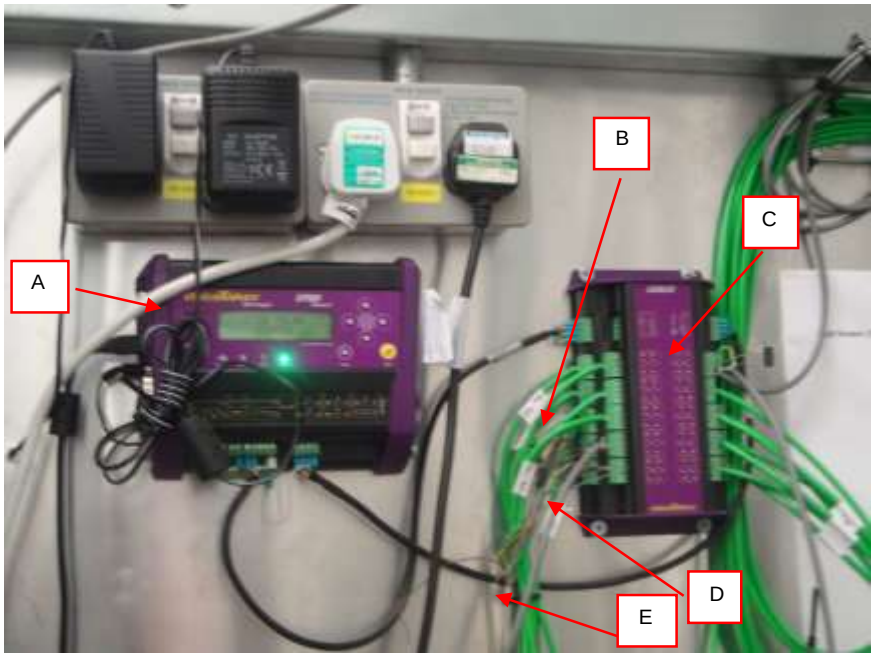

Figure E-2: Picture of the data acquisition system for the PSBFBC: (A) data logger, (B) thermocouple data cable, (C) data logger extension box, (D) pressure transducer data cable, (E) flue gas analyser data cable

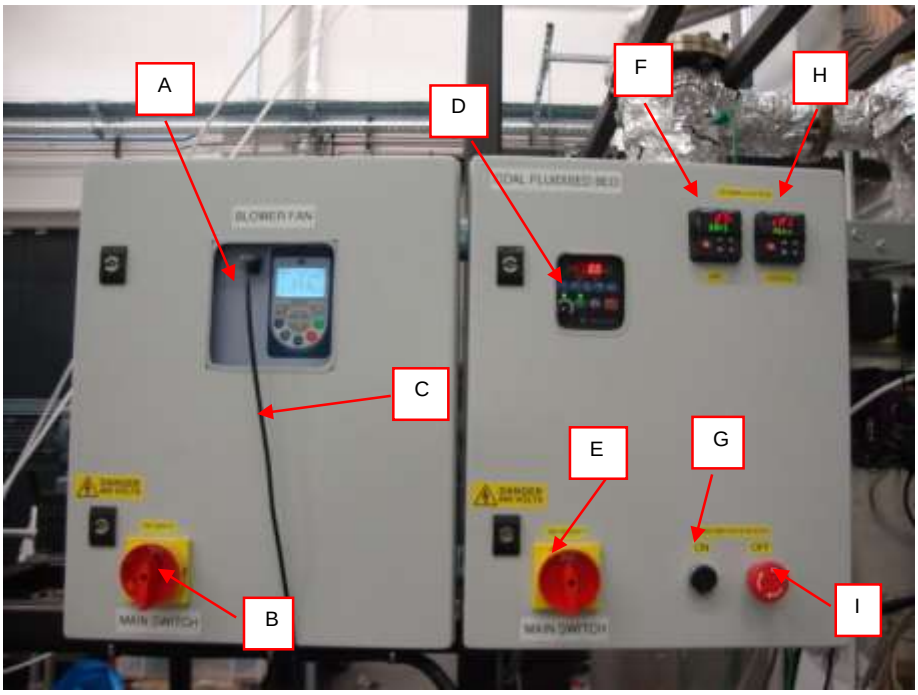

Figure E-3: BFBR heater, fluidising fan and coal feeder control system for the PSBFBC: (A) fluidising fan inverter, (B) main switch for fluidising fan controller, (C) fluidising fan remote control data cable, (D) coal feeder inverter, (E) main switch for the coal feeder and BFBR heater controller, (F) temperature limit controller, (G) on / reset button for the coal feeder and BFBR heater control system, (H) temperature heating controller, (I) emergency stop button 2

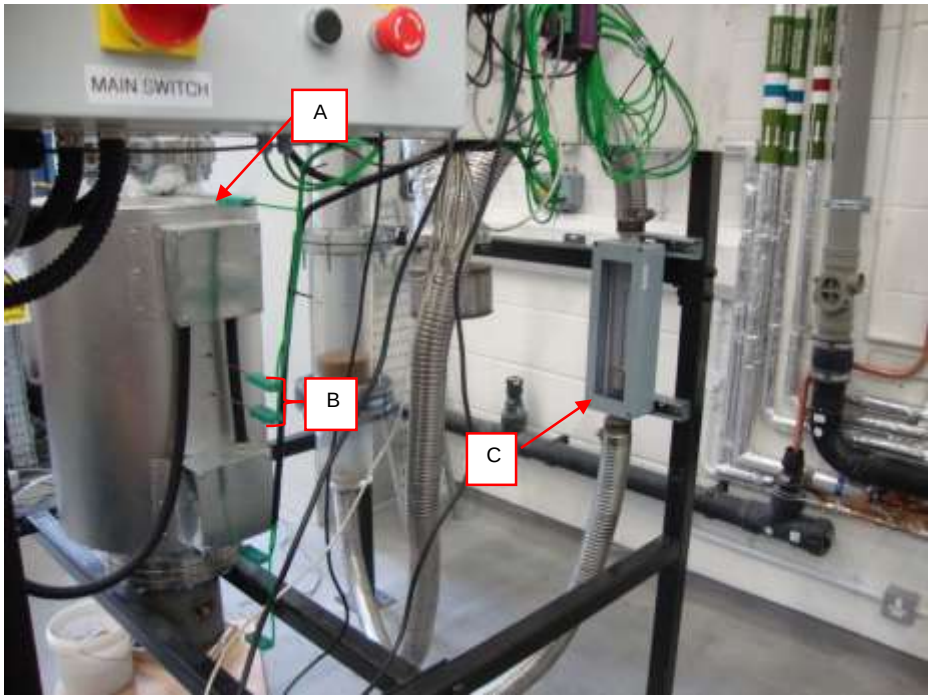

Figure E-4: The flue gas extraction unit control system for the PSBFBC: (A) main switch for extraction fan controller, (B) extraction fan speed regulator

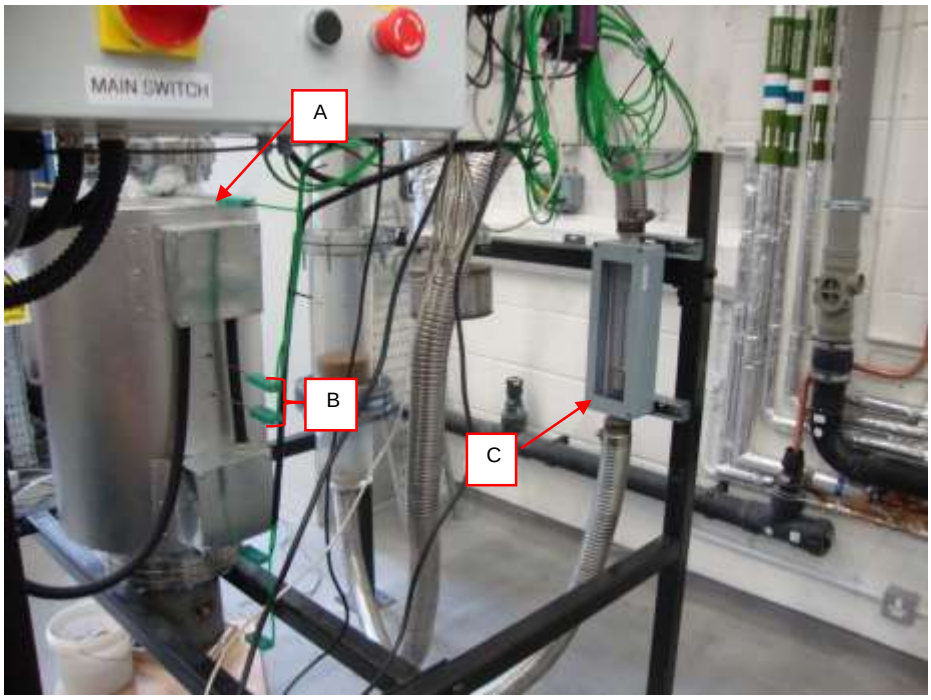

Figure E-5: The BFBR heater and variable area flow meter units on the PSBFBC: (A) thermocouple (PSBFBC operation monitoring), (B) limit and heating BFBR furnace controller thermocouples, (C) variable area flowmeter

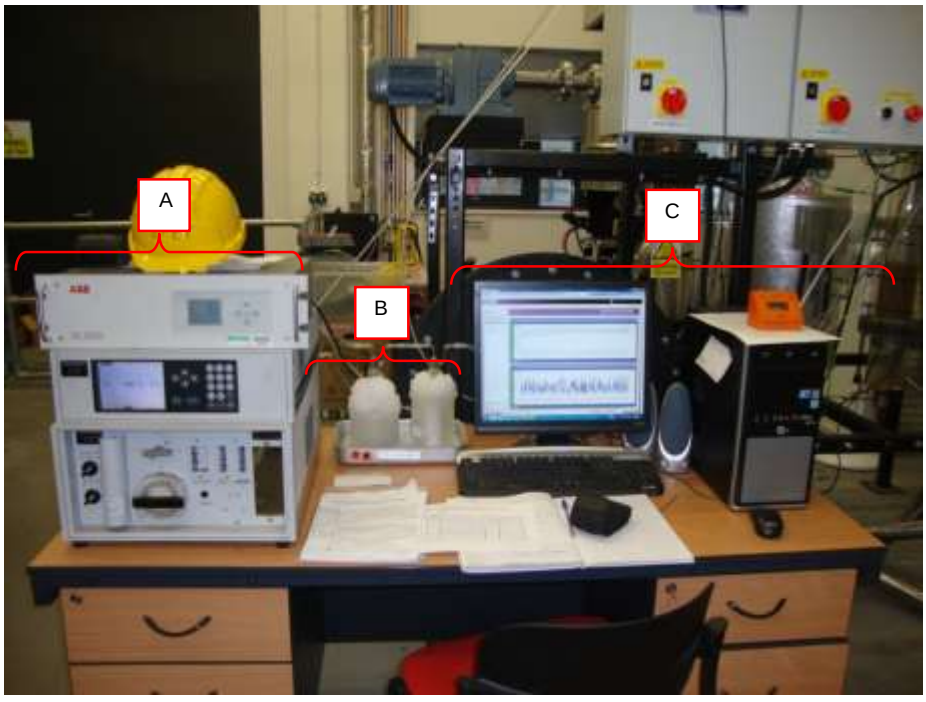

Figure E-6: The flue gas analyser and computer system for the PSBFBC: (A) flue gas analyser, (B) flue gas conditioning unit, (C) computer for monitoring, controlling and data collection

Appendix F: PSBFBC Coal Combustion Pre Start-up and Shutdown Check List

This checklist form must be filled prior to the start-up of the PSBFBC combustion rig and at the end of every experimental run.

Name of Operator:

Date: **Start Time:** **End Time:**

Prestart – Up List

	Activity	**Checked**
1	Switch “ON” the extraction fan	
2	Check and empty that the cyclone reject container	
3	Check and release the emergency stop buttons	
4	Check coal level in the hopper and top up if needed	
5	Turn the manual ball valve 1 to “OPEN” position	
6	Insert the cooling water flue gas sampling probe and turn “OPEN” the cooling water supply valve for the probe	
7	Turn “OPEN” the nitrogen / air supply into the coal hopper and set the flowrate to 25 litres/minute	
8	Turn “ON” the data logger, gas analyser and the computer	
9	Connect the flue gas analyser exhaust gas lines to the extraction vent	
10	Check that a blank flange is around the rig for emergency	
11	Double click on the “DataTaker” software to start the monitoring and collection of the temperature, pressure and flue gas composition data.	

Shutdown Check List

	Activity	**Checked**
1	Ensure all data logged for the experimental run are saved	
2	Switch the fluidising fan “OFF”	
3	Turn the manual ball valve 1 & 2 to “CLOSE” position	
4	Removing the cooling water flue gas sampling probe and turn “CLOSE” the water supply valve into the probe	
5	Leave the nitrogen / air supply into the coal hopper “ON” but reduce the flowrate to 15 litres/minute	
6	Leave the extractor system “ON”	
7	Switch “OFF” the data logger, gas analyser and the computer	

Appendix G: PSBFBC Coal Feed-rate vs Air Flow-rate Operating Chart

Coal Feeder		Stoichiometry Air Flow rate @ 20°C (l/min)										
Frequency (Hz)	**Feed rate (kg/h)**	**0%**	**10%**	**20%**	**30%**	**40%**	**50%**	**60%**	**70%**	**80%**	**90%**	**100%**
5	3.5	404	445	485	525	566	606	647	687	728	768	808
7.5	4.2	485	534	582	631	679	728	776	825	873	922	970
10	5.5	635	699	762	826	889	953	1016	1080	1143	1207	1270

Gas (%)	Expected Percentage Composition of the Flue Gas assuming Complete Combustion (Dry Basis)										
	0	**10**	**20**	**30**	**40**	**50**	**60**	**70**	**80**	**90**	**100**
Oxygen (O_2) (%)	0.0	1.9	3.6	4.9	6.1	7.1	8.0	8.8	9.5	10.1	10.6
Carbon dioxide (CO_2) (%)	18.2	16.5	15.1	13.9	12.9	12.0	11.2	10.6	10.0	9.4	9.0

Appendix H: SEM / EDX Resin Block and Carbon Tabs Sample Preparation

H-1: Resin Blocks

Struers epofix resin and hardener mixed in a ratio of 8.3:1 by weight was used to mount the agglomerated bed material. The mounted samples were placed in a Struers Epovac vacuum pump for 15 minutes to drive out all the air and left overnight to set, forming a moulded resin block. The moulded resin block was mounted in Struers Rotopol 1 and subjected to three stages of grinding using Struers MD-Piano 1200, 220 and 120 plates which was followed by three stages of polishing with Struers MD-Plan (9 µm), MD-Dac (3 µm) and MD-Dur (1 µm) polishing cloths in order to attain a high quality polished surface. Each grinding and polishing stage was run for 2 minutes and diamond lubricants Struers Dia Duo 9 µm, 3 µm and 1 µm was introduced on to the surface of the polishing cloth for each polishing stage. After polishing, the moulded resin block was then cleaned, allowed to dry in ambient room conditions and examined under light microscope to access the smoothness of the polished surface.

The final stage of the sample preparation is the “carbon coating” stage. The polished surface of the moulded resin blocks was placed inside a Jee 420 vacuum evaporator with the polished surface to be examined under SEM facing upward. The evaporator was then evacuated and a high electric current was passed through carbon rods which evaporates and deposits a very thin layer of carbon, in the order of 20-50 nm on the polished surface of the moulded resin block. The finished resin block, which is 30mm in diameter, is stored away in a 40mm internal diameter dedicated paper box in preparation for SEM.

H-2: Carbon Tabs

A piece of 10mm carbon sticky tab is placed on the surface of the 12.7mm SEM pin stud. A representative sample of the calcinated pure Garside 14/25 sand bed material, mix or loose bed material is spread carefully on the surface of the carbon sticky tab. The edges of the pin stud where there is no carbon sticky tab is cleaned to remove any debris after which it is stored away in the pin stud holder in preparation for SEM

Appendix I: Mass Balance of Ash Deposition in PSBFBC Bed Compared with Industrial FBC Bed

I-1: Mass Balance for PSBFBC

Facts:

1. Percentage (%) composition of ash in washed Blyth coal: 3.9%
2. Percentage (%) composition of ash in unwashed Blyth coal: 6.2%
3. Bed material weight: 6 kg

Assumption:

1. Only 50% of the ash available for deposition is deposited in the PSBFBC bed (% of ash deposited)

Summaries of mass balance obtained for washed and unwashed Blyth coal combusted in the PSBFBC are presented in Tables I-1 and I-2 respectively. Coal federate, total coal used, cyclone reject collected and percentage of ash in reject were all measured during the course of this investigation.

The following were determined as follows:

$$\textit{Amount of ash in coal (g)} : \textit{Total coal used (g)} \times \textit{\% of ash in coal (\%)}$$

$$\textit{Amount of ash in reject (g)} : \textit{Cyclone reject collected (g)} \times \textit{\% of ash in reject (wt.\%)}$$

$$\textit{Ash available for deposition (g)} : \textit{Amount of ash in coal (g)} - \textit{Amount of ash in reject (g)}$$

$$\textit{Amount of ash deposited in bed (g)} : \textit{Ash available for deposition (g)} \times \textit{\% of ash deposited (wt.\%)}$$

$$\textit{Percentage of ash deposited in the bed (\%)}: \frac{\textit{Amount of ash deposited in bed (g)}}{\textit{Bed material weight (g)}} \times 100$$

Table I-1: Mass balance summary for ash deposited in PSBFBC bed during the combustion of unwashed Blyth coal

Run	Run Time (h)	Coal Feedrate (kg/h)	Total Coal Used (kg)	Amount of Ash in coal (g)	Cyclone Reject Collected (g)	Percentage of Ash in Reject (wt.%)	Amount of Ash in Reject (g)	Ash Available for Deposition (g)	Amount of Ash Deposited in Bed (g)
1	5.1	1.9	9.7	380.1	550	45.7	251.2	128.9	64.5
2	5.2	2.4	12.4	483.9	509	47.8	243.3	240.6	120.3
3	5.2	1.9	9.8	383.8	769	48.0	368.9	14.9	7.5
4	5.2	2.4	12.4	484.8	800	50.3	402.3	82.5	41.3
5	5.2	2.4	12.4	484.8	800	48.7	389.7	95.1	47.6
6	5.2	2.1	10.9	424.2	755	48.8	368.3	55.9	28.0
7	5.2	2.1	10.9	424.2	747	47.0	351.4	72.8	36.4
8	5.2	2.2	11.4	444.4	786	45.1	354.8	89.6	44.8
9	5.2	2.2	11.4	444.4	775	45.7	354.5	89.9	45.0
10	5.2	2	10.4	404.0	809	46.4	375.3	28.8	14.4
TOTAL	51.7	21.60	111.8	4359.0	7300	473.6	3459.8	899.2	449.6

Percentage of ash deposited in washed Blyth PSBFBC bed (%): 7.4%

Table I-2: Mass balance summary for ash deposited in PSBFBC bed during the combustion of unwashed Blyth coal

Run	Run Time (h)	Coal Feedrate (kg/h)	Total Coal Used (kg)	Amount of Ash in coal (g)	Cyclone Reject Collected (g)	Percentage of Ash in Reject (wt.%)	Amount of Ash in Reject (g)	Ash Available for Deposition (g)	Amount of Ash Deposited in Bed (g)
1	5.2	2.3	11.9	738.7	703	49.4	347.1	391.6	195.8
2	5.2	2.1	10.9	674.4	685	53.7	367.8	306.6	153.3
3	5.2	2.3	11.9	738.7	703	51.2	359.9	378.7	189.4
4	5.2	2.1	10.9	674.4	802	52.9	424.4	250.0	125.0
5	5.2	2.1	10.9	674.4	701	47.0	329.4	345.1	172.5
6	5.2	2.3	11.9	738.7	748	48.0	358.9	379.7	189.9
7	5.2	2.2	11.4	706.6	809	48.4	391.3	315.2	157.6
8	5.2	2.2	11.4	706.6	828	49.2	407.6	298.9	149.5
9	5.2	2.1	10.9	674.4	826	44.2	365.5	308.9	154.5
10	5.2	2.2	11.4	706.6	807	47.2	380.6	326.0	163.0
TOTAL	51.8	21.90	113.4	7033.4	7612	491.2	3732.5	3300.9	1650.5

Percentage of ash deposited in washed Blyth PSBFBC bed (%): 25.6%

I-2: Mass Balance for Industrial FBC

Most of the information required to accurately determine the amount of ash deposited in the industrial bed is unknown. However this was estimated using the facts and assumptions stated below.

Facts:

1. Percentage (%) composition of ash in unwashed Blyth coal: 6.2%

2. Bed material weight: 13 tons
3. Operating period : 240 hours
4. Coal federate (tph): 2.7

Assumption:

1. Only 5% of the ash present in coal during the entire combustion run is deposited in the bed due to the high entrainment rate observed from the operation of the industrial FBC (% of ash deposited)

Summary of mass balance obtained for unwashed Blyth coal combusted in the industrial FBC is presented in Table I-3. The following were determined as follows:

$$Coal\ used\ (tons) : Operating\ period\ (h) \times Coal\ feed\ rate\ (tph)$$

$$Amount\ of\ ash\ in\ coal\ (tons) : Total\ coal\ used\ (tons) \times \%\ of\ ash\ in\ coal\ (\%)$$

$$Amount\ of\ ash\ deposited\ in\ bed\ (tons) : Ash\ available\ for\ deposition\ (tons) \times \%\ of\ ash\ deposited\ (wt.\%)$$

$$Percentage\ of\ ash\ deposited\ in\ the\ bed\ (\%) : \frac{Amount\ of\ ash\ deposited\ in\ bed\ (tons)}{Bed\ material\ weight\ (tons)} \times 100$$

Table I-3: Mass balance summary for ash deposited in industrial FBC bed during the combustion of unwashed Blyth coal

Coal use (tons)	648
Amount of ash in coal (tons)	40.18
Amount of ash deposited in bed (tons)	2.01
Percentage of ash deposited in bed (%)	15.45